8-24-2022 10:00 AM

Efficient Discovery and Utilization of Radio Information in Ultra-Dense Heterogeneous 3D Wireless Networks

Mattaka Gamage Samantha Sriyananda, *The University of Western Ontario*

Abstract

Emergence of new applications, industrial automation and the explosive boost of smart concepts have led to an environment with rapidly increasing device densification and service diversification. This revolutionary upward trend has led the upcoming 6th-Generation (6G) and beyond communication systems to be globally available communication, computing and intelligent systems seamlessly connecting devices, services and infrastructure facilities. In this kind of environment, scarcity of radio resources would be upshot to an unimaginably high level compelling them to be very efficiently utilized. In this case, timely action is taken to deviate from approximate site-specific 2-Dimensional (2D) network concepts in radio resource utilization and network planning replacing them with more accurate 3-Dimensional (3D) network concepts while utilizing spatially distributed location-specific radio characteristics. Empowering this initiative, initially a framework is developed to accurately estimate the location-specific path loss parameters under dynamic environmental conditions in a 3D small cell (SC) heterogeneous networks (HetNets) facilitating efficient radio resource management schemes using crowdsensing data collection principle together with Linear Algebra (LA) and machine learning (ML) techniques. According to the results, the gradient descent technique is with the highest path loss parameter estimation accuracy which is over 98%. At a latter stage, receive signal power is calculated at a slightly extended 3D communication distances from the cluster boundaries based on already estimated propagation parameters with an accuracy of over 74% for certain distances. Coordination in both device-network and network-network interactions is also a critical factor in efficient radio resource utilization while meeting Quality of Service (QoS) requirements in heavily congested future 3D SCs HetNets. Then, overall communication performance enhancement through better utilization of spatially distributed opportunistic radio resources in a 3D SC is addressed with the device and network coordination, ML and Slotted-ALOHA principles together with scheduling, power control and access prioritization schemes. Within this solution, several communication related factors like 3D spatial positions and QoS requirements of the devices in two co-located networks operated in licensed band (LB) and unlicensed band (UB) are considered. To overcome the challenge of maintaining QoS under ongoing network densification and with limited radio resources cellular network traffic is offloaded to UB. Approximately, 70% better overall coordination efficiency is achieved at initial network access with the device network coordinated weighting factor based prioritization scheme powered with the Q-learning (QL) principle over conventional schemes. Subsequently, coverage information of nearby dense NR-Unlicensed (NR-U) base stations (BSs) is investigated for better allocation and utilization of common location-specific spatially distributed radio resources in UB. Firstly, the problem of determining the receive signal power at a given

location due to a transmission done by a neighbor NR-U BS is addressed with a solution based on a deep regression neural network algorithm enabling to predict receive signal or interference power of a neighbor BS at a given location of a 3D cell. Subsequently, the problem of efficient radio resource management is considered while dynamically utilizing UB spectrum for NR-U transmissions through an algorithm based on the double Q-learning (DQL) principle and device collaboration. Over 200% faster algorithm convergence is achieved by the DQL based method over conventional solutions with estimated path loss parameters.

Lay Summary

Emergence of new applications and industrial automation together with the sudden increase of smart cities, smart premises (e.g., houses and buildings) and smart vehicles have led to a rapid increase in not only the number of devices connected to wireless networks but also the services provided through them. This trend has convinced the designers of the upcoming cellular wireless communication systems to make them globally available communication, computing and intelligent systems providing uninterrupted services continuously to both individuals and machines. In this kind of environment, resources used for wireless links between the devices and the serving stations are identified as extremely scarce assets that are to be very efficiently utilized. Moreover, the characteristics of these resources are specific to the locations in the 3D space as well. Based on this reason, one of the best solutions is to deviate from approximate 2-Dimensional (2D) network design principles while replacing them with 3-Dimensional (3D) network design concepts. These 3D network design principles are expected to best use the resources available at a given location in 3D space. In this case, initially a framework is developed to estimate or discover the resources at a given location under dynamic environmental conditions and to better utilize them subsequently. Mathematical modelling and self-learning techniques are used for that with the information provided by several groups of devices in a small 3D network coverage area. Coordination of both device-network and network-network interactions is also identified as one of the critical factors in the efficient utilization of these resources in meeting the Quality of Service (QoS) requirements of the devices in heavily congested future 3D networks. In this case, overall communication performance enhancement is achieved through efficient utilization of resources together with supporting techniques developed based on device and network coordination schemes. For this scenario, much attention is paid to the opportunistically available scarce resources. At the same time, factors like the locations of the devices in the 3D space, their QoS needs and priority requirements of the device congestion situations are also considered. In certain scenarios, devices served by two wireless networks are also considered where those networks are operated through different transmitters at the same location. To better facilitate these operations, prediction of receive signal power at a given location due to a transmission done by a nearby serving station is also being investigated with the objective of efficient allocation and utilization of common resources. For that, state of the art machine learning techniques are used while dynamically utilizing the limited resources.

To my parents

Acknowledgments

I would like to express my profound gratitude and appreciation to my thesis supervisor, Dr. Xianbin Wang, for his invaluable guidance, continuous supervision and financial support for my graduate studies. Moreover, I do appreciate his guidance and time spent on numerous discussions on how to successfully shape up a professional career of an engineer while developing necessary skills in facing rapidly evolving competitive global technological environment.

I specially thank Dr. Luiz Capretz and Dr. Serguei Primak for being the members of my thesis advisory committee and providing me with numerous constructive suggestions. At the same time, it was a great privilege for me to have Dr. Aleksander Essex and Dr. Abdallah Shami as the Graduate Chairs, those who always supported my studies in numerous ways.

I gratefully appreciate Dr. Jagath Samarabandu, Dr. Taufiq Rahman, Dr. Ning Zhang and Dr. Yimin Yang for being the members of my examination committee for the thesis defense. Furthermore, it was a great pleasure and honor for me to have Dr. Catherine Nolan as the Chair of the examination committee. I highly value their precious time and constructive suggestions to further improve my thesis and research.

I would also like to convey my warmest regards to my colleagues and friends in my research group for creating a gentle and inclusive working atmosphere, from which I immensely benefited during my doctoral studies. In particular, I appreciate them for making themselves available for discussions not only on the various research related problems but also on the numerous problems in day-to-day life as well.

I always express my sincere appreciation to Dr. Jagath Samarabandu for sharing his professional insights and being an expert mentor for me on numerous occasions. His lab was always open to me and it was a pleasurable experience for me to exchange thoughts and ideas with the friends and colleagues in that lab. Similarly, it was a precious opportunity for me to associate with the friends from the Optimized Computing and Communications research group led by Dr. Abdallah Shami. Their intimate companionship was an unforgettable courage and an asset for me in organizing numerous professional events throughout my stay at the university.

It is a privilege for me to experience the cooperation of the non-academic staff of the Department in various means in a quick and courteous manner where the services of different secretaries and coordinators are highlighted with much recognition.

I extend my sincere and deepest gratitude to my parents, my elder brother and his family for their love and support given throughout my life and the activities I have engaged in. The strong foundation laid by my parents for my life has always been a great strength, not only to face, tolerate and fortify myself against all the foreseen risks and dangers, but also to overcome all the obstacles and barriers in my life.

Contents

List of Figures

List of Tables

List of Acronyms

2D	2-Dimensional
3D	3-Dimensional
2G	2nd-Generation
3G	3rd-Generation
3GPP	3rd-Generation Partnership Progect
4G	4th-Generation
5G	5th-Generation
6G	6th-Generation
eMBB	Enhanced Mobile Broadband
mMIMO	Massive Multiple-Input Multiple-Output
mMTC	Massive Machine-Type Communication
mmWave	Millimeter Wave
uMUB	Ubiquitous Mobile Ultra-Broadband
uHDD	Ultra-High Data Density
uHSLLC	Ultra-High-Speed with Low-Latency Communications
uRLLC	Ultra-Reliable Low-Latency Communications
AI	Artificial Intelligence
ANN	Artificial Neural Network
AP	Access Point
ARQ	Automatic Repeat Request
AWGN	Additive White Gaussian Noise
BS	Base Station
CNN	Convolutional Neural Network
CR	Cognitive Radio
D2D	Device-to-Device
DCNN	Deep Convolution Neural Network
DL	Down-Link
DNN	Deep Neural Network
DQL	Double Q-Learning

DRNN	Deep Regression Neural Network
EE	Energy Efficiency
GD	Gradient Descent
HCS	Human-Centric Services
HetNet	Heterogeneous Network
HBF	Holographic Beamforming
ICT	Information and Communication Technology
IDW	Inverse Distance Weighting
IN	Impulse Noise
IoE	Internet of Everything
IoT	Internet of Things
KPI	Key Performance Indicator
LA	Linear Algebra
LAA	License-Assisted Access
LB	Licensed Band
LBT	Listen Before Talk
LDHMC	Long-Distance and High-Mobility Communications
LIS	Large Intelligent Surface
LOS	Line-of-Sight
LR	Linear Regression
LTE	Long-Term Evolution
LTE-U	LTE-Unlicensed
LS	Least Squire
MDP	Markov Decision Process
MIMO	Multiple-Input Multiple-Output
ML	Machine Learning
MSE	Mean Square Error
NLOS	Non-Line-of-Sight
NMS	Nelder-Mead Simplex
NN	Neural Network
NR	New Radio
NR-U	NR-Unlicensed
OAM	Orbital Angular Momentum
OLS	Ordinary Least Squire

OS	Open Squire
QoS	Quality of Service
QL	Q-Learning
RACH	Random Access Channel
RBL	Regret Based Learning
ReLU	Rectified Linear Unit
REM	Radio Environment Map
RIM	Radio Information Map
RL	Reinforcement Learning
RQ	Repeat Request
RRI	Radio Resource Information
RRM	Radio Resource Management
RSP	Receive Signal Power
S-ALOHA	Slotted-ALOHA
SC	Small Cell
SRE	Smart Radio Environment
SINR	Signal-to-Interference-Plus-Noise Ratio
SNR	Signal-to-Noise Ratio
SM-MIMO	Supermassive Multiple-Input Multiple-Output
TDD	Time Division Duplex
UB	Unlicensed Band
UMa	Urban-Macro
UMi	Urban-Micro
UE	User Equipment
UL	Up-Link
UAV	Unmanned Aerial Vehicle
V2X	Vehicle-to-Everything

Chapter 1

Introduction

1.1   Heterogeneous 3D Small Cell Networks

Continuous and increasing growth of global wireless traffic is always forecast through statistical analyses where it is expected to have rate increase in exabytes per month in near future [1]. In comparison with 5th-Generation (5G), 6th-Generation (6G) is expected to enhance the performance of information transmission, peak data rates up to 1 Tbps and ultra-low latency in microseconds. It features terahertz frequency communication and spatial multiplexing, providing as much as 1000 times higher capacity than 5G networks. For upcoming wireless communication generations, three new service classes are identified [2]: ubiquitous mobile ultra-broadband (uMUB), ultra-high-speed with low-latency communications (uHSLLC) and ultra-high data density (uHDD) in supporting massive machine type communications. In order to effectively facilitate these service classes fundamental reforms are needed to the architectural platforms enhancing joint sensing, communication, computing, processing and, above all, an environment that is cooperative and programmable [3]. This visionary concept for upcoming wireless communication systems is introduced as smart radio environment (SRE) [3]. Furthermore, to increase the processing capabilities and the accuracy of decisions while reducing the processing time and increasing the performance aspects of the communication systems,

this SRE is designed with intelligent, proactive, adaptive, situation and content aware principles, algorithms and techniques [4]. As a part of continuous expansion of service classes, growth of service classes from 5G containing massive machine-type communication (mMTC), enhanced mobile broadband (eMBB) and ultra-reliable low-latency communications (uRLLC) to 6G containing uHDD, uMUB and uHSLLC are given in Fig. 1.1. With the development technology and from different viewpoints, more service classes like long-distance and high-mobility communications (LDHMC) and human-centric services (HCS) [5, 6] are identified. Different anticipated use cases in 6G service classes are also given in the same figure.

By this moment, studies on 6G and beyond wireless communication systems have already begun while exploring on new avenues to broaden the existing boundaries surpassing the current horizon. In future, massive machine type communications originated from unmanned devices are anticipated in both ground and sky with a demand for ultra-reliable, highly energy efficient and significantly low latent, networks while supporting very high data rates and a vast number of heterogeneous connections. With increased network densification and information and communication technology (ICT) enabled industry, these dense device deployments at ground level and above may lead to spatially distributed small cells (SCs) in the 3-Dimensional (3D) space while further demanding to establish heterogeneous 3D networks with the use of 3rd spatial dimension for cellular coverage planning. In addition, the use of high radio frequency bands and large scale antenna arrays also may create demands on highly distributed radio resources in time, frequency and spatial domains. Next-generation wireless systems are expected to autonomously utilize technologies in a distributed fashion to satisfy the simultaneous delivery of services with stringent requirements that arise in a dynamic way [7]. In this case, it is very important to understand and pay attention to the natural chronological evolution of radio resource management principles against network coverage planning concepts as indicated Fig. 1.2. The emerging immediate future is going to be SRE for 3D heterogeneous networks (HetNets) operated with dynamic and shared radio resources through situation aware intelligent algorithms. In parallel cell-free networks operated in 3D space [8, 9] is also being
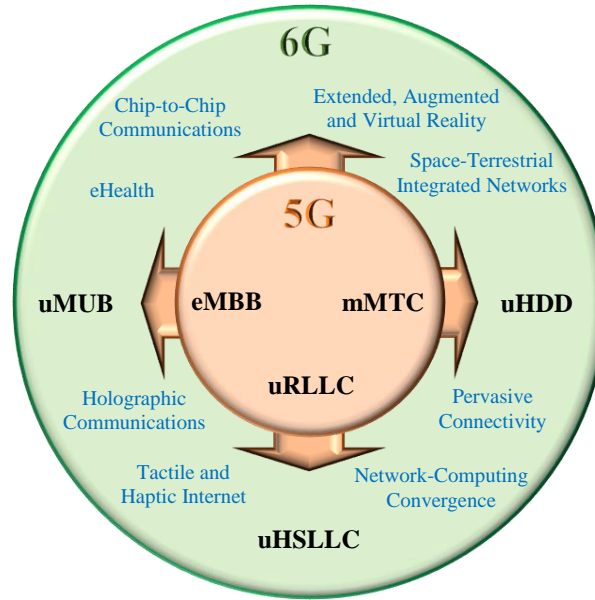
Figure 1.1: Expansion of service classes from 5G to 6G and their use cases.

considered as a strong candidate for the future wireless networks.

1.1.1 3D SC HetNets Over Existing 2D Cellular Networks

With the natural evolution of device locations from ground to different elevated positions limitations in performance could be observed with many of the existing technologies belongs to 4th-Generation (4G) and before generations in utilization of radio resources [5, 10]. On the other hand, integration of ground and airborne networks is also limited by technological constrains. Some of those limitations are arisen due to fundamental design error or the assumption involved with network planning that the network or cell deployment is done on a 2-Dimensional (2D) plane. Particularly, this assumption is predominantly used in the technical areas of network coverage planning (including frequency planning) and radio resource management (including construction of radio maps). In this case, now it is identified as one of the fundamental assumptions that the designers to deviate from in designing and planning the future heterogeneous wireless networks [10] while achieving designated goals associated with upcoming wireless cellular networks.

The emerging requirements over and above existing technologies includes, measurement
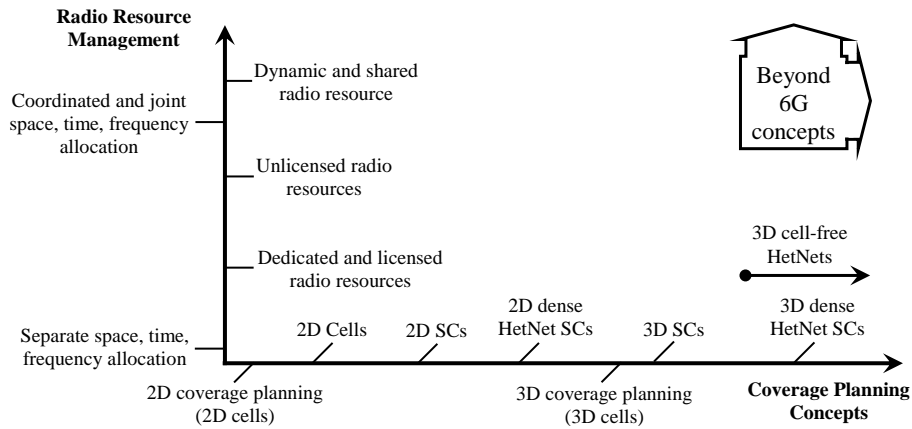
Figure 1.2: Evolution of radio resource management principles against network coverage planning concepts.

and (data-driven) modeling of the 3D propagation environment, 3D frequency and network planning (including where and how to deploy base stations (BSs)), new network optimization, mobility management, routing, and resource management in 3D environment. In this case, it has already envisioned that all the solutions and techniques designed for 6G and beyond communication systems are for ground and aerial or airborne transceivers.

In order to become a fully functional 3D network at least four basic technical requirements are to be fulfilled.

1. Utilization of 3D coordinate system to identify locations of the devices.

2. Utilization of location-specific spatially distributed 3D radio resources.

3. Following the 3D planning concepts (including frequency and coverage planning) to serve the devices [10].

4. Employment of techniques where 3D characteristics related to the device distributions, the radio resources and/or environment are leveraged.

These requirements for a 3D network is given in Fig. 1.3. Any network that uses fewer elements than these key properties is not identified as a fully functional and fully featured 3D network. The concepts, algorithms, theories and techniques that utilize one or more of these
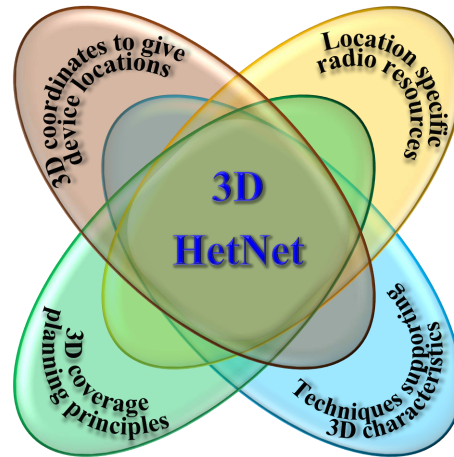
Figure 1.3: Main technical requirements for a 3D wireless network.

main components are recognized as supportive concepts, algorithms, theories and techniques for the 3D networks. In addition, efficient use of 3D spatial parameters should be reflected through some of the performance metrics as well.

1.1.2 3D Networks and Associated Performance Measures

Primarily the demand for the 3D networks is arisen from two main sources viz the communication devices positioned at different elevations and the numerous types of flying objects at different altitudes [11] with numerous BS-device vertical angles including certain scenarios of vehicle-to-everything (V2X) communication. However, at present, they are catered by the existing 2D network technologies and architectures [12] which are incapable of meeting the requirements of the future networks. Initially, the demands for the 3D networks were driven by a set of extensive and inevitable applications like environmental and natural monitoring, patrolling and disaster recovery, search and rescue, transportation and different types of combats (e.g., air-to-air, air-to-ground). In reorganizing and reconfiguring existing network architectures and concepts, it is very important not to limit the usage of 3D networks to flying objects where existing 2D networks are to be completely replaced with 3D HetNets in the long run. However, coexistence of 2D and 3D networks could be identified as an medium term or indeterminate solution during the process of evolution which is with a high demand.

When catering to future networks and communication systems with airborne (above ground level) mobile or stationary transceivers, the protocols must operate in 3D space across different propagation environments, solutions should meet the requirements of heterogeneous devices with different mobility patterns and algorithms ought to learn and adapt to the dynamic and complex environment conditions. In addition, network architecture and infrastructure facilities should also be aligned accordingly to expedite these emerging developments.
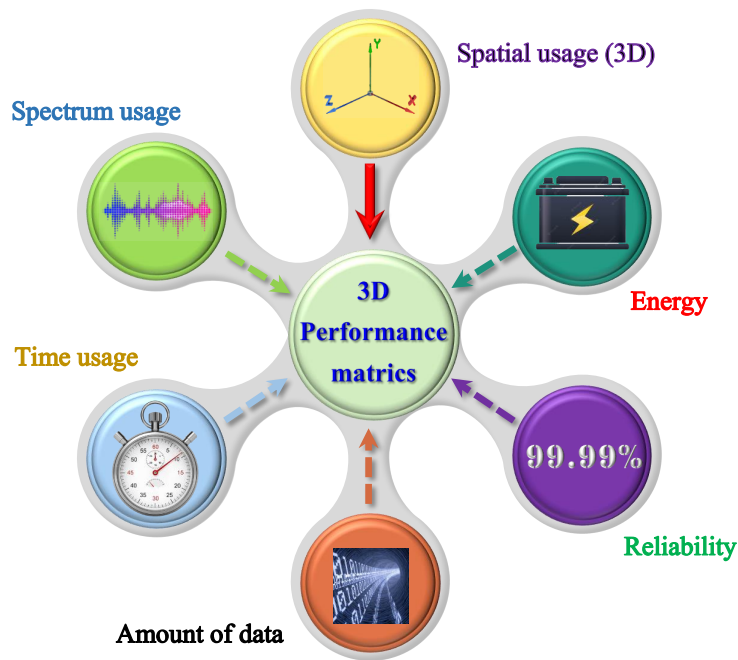
Figure 1.4: Basis for performance indicators.

Apart from those requirements, even performance analysis of any of the solutions provided for 6G and beyond networks should be capable of reflect the true impact of the 3D background generated by spatially distributed resources together with dynamism created by surrounding environment and the relative movements of the devices. In other words this is the right time to move away from conventional performance metrics towards fine-grained [5] location and spatial volume sensitive performance metrics. Many of the key performance indicators (KPIs) for the upcoming wireless communication systems are developed based on the principle use of several basic resources and return on utilization of those resources. A number of possible combinations in supporting these performance indicators can be found in Fig. 1.4. One of the

Table 1.1: Required values for KPIs in 6G HetNets

Data Rate	Bandwidth (MHz)	Latency (µs)	Reliability (%)	Spectral Efficiency	Energy Efficiency	Connection Density	Traffic Capacity	Mobility (km/h)	Processing delay (ns)
1 Tb/s	400	1-100	99.99999	5–10× that of 5G	10–100× that of 5G	10^7 devices/km^2	1-10 Gb/s/m^3	1,000	1

simplest early stage example is "amount of data" together with "time usage" may give data rate or "latency" which is the time taken to deliver some data to a destination location in a network. However, these performance metrics are also evolving over time.

As an example measurement units for spectral and energy efficiency requirements can be considered. For the 2nd-Generation (2G) it is in bps, for the 3rd-Generation (3G) it is in bps/Hz, for the 4G it is in bps/Hz/m^2 and for the 5G is in bps/Hz/m^2/Joules. For the 6G it should be as bps/Hz/m^3/Joules. As it is indicated, from 2G to 4G there had not been much concern on energy efficiency (EE). However, for the 6G and beyond communication systems, volume is also taken into consideration when and KPI is developed under 3D HetNet environment [5]. In this case, these requirements may lead to developments along several key streams namely, accuracy of 3D propagation modeling, efficiency of radio resource management in 3D space, 3D performance metrics for the devices and the networks, 3D mobility management and 3D network optimization. The minimum required values for the KPIs in 6G HetNets are given in Table 1.1 [5, 6, 13, 14]. The value for the spectral and energy efficiency gains with respect to 5G networks is given as $1000 \times$ in bps/Hz/m^3/Joules [5].

1.2 Challenges in Path Loss Estimation and Radio Resource Utilization in 3D HetNets

This study is motivated by the demand on solving the technical problems with scarce radio resource and the deployment of 3D networks followed by a set of benefits. However, in designing solutions for these problems several challenges were identified particularly in determining location-specific path loss parameters, location-specific radio resources and efficient utilization

of them. Some of the challenges are arisen due to incompatibility of conventional techniques and methods used in 2D networks with the upcoming 3D networks.

1.2.1 Dynamism of the Device Distributions and the Environment

Due to continuous changes in the environment and the device distributions, conventional site-specific path loss models and associated algorithms for radio resource management cannot be considered as effective models and efficient mechanisms anymore [15]. Negligence of these dynamic conditions has led to significant errors and performance degradation in results when they are being applied for the dense real life scenarios [16, 17]. Technically, many of these path loss models and values for their parameters are being held constant over time and insensitive to the changes of the environment or the device distributions during the process of they are being used for radio resource management [18–21]. That means, many of these models and algorithms have been developed and they are being used under the assumption of static environments and the device distribution scenarios. Even in the long run they cannot be successfully used in the environments and the terrain conditions that they were originally developed for. As almost all the real life scenarios are associated with highly dynamic environments and device deployments, in order to be more realistic and enhance performance, at least parameters of current path loss models and radio resource management schemes are to be updated dynamically accounting for dynamism of the environment and device distributions while facilitating collection and processing of data to determine characteristics of radio links and construction of radio maps in real-time basis [15].

1.2.2 Knowledge on 3D Spatially Distributed Path Loss Parameters

For the conventional signal processing algorithms and technique used for radio resource management, knowledge on path loss parameters and fading characteristics are vital information. One of the main assumptions made with those techniques is that the values of the path loss parameters are common for a given cell (i.e., site-specific values). However, in the reality

they are location-specific parameters and values. Due to this reason, many of the path loss models cannot be generalized reasonably to use at all the locations in a cell and all cells with similar kind of terrain characteristics other than the locations that they were developed for. There is a considerable adverse impact to the performance of the future communication systems operated in dense device distributions under very scarce radio resource conditions due to this assumption. In this case, it is considerable challenge to develop a mechanism to calculate location-specific values for the parameters of a selected path loss model in order to calculate receive signal power or interference values for radio resource management.

1.2.3 Device Dependent Errors Associated with Readings

In taking measurements on receive signal power and signal-to-interference-plus-noise ratio (SINR), the reading can be contaminated with device dependent errors gains and losses [22,23]. In a highly congested SC environment these errors are capable of generating non-negligible adverse impact to the decisions on radio resource management which are taken based on the different measurement values sent by the receivers. Subsequently, these errors can cause reduction in radio resource utilization efficiency leading to have degradation in overall performance and Quality of Service (QoS). In a SC environment, when the devices are in the vicinity of each other avoidance of third spacial dimension in coverage planning makes the situation even worse. In this case, several steps are to be taken to avoid this challenge including employing suitable post acquisition data processing schemes, avoidance of taking readings from the same or a single device and to use of specifically developed field measurement devices to take readings. In addition, a large number of readings are to be taken from each device to avoid errors with a single reading and a group of devices can be employed reduce the device dependent errors.

1.2.4 Overhead and Costs Associated with Network Resources and Equipment

Due to scarcity of network resources and the associated costs, it is difficult to allocate dedicated resources like a separate channel or a portion of a frame from the network to report field measurements and to exchange control information related to their subsequent processing operations. Furthermore, there is a difficulty and significant costs associated with positioning the field measurement devices in different required locations of all the cells for some of the future real-time operations like location-specific path loss parameter estimation and radio map constructions [19, 24, 25]. In certain occasions, there could be man made access restrictions to the locations preventing deployment third party or operator devices at the required locations due to numerous reasons like security and privacy. In addition, managing conventional processing operations related to development of 3D radio maps and determining spatially distributed propagation parameters for all the cells in a network are also beyond the limits of human capacities. In this case, it is highly desirable to have intelligent autonomous process for all those operations thorough a network wide technological upgrade. As a result, it is highly encouraged to use available network resources and the devices strategically for these real-time field measurements campaigns and subsequent real-time information management operations. In order to support these amendments, it may be necessary to have amendment in the network architecture as well. The new architecture should be able to facilitate operations related to real-time data collection, data processing, coverage discovery, resource allocation, usual communication aspects, geographical coverage planning [26] and network control [27]. In addition, it should be able to efficiently handle cooperative and coordinated learning and processing operations while supporting mutual data exchange between BSs, devices and cloud.

To provide very effective solutions, it is always better to be aware on the general key challenges related to upcoming communication concepts beyond 6G wireless systems and associated enabling technologies like opening the subterahertz spectrum for increased band-

widths, pushing the limits of semiconductor technologies to support these bands, developing transceiver designs and architectures to realize the high data rates and achieving submillisecond latencies at the network level [13, 28]. These challenges are arisen on top of several conventional challenges like maintenance of different types of efficiencies like energy efficiency, spectrum efficiency and data processing efficiency which are directly linked with the traditional KPIs. In the case of new research challenges, a set of new KPIs are also being designed to measure the performance enhancement achieved through the solutions provided for these new challenges particularly aiming 6G and beyond communication systems.

In this study, much attention is paid for the most closely related challenges and problems related to path loss estimation and radio resource management in 3D wireless networks. Some of the most prominent general challenges related to progression of 3D networks include coverage planning, cell association [29] and frequency planning [30]. With the increase of device density with uncoordinated massive number of heterogeneous devices, particularly in unlicensed band (UB) more and more intensified additional challenges are expected including avoidance of access attempts for already allocated radio resources, coordinated use of location-specific opportunistic radio resources in a precise and efficient manner, management of channel access for the new devices [31, 32] while minimizing access collisions, reduction of access delays while increasing access probability for prioritized devices. Even though some of the general challenges are being well investigated, due to exponentially growing device density and wireless traffic still they are in the forefront of future wireless network design challenges and problems. Because, machine type devices can continuously compete for scarce radio resources in a small 3D space generating interference and access congestion concessions leading to highly inefficient utilization of radio resources.

1.3 Research Motivations

This study is motivated by several motivation factors. Some of the key motivation factors in favor of 3D networks could also be highlighted.

- **Increase use of sky:** Since recent past, there is an increase in use of the sky by different low flying objects like balloons, drones, low altitude air-crafts and unmanned aerial vehicles (UAVs) [11]. Particularly, there is a significant increase in the amount of flying objects within first the 500 m from the ground [33]. In addition, due to continuous and rapid urbanization and industrialization, there is a tremendous growth in man made structures towards the sky like high-rise buildings, bridges, towers and elevated highways where mobile wireless devices are being widely used. The current 2D networks established on many of those high-rise structures are based on floors of individual buildings where level of interference is high. In this case it is an apparent fact that, there is no well structured cellular-network planning approach for them while considering the elevation as an element of cellular network planning.

- **Scarce radio resources:** With the increase of device density and service diversification there always is a aggressively growing demand high data rates [27]. In order to successfully face that demand successfully, designers have been compelled to consider high frequency bands for the radio links of the wireless communication systems [34]. With this frequency band shift, there is a considerable decrease in feasible transmission distance leading to reduction in size of the cells in cellular wireless networks creating dense SCs. In this dense SC environment with extremely data hungry devices, it is very clear that all the radio resources including spectrum become well demanded scarce resources. Any error or inefficiency in radio resource management may lead to non-negligible performance degradation not only in own network but also in neighbor and collaborating networks. Since coexistence of networks is pivotal factor, it is important to consider accurate and precise radio resource management and utilization strategies for dedicated,

shared and common radio resources for both upcoming 3D and conventional 2D networks.

- **Requirements of devices and their applications at elevated locations:** There is an exponentially growing demand on wireless traffic from the devices that are operated from non-ground level positions. They are are possessing numerous service requirements and traffic types based on their elevation. Control signal to some of the drones and emergency call originated from a low flying balloon may be critical be prioritized to avoid possible accident and crashes. Currently, these service requirements and traffic types associated with the elevation are not considered in wireless service provisioning or radio resource management.

- **Future HetNet environments:** It is very important that all the wireless communication systems to be compatible with the future HetNet environment. Future wireless communication environment is going to be equipped with ultra-reliable, dense, low latent, fast, situation aware, self configurable, adaptive, intelligent and proactive networks and devices operated in the 3D space. In addition, it is expected to have a large number of machine type devices supporting resource hungry vertical applications. However, many of the techniques used in current 2D networks related to network expansion planning like frequency planning and coverage planning are not going to be compatible with the 3D networks. However, negligence of the third spacial dimension and continuation of network expansion leads to inappropriate use data related to radio resources in many of the techniques and algorithms related to operations associated with interference and radio resource management leading to degradation in performance. In addition, it is necessity to consider the vertical spatial dimension for in several emerging sport technologies and their applications related to cellular communication. Assistance received from drone technologies in expansion of wireless cellular networks is an example for that where drone BSs are suggested for cellular network coverage expansion for some applications under certain scenarios [35–38].

1.4   Goals and Objectives

The overall goal of this thesis is to improve the operational effectiveness of 3D wireless HetNets through timely observing the communication environment/surrounding and application related requirements against opportunistic utilization of available resources through system adaptation and network coordination. While achieving this main objective a set of other aspects are also considered where they are converted to problems and challenges during the study. These aspects include:

- To support sporadic (or random), dynamic and efficient use of radio resources based on their availability while facilitating high data rates and traffic from machine type devices including traffic from Internet of Things (IoT) devices those are with random radio resource demand patterns.

- To ameliorate the adverse effects of cell densification. With reduced cell sizes, large number of connections and short wavelengths, radio signals will be congested in time, frequency, power and space domains where they could be easily affected by several physical objects, device dependent errors, inaccurate estimation of radio information and inaccurate utilization radio resources.

- To reduce the adverse impact due to uncoordinated use of radio resources in licensed band (LB) and UB network operations. Due to lack of coordination and collaboration among devices and their serving networks, radio resources are very inefficiently utilized where the utilization efficiency is to be increased through device network coordination through collaborative processes.

- To facilitate network operation under dynamic network, device distribution and environmental conditions through real-time, proactive, less complex and low power consuming algorithms and techniques.

For the convenience of achieving this overall objective, the study is carried out under three different topics containing several objectives related to the overall goal or the main objective.

- Crowdsensing-assisted path loss estimation and management of dynamic coverage in 3D wireless networks with dense SCs.

- Device and network coordination for opportunistic utilization of radio resources in 3D networks.

- Learning based neighboring station coverage identification, dynamic spectrum utilization and resource allocation for 3D cells in NR-Unlicensed (NR-U) networks.

1.5 Technical Contributions of the Thesis

In solving the general problems associated with platform migration from 2D networks to 3D networks, several technical contributions are achieved with this study. In addition, a number of technical challenges are also addressed with these contributions, problem formulation and the solutions provided for them. However, the main value of the contributions is due to prominence of the solutions and necessity of them as enabling technologies for rapidly evolving 3D cellular networks in fulfilling future communication needs in a cost effective and efficient manner. Furthermore, due to applicability of many of the solutions, they are capable of generating a considerable impact in terms of performance not only for the upcoming cellular networks but also for the existing wireless networks as well. Then, the main contributions of this study are summarized as:

- To solve the problem of estimate location-specific path loss parameters and then receive signal power or coverage of a 3D SCs, three simple real-time mechanisms based on Linear Algebra (LA) and machine learning (ML) principles are presented. Subsequently, radio maps are also constructed. To address the challenges of managing radio data from 3D cells on real-time basis, capture the dynamism with devices and the environment, and to eliminate inaccuracies associated with a reading taken by a single device, an algorithm based on crowdsensing technique is discussed leading to have dynamic radio maps for the SCs. To overcome the challenges of avoiding device dependent errors and noise, a

simple signal preprocessing stage is employed. This solution can be implemented at all the SCs serving to device clusters.

- To solve the problem of estimation of location-specific receive signal or interference power values of a NR-U neighbor 3D SC a deep regression neural network (DRNN) based model is presented. With this solution challenges of estimation of location-specific path loss parameters and nullifying of influences caused due to results obtained from the unevenly distributed device locations in 3D space are mitigated. To overcome the challenge of increasing the resolution or the granularity of the readings and then the accuracy of the estimations, the SC is divided into smaller cubic volumes and each volume is assigned with a separate DRNN. This solution can be implemented at the SC BSs or at the cloud.

- To reduce the time taken for the process of up-link (UL) random access channel (RACH) access and to increase the utilization efficiency of opportunistic 3D radio resources on LB and UB, Q-learning (QL) based device and network coordination assisted algorithm is presented while coordinating the networks operated on both bands. To address the challenges of selection of the best devices to grant channel access, utilization of location-specific and other related information to get priority in communication, and to eliminate performance degradation and failures in meeting QoS aspects, an device network coordination assisted scheduling, transmit power control and prioritized access granting scheme is also introduced considering data types and the elevation of the devices in 3D space.

- To solve the problem of managing the coverage at the cluster borders in achieving better connectivity, two algorithms are presented based on inverse distance weighting (IDW) and Nelder-Mead Simplex (NMS) principles. With them, propagation parameters are extrapolated for the extended distances and 3D communication distances are extended while constructing radio environment maps (REMs). Other than the challenges related to

data collection, additional challenge of interference to the other devices is addressed with directional beams using precoded massive multiple-input multiple-output (mMIMO) antennas.

- In order to enhance performance of the devices through efficient radio resource utilization in UB, algorithms are introduced based on regret based learning (RBL) and double Q-learning (DQL) techniques to efficiently manage the opportunistically available radio resource in the UB. With these solutions, challenges of limited time availability for training, devices becoming excessively competitive in utilizing radio resources, facing the dynamic environment, unavailability of data for training are also mitigated while enabling real-time training and operations.

- In order to facilitate 3D cell deployment scenarios, smooth flow of data and information, real-time operations and convenient implementation of solutions network architectures and functional protocols for cellular networks with 3D SCs are also discussed appropriately. They are made compatible for the operations of both future and current networks operated in LB and UB.

In this study, all the operations related to "efficient discovery and utilization of radio information" is supported by well established and state of the art techniques, algorithms, procedures and protocols used for radio resource information gathering, processing and utilization.

1.6 Thesis Outline

The organization of the chapters of this thesis is summarized as follows and the organization of the thesis is presented in Fig. 1.5:

Research background for the subtopics is briefly presented in Chapter 2 aligning with the emerging and pioneering technologies related to 6G and beyond communication systems. Because these technologies are identified as the enabling technologies for 3D HetNets. In particular, the technologies related to coverage planning, spectrum management and some of the

ML technologies used in 3D space are discussed. A high attention is paid for some of the modern tools suitable for the operations of the 3D HetNets like reinforcement learning (RL) and artificial neural network (ANN).

In Chapter 3, it is focused on establishment of a framework to estimate location-specific path loss parameters and to manage dynamic coverage of 3D wireless networks with dense SCs. In other words, schemes for location-specific path loss estimation are developed for efficient radio resource management based on the principle of crowdsensing together with LA and ML techniques. At the same time, corresponding procedure for capturing dynamic coverage of a SC BS serving to an arbitrary cluster is also discussed based on its 3D propagation characteristics. Within the second stage of the study, the estimated values for the parameters are extrapolated to slightly extended 3D communication distances from the cluster boundary improving the cluster edge radio coverage in facilitating a seamless connectivity while meeting the QoS aspects of the devices.

In Chapter 4, attention is paid to develop a mechanism to achieve device and network coordination in order to opportunistically utilize radio resources in 3D networks considering both LB and UB. In this work, problem of performance degradation due to negligence of operational conditions of devices, their data types, availability of spectrum for communication and delays in radio resource allocation in a 3D network is addressed. In the case of LB, a solution is developed based on QL and S-ALOHA principles with the help of device cooperation and network coordination. In the case of UB, a algorithm is developed based on RBL principles to utilize the already allocated and opportunistically available radio resources in an optimal manner. Moreover, functional protocols for both device and BS are also discussed while easing the implementation of the solutions.

In Chapter 5, it is concentrated to develop a learning based mechanisms to identify neighbor station coverage, dynamic spectrum utilization and resource allocation for 3D SCs in NR-U networks. Within the initial part of the study, problem of neighbor BS coverage identification is addressed. As a solution, a DRNN based algorithm is suggested to predict receive signal

or interference power from a neighbor BS at a given location of a 3D SC. At the second part of the study, problem of efficient radio resources allocation for dynamic spectrum utilization is addressed leading to have an algorithm based on DQL technique with device collaboration. However, this solution is developed using the outcomes of the first part of the study. Moreover, overall network architecture is also discussed facilitating deployment of the solutions for the corresponding scenarios.

Finally, in Chapter 6, the thesis contributions are briefed while recognizing some of the apparent future research directions.

Efficient Discovery and Utilization of Radio Information in Ultra-Dense Heterogeneous 3D Wireless Networks

Research Goal: To improve 3D wireless HetNets by observing the environment and requirements of the applications against opportunistic utilization of resources with system adaptation.

Motivations: 1. Increase use of sky 2. Scarcity in radio resources 3. Requirements of the devices and applications from elevated positions, 4. Future HetNet environment.

Chapter 3 (Topic 1)	**Chapter 4 (Topic 2)**	**Chapter 5 (Topic 3)**

Objectives

1. To estimate location-specific path loss parameters in 4G LTE and 5G NR 3D SCs.	**1.** To better allocate opportunistic LB and UB radio resources considering multiple factors.	**1.** To identify coverage and predict radio information of a neighbor 3D SC in real-time.
2. To extend 3D communication distance.	**2.** To optimally utilize radio resources in UB of 3D SCs.	**2.** To allocate and utilize radio resources in 3D SCs.

100% LB → **50% LB, 50% UB** → **100% UB**

Solutions

Phase 1: LA, LS and GD based methods to estimate PL parameters.	**Phase 1:** Device and network coordinated weighting based prioritized UL access scheme.	**Phase 1:** DRNN based approach to discover and predict radio information.
Phase 2: IDW and NMS based methods to extrapolate 3D coverage.	**Phase 2:** Device and network coordination aided QL for RACH access in LB and UB.	**Phase 2:** Collaborative learning algorithm based on DQL to utilize UB radio resources.

Utilize radio information   Utilize channel access   An alternative approach to predict radio information

Contributions

1. A crowdsensing algorithm to manage data. **Challenges:** ①, ②, ③	**1.** An algorithm to support access granting schemes. **Challenges:** ⑥, ⑦	**1.** An algorithm to support DRNN based solution. **Challenges:** ②, ⑩, ⑪, ⑬
2. An algorithm to facilitate PL estimation techniques. **Challenges:** ⑧	**2.** Device network coordination assisted ML algorithm. **Challenges:** ⑨, ⑩, ⑪, ⑫	**2.** An algorithm to support DQL based solution. **Challenges:** ⑪, ⑫, ⑭, ⑮
3. An algorithm to facilitate 3D coverage extension. **Challenges:** ⑤	**3.** A RL algorithm to efficient radio resource utilization. **Challenges:** ①, ⑨	**3.** An algorithm to train and utilize DRNN based solution. **Challenges:** ①, ⑯
4. Design of a compatible network architecture. **Challenges:** ①, ④, ⑧	**4.** Design of functional protocols for UE and BSs. **Challenges:** ④, ⑧	**4.** Design of a compatible network architecture. **Challenges:** ①, ④, ⑧

Challenges: ① Facing the dynamism ② Restrictions on measurement devices ③ Device dependent errors ④ Scarcity of network resource ⑤ Knowledge on path loss parameters ⑥ Maximization of access probability ⑦ Minimization of waiting time ⑧ Data and information exchange ⑨ Making devices proactive ⑩ Situation awareness ⑪ Fast adaptation to the environment ⑫ Coordinated use of radio resources ⑬ Knowledge on propagation model ⑭ Collaborative learning ⑮ Neighbor SC interference management ⑯ Increasing the granularity of the solution

Figure 1.5: Organization of the thesis.

Chapter 2

Enabling Technologies for 3D HetNets

Since the recent past, societies are becoming more and more data-centric, data-dependent and automated while productivity is driven through the automation of industrial processes and individual activities [39]. With the launch of future communication systems, full realization of the Internet of Everything (IoE) paradigm is expected while connecting people, computing resources, vehicles, devices, wearables, sensors and robotic agents. That means the initialization of a fully connected, intelligent digital world [6]. This highly digitized and intelligent information society is going to be a globally or universally data driven pool of information which is enabled by a near-instant and unlimited full wireless connectivity. Autonomous systems are occupying the ground, oceans and sky more rapidly than ever before while assisting numerous applications where upcoming 3D HetNets are only a part of that. In this case, it is inevitable that HetNets in 6G and beyond generations are going to be immensely complex communication networks [40] requiring significant support from autonomous, intelligent, fast learning and fast processing technologies. Moreover, high performing communication technologies, underlying network architectures and their deployment models are also needed to power these upcoming generations of communication networks [39] where the 3D HetNet model is one of the strongest candidates for that. In this environment, future devices will no longer be conventional smart devices only. They would be resource donors for the collaborative operations in the

future networks in terms of many functionalities like processing, caching and relaying [6, 41]. Then, the fundamental technology will no longer be limited to software-defined radio and the network architecture will be an upgrade of CloudRANs [6, 41].

2.1 Pioneering Technologies for 6G and Beyond Communication Systems

6G and beyond wireless communication systems are to be extremely carefully and rapidly shaped up to meet the societal visions for future information, communication and computing sectors facilitated by near-instant and unlimited full wireless connectivity [6]. Because, 6G and beyond systems are the key enabler for the highly digitized, intelligence inspired, globally data driven and rapidly evolving information society by 2030 and beyond. These systems are expected to connect everything, provide full dimensional wireless coverage, and integrate all functions, including sensing, communication, computing, storage, control, positioning, radar, navigation and imaging while supporting full-vertical applications and being operated autonomously with intelligence and consciousness [6].

To make this vision a reality, it is essential to design the 6G HetNets as large dimensional, autonomous and intelligent networks covering communication in the space, sky, terrestrial and sea domains seamlessly [6, 41]. Then, the 6G mobile network architecture is to be a genuinely intelligent system architecture powered by artificial intelligence (AI) in managing and connecting space–air–ground–underwater sub-networks while providing a near-instant and unlimited superconnectivity [39]. This architecture has to maintain the heterogeneity in all kinds of entities like device interfaces, applications, services, data types and other networks. Furthermore, it has to support all the upcoming functions like virtualization of network equipment while complying with the deployment models through distributed and centralized learning, processing and computing functions through coordinated, cooperative and situation aware operations. Some of those operations will be performed at the radio AI engines developed with electronic

neural networks or similar modern integrated neural processing units [6]. In this case, a pivotal role is expected to be played by the 3D HetNets [39] in the provisioning of "full coverage" for all the communicating entities while empowering a systematic and revolutionary transformation against conventional 2D networks.

The revolution or the transformation towards the 6G concept of full coverage networks is going to be realized and pioneered with several key technologies like THz communications, supermassive multiple-input multiple-output (SM-MIMO) antenna systems, large intelligent surfaces (LISs), holographic beamforming (HBF), orbital angular momentum (OAM), laser and visible-light communications, quantum communications and computing, molecular communications and IoE [5, 6, 42, 43]. In addition, future wireless communication systems are going to be further strengthened with full-duplex channels, device-to-device communication techniques, AI/ML and 3D networking tools, including 3D propagation models [5]. However, background technologies related to this study are limited to several areas like signal processing, AI/ML and 3D propagation models which are among the key empowering technologies of the future 3D HetNets. Based on this information, the relationship between radio resources, the main physical layer enabling technologies of future 3D HetNet (THz communications, SM-MIMO, LISs, HBF, OAM, AI/ML and 3D networking tools) and the service classes (uHDD, uMUB, uHSLLC, LDHMC and HCS) is explained in Fig. 2.1.

2.2 Recent Developments on 3D HetNets

Recent developments on 3D HetNets are in several directions including cellular coverage planning, frequency planning, energy coverage planning and beam steering in the 3D space. As it was done in 2D networks, planning processes are initiated with basic theoretical cell shapes. Even though the main objectives of certain developments are not directly connected to cellular wireless communication concepts, they can be effectively used to improve future wireless cellular networks.
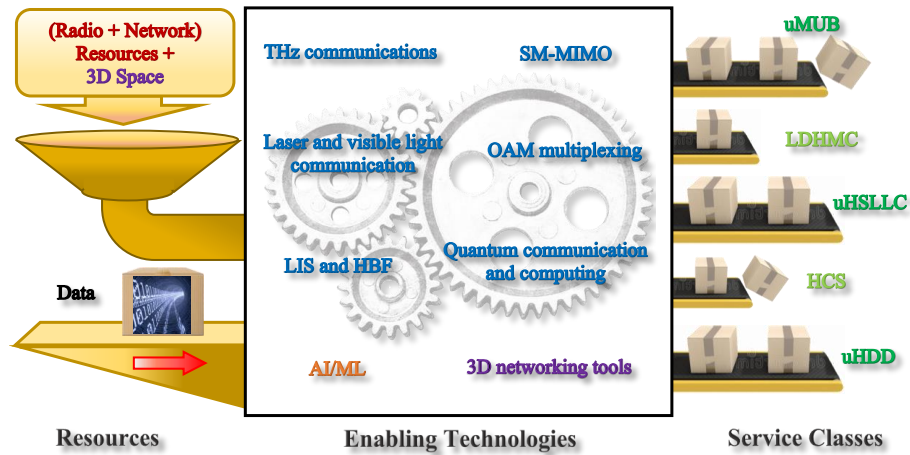
Figure 2.1: Relationship between radio resources, enabling technologies and services classes.

2.2.1   Coverage Planning in 3D Space

The standard concept of planar cellular networks is extended into space with 3D SCs to meet the growing number of communication services [44]. At the same time, the importance of using SCs designed based on hexagonal tessellations is also highlighted while suggesting to place antennas in 3D space of buildings. Coverage and connectivity issues for 3D networks are are also among the burning problems of 3D HetNets [45]. Solutions for some of those problems are developed while assuming random and uncontrollable node locations where the goal is to find a node placement strategy with 100% sensing coverage of a 3D space [45]. In this work, a 3D network volume is divided into virtual regions or cells and used for the analysis where truncated octahedral tessellation of 3D volumes is used for that. Although some of the 3D underwater networks are used in that study, much of the outcomes can be prominently applicable to other 3D networks designed for airborne applications like space exploration and storm tracking.

A mechanism to place a drone BS in a 3D space is also an important component [46] in maximizing the number of covered users with different QoS requirements. The placement problem for a drone BS can be formulated as a multiple circle placement problem. For the same problem, a low-complexity algorithm, namely, the maximal weighted area algorithm can

also be employed [46]. 3D cells powered by drone BSs and cellular-connected drone users are introduced leveraging the concept of 3D cellular networks [10]. At the same time, a framework for network coverage planning done with drone BSs and latency-minimal cell association for drone user equipment (UE) is also discussed. Subsequently, based on the spatial distribution of drone UE and the locations of drone BSs, the latency-minimal 3D cell association for drone UE is also derived [10].

In empowering 3D HetNets, it's worth jointly considering down-link (DL) simultaneous wireless information and power transfer together with UL information transmission for UAV-assisted millimeter wave (mmWave) cellular networks [47]. In this kind of scenario, UE locations can be modeled using Poisson cluster processes while UAV BSs are positioned in 3D space in the sky [47]. Distinguishing features of mmWave communications like different path loss models for line-of-sight (LOS), non-line-of-sight (NLOS) links and directional transmissions are considered. In contrast to conventional approaches, successful transmission probability to jointly present the energy and SINR coverage is derived. The optimal placement of tethered UAVs to minimize the average path loss between the UAVs and a receiver located on the ground is discussed by Kishk *et al.* [48]. In the same study, upper and lower bounds for the optimal values of the tether length and inclination angle are also derived. At the same time, the probability distribution of the minimum inclination angle of the tether length is also derived.

In another study, concepts in stochastic geometry are applied to investigate the DL performance of a vertical heterogeneous network comprising aerial and terrestrial BSs [49]. In this study, BSs are deployed at a particular altitude while the terrestrial BSs are deployed on the ground. An air-to-ground channel model that incorporates both LOS and NLOS transmissions is used for the radio links. Coverage performance of a reference UE in a finite network of multiple 3D drones is analyzed by Shen *et al.* [50] while presenting a mixed mobility model to support the movement process of a drone in a 3D cylindrical region. By using the same mobility model and the network, the coverage probability of a reference UE under uniform and closest drone associations are also analyzed in one snapshot.

2.2.2 Spectrum Usage in 3D Space

A frequency planning mechanism with an analytical expression for the feasible integer frequency reuse factors is presented by Mozaffari *et al.* [10] considering the cells with truncated octahedron shapes. In the same way, as in 2D cellular networks, the frequency reuse factor is equal to the number of non-interfering cells within a cluster of cells. In this work, two sizes of truncated octahedron cells in the same network are considered and the locations of drone BSs are also determined. In parallel, frequency reuse mechanisms and channel allocation schemes are also investigated [44] to facilitate efficient network operations.

A spectrum sharing mechanism for UAV SC networks modeled by the 3D Poisson point process is suggested by Zhang *et al.* [51]. In this study, underlay spectrum sharing between the UAV SCs in the 3D network and traditional 2D cellular networks is modeled with 2D Poisson point processes. To further protect the cellular network in the spectrum underlay, the effect of primary exclusive regions in a 3D space is investigated. In contrast to circular regions in traditional cellular spectrum sharing in the 2D space, the shape of the 3D region is found as a half-spherical segment, depending on the radius of the region and the height limit of the UAV SCs. The radii of primary exclusive regions are restricted for small UAV SC constraints and limited UAV SC heights.

The importance of a frequency assignment method based on cell geometrical characteristics is identified by Ellatifi *et al.* [52] while accounting for co-channel and adjacent channel interference. For this, spatial tiling methods are used. Reuse distance and frequency group numbers are obtained with only co-channel interference constraints. In conclusion, the two most suitable 3D cells for 3D networks are selected.

A 3D model is proposed by Chen *et al.* [53] for a K-tier HetNet with multi-antenna BSs, where different tiers share the same frequency band with different BS heights, BS densities, the number of antennas per BS, BS transmit power values, association biases and path loss exponents. In the same study, analytical expressions are derived for the per-tier association

probability under both the strongest received signal and the closest BS cell-association strategies.

2.2.3 ML Technologies for 3D HetNets

ML is a branch of AI and also a data driven concept. ML algorithms are capable of learning and improving themselves using data without being explicitly programmed or any third party intervention [54]. The goal of ML is to understand the structure and patterns of data and fit that data into models that can be understood and utilized. There are many advantages associated with this concept over other techniques including compatibility with autonomous operations, capability to identify patterns, ability to continuous improvement, capacity to handle data efficiently and competency to handle a wide range of applications. Since ML techniques are mostly data driven methods, they are good for when the model is unknown, difficult to be derived, difficult to be adopted or suspicious. Due to these reasons and the attractive performance of ML algorithms even under complex conditions and constraints, many of the ML techniques belonging to all the major branches, including supervised learning, unsupervised learning, semi-supervised learning and RL have become popular in the sphere of wireless communication, even empowering many of the operations in 3D HetNet. In another study [10], drone BSs use ML tools to estimate the spatial probability distribution of drone UE using available prior information on the drone UE locations in the 3D space. Meanwhile, the problem of joint 3D deployment and power allocation for maximizing the system throughput in a UAV BS system is addressed by Zhang *et al.* [55]. Out of many data processing techniques and algorithms, RL and ANN based techniques are widely used in that study.

Reinforcement Learning

RL is an area of ML concerned with how intelligent agents ought to take actions in an environment in order to maximize the notion of cumulative reward [56]. For the algorithms developed based on these principles, no prior data is needed for training while making them unbiased on

training data. In addition, these computationally simple algorithms can be trained and operated on a real-time basis in a goal oriented manner under complex environmental conditions without any knowledge on the model or the exact input-output relationship. In conventional systems and algorithms, knowledge on the model is an essential feature. Furthermore, RL based algorithms are with a high degree of adaptability as they are continuously trained during the operation with the fast converging property. These schemes are with greater design flexibility supporting cooperative, coordinated or independent systems under situation and environment aware or unaware conditions. All of these advantages and their performance have made them a very passionate set of tools for the wireless communication system designers.

There are two main types of RL techniques, namely positive RL which tries to maximize performance and negative positive RL which attempts to increase behavior [56]. QL [57], RBL [58], multi-armed bandit [59], SARSA [60] and AC3 [61] are some of the well-known RL techniques used to support wireless communication systems. A QL based approach can also be used to solve the problem of dynamic channel assignment [57] while a RBL principle assisted algorithm can be developed for DL inter-cell interference coordination in a HetNet deployment with macro and pico cells [58].

Artificial Neural Networks

ANNs are biologically inspired computational networks possessing the advantages of ML [54]. They are with the ability to learn by themselves and produce outputs that are not limited to the inputs provided to them where the inputs are stored in their own networks instead of a database, avoiding any impact from a loss of data. In a case of missing information, an ANN can produce the output. On the other hand, they are capable of outperforming many of the conventional signal processing techniques particularly complicated problems under complex conditions and tight constraints. Upon training, deep learning techniques are also with fast prediction properties while giving sub-optimal solutions with acceptable accuracy. Apart from that, ANN and other supervised learning methods are outperformed by deep learning techniques provided that

sufficient amounts of data, training time and processing power are available. In the estimation of path loss parameters and receive signal strength values, it is shown that ANN based algorithms can outperform conventional signal processing techniques [62]. A limited number of parameters can be handled by almost all the conventional signal processing based path loss model derivation mechanisms.

Feedforward, regulatory feedback, radial basis function, recurrent, modular and physical are the most prominent types of ANNs. ANNs with a higher number of hidden layers, known as deep-ANNs are capable of performing better than single layer ANNs [63]. Due to their outstanding capacity to replace conventional regression techniques, much attention is drawn to them [64, 65]. In addition, DRNN techniques are highly compatible with the architectures of upcoming neural processing units as well [66]. In the case of path loss estimation, the application of deep neural network (DNN) techniques against conventional signal processing techniques is shown in Fig. 2.2. Further knowledge is gathered through a comparison between the results of traditional channel models and the results obtained with a DRNN aided simple path loss model developed by analyzing satellite images [65]. A DRNN-assisted adaptive multi-attribute fusion method [64] can be used to re-identification of persons as regression analysis.

Currently, research and development activities are being carried out to apply different categories of AI and ML schemes, including supervised, semi-supervised, unsupervised and RL for almost all the operations of the wireless communication systems [67, 68]. For the simplicity, some of the main ML techniques used in the cloud, BSs and the devices related to the physical, medium access control and network layers are presented in Fig. 2.3. A list of applications and a description of the possible modes of operation are also given in the same figure. In this figure, the term management refers to all the relevant tasks and operations like information gathering, optimization, allocation and scheduling in the cellular mobile communication systems. In upcoming wireless communication systems, it is planned to administer these three layers through a single AI based architecture while facilitating both distributed and centralized

Signal processing and curve fitting techniques

1. Model approximation/selection
2. Path loss parameter estimation (i.e, α, β)

Observations (Data gathering)

Radio information prediction

DNN techniques
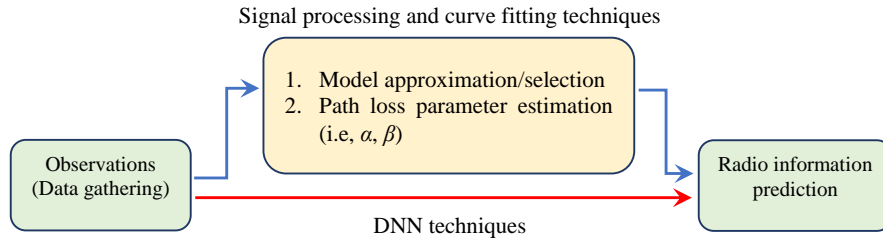
Figure 2.2: Signal processing vs DNN for path loss prediction.

functions related to communication, computing and sensing operations. These operations may be carried out in an autonomous, independent, collaborative and/or cooperative manner with or without coordination. Moreover, these AI/ML infrastructure facilities and algorithms are going to be scalable and decomposable platforms supporting the human in the loop feature and ubiquitous AI services for on-line (real-time) and off-line operations [69]. Generally, future HetNets are expected to be featured with many self-supportive properties enabling them to be self-configurable, self-learning, self-optimization, self-diagnostic and self-healing, networks and entities.

2.2.4   ML Based Receive Signal Estimation Methods in 3D Environments

It's a well-known fact that neural network (NN) and DNN based solutions are widely used to solve different problems in wireless communication and related areas. However, in this study, high attention is paid to explore the work done to replace the conventional signal processing based approaches to estimate the path loss characteristics. A channel model obtained using deep learning techniques by utilizing satellite images and a simple path loss model is presented by Thrane *et al.* [70]. For this model, experimental measurements are gathered and composed for the training and test sets. Dai *et al.* [71] have carried out a study on a ML based received signal strength predictor that can be trained and optimized for the coverage performance of BS deployments via multi-objective heuristic methods. Many practical features that are capable of influencing the phenomenon of signal propagation like geographical characteristics and operating parameters of BSs are fed into ML models to predict received signal strength values in a

Location	AI/ML Algorithm	Application	Description
Cloud	All the AI/ML algorithms ①-⑭ can be implemented. Performance of the algorithms and the system is prioritized over resource consumption and complexity when selection of the best set of algorithms.	Applications including ①, ④, ⑨-⑫, ⑭-⑯ are executed (not limited to).	Supports some modes of operations including ①-③, ⑤-⑩.
BS	All the AI/ML algorithms ①-⑭ can be implemented. There may be occasions where resources can be a limiting factor where it can be considered when selection of the most suitable set of algorithms.	Applications including ①-⑬, ⑮ and ⑯ are run. There may be limitations.	Supports some modes of operations including ①-③, ⑤-⑨.
Device	A limited number of AI/ML algorithms can be implemented. E.g., variants in ①, ⑨, ⑦ and ⑭. Mostly limited by resources and complexity. Prefer to accept trained NN or algorithms.	Applications including ②- ⑧, ⑪, ⑬, ⑮, ⑯. Limited by resources.	Supports certain modes of operations including ①-⑨.

AI/ML Algorithm: (examples) ① Reinforcement learning (RL, QL, DQL, DQL, Deep-QL, multi-armed bandit, Double deep QL, C51, QR-DQN, DDPG) ② ANN (CNN, generative adversarial networks, DRNN, graph NN, recursive NN, recurrent NN, self-organizing maps, deep generative NN, feed-forward NN, radial basis function network) ③ Federated learning ④ Decision tree ⑤ Naive Bayesian ⑥ *K*-nearest neighbors ⑦ Logistic regression ⑧ *K*-means/*C*-means ⑨ Autoencoder ⑩ ISOMAP ⑪ Support/relevance vector machine ⑫ Deep belief network ⑬ Boltzmann machine ⑭ Game based learning (mean-field game, Markov game, stochastic game)

Applications: ① Propagation models and path loss prediction ② Channel estimation, prediction and equalization ③ Radio resource management ④ Latency management ⑤ Access management ⑥ Symbol detection ⑦ Modulation and coding ⑧ Antenna related operations ⑨ User traffic management ⑩ Frequency band management ⑪ Data management and caching ⑫ Mobility and handover management ⑬ Security management ⑭ Cell management ⑮ Fault identification and recovery ⑯ QoS (including QoE and QoPE) management

Description: ① Centralized processing ② Collaborative processing ③ Coordinated operations ④ Prefer to offload operations ⑤ Distributed processing ⑥ Scalable and decomposable ⑦ Self properties (configurable, learning, optimization, diagnostic and healing) for the architecture and algorithms ⑧ On-line (real-time) operations ⑨ Off-line operations ⑩ Accept operations

Figure 2.3: Main ML techniques used in cloud, BSs and the devices related to physical, medium access control and network layers.

rasterized area. Furthermore, ANN models can be used to predict the macrocell path losses as well [62]. In that study, measurement data obtained using an IS-95 pilot signal from a commercial code-division multiple-access mobile network operated in rural Australia is used to train and evaluate the models.

In a deep convolution neural network (DCNN) based approach to predict the path loss distributions using 2D satellite images, the inference is calculated in real-time for different

communication frequencies and transmitter heights [72]. Instead of using a 3D model, area images are used as the inputs to calculate the interference. In a separate study, a multilayer perceptron NN is employed to accurately predict the path losses in a 3D environment [73]. In that study, several environmental features are used to describe the propagation environment instead of complex 3D environment modeling mechanisms. Information on BSs and the receivers including their 3D locations, transmission frequency, transmit power values, antenna information, feeder losses and receive power values are among them. At the same time, a DCNN based solution to estimate channel parameters (specifically, path loss exponent and standard deviation of shadowing) in the 3D space using 2D satellite images without 3D model generation is suggested by Ates *et al.* [74].

A DCNN based autoencoder is used as the urban canyon 3D path loss prediction model for the communication systems operated in 28 GHz frequency band in Manhattan. In that study, street clutters are modeled via a LiDAR point cloud dataset and buildings are modeled with a mesh-grid building dataset [75]. In contrast to 3D ray tracing approaches with geometrical information to model physical radio propagation phenomena, in a study conducted by Qiu *et al.* [76], a two sub-NNs assisted DCNN based approach is used to predict the outdoor path losses in an urban 5G scenario operated in 30 GHz band. An ANN based model is developed by Egi *et al.* [77] to account for the effect of tree canopies which can be applicable to any other environments as well. In this solution, a 2D image color classification mechanism is used to extract the features from a 3D point cloud and an ANN based algorithm is employed to predict the path losses. Furthermore, in 3D channel models, AI and ML are recommended to be used for multipath component clustering, scenario classification and channel prediction by using clustering, classification, and regression algorithms like ANN, convolutional neural network (CNN), and generative adversarial networks, respectively [78].

2.2.5 Signal Processing Based Receive Signal Estimation Methods in 3D Environments

Development of path loss or propagation models is the main avenue associated with the receive signal estimation techniques for those who are assisted with signal processing based approaches. Literature on the development of propagation models for 3D environments is available in numerous directions while paying attention to numerous use cases or deployment scenarios and frequency bands with their propagation characteristics of interest. In supporting this approach, a 3D statistical channel impulse response model is discussed for urban LOS and NLOS channels from 28 GHz and 73 GHz ultra-wideband propagation measurements in New York City [79]. For this, a mathematical framework is also used [79]. The derived model of that study is recommended for 5G wireless systems that are operated in both ultrahigh frequency/microwave and mmWave spectrum bands with the expectation of increasing the channel capacities. In another parallel study, an empirical indoor 3D spatial statistical channel model for mmWave and sub-THz frequencies is developed based on the radio propagation measurements done on 28 GHz and 140 GHz bands on an entire floor of an office building [21]. A 3D propagation model is discussed to predict the radio losses in a corridor environment [80] where a ray-tracing technique is used and combined with a ray-fixed coordinate system to simplify the computations of transmission, reflection, and diffraction coefficients. At the same time, a 3D propagation model for path loss prediction in a typical urban site, with the use of geometrical optics and uniform theory of diffraction is presented by Kanatas *et al.* [81] while paying attention to numerous rays that undergo reflections and diffraction. By considering the factors of 3D scattering space, 3D trajectory, and 3D antenna arrays, a non-stationary ray-based channel model for UAV-to-vehicle mmWave communications is proposed [82]. In that study, computation and generation methods for channel parameters, including inter-path and intra-path are developed and illustrated in detail.

An air-to-ground two-piece path loss model for mmWave channels with both LOS and

NLOS is presented by Alkama *et al.* [83]. This model is used with 3D directional beamforming to derive an analytical framework to study coverage probability and capacity using stochastic geometry for coverage done with an UAV. Meanwhile, a simple theoretical 3D propagation model is proposed for UAVs equipped with intelligent reflecting surfaces [84] with the expectation of using them in massive, ultra-reliable and low-latent communication systems. An analytical 3D channel model is presented for reconfigurable intelligent surface-assisted multiple-input multiple-output (MIMO) communication systems based on 3D cylindrical shapes containing LOS for single and double-bounced modes at the surface for the reflected and near scattered radio waves [85]. Propagation conditions pertaining to reception and transmission at the mobile terminals measured using a wideband channel sounder and a dual-polarized spherical antenna array are presented by Kalliola *et al.* [86]. Subsequently, results are refined and extended to full, double-directional 3D channels.

2.3   Reasons and Benefits of Efficient Information Management in Wireless Networks

Some of the strategies used for information management in this study and the benefits associated with them are discussed as follows.

- **Intermediate data processing stage:** For the system models in this study, an intermediate post-acquisition data processing stage or data preprocessing stage is introduced to identify and correct the data or the imperfect information [87]. Because, utilization of perfect or near-perfect information is a critical factor for the performances of many of the technologies that are going to be used in near future wireless communication systems under scarce and competitive radio resource conditions [88–91]. As an example, improved performance for signal detection and resource allocation can be achieved with near-perfect information.

- **Cloud for information sharing:** Information sharing and global availability are facilitated through a cloud while leading to the advantages associated with deterministic network environments [92]. In addition, after the wireless network is being operated for a reasonable time duration, a reduction in overall operational cost for the network is expected to be achieved due to reuse and sharing of relevant information through the cloud [93]. Moreover, the reduction of time for network operations is a key element in future wireless networks which are being strongly supported with cloud-based information sharing [94]. In this study, the concept of radio map, a cloud-based concept, is expected to be used to achieve a considerable time reduction in network operations.

- **Simple and backward compatible network architectures:** 3D wireless HetNet architectures used for the implementations are suggested to be simple and compatible with the existing wireless network architectures. Then, most of the processing functionalities can be replaced with information exchange operations paving the way to reduce the processing requirements at the node level.

- **Real-time data processing:** Real-time information is very essential for many of the physical layer technologies like SM-MIMO [88], beamforming [89], device-to-device (D2D) communication [90] and interference management [91]. In addition, these technologies are very sensitive to the accuracy of certain parameter values like location information, radio resource information (RRI) and overall latency [95]. The solutions are expected to be enablers for them through real-time data processing and information provisioning while correcting imperfections [96].

- **Energy saving through information sharing:** Energy saving and energy utilization efficiency can be increased through information sharing leading to much greener and cost-effective [97] networks.

2.4   Assumptions

This study is carried out subject to several limitations and assumptions, unless specifically stated otherwise.

1. The behavior of all the channels is taken place according to the models used for them. In other words, ideal channel characteristics are assumed unless otherwise specifically mentioned.

2. Mobility related phenomena (e.g., Doppler, trajectory optimization) and handover of UE are not taken into account.

3. Perfect synchronization in terms of time and frequency is assumed.

4. DL streams are considered as the default direction of communication. Both in UL and DL, upon channel acquisition, the number of users is assumed to be constant throughout the operations with a full buffer condition. No feedback mechanisms are considered for the correction of data (i.e., at least no repeat request (RQ) or automatic repeat request (ARQ) schemes).

5. Properly planned cells in a cellular wireless network are considered where there is no interference from other BSs or the devices unless otherwise it is specifically mentioned.

6. Delays and latency associated with the network and related issues are not considered.

7. Channel state information is valid for the frequency ranges considered and perfectly known if not stated.

8. All the flying BSs and UE are capable of maintaining their operations irrespective of non-wireless communication related constraints like power requirements for flying.

2.5   Chapter Summary

Enabling technologies related to 3D HetNets, 6G and beyond communication systems are discussed. Initially, recent developments on 3D HetNets are presented. Under this, special atten-

tion is paid to the coverage planning, spectrum management and ML technologies used in 3D space and 3D HetNets. Subsequently, recent related work is briefly presented on ML and signal processing based receive signal estimation methods that can be used in 3D environments. Under the ML technologies used in 3D space, different types, their advantages and the use cases of RL and ANN technologies are discussed. In addition, the reasons and benefits of efficient information management in wireless networks are also highlighted. That is followed by a list of the main assumptions used in this study. The preliminaries presented in this chapter are used to develop efficient information management schemes for ultra-dense 3D HetNets.

Chapter 3

Crowdsensing-Assisted Path Loss Estimation and Management of Dynamic Coverage in Dense 3D SC Networks

Emerging vertical applications enabled by connected devices and smart infrastructures have created an ever-increasing demand for high data rates over 5G and beyond wireless networks. Deployment of dense SCs and mmWave communication systems have become inevitable in future wireless networks. Consequently, it is more accurate to model such networks in the 3D space due to the spatially distributed nature of the SCs, locations of the devices, radio resources and propagation environment. Accurate estimation of location-specific path loss parameters is then essential for efficient utilization of radio resources and management of dynamic coverage in 3D SC networks. In this paper, a framework for location-specific path loss estimation is developed for efficient radio resource management, based on the principle of crowdsensing together with Linear Algebra (LA) and ML techniques considering 2.5 GHz and 28 GHz bands. The corresponding procedure for capturing dynamic coverage of a SC BS serving to an arbitrary cluster is proposed and examined based on its 3D propagation characteristics. Results show that the accuracy of 3D path loss parameter estimation using gradient descent (GD)

38

techniques is superior compared to LA technique and can achieve over 98% estimation accuracy. Although numerical results are presented for a single amorphous 3D cell of a wireless network, the framework given in this paper can be extended to any arbitrary 3D wireless cellular network. The highest path loss parameter estimation accuracy is shown by GD technique which is over 98%. In the case of receive signal power calculations at slightly extended 3D communication distances from the cluster boundaries, over 74% accuracy is shown for certain scenarios when the calculations are done with the already estimated propagation parameters.

3.1 Introduction

The data traffic over wireless networks has been increasing dramatically over the past several decades and statistics show that globally this traffic increases by nearly a 1,000 times every 15 years [98]. This trend is expected to continue as a massive number of devices requiring connection to wireless networks for Internet access and also due to a variety of new services. It is estimated that the global traffic over wireless networks is likely to exceed one zettabyte/month by the year 2028, due to over 5 billion user communication devices expected to be connected to networks [98]. Furthermore, the expected number of IoT device connections using wireless networks is likely to exceed 500 billion by the year 2025 [99]. As the number of mobile devices and demand for new mobile services continue to increase, it becomes challenging to characterize the dynamic wireless signal propagation environment accurately for efficient utilization of limited radio resources and QoS provisioning [100].

A paradigm shift is expected in the design and operation of emerging wireless networks to support massive data traffic from a huge number of devices connected to them. It is, therefore, imperative to employ spectrum resources in the mmWave band for communication in 5G and beyond networks [101]. An immediate consequence of this is considerable reduction in cell size, leading to networks with dense SCs [25]. Thus, in designing such networks, it is important to consider the signal propagation environment where the networks are going to be deployed.

Specifically, the environment for 5G and beyond could comprise of high-rise structures and objects including smart homes, offices, hospitals, businesses, industries, multi-level flyovers, drones and other flying objects. The locations of devices in a SC of such an environment are best described in 3D space due to significantly reduced cell size. Further, they may be dynamic in terms of locations with diverse data and QoS requirements while interacting with machines and humans. Thus, to serve the needs in such a complex environment, a 3D model of network [102] is appropriate as opposed to existing 2D network model while utilizing the third spatial dimension for cellular coverage planning and radio resource management. Since there are no fixed boundaries or coverage areas for the cells in real life, it is beneficial to model cells in 3D SC networks to be amorphous or semi-rigid [103] while paving the way to change their sizes in overcoming problems like elimination of coverage holes, managing the number of devices served, strengthening cell or cluster boundary coverage and avoidance of undue coverage overlaps. In this study, 3D SC network or 3D network is a cellular wireless network consists of 3D SCs and a cluster is a set of collocated devices or a group of devices in the close vicinity of each other.

In-depth understanding and accurate estimation of path losses for radio channels are critical for the overall coverage planning, efficient operation and radio resource management in both conventional 2D and emerging 3D wireless networks. Furthermore, with reduced cell size, surrounding environment introduces more significant location-related impact to wireless signal propagation. As a result, location-specific path loss modeling and parameter estimation becomes essential for cell coverage management particularly for emerging 3D SCs in 5G and beyond cellular networks [104] and even for cell-free mMIMO systems [105]. Moreover, it is also important to guarantee a seamless connectivity and QoS at the borders of clusters or 3D cells. For this reason, 3D communication distance at the cluster or cell boundaries has to be adjusted based on the actual coverage of the small base station, which is often severely impacted by the surrounding environment. Due to advancement of mMIMO-assisted beamforming techniques [96,106], radio footprints can be more accurately controlled while facilitating to achieve

this objective without any significant effort. Here extension of 3D communication distance is defined as a process of limited expansion of the coverage of a SC BS at a selected direction in the 3D space to provide better support for devices at cell boundary through BS transmit power adjustments.

When the closest or most related work on 3D modeling of cellular networks is surveyed, concept of 3D cells has been used in some occasions, in particular, for finding solutions to specific problems associated with drones [36–38, 102]. For example, an octahedron cellular structure has been used to investigate coverage area with a drone in each cell acting as BS [36–38, 102]. When considering studies on estimation of propagation parameters, with the observation of differences between theoretical and measured values, importance of estimation of them through field measurements is discussed as early as in 1957 [107, 108]. Usefulness of knowledge on location-specific parameters has also been recognized many years ago [19]. By this moment, several powerful tools like Kriging method [24] are available for path loss estimation and prediction even to the locations with no radio coverage. Guidelines on modeling 3D cells are discussed for the frequency bands used in 4G Long-Term Evolution (LTE) and 5G new radio (NR) systems for certain cell types including urban-macro (UMa) and urban-micro (UMi) in 3rd-Generation Partnership Progect (3GPP) standards [109–111] as well. In those standards, a high attention is paid on deriving the impact through the direction of wave propagation rather than capturing location-specific propagation characteristics. However, due to ignorance of third spatial dimension in estimation of certain parameters, excessive complexity [112] and difficulties in data gathering those techniques have become less attractive for modeling 3D cells and even to face dynamic environmental conditions.

Once location-specific radio information is available, as a general practice, it is presented in form of 3D radio maps [24] for the convenience of subsequent use of it for efficient coverage and radio resource management in ensuring QoS aspects in wireless communication systems [25]. A radio map, REM or radio information map (RIM) is a database constructed by storing radio information against its locations [24] in a cell. The information could be path loss,

interference, receive signal power (RSP) values or combination of them at a location. Eleventh there are many techniques in literature to find location-specific radio information and construct radio maps for 2D cells, only a few of them can be improved to use for 3D SCs.

This work is primarily motivated by the technical problems associated with discovery of spatially distributed location-specific path loss parameters in 3D cells where there is no universal set of propagation parameters, which can be used to estimate radio information at different locations or areas within a SC. This location-specific information is with a paramount importance for efficient utilization of radio resources to improve communication performance and also for effective coverage management of devices for good QoS [113] while serving a large number of communication links. Then, the problem is how to capture those spatially distributed location-specific propagation characteristics of a 3D SC to construct radio maps. Since the provisions provided by 3GPP standards are not strong enough estimate location-specific propagation parameters under dynamic conditions for the 4G LTE [109, 110] and 5G NR [111] networks, still more studies are needed to further improve efficient radio resource utilization. When ensuring a seamless coverage, QoS and facilitating cell-free mMIMO systems [105], same way as in 2D networks [114, 115], having a proper mechanism for extending the 3D communication distance at the border of a 3D cell or a cluster with extended radio maps is also considered as a critical aspect. Furthermore, it is also a process linked with the 3D spatial positions due to use of location-specific propagation parameters while leading to an expansion of 3D SC coverage as a whole. Even though there is a large number of techniques to estimate those parameters, construct RIMs and support coverage management, the problem is that they are highly inefficient and inaccurate due to consideration 2D space rather than in 3D space.

3.1.1 Technical Challenges

There are several challenges against development of solutions for both problems on future 3D SC networks viz. propagation parameter estimation and 3D communication distance extension,

using conventional techniques and methods used in 2D networks. The challenges considered in this study are common for both problems as information and data are collected from the same devices and exchanged all over the network appropriately. In addition, the solutions should be compatible with future agile, flexible, environment-aware and self-configurable cellular networks as well.

When some of the relevant challenges are considered, the first challenge is to face the dynamism of the device distributions and the environment in collection and processing data in real-time to construct radio maps. The second challenge is arisen due to significant difficulty and costs associated with deployment of measurement devices at required locations all over the cell to take readings. Sometimes, there may be restrictions in accessing certain locations as well. The third challenge is to eliminate the device dependent errors associated with the readings. They are pivotal when readings are taken by a single device. Fourth technical challenge is arisen due to scarcity of network resource as there is a significant overhead and a cost in using dedicated channel or a frame to report measurement results. Currently, there is no autonomous method to perform these operations in an opportunistic manner while utilizing available devices and network resources without any extra cost. Lack of knowledge on path loss parameters and reporting devices are identified as the main challenges for the communication distance extension. The next hurdle is to manage data processing operations related to estimation of path loss parameters and subsequent constructions of radio maps. In this case, a network architecture is to be designed that can effectively support several operations like data collection, data processing, communication, geographical coverage planning [26] and network control [27] aspects.

3.1.2   Proposed Solution

Giving solutions for the problems discussed in this study is started with modeling 3D SCs. That is followed by presentation of mechanisms for real-time data gathering and path loss parameter estimation for the same cells. A cloud-assisted network protocol is discussed to construct ra-

dio maps with estimated propagation parameters on real-time basis under dynamic conditions. Then, two algorithms are presented, to extend the 3D communication distance at cluster borders including parameter prediction for the extended areas. Classrooms in universities, certain shops in shopping malls and meeting rooms in offices can be given as examples for the device clusters.

The solutions are developed based on several principles and techniques while simplifying a number of challenges. In mitigating the first most challenge, 3D coordinate system is used to give precise locations of devices and radio information in the 3D space while helping to manage massive number of connections [116] for a 3D SC network. Crowdsensing-assisted [117, 118] algorithm is proposed to collect and manage radio data on real-time basis. This scheme together with signal preprocessing stage are expected to reduce the inaccuracies caused by measurements taken by individual devices like device-specific errors, noise, gains and losses. Further, the same devices and resources, including receive signal, are used to take measurements based on their opportunistic availability at a given location and a moment yielding a considerable cost reduction in terms of capital expenditure, labor, time and network resources while beating the challenges on resource utilization and accessing locations.

Subsequently, LA and ML principles are used to estimate location-specific path loss parameters. In the LA method, sets of linear equations, describing all device pairs in a cluster, are solved. In the ML methods, least squire (LS) and GD algorithms are used. For the 3D communication distance extension at the cluster border, inverse distance weighting (IDW) or Shepard method [119, 120] assisted algorithm is developed. To extrapolate propagation parameters and to arrive at realistic radio maps at the vicinity of extended cluster boundary, in solving the problem of weak radio coverage at the borders, Nelder-Mead Simplex (NMS) technique [121, 122] based approach is used. Use of ML techniques also have several advantages, where they are capable of converging fast giving sub-optimum solutions while supporting to overcome the challenge of dynamic operational conditions. Moreover, they are expected to outperform conventional signal processing techniques by adjusting the parameters under complex conditions

and constraints.

The solutions discussed in this study are with several general advantages while mitigating several challenges. Having a customized and agile cell coverage, dynamic RIMs and sensitivity to environmental changes are the apparent merits of the solutions. Furthermore, solutions are backward and forward compatible with existing and near future systems, protocols, networks and their performance aspects particularly with emerging intelligent and autonomous network concepts by and large [123]. In addition, all the algorithms are easy-to-implement and less-complex compared to the methods with large number of measurement points [24]. As an example, in certain scenarios used for Kriging method [24] over 30,000 measurement points are considered compared to 50 devices dropped over 5 clusters in this study.

3.1.3 Technical Contributions

In solving the general problems associated with platform migration from 2D and 3D networks, several technical contributions are presented with this study. The main value of the contributions is due to their prominence and necessity as enabling technologies for rapidly evolving 3D cellular networks in fulfilling future communication needs in a cost effective and efficient manner. Furthermore, due to their applicability, they are capable of generating a significant impact not only for upcoming cellular networks but also for the existing wireless networks for their performance enhancement. The contributions are summarized as:

- To address the challenges 1. managing radio data from 3D cells on real-time basis 2. capture the dynamism associated with devices and the environment 3. eliminate inaccuracies associated with a reading taken by a single device, an algorithm based on crowdsensing technique is discussed while facilitating to have much realistic and dynamic radio maps.

- To solve the problem of estimation of location-specific path loss parameters of 3D SCs, three simple real-time mechanisms based on LA and ML principles are presented for both indoor and outdoor scenarios and frequency bands used in 4G LTE and 5G NR

deployments followed by construction of their radio maps. According to the results, GD algorithm is the best technique to estimate 3D path loss parameters showing over 98% estimation accuracy.

- To solve the problem of managing the coverage at the cluster borders in achieving better connectivity, two algorithms are presented based on IDW and NMS principles. With them, 3D communication distances are extended and propagation parameters are found for the extended distances while constructing REMs. In the case of receive signal power calculations at a slightly extended 3D communication distances from the cluster boundaries, by using already estimated propagation parameters, over 74% accuracy is shown for certain scenarios.

- In order to facilitate smooth flow of data and information, real-time operations and convenient implementation a feasible network architecture or a structured model of a cellular network with 3D cells consisting of clusters or crowds of devices in each cell is also discussed.

3.2   System Model and Problem Formulation

As shown in Fig. 3.1, a layout of a 3D SC containing several randomly dropped device clusters at time instances $\mathcal{T}_{\upsilon}$ and $\mathcal{T}_{(\upsilon+1)}$ is considered. Neither other types of cells like micro, pico or femto cells nor relay transmitters are considered within a given SC. The clusters are formed in both indoor or outdoor environments where the devices in them are directly served by the BS of the SC. In addition, with proper frequency planning there are no cell overlaps leading to have no inter-cell interference as well. An independent device and cluster deployment setup is indicated by υ and each cluster is with randomly dropped nearby M devices in the 3D space where devices are indexed with m, $m \in \mathcal{M}$, $\mathcal{M} = \{1, 2, 3, \ldots, m, \ldots, M\}$ and M can be a cluster-specific number as well. During time window $\mathcal{T}_{\upsilon}$, RSP values and location information are reported back to the BS by the devices which are opportunistic observations for the BS. For
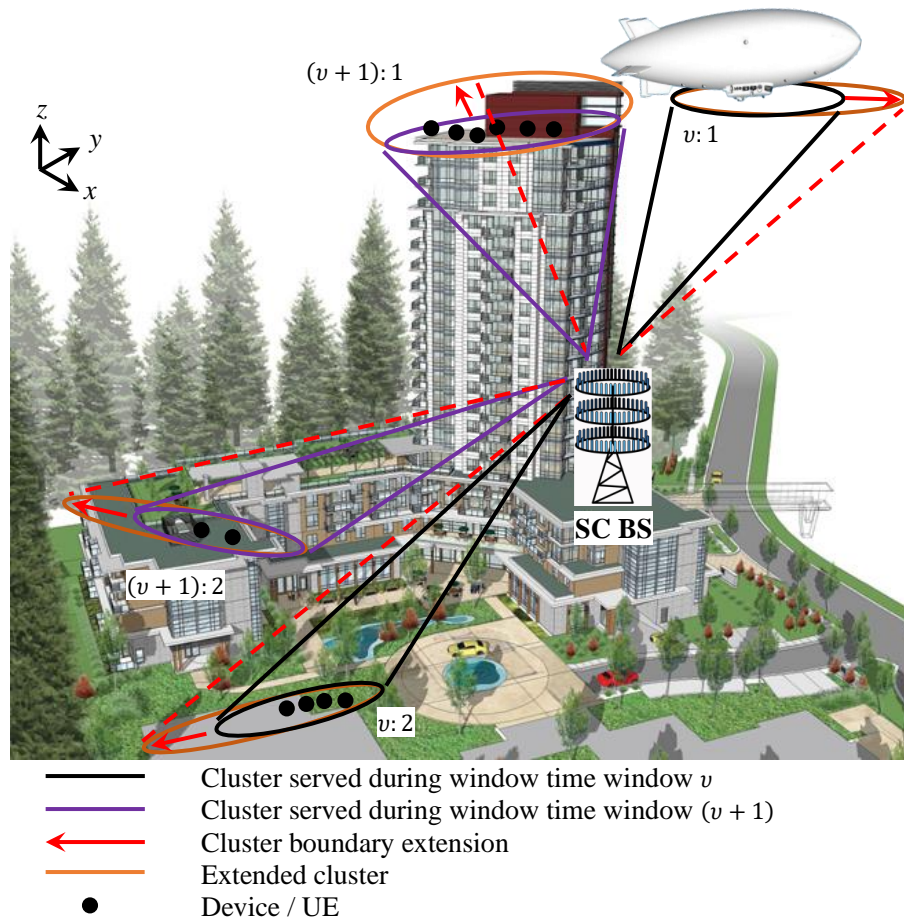
Figure 3.1: Layout of a 3D SC with device clusters and extension of their coverage at the boundaries when they are served at two time windows indexed by v and $(v + 1)$.

the simplicity C clusters served within $\mathcal{T}_v$ are named as $v : 1$, $v : 2$, $v : \ldots$, $v : C$. Generally, a device cluster can be a set of user equipment (UE) in a room where there is a high possibility to have a negligible variation in the vertical elevation for the devices within the same cluster. Further, 3D communication distance extensions at the cluster boundary are given by the red arrows where they are always pointed away from the center of the SC. The center of SC is selected as the origin of the 3D Cartesian coordinate system as well.

3.2.1   Overall Architecture and Overview on Path Loss and Radio Data Management

The overall operation of the network is divided into two main parts namely 3D network management and information management. Overall network architecture to manage the process of path loss estimation and radio map construction for 3D network is given in Fig. 3.2. Functionalities for stages ① - ⑦ are briefed as,

① Data collection: Data like RSP, SINR, interference and location data are opportunistically observed by the devices in a cluster.

② UL: Collected data is passed to the BS.

③ DL: Link considered for observations.

④ BS: Optional intermediate preprocessing stage to get information like path losses. Own 3D radio map can be constructed with data from own UE.

⑤ Backhaul, UL from BS to cloud: Necessary data and information are passed to the cloud.

⑥ Backhaul, DL from cloud to BS: Information needed for DL transmission and network management are passed.

⑦ Cloud: If not done at ④, this is the main location of 3D network and information management. Radio map is constructed where it is used by BSs and UE.

When managing the 3D network, BS admission control, identification of BSs whether they are from a 3D network and facilitation of continuous operation of the network are among some of the main functions [124]. Primarily, a BS indicated by ④ should be technically competent to manage the 3D coordinate system of the cell as well. Admission of 2D BSs are highly discouraged and they are restricted to the first or ground layer of the network. It is very important to identify whether a BS is going to be connected to a 2D network or a 3D network.
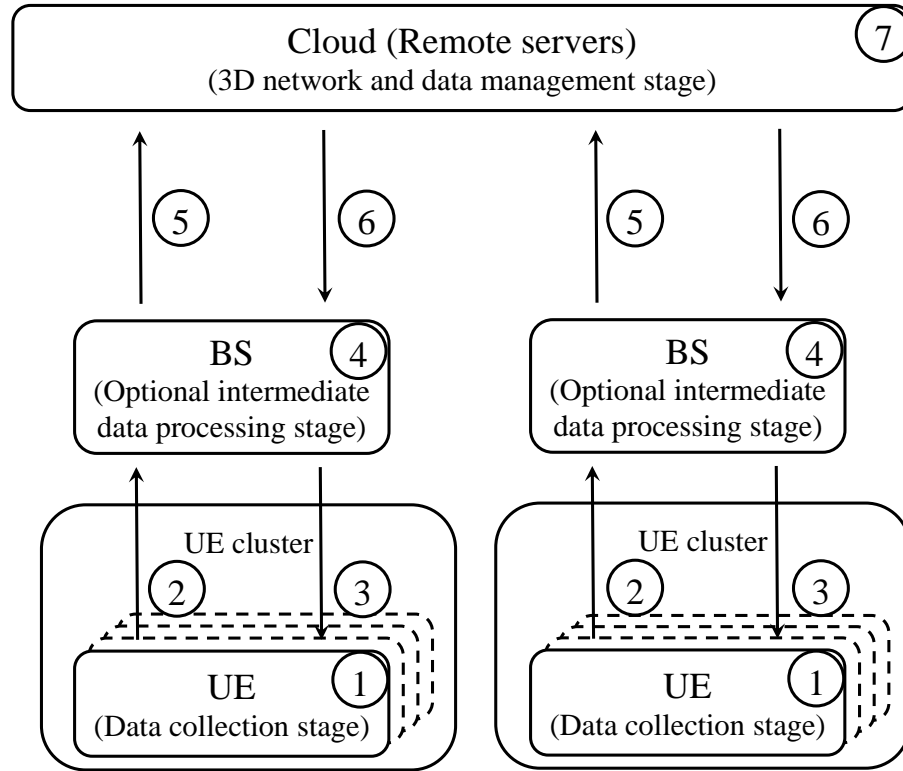
Figure 3.2: Network architecture of 3D network and information management.

This can be done through one of two main approaches. First and the easiest method is to get a confirmation about the location of the BS from the cloud server ⑦ whether the location is already in a 3D network coverage plan or suitable for that. This is done with the help of an already available cellular coverage map in ⑦. Second method is based on signal sensing done by BSs. At any moment, specially at the initialization, if a 3D capable BS receives signals from one of the BSs at her neighbor locations, a verification request is sent to the cloud asking whether her location can also be included to the 3D BS coverage plan [125]. In this way infrastructure framework for a flexible and agile 3D network can be developed. However, BS admission control is not discussed in this study.

There are three main stages associated with information management, viz. data gathering, data processing and information utilization. Functions of sharing and storage of information are also discussed under information utilization. In the case of data gathering, based on the observations, SINR, interference and location data are collected at ①. Collected data is pro-

cessed at ④ or ⑦, appropriately. In utilizing information, many of them like RSP values on DL from previous occasions are used at ④ and ⑦ for numerous algorithms in achieving different objectives. The same values are used at ① and ④ to define transmission resource blocks as well. For storage also, some data is passed to ⑦ by ④ where they are used for processing and decision making purposes at different places including both locations.

3.2.2   Problem Formulation

The research problem is defined with two main components viz. 3D path loss parameter estimation and cell border 3D communication distance extension where results of the first part are used for the second part of the study.

Location-Specific 3D Path Loss Estimation

In the first stage, the problem of finding location-specific, spatially distributed and dynamically updating or real-time path loss parameters for a 3D SC is addressed. Each set of estimated parameters is only valid for a specific location. The purpose of handling this problem is to use them to find 3D cell coverage information, radio resource management (including RIM construction and interference management), and radio coverage prediction at cluster or cell boundaries in a more realistic and effective manner at a subsequent occasion. In this way, efficient and deterministic utilization of radio resources in real-time operations is assured. The technical challenges associated with this problem include unreliability of data collected from single device (i.e., single device, single reading), limited availability of data at a given time instance, dynamism of the environment, volatility in reporting device deployments (i.e., changes in locations over time), mitigation of influence of equipment-specific gains (i.e., transmitter and receiver-specific losses and gains) and reduction of effect of noise (there can be interference as well). To address some of these challenges, receive signal is to be analyzed in detail.

The observed receive signal $y[t]$ of a device served by the BS at time t with transmit power p, transmit symbol $x[t]$ and additive white Gaussian noise (AWGN) $\eta[t]$, $\eta[t] \sim \mathcal{N}_c\left(0, \sigma^2\right)$, is

given as $y[t] = \sqrt{p\bar{G}}hx[t] + \eta[t]$. The channel coefficient h, $|h|^2 = |h^{\mathrm{f}}|^2 \, 10^{-\frac{L_{\mathrm{P}}}{10}}$, $|h^{\mathrm{f}}|^2 \sim \mathcal{U}(0.9, 1.1)$, is with location based fading coefficient h^{f} and path loss L_{P} (in dB). $\mathcal{U}(0.9, 1.1)$ is used to represent an uniform distribution in the close interval $[0.9, 1.1]$ where this interval is used to represent the slight variations in parameter $|h^{\mathrm{f}}|^2$ due to non-significant general changes in the environment relative to the device within a small period of time. With transmit antenna gain G_{T}, receive antenna gain G_{R} and transmitter losses (e.g., feeder loss) L_{T}, parameter for the other losses and gains $\bar{G}$ (in Watts) is given as $\bar{G} = G_{\mathrm{T}} G_{\mathrm{R}} (L_{\mathrm{T}})^{-1}$ [24] where all the transmitter and some of the device-specific parameters (e.g., G_{R}) are known. Even though L_{P} is a location dependent value, for the simplicity of the presentation they are not indexed with 3D location coordinates. With $\mathbb{E}\left[x[t]^2\right] = 1$, the receive signal power of a symbol from a frame without influence of the receiver-specific parameters is given as

$$p_{\mathrm{R}} = \frac{|y[t]|^2}{G_{\mathrm{R}}} = \frac{pG_{\mathrm{T}} \, |h^{\mathrm{f}}|^2 \, 10^{-\frac{L_{\mathrm{P}}}{10}}}{L_{\mathrm{T}}} + \frac{\eta^2}{G_{\mathrm{R}}}. \tag{3.1}$$

With this formulation, the challenge of mitigation of impact of device dependent gains and losses is also addressed.

Consider a device m at distance d_m from the transmitter in a cluster with location-specific path loss L_{P}^m and its estimated value $\hat{L}_{\mathrm{P}}^m$, $\hat{L}_{\mathrm{P}}^m = \hat{\alpha}_{(x,y,z)} + 10\log_{10}(d_m)\hat{\beta}_{(x,y,z)} + \hat{\xi}_{(x,y,z)} + \hat{L}_{(x,y,z)}^{\mathrm{O}}$ dB [24, 111]. $\hat{\alpha}_{(x,y,z)}$, $\hat{\beta}_{(x,y,z)}$, $\hat{\xi}_{(x,y,z)}$ and $\hat{L}_{(x,y,z)}^{\mathrm{O}}$ are the estimated values of least square fit of floating intercept, slope over the measured distances, log-normal shadowing, and location-specific other loss at 3D spatial location (x, y, z), respectively. Their original values are given as $\alpha_{(x,y,z)}$, $\beta_{(x,y,z)}$, $\xi_{(x,y,z)}$ and $L_{(x,y,z)}^{\mathrm{O}}$, accordingly and with $\xi_{(x,y,z)} \sim \mathcal{N}\left(0, \sigma_{\mathrm{PL}}^2\right)$. σ_{PL}^2 is the log-normal shadowing variance. Building penetration and inside losses are included to $L_{(x,y,z)}^{\mathrm{O}}$ [111]. Even though, this loss is not discussed many of the related studies, it is included to the main path loss equation by considering the importance of outdoor-to-indoor cell coverage scenarios. However, it can be totally neglected for the scenarios related to outdoor-to-outdoor coverages. For the simplicity, here onward this model is referred as NYUW (modified) path loss

model. The devices are in the close vicinity of each other and their propagation parameters are correlated in space domain within the cluster where parameters $\hat{\alpha}_{(x,y,z)}$, $\hat{\beta}_{(x,y,z)}$, $\hat{\xi}_{(x,y,z)}$ and $\hat{L}^{O}_{(x,y,z)}$ are considered to be common for the cluster. In the estimation process, parameters $\left(\hat{\alpha}_{(x,y,z)} + \hat{\xi}_{(x,y,z)} + \hat{L}^{O}_{(x,y,z)} \right)$ is considered as a single entity as $\hat{\zeta}_{(x,y,z)} = \left(\widehat{\alpha_{(x,y,z)} + \xi_{(x,y,z)} + L^{O}_{(x,y,z)}} \right)$ leading to have $\hat{L}^{m}_{P} = 10\log_{10}(d_m)\hat{\beta}_{(x,y,z)} + \hat{\zeta}_{(x,y,z)}$ where both $\hat{\beta}_{(x,y,z)}$ and $\hat{\zeta}_{(x,y,z)}$ are to be estimated.

Discovery and Extension of 3D Communication Distance

In the second stage, problem of 3D communication distance extension is addressed. More precisely, two branches of the problem, determination of extended 3D communication distance with existing parameters and extrapolation of propagation parameters at an extended distance are considered separately. 3D communication distance is extended through a directional transmission in 3D space [96] using a matched-filter precoded mMIMO system [96, 106]. In this problem also, the same set of technical challenges like increasing the reliability of data collected from single device, increasing amount of data at a given time instance, combating against volatility in reporting device deployments, mitigation of influence of equipment-specific gains and suppression of effect of noise are encountered. In addition, avoidance of interference for other devices is identified as an additional challenge which is overcome with directional beams [96, 106] while efficiently managed radio footprints. The main reasons to handle this problem are to achieve better connectivity, precise coverage and efficient use of radio resources with guaranteed QoS at the cluster boundaries [114, 115] and cell-free systems [105]. In addition, a radio map also can be constructed for the extended distances.

Similar to (3.1), the receive signal power of the mMIMO system containing A ($A \gg 1$) BS antenna elements serving to a single antenna devices [106] is expressed as

$$p_{R'} = \frac{pG_T \left| \boldsymbol{h}^{f} \left(\boldsymbol{h}^{f} \right)^{\mathbf{H}} \right|^2 10^{-\frac{L_P}{10}}}{AL_T} + \frac{\eta^2}{AG_R}, \qquad (3.2)$$

where $\boldsymbol{h}^{f}$ be the channel vector of $1 \times A$ components from BS antennas to a device and power

of each component is in $\mathcal{U}(0.9, 1.1)$. All noises are assumed to be independent and with the same variance. In this case, process of distance estimation is modeled as problem of finding extended distance $\bar{d}_E$ from the BS of the SC.

Consider a device dropped at the farthest location of a cluster at distance d_o from the BS where there is a distance error of e_o, $e_o \sim \mathcal{U}(-e_{max}^o, e_{max}^o)$, due to location reporting. With increase of transmit power, further d_a is added to the distance. There is an error of e_a, assuming $e_a \sim \mathcal{U}(-0.1d_a, 0.1d_a)$ for that with the maximum allowed error of e_{max}^a. $d_e = d_o + d_a$ and d_e is estimated based on the path loss L_P^E. In this case, total distance from BS to the estimated point which is directly away from the BS is given as $d_E = d_e + e_o + e_a$ [126]. When receiver expected threshold value is P_E, path loss is L^E and $p - P_E = L^E$, the ideally estimated 3D communication distance d_e is expressed as

$$d_e = 10^{\frac{1}{10\beta_{(x,y,z)}}\left(10\log_{10}\left(\frac{p_T}{P_E}\right) - \left(\alpha_{(x,y,z)} + \xi_{(x,y,z)}\right)\right)}, \tag{3.3}$$

where transmit power after transmitter gains and losses p_T is modeled as $p_T = pG_T L_T^{-1}$. Using (3.2), the receive signal is given as $p_{R'}$. Since it is not a good idea to rely on a single readings of a device, average is taken over M' devices that are closer to the far most device. In this case, p_R^m, e_a^m, p^m, p_T^m, d_E^m and d_a^m are the indexed versions of $p_{R'}$, e_a, p, p_T, d_E and d_a with device m, respectively. As it is indicated in Fig. 3.3, the planned distance d_P is the distance extension from the farthest device to the planned point (x_E, y_E, z_E) while d_m is used to represent distance for the same point from any other device at (x_m, y_m, z_m) subject to the maximum distance of d_{max}. For the farthest device $d_P = d_a = d_m$. The errors associated with estimations should be limited to a maximum value giving $e_a^m \leq e_{max}^a$. With these conditions, problem of finding the maximum average coverage distances $\bar{d}_E$, is formulated. For this overall accuracy for this estimation δ is also to be ascertained.

In the previous phase of the problem, the same propagation parameters are assumed for 3D communication distance extension. However, this phase, the problem of extrapolation
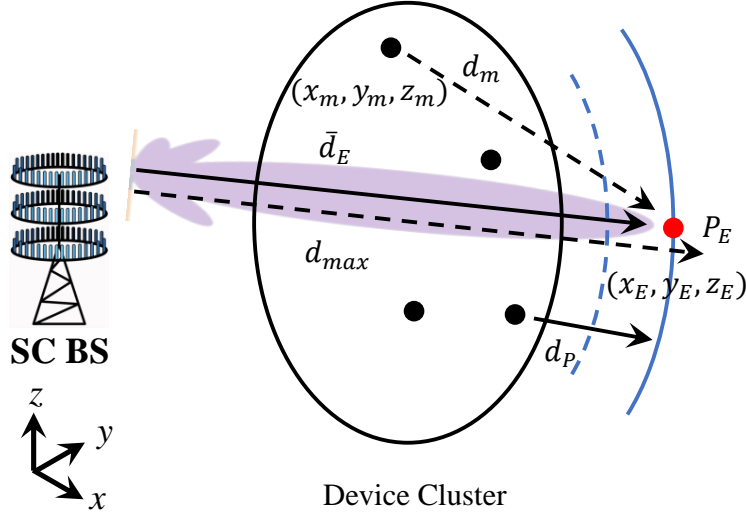
Figure 3.3: Extension of 3D communication distance.

of parameters for extended coverage is addressed. Similar to the first phase, the same sets of purposes and technical challenges are found in handling the problem. In this case for a given extended 3D communication distance d_E, path loss parameters $\beta_{(x,y,z)}$ and $\zeta_{(x,y,z)}$ are to be predicted as $\hat{\beta}^E_{(x,y,z)}$ and $\hat{\zeta}^E_{(x,y,z)}$, accordingly. For this extrapolation the relationship established by formulation $L^E_P = 10\hat{\beta}^E_{(x,y,z)}\log_{10}(d_E) + \hat{\zeta}^E_{(x,y,z)}$ is used. L^E_P is the expected path loss at the extension or beyond the border.

3.3   Data Gathering and Path Loss Estimation

Two main aspects are considered in providing solutions for the problems. First aspect is to establish a mechanism to handle the dynamism of the cell coverage while managing the UE admission and exit from the coverage area. Second aspect is to estimate path loss parameters while eliminating influence caused by receiver-specific gains and losses, and discovery of overall cell coverage through real-time radio data gathering and management.

3.3.1 Crowdsensing-Assisted Algorithm for Discovery of 3D Cell Coverage

In selecting a method for data collection, spatial-temporal 3D crowdsensing-assisted [117,118] data gathering approach is used. With this approach uncertainties and inaccuracies caused by a single reading taken from a single device is reduced where quality of data is further improved with a post-acquisition data processing stage. Since a large amount of data can be collected over time on real-time basis without any extra effort using many devices in a cluster and this solution appears more effective and convenient over conventional data collection techniques. Dynamism of the cell coverage area is captured in terms of multiple time windows leading to have a composite RIM where it is generated and continuously updated using information derived out of gathered data. Clusters and device deployment setup at window υ is considered as an independent crowdsensing [117] incident. It is assumed that the setup is going to last for a period of time which is sufficient to run the algorithms for all C clusters in the SC and find the optimum or suboptimum values for the parameters for that time window. Υ windows are considered to construct a composite coverage or RIM. Number of active windows can be varied at any time where there is no maximum or minimum value for that. For a newly formed cell, a window is originated with arrival of a set of mobile devices to a coverage area. $\mathcal{T}_v$ and $\mathcal{T}_{\max}$ are the time for the window v and the maximum time allowed to keep the coverage and radio information of a window without deletion or archiving from the system, respectively. The changes in device distributions are monitored and the composite coverage map is created by the Algorithm 1. Windows are monitored periodically to identify changes on the locations of the device and clusters deployments. If there is any major change, it is recognized as a new window. Then one of the Algorithms 2, 3 or 4 and one of the Algorithms 5 or 6 are run to extend 3D communication distance, determine the parameters and to get new radio information. Upon convergence of those algorithms cloud and RIM is updated with radio coverage and other information (e.g., distance, accuracy, RSP). If a current window is equivalent to one of the

previous windows or continuation of an existing window, the required parameter values for the other functionalities are obtained from the cloud and RIM is not updated.

3.3.2   Data Preprocessing Stage

A simple and important data preprocessing stage is introduced to reduce the influence caused by the fading channel and AWGN. For that, considering one device in a cluster, similar to (3.1) one receive symbol from each frame n, p_R^n, is taken and they are averaged over N frames or symbols giving

$$p_R^{\text{Av}} = \frac{1}{N} \sum_{n=1}^{N} p_R^n = \frac{pG_T 10^{-\frac{L_P}{10}}}{L_T} \sum_{n=1}^{N} \frac{\left| h_n^{\text{f}} \right|^2}{N} + \frac{1}{G_R} \sum_{n=1}^{N} \frac{\eta_n^2}{N}. \tag{3.4}$$

Since $\eta_n \sim \mathcal{N}_c (0, 1/2)$ and for sufficiently large N, $\frac{1}{N} \sum_{n=1}^{N} \left| h_n^{\text{f}} \right|^2 \approx 1$ and $\frac{1}{N} \sum_{n=1}^{N} \eta_n^2 = \frac{\sigma^2}{2}$ giving

$$p_R^{\text{Av}} = \frac{pG_T 10^{-\frac{L_P}{10}}}{L_T} + \frac{\sigma^2}{2G_R}. \tag{3.5}$$

Since noise variance and G_R are known $\frac{\sigma^2}{2G_R}$ is modeled and reduced from the averaged observed signal. Then considering $10 \log_{10}$ for (3.5) and simplifying

$$-10 \log_{10} \left(\frac{L_T}{pG_T} \left(p_R^{\text{Av}} - \frac{\sigma^2}{2G_R} \right) \right) \approx L_P. \tag{3.6}$$

In this work, three mechanisms are discussed to estimate the path loss parameters namely LA, ordinary least squire (OLS) and GD methods where latter two methods are linear regression techniques based on ML principles [127]. In general, implementation simplicity, ability to be operated on real-time basis and compatibility with complex environments are among the main reasons behind the effectiveness of these solutions. Particularly, the complexity is created by dynamic nature of different factors like device distributions in a cluster, background environment and cluster distributions in a SC. On the other hand, there is no need to have field measurement campaigns for these solutions where the devices in operation are used for report-

---

Algorithm 1: Algorithm for Capturing Dynamic 3D Cell Radio Information with Crowdsensing

---

1: **Initialization**
2: Identification of cellular layout
3: **for** $\upsilon = 1, 2, 3, \ldots \Upsilon$ **do**
4:     **if** *Window υ is active* **then**
5:         **if** *Window $\upsilon \approx$ One of the Current Windows* **then**
6:             Use existing values for the window υ
7:         **else**
8:             **for** $c = 1, 2, 3, ..., C$ **do**
9:                 Crowdsensing and data preprocessing
10:                 Run Algorithm 2, 3 or 4 for υ.
11:                 Run Algorithm 5 or 6
12:                 Add the locations to the map
13:                 Update coverage and radio information
14:             **end**
15:             $\Upsilon \leftarrow \Upsilon + 1$
16:         **end**
17:         Set $\mathcal{T}_\upsilon = 0$
18:     **else**
19:         **if** $\mathcal{T}_\upsilon \geq \mathcal{T}_{max}$ **then**
20:             Archive / Delete radio and coverage information
21:             $\Upsilon \leftarrow \Upsilon - 1$.
22:         **else**
23:             Update $\mathcal{T}_\upsilon \leftarrow \mathcal{T}_\upsilon + 1$
24:         **end**
25:     **end**
26: **end**

---

ing and data collection. That is one of the most prominent advantage associated with these solutions, when compared with most of the conventional approaches used for the empirical models. Even though all these methods are for the systems with linear relationships between independent and dependent variables, there is no similar relationship between distance and the power in path loss models. In this case, the linear relationship is established by considering the term $10 \log_{10}(d_m)$ as the independent variable. However, with this transformation sensitivity of the dependent variable is reduced to a certain extent. That challenge is mitigated by taking readings from spatially distributed devices within the cluster. L_P^m is used to represent L_P of device m.

3.3.3   Linear Algebraic Method

In this method, linear equations for the path losses of two devices m and m' are solved. In solving the pairs, $\binom{M}{2}$ equation pair combinations are to be considered for a single set of solutions. Then the solutions for a given device pair m and m' is given as,

$$\hat{\beta}'_{(x,y,z)} = \frac{L_P^m - L_P^{m'}}{10 \log_{10}(d_m/d_{m'})}, \tag{3.7}$$

$$\hat{\zeta}'_{(x,y,z)} = \frac{-L_P^m \log_{10}(d_{m'}) + L_P^{m'} \log_{10}(d_m)}{\log_{10}(d_m/d_{m'})}. \tag{3.8}$$

where terms L_P^m and $L_P^{m'}$ are to be modeled with the left hand side of (3.6). To get the most appropriate values, the process indicated in the Algorithm 2 is to be followed. In this process, a set of possible solutions are averaged to determine the best values.

Algorithm 2: Algorithm with LA Method

1: **Initialization**
2: For all the devices in a cluster, collect p_R, σ^2, G_R and d_m. Calculate L_P^m.
3: **for** $m = 1, 2, 3, ..., M$ **do**
4:     **for** $m' = m + 1, m + 2, m + 3, ..., M$ **do**
5:         Get the solution $\hat{\beta}'_{(x,y,z),m,m'}$ with (3.7)
6:         **if** $\beta_{(x,y,z)}^{min} < \hat{\beta}'_{(x,y,z)} < \beta_{(x,y,z)}^{max}$ **then**
7:             Get the solution $\hat{\zeta}'_{(x,y,z),m,m'}$ with (3.8)
8:         **end**
9:     **end**
10: **end**
11: $\hat{\beta}_{(x,y,z)} = Avg\left\{\sum_{m\in M}\sum_{m'\in M}\hat{\beta}'_{(x,y,z),m,m'}\right\}, \hat{\zeta}_{(x,y,z)} = Avg\left\{\sum_{m\in M}\sum_{m'\in M}\hat{\zeta}'_{(x,y,z),m,m'}\right\}$

3.3.4   Linear Regression: Ordinary Least Square Method

This a Linear Regression (LR) method and also a basic ML technique used to establish relationship between the input/independent and the dependent variables [127]. Then the related

terms $\bar{X} = \frac{10 \sum_{m=1}^{M} \log_{10}(d_m)}{M}$ and $\bar{Y} = \frac{\sum_{m=1}^{M} L_{\mathrm{P}}^{m}}{M}$ are calculated and estimated parameters are given as

$$\hat{\beta}_{(x,y,z)} = \frac{\sum_{m=1}^{M} \left(10 \log_{10}(d_m) - \bar{X}\right)\left(L_{\mathrm{P}}^{m} - \bar{Y}\right)}{\sum_{m=1}^{M} \left(10 \log_{10}(d_m) - \bar{X}\right)^2}, \tag{3.9}$$

$$\hat{\zeta}_{(x,y,z)} = \bar{Y} + \hat{\beta}_{(x,y,z)}\bar{X}. \tag{3.10}$$

For the completeness, the procedure of implementation is given with Algorithm 3.

Algorithm 3: Algorithm with OLS Method

1: **Initialization**
2: For all the devices in a cluster, collect $p_{\mathrm{R}}, \sigma^2, G_{\mathrm{R}}$ and d_m. Calculate L_{P}^{m}.
3: Calculate $\bar{X}$ and $\bar{Y}$.
4: Calculate $\hat{\beta}_{(x,y,z)}$ with (3.9) and then $\hat{\zeta}_{(x,y,z)}$ with (3.10).

3.3.5 Linear Regression: Gradient Descent Method

This is also a basic ML technique falling under the category of LR techniques [127]. For this, with $\hat{L}_{\mathrm{P}}^{m} = 10 \log_{10}(d_m)\hat{\beta}_{(x,y,z)} + \hat{\zeta}_{(x,y,z)}$, it is considered to minimize the mean of square errors E associated with the estimated path loss values of the devices in the cluster. That is given as

$$\min_{\hat{\beta}_{(x,y,z)},\hat{\zeta}_{(x,y,z)}} E = \frac{1}{M} \sum_{m=1}^{M} \left(L_{\mathrm{P}}^{m} - \hat{L}_{\mathrm{P}}^{m}\right)^2. \tag{3.11}$$

For this $\hat{\beta}_{(x,y,z)}$ and $\hat{\zeta}_{(x,y,z)}$ values are selected based on an iterative process given by

$$\hat{\beta}_{(x,y,z)t} = \hat{\beta}_{(x,y,z)(t-1)} + \gamma D_{\beta_{(x,y,z)}}, \tag{3.12}$$

$$\hat{\zeta}_{(x,y,z)t} = \hat{\zeta}_{(x,y,z)(t-1)} + \gamma D_{\zeta_{(x,y,z)}}, \tag{3.13}$$

where γ is the learning rate. Considering expression $\hat{L}_{\mathrm{P}}^{m} = 10 \log_{10}(d_m)\hat{\beta}_{(x,y,z)} + \hat{\zeta}_{(x,y,z)}$, $\hat{\beta}_{(x,y,z)t}$ and $\hat{\zeta}_{(x,y,z)t}$ are randomly initialized and for $\hat{\beta}_{(x,y,z)t}$ its a value in the range $\beta_{(x,y,z)}^{\min} \leq \hat{\beta}_{(x,y,z)} \leq \beta_{(x,y,z)}^{\max}$.

Then $D_{\beta_{(x,y,z)}}$ and $D_{\zeta_{(x,y,z)}}$ are given as

$$D_{\beta_{(x,y,z)}} = \frac{\partial \hat{L}_P^m}{\partial \hat{\beta}_{(x,y,z)}} = -\frac{20}{M} \sum_{m=1}^{M} \log 10(d_m) \left(L_P^m - \hat{L}_P^m \right), \tag{3.14}$$

$$D_{\zeta_{(x,y,z)}} = \frac{\partial \hat{L}_P^m}{\partial \hat{\zeta}_{(x,y,z)}} = -\frac{2}{M} \sum_{m=1}^{M} \left(L_P^m - \hat{L}_P^m \right). \tag{3.15}$$

The process of implementation of GD scheme with multiple iterations is explained in Algorithm 4.

Algorithm 4: Algorithm with GD Method

1: **Initialization**
2: Collect p_R, σ^2, G_R, d_m and calculate $L_P^m, \forall m \in \mathcal{M}$. Calculate $D_{\beta_{(x,y,z)}}$ and $D_{\beta_{(x,y,z)}}$. Set a value for
   $\gamma, \hat{\beta}_{(x,y,z)t} \sim \mathcal{U}\left(\beta_{(x,y,z)}^{\min}, \beta_{(x,y,z)}^{\max} \right), \hat{\zeta}_{(x,y,z)t} \sim \mathcal{N}\left(0, \sigma_{PL}^2 \right).$
3: **repeat**
4:     Update $\hat{\beta}_{(x,y,z)t} \leftarrow \hat{\beta}_{(x,y,z)(t-1)} + \gamma D_{\beta_{(x,y,z)}}.$
5:     Update $\hat{\zeta}_{(x,y,z)t} \leftarrow \hat{\zeta}_{(x,y,z)(t-1)} + \gamma D_{\zeta_{(x,y,z)}}.$
6:     Calculate E_t.
7: **until** *Convergence OR $E_t < E_{t-1}$*;
8: $\hat{\beta}_{(x,y,z)} = \hat{\beta}_{(x,y,z)t}, \hat{\zeta}_{(x,y,z)} = \hat{\zeta}_{(x,y,z)t}$

3.4   3D Communication Distance Extension and RIM Construction

Extension of cluster boundary coverage and construction of RIM under dynamic conditions are the main objectives of the second part of the solution. In this case, two solutions are developed to extend the 3D communication distance using already estimated parameters, and to estimate parameters for extrapolation of limited coverage distance while updating the REM. Coverage extension is achieved with transmit power control and estimation of corresponding propagation distances. In this case principles of crowdsensing, IDW [119, 120] and NMS algorithm [122] are used for data gathering, distance extension and path loss parameter predictions, accordingly.

By considering complexity of the problem (including dynamism and unpredictable na-

ture of environment) and requirements of the future communication systems, IDW [119, 120] method is selected to solve the problem. These solutions become even effective as it does not require any knowledge on propagation parameters for the extended distance. Robustness against the dynamism of the environment (e.g., changes in the background), real-time implementation, compatibility with 2D and other future networks, and applicability for the networks with irregular cell shapes are some of the advantages with these solutions over existing methods. In this work, the main technical challenge of taking readings at the location where there is no device to report. That challenge is mitigated with distance estimations done towards a predefined location with reasonable accuracy.

3.4.1 Inverse Distance Weighting Assisted Algorithm

To extrapolate 3D communication distance with a planned distance d_P from the farthest device, a scheme based on IDW principle [119, 120] is proposed. Originally, this method is used for extrapolation of multiple transmitters in indoor environments. Using this approach, the receive power at a desired location is given as

$$P_E = \sum_{m=1}^{M'} w_m p_{\text{R}}^m, \tag{3.16}$$

where the weighting factor for device m, w_m, and the distance to the device m, d_m are given as $w_m = \frac{d_m^{-b}}{\sum_{m'=1}^{M'} d_{m'}^{-b}}$ is the and $d_m = \sqrt{(x_E - x_m)^2 + (y_E - y_m)^2 + (z_E - z_m)^2}$, accordingly. Based on (3.3), the distance with estimated parameters $\hat{d}_e$ is given as $\hat{d}_e = 10^{\frac{1}{10\hat{\beta}_{(x,y,z)}}\left(10\log_{10}\left(\frac{p_{\text{T}}}{P_E}\right) - \hat{\zeta}_{(x,y,z)}\right)}$. Furthermore, similar to d_E^m the estimated distance with errors is given as $\hat{d}_E^m = \hat{d}_e + e_o^m + e_a^m$ where $e_a^m \sim \mathcal{U}(-0.1d_m, 0.1d_m)$. Then, estimated distance $\bar{d}_E$ is expressed as

$$\bar{d}_E = \frac{\sum_{m=1}^{M'} \hat{d}_E^m}{M'}. \tag{3.17}$$

When calculation of $\bar{d}_E$, the overall accuracy of extension of 3D communication distance

δ_m is defined as

$$
\begin{aligned}
\delta_m &= \frac{1}{2}\left[\left(1 - \left|\frac{e_a^m}{e_{\max}^a}\right|\right) + \left(1 - \left|\frac{e_o^m}{e_{\max}}\right|\right)\right] \\
&= \frac{1}{2}\left[2 - \left(\left|\frac{e_a^m}{e_{\max}^a}\right| + \left|\frac{e_o^m}{e_{\max}}\right|\right)\right],
\end{aligned}
\tag{3.18}
$$

where $e_{\max}$ is the maximum error when reporting the locations of the devices. Then the average

accuracy is given by

$$
\delta = \frac{\sum_{m=1}^{M'} \delta_m}{M'}.
\tag{3.19}
$$

This process is further explained in by the Algorithm 5.

Algorithm 5: Algorithm for 3D Communication Distance Extension

---

1: **Initialization**
2: Set $e_{\max}^o$, $e_{\max}^a$, d_p and $d_{\max}$.
3: Get d_m, $\forall m \in \mathcal{M}'$.
4: **if** $d_m < d_{max}$, $\forall m \in \mathcal{M}'$ **then**
5:    | **Initialization**
6:    | **for** $l = 1, 2, 3, ..., L$ **do**
7:    | | **for** $m = 1, 2, 3, ..., M'$ **do**
8:    | | | Transmit with p_{T}^m.
9:    | | | Crowdsensensing and data preprocessing
10:   | | | Get P_E, d_e^m, e_a^m and e_o^m.
11:   | | | **if** $e_a^m \le e_{max}^a$ **then**
12:   | | | | Calculate $d_E^m(l)$ and $\delta_m(l)$.
13:   | | | **else**
14:   | | | | Reduce d_P,
15:   | | | | Go to Step 3.
16:   | | | **end**
17:   | | **end**
18:   | | Calculate $\bar{d}_E(l)$ with (3.17) and $\delta(l)$ with (3.19).
19:   | **end**
20:   | Calculate $\bar{d}_E = \frac{\sum_{l=1}^{L} \bar{d}_E(l)}{L}$ and $\delta = \frac{\sum_{l=1}^{L} \delta(l)}{L}$.
21: **else**
22:   | Reduce d_P,
23:   | Go to Step 3.
24: **end**

3.4.2   Nelder-Mead Simplex Algorithm

In order to extrapolate parameters an extended 3D communication distance a mechanism based on NMS algorithm [122] is suggested. Originally, this method is used for interpolation using higher order Voronoi tessellation. In this work it is used for extrapolation of parameters for limited distances. For that sum of the weighted residual squares are minimized and corresponding arguments are found as

$$\left(\hat{x}_E, \hat{y}_E, \hat{z}_E, \hat{\beta}^E_{(x,y,z)}, \hat{p}_{R`_1}\right) = \underset{\hat{x}'_E, \hat{y}'_E, \hat{z}'_E, \beta'_{(x,y,z)}, p'_{R`_1}}{\arg\max} \left(\frac{1}{J} \sum_{m=1}^{M} w_m \lambda_m^2\right), \tag{3.20}$$

where w_m, λ_m and J are given as $w_m = 1/\left|p^m_{Av`}\right|^b$, $\lambda_m = p^m_{Av`} - p_{R`_1} + 10\hat{\beta}_{(x,y,z)} \log_{10}\left(d^E_m\right)$ and $J = \sum_m^M w_m$, accordingly. $(\hat{x}_E, \hat{y}_E, \hat{z}_E)$, $b$, $d^E_m$, $p^m_{Av`}$ and $p_{R`_1}$ are extended position by the prediction, power parameter, slightly extended 3D communication distance related to each device, average and reference receive powers, respectively. By averaging similar to (3.5) and with reduction of noise component $\frac{\sigma^2}{2G_R}$ from the averaged signal over N frames, $p^m_{Av`}$ is given as

$$p^m_{Av`} = \left(\frac{1}{N} \sum_{n=1}^{N} p^n_{R`} - \frac{\sigma^2}{2G_R}\right). \tag{3.21}$$

By using known $\hat{p}_{R`_1}$, (3.20) is further simplified to

$$\hat{\beta}^E_{(x,y,z)} = \underset{\beta'_{(x,y,z)}}{\arg\max} \left(\frac{1}{J} \sum_{m=1}^{M} w_m \lambda_m^2\right). \tag{3.22}$$

Since Heuristic search criterion is used for (3.22), there can be multiple solutions. Range for $\hat{\beta}^E_{(x,y,z)}$ and $\beta'_{(x,y,z)}$ is set as $\pm$ 20% than $\hat{\beta}_{(x,y,z)}$ for the considered cluster. d_m is increased by the same step size for all the devices to get d^E_m. Then, extended 3D communication distance d_E is given as $d_E = \max\left(d^E_1, d^E_2, \ldots, d^E_M\right)$. Considering the device with d_E and for a close value to L^m_P, $\hat{\zeta}^E_{(x,y,z)}$ is given as $\hat{\zeta}^E_{(x,y,z)} = L^E_P - 10\hat{\beta}^E_{(x,y,z)} \log_{10}(d_E)$. For L^E_P a suitable value that is greater than the loss at the location of the farthest device is to be selected. The process of implementation

is detailed in Algorithm 6.

Algorithm 6: Algorithm with for Extrapolation of Parameters and Distance

---

1: **Initialization**
2: Crowdsensensing and data preprocessing
3: Calculate p_{Av}^m, with (3.21), $\forall m \in \mathcal{M}$.
4: Calculate w_m and λ_m, $\forall m \in \mathcal{M}$.
5: Calculate $J = \sum_j^M w_m$.
6: Set the range for $\hat{\beta}_{(x,y,z)}^E$:
$\hat{\beta}'^L_{(x,y,z)} = 0.8\hat{\beta}_{(x,y,z)}$,
$\hat{\beta}'^U_{(x,y,z)} = 1.2\hat{\beta}_{(x,y,z)}$.
7: Find $\hat{\beta}_{(x,y,z)}^E$ using (3.22) and then decide d_E
8: Use $\hat{\beta}_{(x,y,z)}^E$ to find $\hat{\zeta}_{(x,y,z)}^E$ at d_E

3.5   Simulation Results

Simulation results are presented considering a 3D SC of 50 m in approximate geographical radius where BS is at the center. For the implementation, both 4G LTE system operated in 2.5 GHz band (band 41) [109, 110] and 5G NR system operated in 28 GHz band (band n257 in frequency range 2) [25, 128] are considered where the operating frequency 2.5 GHz is very closely related to the bands 7 and 53 [109] that are used in certain variants of LTE networks in different geographical regions. It is assumed that DLs of the BS are with an uniform and continuous traffic flow with full buffer status. In construction of composite coverage map, moving window size is set to two for windows υ and $(\upsilon + 1)$. For each window five cluster deployments are considered and each cluster is 2-4 m radius with randomly dropped devices of approximately 10 in number. For the simplicity, cluster deployments are considered with NLOS properties covering both outdoor-to-outdoor and outdoor-to-indoor scenarios. Information on the four propagation models used for the comparison UMa, UMi, UMi-street canyon and NYUW (modified) [25, 109] are made available in Table 3.1. In the case of deployments, except for the NYUW (modified) model, parameters $\alpha_{(x,y,z)}$, $\beta_{(x,y,z)}$ are modeled with a variation of ±10% with respect to the values given in the Table 3.1. L_{Tw}, $L_{(x,y,z)}^{In}$, L_{Npi}, L_{Gls}, L_{Con}

and L_{Pe}^2 are the building penetration loss through the external wall, the inside loss dependent on the depth into the building, additional loss to the external wall loss to account for non-perpendicular incidence, standard multi-pane glass loss, concrete loss and is the standard deviation for the penetration loss, respectively. How to measure outdoor-to-indoor 2D distance for the device m, d_{2Din}^m, is shown in Fig. 3.4. Transmission frames of 10 ms are used and each frame is equally divided among the devices in a cluster. Values for the common simulation parameters for the 3D SC network is given in Table 3.2. In the case of sample size, 10,000 readings are averaged from each device. In this study, it is assumed that all the devices, BSs and servers are properly synchronized in both time and frequency domains where they are well coordinated with no network or processing delays.

3.5.1 Estimation of Path Loss Parameters

Estimated parameters for path loss model related to two time windows $\mathcal{T}_\nu$ and $\mathcal{T}_{(\nu+1)}$ are presented in Table 3.3. Five clusters are considered for each time window and estimated parameter values under three methods LA, OLS and GD are tabulated. Estimated values for $\beta_{(x,y,z)}$ and $\zeta_{(x,y,z)}$ are given in Table 3.3 (a) and Table 3.3 (b), accordingly. In these tables, actual and estimated parameter values are compared against each other and errors percentages are also presented for individual cluster at each time window. In the case of $\hat{\beta}_{(x,y,z)}$, 9.244% for 28 GHz NYUW (modified) model and 1.085% for 2.5 GHz UMa NLOS model are the highest and the lowest error percentages, accordingly. Similarly, 10.621% for 2.5 GHz UMa NLOS model and 1.009% for 28 GHz NYUW (modified) model are the highest and the lowest error percentages for $\hat{\zeta}_{(x,y,z)}$, respectively. In the case of UMi-street canyon model, values of the estimated parameters are given in Table 3.4. Considering parameter $\hat{\beta}_{(x,y,z)}$ as given in Table 3.4 (a), 6.49% and 2.642% are the highest and the lowest error percentages, respectively. Furthermore, as given in Table 3.4 (b), 6.847% with OLS method and 1.743% with GD method are the highest and the lowest error percentages for $\hat{\zeta}_{(x,y,z)}$, respectively. However, by considering the average errors, in general the best performance is shown by GD method.

Table 3.1: Path loss models, their parameter values and penetration losses under NLOS condition used in cell deployment scenarios in 4G LTE and 5G NR systems operated in frequency bands 2.5 GHz and 28 GHz.

Parameter	Explanations and Values											
Band (Name)	**2.5 GHz (4G LTE)**			**28 GHz (5G NR)**								
Model name	**UMa NLOS**			**UMa NLOS**			**UMi - Street Canyon**			**NYUW (modified)**		
Model equation	$L_P^m = \alpha_{(x,y,z)} + 10\log_{10}(d_m)\beta_{(x,y,z)}$ $-0.3(h_m - 1.5) + \xi_{(x,y,z)} + L_{(x,y,z)}^O$ $\alpha_{(x,y,z)} = 22.7 + 26\log_{10}(f_c)$			$L_P^m = \alpha_{(x,y,z)} + 10\log_{10}(d_m)\beta_{(x,y,z)} + \xi_{(x,y,z)}$ $+L_{(x,y,z)}^O$ $\alpha_{(x,y,z)} = 32.4 + 20\log_{10}(f_c)$						$L_P^m = \alpha_{(x,y,z)} + 10\log_{10}(d_m)\beta_{(x,y,z)}$ $+\xi_{(x,y,z)} + L_{(x,y,z)}^O$		
Parameter	$\alpha_{(x,y,z)}$	$\beta_{(x,y,z)}$	σ_{PL}	$\alpha_{(x,y,z)}$	$\beta_{(x,y,z)}$	σ_{PL}	$\alpha_{(x,y,z)}$	$\beta_{(x,y,z)}$	σ_{PL}	$\alpha_{(x,y,z)}$	$\beta_{(x,y,z)}$	σ_{PL}
Value	33.05	3.67	4	61.34	3	7.8	61.34	3.19	8.2	$61\leq \alpha_{(x,y,z)} \leq 72$	$2 \leq \beta_{(x,y,z)} \leq 2.8$	8.7
Penetration loss equation	$L_{(x,y,z)}^O = L_{Tw} + L_{(x,y,z)}^{In} + \mathcal{N}(0, \sigma_{Pe}^2)$, $L_{Tw} = 20$, $L_{(x,y,z)}^{In} = 0.5 d_{2Din}^m$, $\sigma_{Pe} = 0$, $\sigma_{PL} = 7$, $d_{2Din}^m = \mathcal{U}(0,8)$, f_c is in GHz			$L_{(x,y,z)}^O = L_{Tw} + L_{(x,y,z)}^{In} + \mathcal{N}(0, \sigma_{Pe}^2)$, $L_{Tw} = L_{Npi} - 10\log_{10}\left(0.3\cdot 10^{\frac{-L_{Gls}}{10}} + 0.7\cdot 10^{\frac{-L_{Con}}{10}}\right) = 117$, $L_{(x,y,z)}^{In} = 0.5 d_{2Din}^m$, $L_{Npi} = 5$, $\sigma_{Pe} = 4.4$, $L_{Gls} = 2 + 0.2 f_c = 7.6$, $L_{Con} = 5 + 4 f_c = 117$, $d_{2Din}^m = \mathcal{U}(0,8)$, L_{Gls} =Loss with multiplane glass, L_{Con} = Loss with concrete, f_c is in GHz										
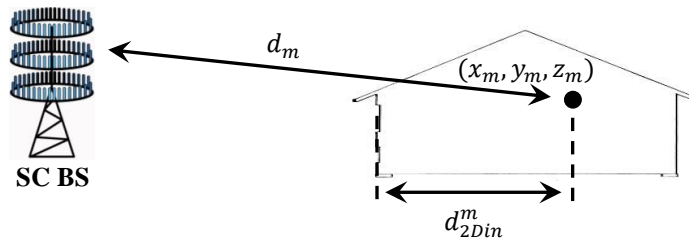
Figure 3.4: Layout of a 3D SC serving to an indoor device.

Table 3.2: Common simulation parameters for the 3D SC network.

Parameter	Value
Maximum transmit power	26 dBm
Minimum transmit powers	2.6 dBm
Power control steps	10
The threshold power for P_E	-90 dBm
Transmitter antenna gain	4 dB
Receiver antenna gain	1 dB
Transmitter feeder losses	2 dB
Receive feeder loss	1 dB
Receiver feeder loss variation	5%
Variance for AWGN, σ^2	-100 dBm/Hz

For the two time windows $\mathcal{T}_\nu$ and $\mathcal{T}_{(\nu+1)}$, plots for the performance of OLS LR technique are shown in Fig. 3.5. Liner plots for the propagation models UMa, UMi, UMi-street canyon and NYUW (modified) [25, 109] are given in Fig. 3.5 (a) to Fig. 3.5 (d), respectively.

For the same time windows, convergence plots for E for the GD method are shown in Fig. 3.6. Plots for the propagation models UMa, UMi, UMi-street canyon and NYUW (modified) [25, 109] are given in Fig. 3.6 (a) to Fig. 3.6 (d), respectively. For this, learning rate γ is set as $\gamma = 1 \times 10^{-3}$.

In the case of outdoor-to-indoor scenarios, estimated parameters for propagation models given in Table 3.5. Estimated values for $\beta_{(x,y,z)}$ and $\zeta_{(x,y,z)}$ are given in Table 3.5 (a) and Table 3.5 (b), accordingly. In this process it is assumed that L_{Tw} and $L^{In}_{(x,y,z)}$ are known. In these tables, actual and estimated parameter values are compared against each other and errors percentages are also presented for individual cluster at each time window. In the case of $\hat{\beta}_{(x,y,z)}$, 14.097% for 28 GHz NYUW (modified) model and 2.323% for 2.5 GHz UMa NLOS model are the highest and the lowest error percentages, accordingly. Similarly, 17.623% for 2.5 GHz UMa NLOS model and 1.398% for 28 GHz NYUW (modified) model are the highest and the lowest

Table 3.3: For consecutive two time windows $\mathcal{T}_v$ and $\mathcal{T}_{(v+1)}$ of the management algorithm, considering a SC serving to five clusters at each window, under three methods, the estimated values for the propagation parameters under different propagation models are shown with corresponding estimation errors for the parameter: (a) $\beta_{(x,y,z)}$. (b) $\zeta_{(x,y,z)}$.

(a) Estimations for the parameter $\beta_{(x,y,z)}$.

Cluster	Location x_0, y_0, z_0 (m)	2.5 GHz (4G LTE) UMa NLOS β	$\hat{\beta}$ LA	$\hat{\beta}$ OLS	$\hat{\beta}$ GD	Error(%) LA	Error(%) OLS	Error(%) GD	28 GHz (5G NR) UMa NLOS β	$\hat{\beta}$ LA	$\hat{\beta}$ OLS	$\hat{\beta}$ GD	Error(%) LA	Error(%) OLS	Error(%) GD	28 GHz (5G NR) NYUW(modified) β	$\hat{\beta}$ LA	$\hat{\beta}$ OLS	$\hat{\beta}$ GD	Error(%) LA	Error(%) OLS	Error(%) GD
v:1	12.06, -31.45, 27.77	3.57	3.651	3.933	3.646	2.373	10.310	2.275	3.13	2.970	3.122	3.122	5.081	2.269	0.229	2.39	2.380	2.800	2.409	0.418	17.155	0.7853
v:2	-1.28, -41.06, 3.96	3.70	3.640	3.470	3.708	1.555	6.148	0.292	2.93	3.001	2.801	2.801	2.249	4.567	4.530	2.09	2.201	2.001	2.103	5.263	4.306	0.613
v:3	14.65, 32.21, 24.91	3.58	3.742	3.774	3.578	4.522	5.467	0.007	2.88	3.060	2.882	2.882	6.195	8.689	0.035	2.66	2.391	2.801	2.738	10.151	5.263	2.934
v:4	15.81, 24.45, -29.12	3.63	3.561	3.403	3.671	1.917	6.243	1.145	2.95	2.981	2.955	2.955	0.897	5.197	0.056	2.40	2.272	2.064	2.414	5.417	14.006	0.595
v:5	-32.25, -4.64, 24.67	3.82	3.631	3.709	3.685	4.986	2.911	3.535	3.02	3.051	2.976	2.976	1.010	1.678	1.435	2.36	2.291	2.204	2.370	2.966	6.591	0.414
(v+1):1	-37.80, -21.79, -11.55	3.77	3.692	3.933	3.795	2.052	4.398	0.733	2.99	3.001	2.906	2.906	0.150	6.827	2.996	2.38	2.442	2.801	2.529	2.521	17.647	6.262
(v+1):2	-1.40, -10.27, -43.55	3.81	3.750	3.403	3.797	1.704	10.799	0.465	3.00	3.081	3.046	3.046	2.718	6.621	1.599	2.24	2.371	2.010	2.212	5.803	10.714	1.239
(v+1):3	28.33, -18.01, 28.35	3.68	3.643	3.933	3.630	1.213	6.738	1.497	2.96	3.030	3.063	3.063	2.382	8.126	3.490	2.77	2.432	2.801	2.788	12.274	1.083	0.661
(v+1):4	-32.19, 27.56, -5.05	3.54	3.631	3.403	3.537	2.603	3.813	0.0314	3.14	2.961	3.183	3.183	5.808	1.830	1.285	2.31	2.381	2.116	2.265	3.030	8.389	1.957
(v+1):5	33.38, -26.33, -11.86	3.57	3.681	3.594	3.598	3.162	0.761	0.864	3.05	2.970	2.935	2.935	2.511	0.442	3.653	2.61	2.290	2.802	2.651	12.261	7.280	1.560
Average error						2.609	5.759	1.085					2.900	4.625	1.931					6.010	9.244	1.702

(b) Estimations for the parameter $\zeta_{(x,y,z)}$.

Cluster	Location x_0, y_0, z_0 (m)	2.5 GHz (4G LTE) UMa NLOS ξ	$\hat{\zeta}$ LA	$\hat{\zeta}$ OLS	$\hat{\zeta}$ GD	Error(%) LA	Error(%) OLS	Error(%) GD	28 GHz (5G NR) UMa NLOS ξ	$\hat{\zeta}$ LA	$\hat{\zeta}$ OLS	$\hat{\zeta}$ GD	Error(%) LA	Error(%) OLS	Error(%) GD	28 GHz (5G NR) NYUW(modified) ξ	$\hat{\zeta}$ LA	$\hat{\zeta}$ OLS	$\hat{\zeta}$ GD	Error(%) LA	Error(%) OLS	Error(%) GD
v:1	12.06, -31.45, 27.77	25.97	24.651	19.968	24.664	5.075	23.105	5.021	64.54	67.312	63.450	0.229	4.297	1.684	0.209	65.06	65.341	58.362	64.770	0.430	10.295	0.446
v:2	-1.28, -41.06, 3.96	36.87	37.732	40.474	36.655	2.343	9.786	0.572	73.82	61.341	75.666	4.530	16.909	2.496	2.924	59.36	57.534	60.767	59.116	3.083	2.370	0.410
v:3	14.65, 32.21, 24.91	34.33	31.601	31.115	34.298	7.955	9.369	0.096	58.70	55.753	54.591	0.035	5.019	6.993	0.061	57.25	61.741	54.942	55.952	7.843	4.031	2.267
v:4	15.81, 24.45, -29.12	32.16	33.331	35.819	31.481	3.644	11.383	2.106	60.92	60.521	63.411	0.056	0.665	4.081	0.018	68.79	70.853	74.226	68.551	2.995	7.902	0.347
v:5	-32.25, -4.64, 24.67	36.43	39.430	38.233	38.614	8.220	4.936	5.981	61.77	61.312	60.955	1.435	0.750	1.324	1.070	66.44	67.613	68.948	66.297	1.761	3.775	0.215
(v+1):1	-37.80, -21.79, -11.55	23.95	25.231	21.195	23.462	5.331	11.513	2.050	47.84	47.560	44.447	2.996	0.587	7.095	3.003	73.77	72.644	66.839	71.320	1.532	9.396	3.322
(v+1):2	-1.40, -10.27, -43.55	42.43	43.612	49.246	42.729	2.783	16.068	0.706	61.20	59.931	64.459	1.599	2.069	5.332	1.276	72.15	70.062	76.123	72.612	2.897	5.506	0.641
(v+1):3	28.33, -18.01, 28.35	33.32	34.031	29.255	34.230	2.128	12.203	2.729	56.73	55.590	52.793	3.490	2.004	6.935	2.979	65.11	70.591	64.613	64.820	8.417	0.763	0.446
(v+1):4	-32.19, 27.56, -5.05	32.36	30.740	34.484	32.317	5.021	6.548	0.148	65.56	69.261	64.634	1.285	5.642	1.415	1.262	60.05	58.890	63.124	60.718	1.932	5.118	1.113
(v+1):5	33.38, -26.33, -11.86	31.86	30.061	31.451	31.391	5.656	1.290	1.479	60.03	61.260	59.816	3.653	2.052	0.354	3.052	71.09	76.381	67.954	70.462	7.441	4.411	0.883
Average error						4.816	10.621	2.089					4.000	3.771	1.585					3.833	5.357	1.009

Table 3.4: In UMa-street canyon scenarios, for consecutive two time windows $\mathcal{T}_v$ and $\mathcal{T}_{(v+1)}$ of the management algorithm, considering a SC serving to five clusters at each window, under three methods, the estimated values for the propagation parameters are shown with corresponding estimation errors for the parameter: (a) $\beta_{(x,y,z)}$. (b) $\zeta_{(x,y,z)}$.

(a) Estimations for the parameter $\beta_{(x,y,z)}$.

Cluster	x_0, y_0, z_0 (m)	β	$\widehat{\beta}$			Error (%)		
			LA	OLS	GD	LA	OLS	GD
v:1	-21.54, -13.69, -28.07	3.28	3.161	3.401	3.363	3.919	3.408	2.244
v:2	5.23, -15.51, -41.93	3.26	3.220	2.971	3.227	1.185	8.826	0.973
v:3	-36.20, 8.66, -16.13	3.33	3.172	3.401	3.343	4.905	2.025	0.298
v:4	21.28, 34.77, -14.32	3.32	3.131	2.971	3.313	5.791	10.577	0.278
v:5	40.80, -11.67, -14.48	3.14	3.190	3.401	3.355	1.676	8.402	6.950
$(v+1)$:1	9.81, 3.06, -35.31	3.21	3.192	3.401	3.449	0.743	5.822	7.309
$(v+1)$:2	-28.38, 18.15, -30.52	3.19	3.341	2.971	3.180	4.545	7.005	0.444
$(v+1)$:3	35.17, 2.39, -20.91	3.09	3.401	3.401	3.186	10.050	10.083	3.124
$(v+1)$:4	-0.246, -25.20, -32.54	3.17	3.171	2.971	3.176	0.123	6.162	0.301
$(v+1)$:5	-42.32, -13.29, -6.19	3.08	3.201	3.163	3.222	3.792	2.591	4.500
Average error						**3.673**	**6.490**	**2.642**

(b) Estimations for the parameter $\zeta_{(x,y,z)}$.

Cluster	x_0, y_0, z_0 (m)	ξ	$\widehat{\xi}$			Error (%)		
			LA	OLS	GD	LA	OLS	GD
v:1	-21.54, -13.69, -28.07	52.22	54.361	51.051	50.406	4.102	3.470	2.235
v:2	5.23, -15.51, -41.93	63.40	63.693	63.820	68.219	0.457	7.601	0.662
v:3	-36.20, 8.66, -16.13	57.26	60.042	57.083	56.188	4.828	1.897	0.336
v:4	21.28, 34.77, -14.32	59.60	62.591	59.759	65.261	5.022	9.504	0.273
v:5	40.80, -11.67, -14.48	77.72	61.340	75.879	76.496	21.080	1.580	2.373
$(v+1)$:1	9.81, 3.06, -35.31	73.94	61.343	70.505	75.217	17.046	1.720	4.652
$(v+1)$:2	-28.38, 18.15, -30.52	58.68	56.221	58.970	62.386	4.192	6.316	0.494
$(v+1)$:3	35.17, 2.39, -20.91	67.80	62.242	66.310	62.535	8.198	7.763	2.195
$(v+1)$:4	-0.246, -25.20, -32.54	57.19	57.030	56.977	60.296	0.282	5.429	0.375
$(v+1)$:5	-42.32, -13.29, -6.19	58.14	56.251	55.916	56.862	3.259	2.207	3.834
Average error						**6.847**	**4.749**	**1.743**

error percentages for $\hat{\zeta}_{(x,y,z)}$, respectively. However, by considering the average errors, except for the case of 28 GHz UMa NLOS model, the best performance is shown by GD method for estimation of $\zeta_{(x,y,z)}$ and $\zeta_{(x,y,z)}$, accordingly.

In the case of conventional 2D models, no parameter value estimations are needed as the values given in the literature [25] and standards [109] are assumed to be correct for $\hat{\zeta}_{(x,y,z)}$ and $\hat{\zeta}_{(x,y,z)}$ where they are constant for a given SC.

Sample size or the number of frames used for averaging, N, is a very important factor to be considered from the implementation point of view and the accuracy of the estimated values. Because, less sample sizes lead to reduced overheads and also reduced window time duration values. To get a clear idea on this, average error values of the estimated parameters

(a) LTE, UMa NLOS.

(b) 5G NR, UMa NLOS.

(c) 5G NR, UMi-Street Canyon.

(d) 5G NR, NYUW (modified).
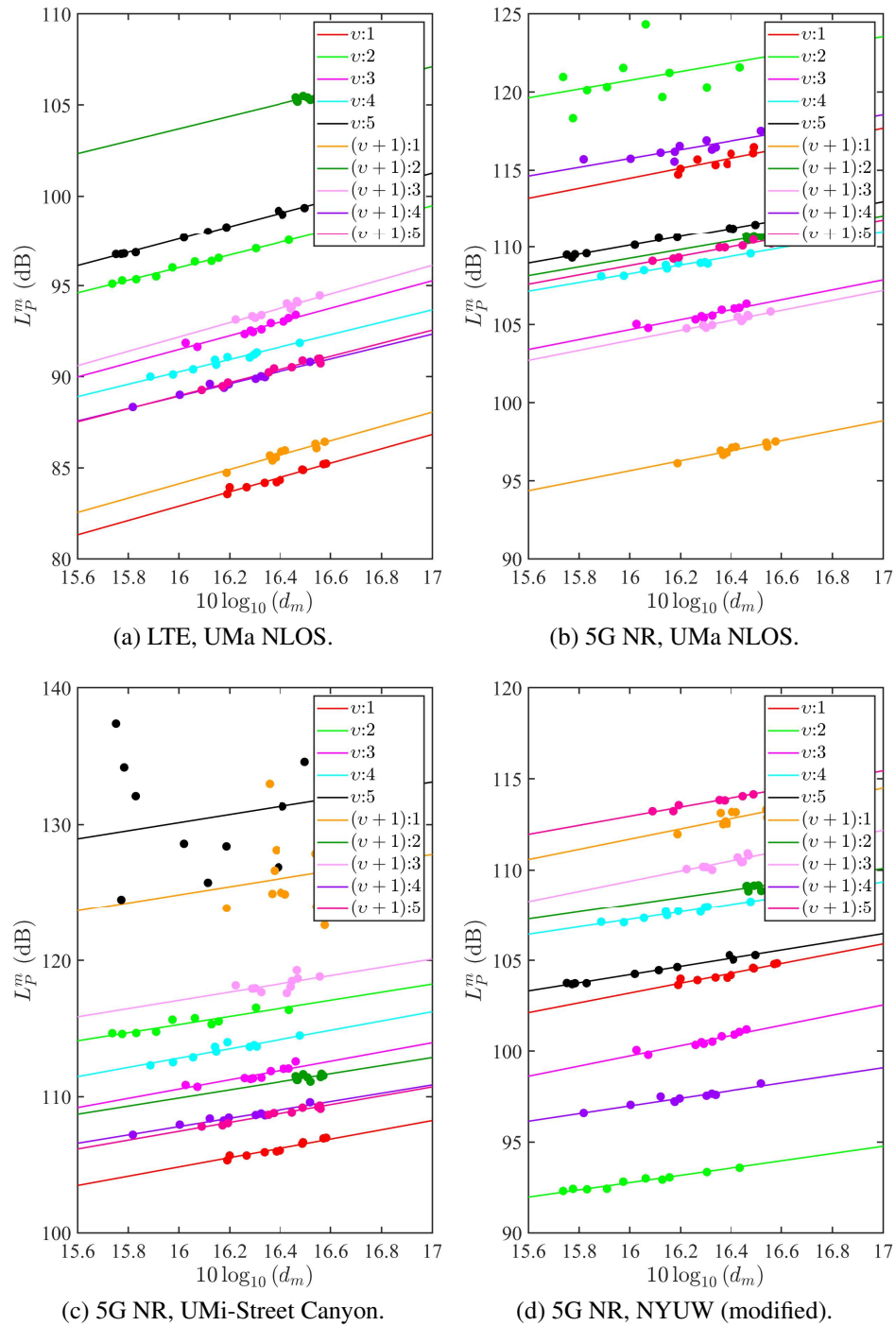
Figure 3.5: For consecutive two time windows, linear plots for parameter estimations with OLS: (a) for 2.5 GHz, 4G LTE UMa NLOS model. (b) for 28 GHz, 5G NR UMa NLOS model. (c) for 28 GHz, 5G NR UMi-street canyon model. (d) for 28 GHz, 5G NR NYUW (modified) model.
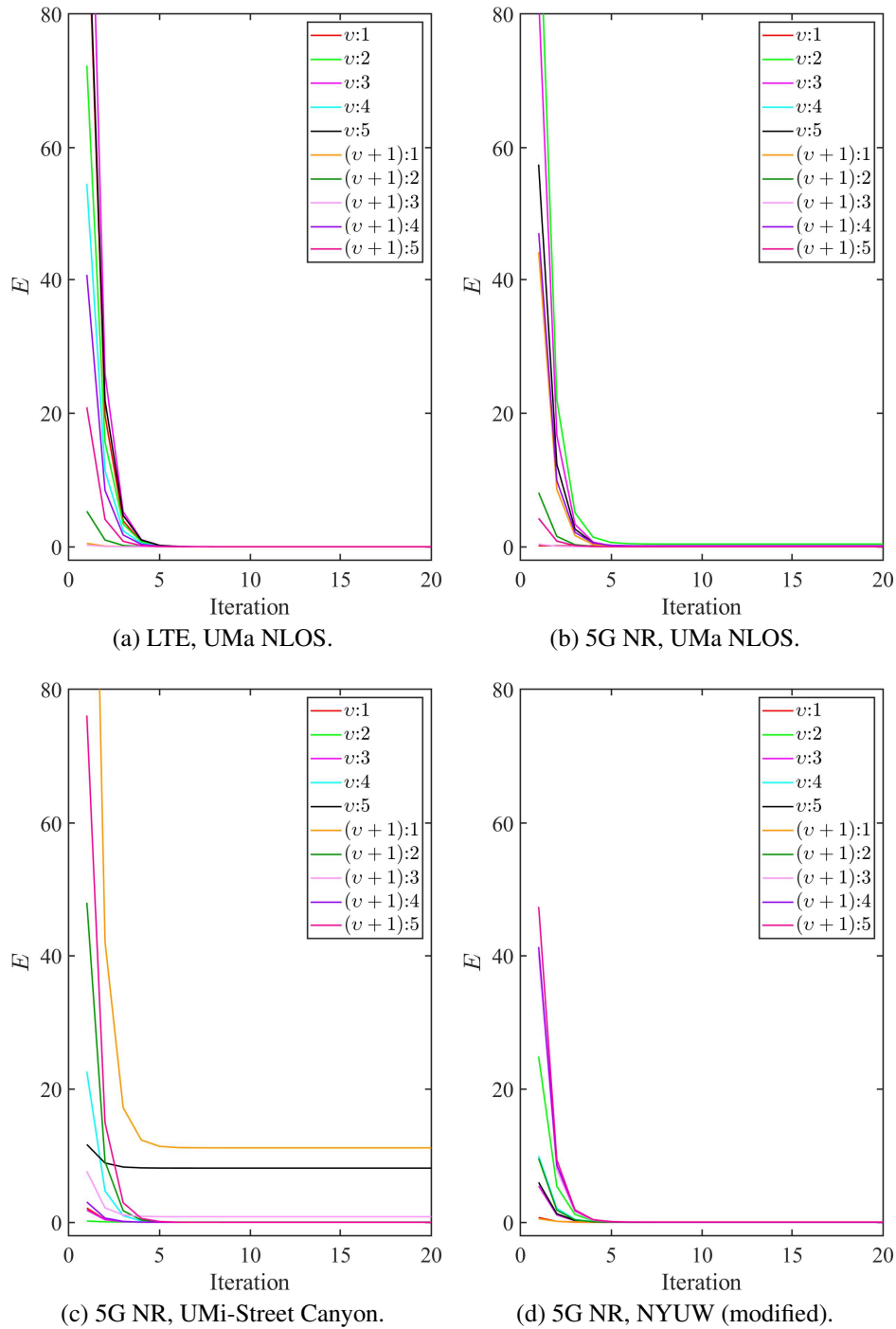
Figure 3.6: For consecutive two time windows, convergence plots of average of square error (E) for parameter estimations with GD method: (a) for 2.5 GHz, 4G LTE UMa NLOS model. (b) for 28 GHz, 5G NR UMa NLOS model. (c) for 28 GHz, 5G NR UMi-street canyon model. (d) for 28 GHz, 5G NR NYUW (modified) model.

against sample size are considered in Fig. 3.7 where the average error values against estimated parameter $\hat{\beta}_{(x,y,z)}$ and $\hat{\zeta}_{(x,y,z)}$ are shown in Fig. 3.7 (a) and Fig. 3.7 (b), accordingly. For this all the three estimation methods LA, OLS and GD are used. Based on results presented in Fig. 3.7, comparatively high stability for the results is shown for the sample size of 1,000 or more.

3.5.2   3D Communication Distance Extension and Radio Map Construction

For the purpose of 3D communication distance extension a cluster in a SC is considered where the devices are served by a BS equipped with 64 antenna element ($A = 64$) mMIMO system considering NYUW (modified).

Inverse Distance Weighting Assisted Algorithm

With the use of IDW method, variations of estimated receive power and estimated extended distance are shown in Fig. 3.8. In this case, it is assumed that path loss parameters are stable enough to be used for extrapolations within 4 m ($d_{\max} = 4$ m) from the farthest device and with $b = 4$. Furthermore, different transmit power levels in the range 24.5 - 26 dBm with estimated path loss parameter values under GD method $\hat{\beta}_{(x,y,z)} = 2.673$ and $\hat{\zeta}_{(x,y,z)} = 64.103$ are used for this part of study. The estimated receive power values at a planned receive location situated away from the farthest device is given in Fig. 3.8(a). It is shown that for a given transmit power level there is no significant variation of estimated receive power against variation of planned distance (d_P). However, there is a apparent change of estimated receive power (about 3-3.25%) with the change of transmit power level under the same estimated path loss parameter values. In Fig. 3.8(b), for $\hat{d}_e$ distances are calculated with parameters estimated with GD method and for d_e distance are calculated with ideal parameters with the use of conventional equations.

For this, a range of expected receiver power P_E values -75.86, -75.6, -75.26 and -75.08 dBm are used for corresponding transmit power values of 24.5, 25, 25.5 and 26 dBm, accordingly. For the error estimation, the maximum values are set as $e^o_{\max} = 0.4$ m and $e^a_{\max} = 0.8$ m,

Table 3.5: In outdoor-to-indoor scenarios, for consecutive two time windows $\mathcal{T}_v$ and $\mathcal{T}_{(v+1)}$ of the management algorithm, considering a SC serving to five clusters at each window, under three methods, the estimated values for the propagation parameters under different base propagation models are shown with corresponding estimation errors for the parameter: (a) $\beta_{(x,y,z)}$. (b) $\zeta_{(x,y,z)}$.

(a) Estimations for the parameter $\beta_{(x,y,z)}$.

Cluster	Location x_0,y_0,z_0 (m)	Indoor distance d_{2Din}^m (m)	2.5 GHz (4G LTE) UMa NLOS β	$\hat{\beta}$ LA	OLS	GD	Error (%) LA	OLS	GD	28 GHz (5G NR) UMa NLOS β	$\hat{\beta}$ LA	OLS	GD	Error (%) LA	OLS	GD	NYUW (modified) β	$\hat{\beta}$ LA	OLS	GD	Error (%) LA	OLS	GD
v:1	15.97, -34.52, 27.77	4.97	3.57	3.781	3.403	3.5567	6.019	4.555	0.244	3.13	3.001	2.801	2.756	4.123	10.515	11.930	2.39	2.401	2.001	2.372	0.418	16.318	0.769
v:2	-4.25, -44.93, 3.96	4.88	3.70	3.670	3.403	3.3201	0.744	7.965	10.208	2.93	3.003	2.802	2.361	2.249	4.567	19.514	2.09	2.420	2.025	2.139	15.789	4.3062	2.374
v:3	12.13, 31.85, 24.90	2.55	3.58	3.622	3.758	3.484	1.168	5.038	2.633	2.88	3.032	3.205	2.952	4.112	11.05	2.430	2.66	2.671	2.801	2.604	0.376	5.2632	2.101
v:4	12.97, 22.70, -29.12	3.32	3.63	3.691	3.403	3.5833	1.664	6.243	1.275	2.95	3.006	2.806	2.873	1.574	5.197	2.735	2.40	2.403	2.804	2.394	0.011	16.667	0.263
v:5	-35.35, -8.49, 24.67	4.94	3.82	3.553	3.924	3.8213	7.080	2.722	0.022	3.02	2.921	3.201	2.581	3.295	5.978	14.503	2.36	2.781	2.806	2.267	17.797	18.644	3.948
$(v+1)$:1	-40.50, -25.21, -11.55	4.36	3.77	3.821	3.933	3.7493	1.399	4.398	0.477	3.00	2.962	2.802	2.879	1.185	6.526	3.890	2.38	2.403	2.068	2.075	0.840	15.966	12.817
$(v+1)$:2	-4.30, -13.43, -43.55	4.28	3.82	3.580	3.403	3.5929	6.160	10.799	5.823	3.00	2.841	2.806	3.028	5.286	6.620	0.980	2.24	2.571	2.056	2.242	14.732	10.714	0.086
$(v+1)$:3	24.86, -21.53, 28.35	4.94	3.68	3.781	3.915	3.6982	2.586	6.239	0.367	2.96	3.045	2.804	2.950	1.368	5.389	0.297	2.77	2.260	2.000	2.423	18.412	27.798	12.541
$(v+1)$:4	-31.72, 28.42, -5.05	0.98	3.54	3.633	3.403	3.4741	2.603	3.813	1.804	3.14	3.016	2.802	2.878	4.535	10.899	8.415	2.31	2.461	2.726	2.208	6.493	18.017	4.420
$(v+1)$:5	34.50, -24.57, -11.86	2.08	3.57	3.701	3.640	3.5807	3.723	2.051	0.379	3.05	2.910	3.208	2.960	4.480	5.039	2.827	2.61	2.780	2.802	2.315	6.513	7.2797	11.284
Average error							3.315	5.382	2.323					3.221	7.178	6.752					8.137	14.097	5.060

(b) Estimations for the parameter $\zeta_{(x,y,z)}$.

Cluster	Location x_0,y_0,z_0 (m)	Indoor distance d_{2Din}^m (m)	2.5 GHz (4G LTE) UMa NLOS ζ	$\hat{\zeta}$ LA	OLS	GD	Error (%) LA	OLS	GD	28 GHz (5G NR) UMa NLOS ζ	$\hat{\zeta}$ LA	OLS	GD	Error (%) LA	OLS	GD	NYUW (modified) ζ	$\hat{\zeta}$ LA	OLS	GD	Error (%) LA	OLS	GD
v:1	15.97, -34.52, 27.77	4.97	59.291	55.801	62.071	59.531	5.890	4.685	0.404	84.20	61.341	81.712	83.673	27.153	2.959	0.630	84.73	66.501	91.604	86.614	21.513	8.117	2.227
v:2	-4.25, -44.93, 3.96	4.88	77.520	33.051	72.816	75.2	57.366	6.067	2.993	94.03	61.342	83.775	90.706	34.768	10.910	3.539	79.57	74.401	80.988	78.886	6.498	1.782	0.860
v:3	12.13, 31.85, 24.90	2.55	48.322	47.520	45.394	49.855	1.666	6.064	3.167	80.12	61.341	76.614	80.510	23.442	4.379	0.484	78.68	77.111	76.804	80.144	1.991	2.380	1.865
v:4	12.97, 22.70, -29.12	3.32	53.811	52.861	57.451	54.621	1.769	6.763	1.503	80.57	61.343	82.545	80.348	23.864	2.455	0.272	88.43	66.502	85.244	88.896	24.801	3.605	0.525
v:5	-35.35, -8.49, 24.67	4.94	54.090	58.223	52.381	54.194	7.637	3.158	0.194	86.47	80.570	77.245	88.007	6.823	10.668	1.778	91.14	81.630	81.664	91.990	10.431	10.393	0.937
$(v+1)$:1	-40.50, -25.21, -11.55	4.36	54.530	53.561	51.695	55.019	1.773	5.194	0.902	71.28	73.391	74.759	73.416	2.962	4.882	2.998	97.20	66.503	96.027	95.441	31.591	1.215	1.819
$(v+1)$:2	-4.30, -13.43, -43.55	4.28	67.602	67.221	73.041	71.806	0.567	8.044	6.218	81.23	78.790	79.552	80.794	3.004	2.066	0.537	92.18	83.791	92.941	90.534	9.106	0.822	1.790
$(v+1)$:3	24.86, -21.53, 28.35	4.94	49.941	48.462	46.228	49.693	2.973	7.441	0.504	82.50	61.341	84.365	81.828	25.649	2.260	0.815	90.88	89.032	96.432	89.322	2.039	6.105	1.718
$(v+1)$:4	-31.72, 28.42, -5.05	0.98	51.890	50.260	54.017	52.859	3.139	4.100	1.870	84.45	61.340	85.611	83.381	27.369	1.369	1.272	78.94	76.781	72.175	80.550	2.740	8.574	2.036
$(v+1)$:5	34.50, -24.57, -11.86	2.08	51.660	49.561	50.521	51.471	4.058	2.196	0.357	80.21	81.170	75.958	79.805	1.198	5.301	0.504	91.27	83.292	83.734	91.087	8.745	8.258	0.203
Average error							8.684	5.371	1.811					17.623	4.725	1.283					11.945	5.125	1.398

(a) Average error with $\hat{\beta}_{(x,y,z)}$.   (b) Average error with $\hat{\zeta}_{(x,y,z)}$.

Figure 3.7: Variation of average error with the estimated parameters against the sample size: (a) Estimated parameter $\hat{\beta}_{(x,y,z)}$. (b) Estimated parameter $\hat{\zeta}_{(x,y,z)}$.

respectively.

For the same cluster, using IDW method, variation of average estimated extended distance and distance estimation accuracy is shown in Fig. 3.9. As it is indicated in Fig. 3.9(a), they are observed against planned estimation distance d_P. Corresponding receive power variation used for that is given in Fig. 3.9(a). In the case of average distance, there is a apparent level of sensitivity of 2.8-2.2% for the change of transmit power in comparison against variation of planned distance. When the estimation accuracy is considered, as shown in Fig. 3.9(b), distance estimation accuracy decreases significantly against increase of planed distance. When the planned distance is about 0.5 m, an estimation accuracy of 74.75% is shown. However, there is no apparent variation i accuracy with considered transmit power levels.

Nelder-Mead Simplex Algorithm

Estimated path loss parameters with NMS algorithm is shown in Table 3.6 using transmit power value of $p_T^m = 26$ dBm, reference distance of $d_r = 1$ m and with $b = 4$. Extrapolated propaga-

(a) Variation of receive power.   (b) Variation of estimated distance.
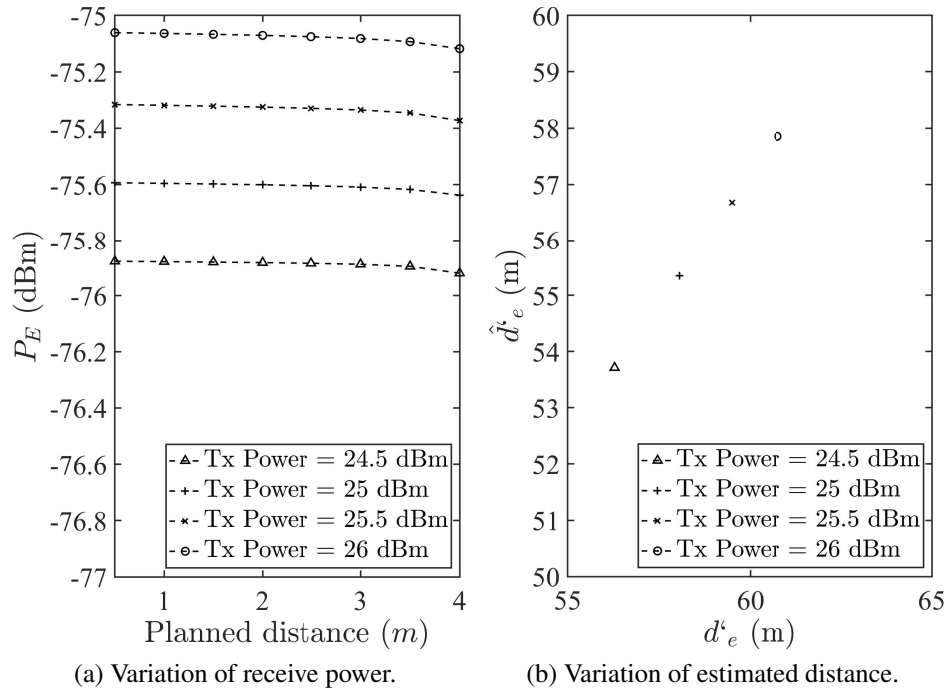
Figure 3.8: Variation of estimated power and distance at different transmit power levels: (a) Estimated receive power at a planned distance. (b) Estimated distance from the BS on the direction of farthest device.

tion parameters for extended distances of 1 m and 4 m are shown by Table 3.6(a) and Table 3.6(b), respectively. They are for two consecutive cluster deployment scenario time windows $\mathcal{T}_v$ and $\mathcal{T}_{(v+1)}$. However, these values cannot be compared against natural values as they are unknown. Further, it is assumed that the parameter values are unchanged over the predicted distance and the variations of them can be successfully captured by the NMS method.

3.6   Chapter Summary

By recognizing necessity of utilization of third spatial dimension for cellular network planning in handling cell densification, wireless connections originated from different spatial poisons in 3D space and dynamic nature of the environment, location-specific path loss estimation and coverage management for dynamic 3D SCs were done in this work. Further, real-time knowledge on path loss parameters was used for 3D communication extension or predication

(a) Average vs planned distance.   (b) Accuracy vs planned distance.
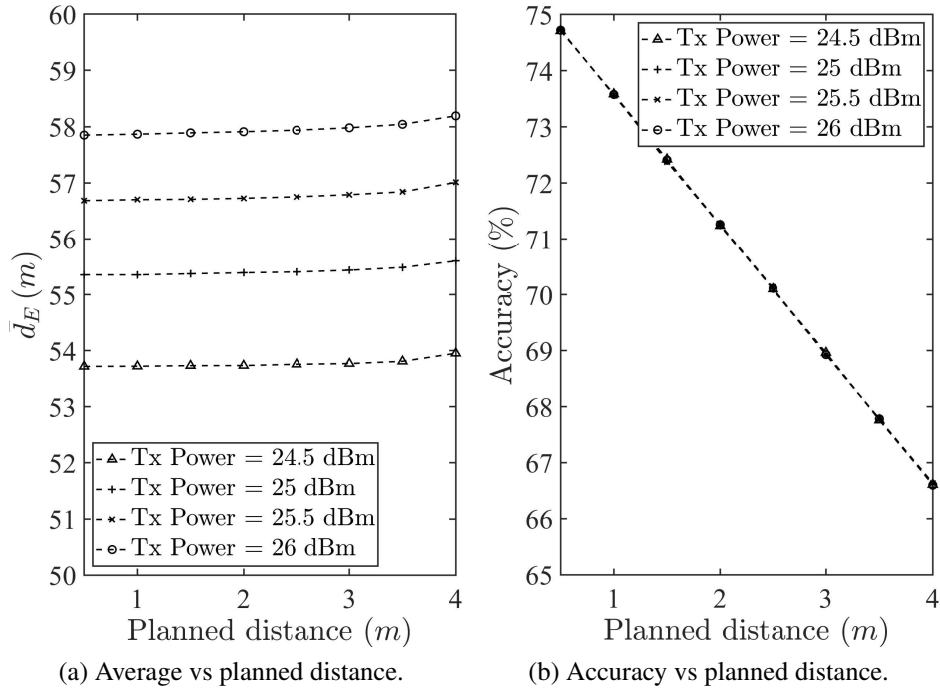
Figure 3.9: Variation of average estimated extended distance and distance estimation accuracy against planned distance: (a) Average estimated extended distance. (b) Accuracy of distance estimation.

of clusters in the SCs while facilitating for efficient radio resource management. For that, data from dynamic device clusters in a 3D SC was gathered using crowdsensing principle where a data management algorithm and supporting network architecture are also discussed in detail. In association with the data management algorithm, three methods namely, LA, OLS and GD were used to estimate path loss parameters considering 2.5 GHz and 28 GHz bands used for 4G LTE and 5G NR systems. Subsequently, IDW and NMS algorithms were used for extension of cluster border coverage and construction of RIM. In the case of 3D communication distance extension, analysis on communication distance extension and accuracy of distance estimation is also presented. Further, with the use of OLS and GD techniques, the solutions are benefited with the advantages of real-time ML techniques as well. With these outcomes of this study, radio resources of 3D SCs can be managed efficiently particularly in assigning transmit power values for the devises while maintaining seamless connectivity, QoS for the devices specially at cluster boundaries. When considering all the contributions, this study can be pronounced

Table 3.6: For consecutive two time windows $\mathcal{T}_v$ and $\mathcal{T}_{(v+1)}$ of the algorithm to capture dynamic 3D cell radio information, estimated parameter values $\hat{\beta}^E_{(x,y,z)}$ and $\hat{\zeta}^E_{(x,y,z)}$ for extrapolation of 3D communication distances from the far most device in the clusters with the extended distances: (a) 1m. (b) 4m.

(a) Parameter predictions with extension of 1m.

Cluster	x_E, y_E, z_E (m)	d_E (m)	$\hat{\beta}$	$\hat{\zeta}$
v:1	-21.09, -41.06, -4.64	46.39	3.125	57.282
v:2	-42.13, 18.61, -5.22	46.35	2.754	58.835
v:3	13.90, 20.09, -39.10	46.11	3.186	55.364
v:4	-27.78, -30.77, -21.04	46.49	2.755	61.003
v:5	18.49, -42.36, 5.25	46.52	2.521	58.881
$(v+1)$:1	14.89, 29.64, 32.12	46.18	2.972	57.565
$(v+1)$:2	-22.47, 5.89, 36.52	43.28	3.242	55.588
$(v+1)$:3	42.86, -7.79, -15.74	46.32	3.184	56.21
$(v+1)$:4	28.48, -11.12, 31.63	43.99	2.755	56.582
$(v+1)$:5	-10.73, 43.11, -9.98	45.53	2.798	50.51

(b) Parameter predictions with extension of 4m.

Cluster	x_E, y_E, z_E (m)	d_E (m)	$\hat{\beta}$	$\hat{\xi}$
v:1	-23.14, -43.11, -6.69	49.39	3.125	57.467
v:2	-44.20, 20.68, -7.29	49.35	2.754	59.041
v:3	15.78, 21.97, -40.98	49.11	3.186	54.859
v:4	-29.53, -32.52, -22.78	49.49	2.755	61.259
v:5	20.57, -44.44, 7.33	49.52	2.521	58.710
$(v+1)$:1	16.69, 31.44, 33.92	49.18	2.972	57.380
$(v+1)$:2	-24.44, 7.86, 38.50	46.28	3.242	57.961
$(v+1)$:3	44.92, -9.85, -17.80	49.32	3.184	57.360
$(v+1)$:4	30.32, -12.96, 33.47	46.99	2.755	56.725
$(v+1)$:5	-12.83, 45.21, -12.08	48.53	2.798	50.464

as an early step of designing an efficient self-configurable, environment aware and flexible 3D cellular networks.

Chapter 4

Device and Network Coordination for Opportunistic Utilization of Radio Resources in 3D HetNets

Device and network coordination is critical for efficient radio resource utilization while meeting QoS requirements in heavily congested future heterogeneous wireless networks featured with 3D SCs. Device and network coordination assisted opportunistic and coordinated use of radio resources in distinct bands could dramatically improve the spectrum utilization in these networks. In this study, overall communication performance enhancement through better utilization of opportunistically available spatially distributed radio resources in a 3D SC is addressed considering two co-located networks operated in LB and UB while jointly accounting for several related factors like 3D spatial positions and QoS requirements of the devices. To confront this problem, a device and network coordination assisted solution is developed using QL and Slotted-ALOHA (S-ALOHA) principles. Then, to maintain performance standards, device and network coordination aided scheduling, power control and access prioritization schemes are discussed. Subsequently, a RBL-assisted algorithm is presented for the UB to optimally utilize radio resources. In these solutions, both device-network and network-network

78

interactions are considered. In the results, an overall coordination efficiency of even over 75% is shown at the initial iterations for the scenarios with the highest device density while demonstrating attractive performance.

4.1 Introduction

With the emergence of IoE and ongoing industry transformation, it is expected that billions of machines and sensors will be connected to Internet through wireless networks, leading to a radical paradigm shift from the rate-centric enhanced mobile broad-band services of yesteryears to an information-centric, ultra-reliable, low latent, intelligent, communication and computing services [129, 130]. In contrast to physical objects in the definition of IoT, encompassing four components namely things, processes, data and people are honored as the key contributors in the definition of IoE in upcoming communication systems [5, 131]. On this path towards a smart world, even the number of conventional IoT devices are expected to grow by hundreds of billions by 2030 [130] exerting an enormous pressure on the wireless infrastructure facilities to cope with dense wireless SCs using scarce radio resources in an efficient manner than ever before. Due to massive number of devices, their priority and QoS requirements, design and operation of wireless networks have become increasingly challenging tasks. In the emerging complex HetNets environment, 3D network rollout aspects [10] together with device and network coordination schemes are to be thoroughly studied for better utilization of critically limited radio resources.

With the increase of network densification and service diversification, there is a significant hike in the number of devices seeking network access through always scarce radio resources in a densely dispersed 3D space. In addition, due to the limitations of the radio resources in the LB, UB is also recognized as a source of opportunistically accessible radio resources for the cellular networks [132] while sharing it with other non-cellular network users [133]. Furthermore, these spatially distributed location-specific radio resources [15] are to be utilized

more accurately and even better than in 2D networks avoiding the assumption used to develop techniques for the 2D networks that the radio resources are constant over the third spatial dimension. On the other hand, devices are with disparate operational conditions and QoS needs while intensely competing for the radio resources and network access. In this case, it is necessary to have more informative device and network coordination assisted mechanisms for systematic exploration of the third spatial dimension for service effective coverage planning, radio resource management, reduction of access delays and meeting the QoS aspects of the devices in an efficient and effective manner in the future HetNets.

One of the key initiatives in device and application prioritization mechanisms is to introduce a distributed scheduling and multiple access mechanism with a basic prioritization option for the devices [134]. However, most of these schemes are not supported with at least the simplest device and network coordination schemes like error feedback algorithms [135]. Moreover, these primary prioritization and feedback schemes have not identified the potential contributions they could have received from the transmit power control mechanisms [136]. In this case, even though these prioritization schemes have evolved up to the 5G NR networks [137], no connection can be seen between device prioritization and the initial transmit power of the devices.

One of the historical milestones on device and network coordination for initial radio resource allocation for wireless channels is marked with the introduction of ML aided S-ALOHA schemes to solve random access channel (RACH) congestion problem in 2012 [138] where the coordination is established with DL coordination farms. Subsequently, this solution is further improved with QL leading to sub-optimum solutions [139, 140]. RACH access in UL is the first occasion where radio resources become opportunistic for the devices seeking communication in the LB. Since, future 3D networks [10] are going to be service and application oriented, information centric, well-coordinated intelligent entities, it is necessary to consider device prioritization, QoS and 3D location-specific radio resource information within the initial device and network coordination scheme along with any of the radio resource utilization processes.

However, in some studies, 3D spatial positions of the devices are considered in certain problems like UL power control for UAVs aided communications [141].

Traffic offloading to UB through opportunistic utilization of radio resources [17, 142, 143] using NR-U [142] and LTE-Unlicensed (LTE-U) [144] concepts is a very common solution for the problem of scarcity of radio spectrum in the LBs rather than employing spectrum sharing and cognitive radio (CR) concepts [145, 146]. To get a much fair understanding, random access and coordinated scheduling schemes for UL of a LTE license-assisted access (LAA) system are also to be compared without accounting for channel access delays [17, 143]. Moreover, to support this traffic offloading concept, total throughput of both DL and UL channels of a NR-U system is maximized while ensuring fair coexistence with a WiFi network in a study done by Huang *et al.* [142]. Moreover, listen before talk (LBT) options are also employed for resource utilization in NR-U in the presence of different wireless networks [147]. In another approach, solutions to mitigate the aliasing effects caused by pseudo paths in 5G NR and NR-U networks are proposed by Wang *et al.* [148].

The main difference between the solutions presented in this study and radio resource utilization in CR [149, 150] is that the opportunistic radio resource utilization algorithms discussed in this study focus on how to use the 3D spatially distributed radio resources rather than to decide whether a particular frequency band can be used for communication or not. Furthermore, availability of a frequency band is opportunistic in CR [149, 150] and channel access is opportunistic in the solution analyzed in this study. Moreover, in the solutions of this investigation, attention is paid to 3D spatial domain utilization of radio spectrum. In many of the solutions presented with RBL [58] and other learning techniques [132, 133, 144, 151] for dynamic radio resource management in LTE-U in 2D networks are highly inefficient as they don't consider 3D spatial distribution of location-specific radio resources and avoid device access prioritization needs in utilization of radio resources for the UL channel access problem.

Other than the timely demand on 3D SC networks, this work is highly motivated by a number of other reasons as well. First, the need of a mechanism to account for different priority

requirements of the data types, services and devices in future 3D SC HetNets by recognizing their 3D location-specific properties and radio resources. There should be enough provisions to represent numerous types of physical parameters (e.g., altitude of a device), QoS needs and priority requirements (e.g., priority for mission critical data) in physical or MAC layer problem formulation, enabling them to be accounted for subsequent solutions. Secondly, the necessity of having a more efficient and fast channel access mechanisms leading to low latent and reliable networks. Prominent delays in the networks are in the areas of grant acquisition (5 ms), random access (9.5 ms), transmit time interval (1 ms), signal processing (3 ms), packet retransmission (8 ms) and core network/Internet (vary vastly) [27, 94] where random access mechanisms are with significantly high delays. Furthermore, most of the algorithms in cellular networks are executed at the BSs resulting not only large waiting times for RACH access and radio resource utilization [17, 143] but also heavy UL access interference as well [152, 153]. These delays can be reduced with the use of intelligent, proactive, independent and coordinated devices and algorithms. Thirdly, to support radio resource and interference management by utilizing opportunistically available radio resources in different networks operated in distinct frequency bands. Forth factor is to promote environment and situation aware, self-configurable technical background for future intelligent HetNets consisting of proactive devices.

In the past, there had been less device density in the 3D space due to the small number of devices and low flying objects [33, 154] leading to have comparatively low demand for the radio resources. Under that condition, there was no significant scarcity of radio resources where many of the challenges and motivations discussed in this study were not at the forefront of designing cellular wireless networks. With the increase in device density and the demand for high throughput rates, it was compelled to use high frequency bands with reduced communication distances for the cellular networks, leading to dense SCs. In this environment, radio resources are going to be extremely scarce and they are to be very carefully used. However, even under this situation, with 2D network design and operation principles, on most occasions approximate site-specific path loss parameters are used for the allocation and utilization of ra-

dio resources. Then, in a highly dense environment and with these approximate parameters, the errors and performance degradation caused due to inaccurate and inefficient use of radio resources are not going to be negligible anymore. As a solution for this problem, the third spatial dimension is suggested to be used for cellular network planning and radio resource management together with spatially distributed location-specific path loss parameters, leading to have better performing 3D SC HetNets through efficient and much accurate use of radio resources.

4.1.1 Technical Challenges

There are several challenges to overcome in achieving highly efficient communication in 3D SC HetNets. These challenges include, coordinated use of location-specific opportunistic radio resources in a precise and efficient manner, management of channel access [31, 32] while minimizing access collisions and relevant delays (i.e., increase of access probability through mitigation of collisions), and avoidance of access attempts for already allocated radio resources. Due to addition of uncoordinated massive number of heterogeneous devices, these challenges are still at the forefront of future wireless network designs. The situation becomes even worse as machine type devices can continuously compete for limited radio resources in a small 3D space, even risking connections for the most needed devices.

4.1.2 Proposed Solution

This study is developed based on the overall objective of efficient utilization of opportunistically available LB and UB radio resources in 3D cellular networks through device and network coordination while prioritizing the requirements of the devices and their associated services by identifying some of them as location-specific 3D spatially distributed parameters. Here, device and network coordination is defined by inclusion of two background interaction processes in supporting the main communication viz. the interaction between devices and the serving BS or the access point (AP) and inter-network interaction or interaction between co-located BS and AP. In addition, several congested locations in a SC are identified as critical areas (e.g., opera-

tion theaters) where some of the nearby devices are facilitated to use historical data on devices and services at those regions during the process of channel access. To successfully achieve the objective of this study, device and network coordination assisted learning based schemes are developed as the solutions by using principles of QL [57], S-ALOHA [155] and RBL [58]. Moreover, these solutions are capable of accounting for multiple prioritization needs of the devices operated in both LB and UB even addressing conventional RACH access problem in congested environments. The success of the solutions is evaluated using several performance metrics like overall coordination efficiency, sum weighted volume capacity, network access delay and channel occupancy. Furthermore, solutions are with several general advantages like capacity to be operated in real-time, fast convergence and less processing power consumption as well.

4.1.3 Technical Contributions

The contributions of this study are identified in numerous directions in addressing problems related to 3D radio resource utilization through device and network coordination while accounting for QoS and access prioritization needs of the devices. Compared to all the existing work, this study well adheres to the definition of a fully functional 3D network by inclusion of the four main components within the design and implementation phases. Then, the main contributions are summarized as:

- In order to maintain performance standards and in meeting QoS aspects we introduce device network coordination assisted scheduling, transmit power control and prioritized access granting schemes. In contrast to conventional approaches, 3D spatial positions of the devices and several other related factors are used in these schemes to achieve better performance. Several challenges like maximizing the access probability and minimizing waiting time for prioritized devices are also addressed with this solution.

- To expedite the process of UL RACH access and to increase the utilization efficiency

of opportunistic 3D radio resources on LB and UB, device and network coordination assisted learning algorithms are presented. When comparing against the previous studies, simultaneous access of LB and UB 3D radio resources is considered with the inter network and inter device-network coordination. Same time, challenges of increasing the situation awareness, fast adaptation to the environment and coordinated use of opportunistic radio resources are also addressed. With this approach, for the LB 66.42% coordination efficiency for the first iteration and 50% less time for the full frame occupancy over regular schemes are achieved. The results for the same performance metrics related to UB are 76% and 50%, respectively.

- In order to further enhance the utilization efficiency of opportunistic 3D radio resources in UB, a RBL algorithm is discussed while addressing the challenges of making the devices more proactive and ensuring use of UB radio resources in a fair manner. With this solution, nearly 16% more sum volume capacity value is achieved over ordinary schemes.

- For the purpose of implementation, functional protocols are discussed for the operations of the devices, BSs, algorithms and mechanisms used in UB and UB networks while addressing the challenges related to data and information exchange among different entities.

4.2 System Model and Problem Formulation

A deployment setup of three 3D SCs of a multi layer 3D cellular network is shown in Fig. 4.1. Each SC is with randomly dropped M devices indexed with m and they are served by a BS in the center of the cell where every BS is co-located with a WiFi AP as well. In this case, BSs are with the capacity to handle both 5G NR and NR-U traffic through LB and UB, respectively. Even though, the solutions presented in this study are highly compatible with the LTE [156] and LTE-U [144] systems, they are not considered in the system model as they are going to
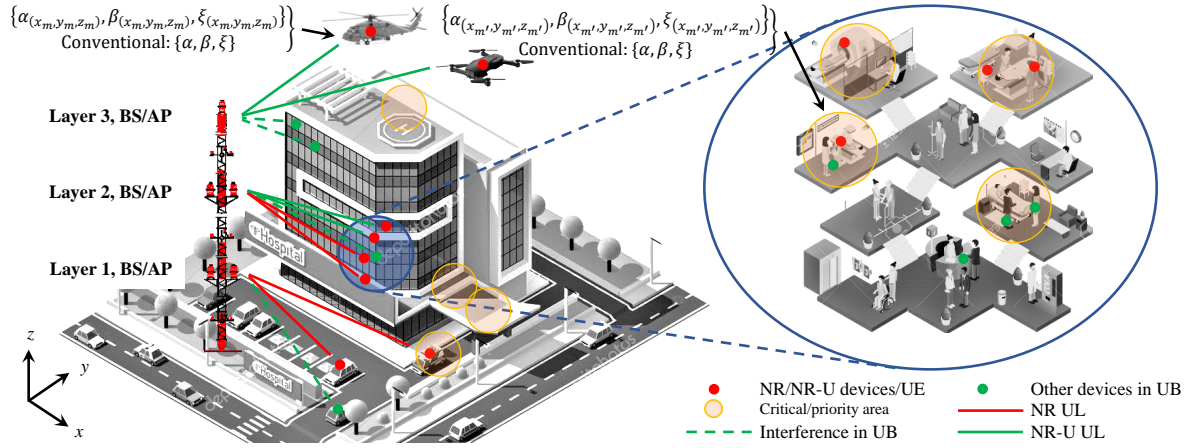
Figure 4.1: Deployment setup of three layers of a 3D cellular network created with three 3D SCs with 5G NR BSs capable of handling LB and UB links.

be obsolete and fully replaced with 5G NR and NR-U systems in the near future. In addition, considering the simplicity of the presentation and the study, only the middle cell is considered for the subsequent derivations and calculations. Some of the important symbols those are used in the system model and problem formulation together with some of the performance metrics are summarized in Table 4.1.

Fading channel for the device m is modeled as $|h_m|^2 = |h_m^{\mathrm{f}}|^2 10^{\frac{-L_m^{\mathrm{P}}}{10}}$, $h_m^{\mathrm{f}} \sim \mathcal{N}_{\mathrm{c}}(0, 1)$, with path loss L_m^{P}, $L_m^{\mathrm{P}} = \alpha_{(x,y,z)} + 10\beta_{(x,y,z)} \log_{10}(d_m) + \xi_{(x,y,z)}$ dB [25] where h_m^{f} is the fading channel coefficient for the device m at distance d_m, $d_m = \sqrt{x_m^2 + y_m^2 + z_m^2}$. Here, (x_m, y_m, z_m) are the Cartesian coordinates for the location of the same device. Floating intercept, line slope parameter and lognormal shadowing for the path loss model are given by $\alpha_{(x,y,z)}$, $\beta_{(x,y,z)}$ and $\xi_{(x,y,z)}$, accordingly [15]. Site-specific path loss parameters used in conventional 2D networks are not indexed with Cartesian coordinates as they are considered to be constant for a particular cell. Then, corresponding site-specific parameters for $\alpha_{(x,y,z)}$, $\beta_{(x,y,z)}$ and $\xi_{(x,y,z)}$ are given as α, β and ξ [25], accordingly. However, based on the scenario, there are certain provisions to model shadowing parameter as a sub-region or sub-site specific parameter [25]. For the simplicity of the presentation, these location-specific and frequency dependent path loss parameters [15] are not indexed with the frequency band. In Fig. 4.1, location-specific path loss parameters and common site-specific path loss parameters based on conventional methods are marked. How-

Table 4.1: Summary of Symbols and Performance Metrics Used in the System Model and Problem Formulation

Symbol	Definition
d_m	Distance to device m in 3D space
d_r	Radius of the SC
h_m	Channel coefficient for device m including path loss
h_m^{f}	Fading channel coefficient for device m
k	Index for a time slots in a frame
p_s^m	UL transmit power of device m with control step s
$p_{s,\mathrm{R}}^m$	Receive signal power at device m at time t
$p_{s,\mathrm{R}}^{m'}$	Instantaneous interference from device m' to the BS
$t_{\min}/t_{\max}$	The minimum/maximum UL transmission time allowed for a device
t_q^m	UL transmit time of device m with control step q
t_{U}	Total time allocated for UL transmission
(x_m, y_m, z_m)	3D or (x, y, z) Cartesian coordinates for device m
$x[t]$	One of the symbols in a sequence sent by a device
$y_m[t]$	Receive signal at device m at time t
$w_{(x,y,z)}^m / w_{(x,y,z)}^{N_w,m}$	Normalized weighting factor of device m/Weight N_w of device m
$C_{\mathrm{E},t}^V$	Sum volume capacity enhancement
C_m^V	Throughput volume capacity of device m
$C_{\min}^V$	The minimum volume capacity required by a device
$C_{\mathrm{Sum}}^{\mathrm{W},V}$	Sum weighted volume capacity
$C_{\mathrm{Sum},t}^{\mathrm{Par},V}/C_{\mathrm{Sum},t}^{\mathrm{Seq},V}$	Sum volume capacity at iteration t with sequential/parallel band utilization
$C_{\mathrm{Sum},t}^V/C_{\mathrm{Sum},t}^{\mathrm{R},V}$	Sum volume capacity at iteration t with the proposed/reference method
$E_{\mathrm{C},t}/E_{\mathrm{OC},t}$	Coordination efficiency/Overall coordination efficiency
$I_{\max}$	Maximum interference limit for a device
$K/\mathcal{K}$	Number/Set of time slots in a frame
L_m^{P}	Path loss for device m
$M/\mathcal{M}$	Number/Set of transmit devices of the SC
$M_{\mathrm{U}}/\mathcal{M}_{\mathrm{U}}$	Number/Set of access granted devices in the UB
N_w	Number of weights considered
O_t/O_t^{R}	Frame occupancy at iteration t with the proposed/reference method
$O_t^{\mathrm{Para}}/O_t^{\mathrm{Seq}}$	Frame occupancy at iteration t with parallel/sequential band utilization
$\mathcal{P}$	Transmit power values set
$P_{\min}/P_{\max}$	The minimum/maximum UL transmission power allowed for a device
$Q/\mathcal{Q}$	Number/Set of transmit time steps
$S/\mathcal{S}$	Number/Set of transmit power steps
W	Bandwidth of the radio link
$\alpha_{(x,y,z)}/\alpha$	Location/site-specific floating intercept for the path loss model [15]
$\beta_{(x,y,z)}/\beta$	Location/site-specific line slope parameter for the path loss model [15]
$\xi_{(x,y,z)}/\xi$	Location/site-specific lognormal shadowing for the path loss model [15]

ever, both locations of the devices and the path loss parameters related to those locations are assumed to be known. It is considered that the channel is constant over a period of a frame and the channel information can be estimated perfectly.

In addition, a finite set of critical or priority areas are also considered where they are created by identifying the requirements of the applications, data types and the devices. Operation theaters, fire routes and entrances to emergency rooms in hospitals are some of the examples for them. Based on the applications, devices in and nearby those areas may need stable radio links, access prioritization and maintenance of high QoS standards. Then, those devices are facilitated to use historical data from the network during the processes of channel access, initial resource allocation and algorithm training while reducing information processing and channel access delays. In this case, it is reasonable to be considered that certain device related characteristics are also 3D spatially distributed parameters.

The observed receive signal at time t, $y_m[t]$, with AWGN $\eta[t]$, $\eta[t] \sim \mathcal{N}_c\left(0, \sigma^2\right)$, due to signal transmitted from device m is given as $y_m[t] = \sqrt{p_s^m} h_m x[t] + \eta[t]$. Power of the symbol $x[t]$ is normalized to unity as $\mathbb{E}\left[x[t]^2\right] = 1$ and p_s^m is the UL transmit power of the device m with power control step s. Since noise and signal are uncorrelated, the receive signal power $p_{s,\mathrm{R}}^m$ is given as

$$p_{s,\mathrm{R}}^m = |y_m[t]|^2 = \underbrace{p_s^m\, |h_m|^2}_{p_{s,m}^{\mathrm{RC}}} + \eta^2. \tag{4.1}$$

In practice, receive signal strength is measured including noise power η^2 and it cannot be further purified to get only $p_{s,m}^{\mathrm{RC}}$. In this case, $p_{s,\mathrm{R}}^m$ is used as the receive signal power for the subsequent calculations. Then, throughput volume capacity C_m^V of device m is given by $C_m^V = \frac{W}{\pi d_r^3}\log_2\left(1 + \frac{p_{s,\mathrm{R}}^m}{\sum_{m' \in \mathcal{M}\backslash m} p_{s,\mathrm{R}}^{m'} + \eta^2}\right)t_{\mathrm{U}}$ [157, (36)] where W, d_r, $\mathcal{M}$ and t_{U} are bandwidth of the radio link, radius of the SC, set of devices in the SC and the time allocated for UL transmission, respectively. Since 3D SCs are considered for this study, in contrast to 2D cellular network

designs, volume capacity is used as a performance metric where it is defined as the throughput capacity for a given unit volume in 3D space. Then, the maximum interference limit $I_{\max}$ for the instantaneous interference $p_{s,\mathrm{R}}^{m'}$ is established as

$$p_{s,\mathrm{R}}^{m'} \leq I_{\max}. \tag{4.2}$$

4.2.1 Data Prioritization in 3D Networks

A brief overview of a very high-level architecture of a 3D SC HetNet containing a set of co-located UB enabled SC BS and AP combinations is given in Fig. 4.2. This architecture is developed based on already available network architecture development principles [158, 159]. The coordination operations are managed by the UB enabled BS and the coordination interaction between each BS-AP pair is given by double-headed dashed arrows. In this network, types of data associated with the devices are considered as the prioritization factor for them. There could be mission critical data like real-time information exchange within a tele-surgery at lower layer and control data of an UAV at a higher layer. Delays related to them should be minimized while increasing the reliability of the transmissions [27].

In this multilayer 3D SC network, layer 1 or the ground level BSs, APs and associated devices are with the lowest elevation. Basically, all the devices on the ground are included to this layer. BSs, APs and associated devices with highest elevation are referred to the layer n or the top layer. There can be several other layers in between layer 1 and n based on their separation distance.

For a given device in a certain altitude, different types of data are expected in numerous quantities where they are handled under four sequential stages explained as

1. Classification: Data is classified on arrival using the headers from multimedia to control and emergency data. Then they are placed on temporary buffers.
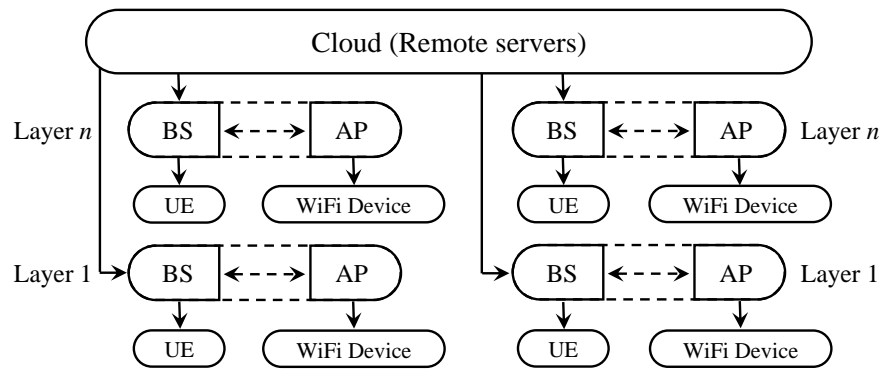
Figure 4.2: Overview of the 3D SC network with co-located BSs and APs.
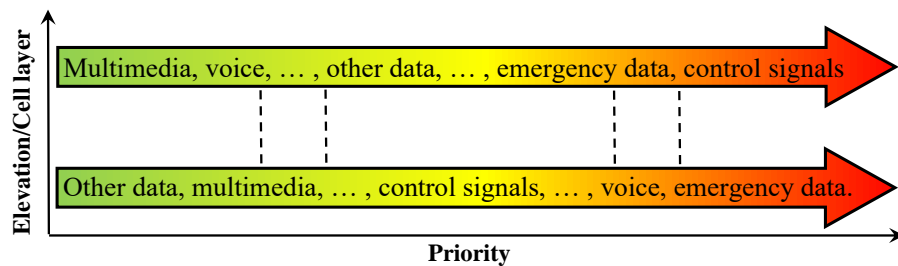
Figure 4.3: Data prioritization policy considering equal volume for each category.

2. Quantification: The quantity of data is determined based on the time a temporary buffer of a device is being held "full". If the duration is high, it is considered that the volume that data is also high.

3. Prioritization: Data is prioritized considering data volume, importance of data, elevation of the device and availability of radio resource in an alternative band as given in Fig. 4.3. Priorities could be varied according to elevation of a device as well.

4. Queuing: Data is buffered until been transferred to the BS.

Based on this approach, 3D spatial distribution of different services, their QoS needs and priority requirements are well recognized.

4.2.2   Medium Access with Opportunistic Radio Resources

The devices are allowed to connect to the BS using frame based S-ALOHA scheme [140]. There are K slots in a frame indexed with k where a device can bid for any kth slot or sub-

frame in that data frame. Even though the LB is allocated for a particular operator and then to a cell through frequency planning, availability of time slots are entirely opportunistic for the devices during the process of UL RACH access. Initially, all the devices are allowed to access the UL time slots of the LB. Once all the time slots are filled, accessing the opportunistically available radio resources in UB is initiated. Within the final study scenario, devices are allowed to access both bands in parallel.

4.2.3   Decisions with Weighted Volume Channel Capacity

In selection of devices to grant channel access, weighting factors are collectively defined by the devices and the BS as $w^m_{(x,y,z)} = \frac{\left(w^{1,m}_{(x,y,z)} + w^{2,m}_{(x,y,z)} + \cdots + w^{N_w,m}_{(x,y,z)}\right)}{N_w}$ where there are N_w weights for the device m at (x, y, z). These weights are adjusted by the BS based on the priority requirements of the devices. As an example, $w^{1,m}_{(x,y,z)}$ can be proportionately adjusted according to the altitude of a device z_m. Let $w^{2,m}_{(x,y,z)}$ be adjusted according to priority of data which is defined using current or historical data related to the nearest critical area as given in the horizontal arrows in Fig. 4.3. $w^{3,m}_{(x,y,z)}$ can be based on availability of an alternative band for communication. If a band is available, the weight is set to 0 and some other value otherwise. In this way prioritized channel access problem is converted to a RACH access problem supported with weighted volume channel capacity values.

4.2.4   Problem Formulation

There are two main components of the problem viz. acquisition of opportunistic radio resources in any of the bands and efficient utilization of radio resources in UB. With the first problem, devices face the same RACH access problem.

Acquisition of Opportunistic Radio Resources

In this study the problem of performance enhancement through better utilization of opportunistically available spatially distributed radio resources in a 3D SC HetNet is addressed.

Conventionally, in LB, it is known as RACH access congestion or RACH access problem. In this study, radio resources in both LB and UB are utilized for the same problem while jointly accounting for several other important communication related factors like 3D spatial positions of the devices, their priority needs and the data types.

Efficient Utilization of Radio Resources in UB

In contrast to LB, UB is with a greater flexibility in varying both transmit power and time for communication. In this case, problem of efficient use of opportunistically available UB radio resources for communication is addressed while deviating from LB. For that, an optimization problem is formulated to maximize the sum weighted volume capacity $C_{\text{Sum}}^{\text{W},V}$ of a SC considering those radio resources as variables subject to a set of constraints:

$$\underset{p_s^m, t_q^m}{\text{maximize}} \quad C_{\text{Sum}}^{\text{W},V} = \sum_{m=1}^{M_{\text{U}}} w_{(x,y,z)}^m C_m^V \tag{4.3a}$$

$$\text{subject to} \quad t_q^m \geq t_{\min}, \quad \forall m \in \mathcal{M}_{\text{U}} \tag{4.3b}$$

$$p_s^m \geq P_{\min}, \quad \forall m \in \mathcal{M}_{\text{U}} \tag{4.3c}$$

$$p_s^m \leq P_{\max}, \quad \forall m \in \mathcal{M}_{\text{U}} \tag{4.3d}$$

$$C_m^V \geq C_{\min}^V, \quad \forall m \in \mathcal{M}_{\text{U}} \tag{4.3e}$$

$$t_q^m \leq t_{\max}, \quad \forall m \in \mathcal{M}_{\text{U}} \tag{4.3f}$$

$$p_{s,\text{R}}^{m'} \leq I_{\max}, \tag{4.3g}$$

where M_{U} and $\mathcal{M}_{\text{U}}$ are the number and the set of access granted devices in UL of the UB, accordingly. Transmit time with time control step q for the device m is given by t_q^m, $q \in Q$ where Q, $Q = \{1, 2, \ldots, q, \ldots, Q\}$, is the set of time steps with the highest step Q. The lower and the upper limits for t_q^m are controlled by (4.3b) and (4.3f) with the minimum and the maximum allowed UL transmission times $t_{\min}$ and $t_{\max}$, accordingly. Similarly, the lower and the upper limits for p_s^m are managed with (4.3c) and (4.3d) with the minimum and the maximum

allowed UL transmission power values $P_{\min}$ and $P_{\max}$, respectively. QoS needs are maintained by (4.3e) with $C_{\min}^V$ where $C_{\min}^V$ is the minimum volume capacity that the device m is required to achieve. Furthermore, interference to the BS from the other devices is controlled with (4.3g) as discussed in (4.2).

There are several purposes for addressing these problems. Some of them include facilitation of fast channel access for the devices, better serving their applications with enhanced sum volume capacity values and guaranteeing QoS through efficient radio resource management. The technical challenges associated with these problems include exchanging information among waiting devices, selection of the best devices to grant channel access, utilization of location-specific and other related information to get priority in communication, and utilization of opportunistically available UB in a fair and efficient manner.

4.3   Coordinated Learning Schemes for Opportunistic Radio Resources Utilization

Mainly, the principles of RL are used in developing device and network coordination assisted solutions for the problems of efficient radio resource management in 3D SCs. Their proven performance for real-time operations over conventional approaches, even without prior knowledge on the environment [140] is the main reason to select them. Since they are with the property of fast adaptability to the operational environment, these model-free, less complex algorithms are capable of quickly converging to sub-optimal solutions within a limited number of iterations. In addition, less amount of energy, processing power and device memory are required by them while leading to the best solutions under model unaware complex environments like the HetNet 3D SCs considered in this study. In this case, these RL based solutions are identified as very effective, stable and efficient approaches over conventional methods and even data driven learning techniques. When compared to traditional dumb and reactive wireless devices, the devices equipped with these solutions become intelligent and proactive equipment. A summary

of symbols, functions and notations used in the solutions developed in this study is given in Table 4.2.

Table 4.2: Summary of Important Symbols, Functions and Notations Used in the Solutions

Symbol	Definition
$d_{\max}^C$	The maximum allowed distance from a device to the center of the nearest critical area
d_C^m	Distance from device m to the center of the nearest critical area
$\{i, k\}$	State-action pair
l	Game round or iteration in RL
r_t	Reward at time t
s_m	Power step by self estimated device priority level
s_C	Power step recommended by the BS
$\mathcal{A}_m$	Action set of device m in RL
$C_{\max}^V$	The maximum volume capacity of the SC
C_{tar}^V	Volume capacity target for the RL algorithm
C_{CAvg}^V	Average volume capacity for the SC
$\mathcal{G}$	RL game
$\mathcal{I}_S$	Set of states in QL
$\mathcal{K}_A$	Set of actions in QL
L	Total game rounds or iterations
$L_m^{P,L}$	Path loss in LB
$L_m^{P,U}$	Path loss in UB
$M_D / \mathcal{M}_D$	Number/Set of devices detected
$Q_t(i, k)$	Q-value at iteration or time t
$Q^*(i, k)$	The optimum Q-function
$Q^{\pi_{QL}}(i, k)$	Q-function with policy π_{QL}
$R_{(x,y,z)}(m, k)$	Reward function at a particular 3D spatial position
$R_C(k)$	Penalty for a collision
$\mathbf{R}_C$	Congestion report
γ	Discount factor
λ	Learning rate
$\pi_m(l)$	Probability value set for RL algorithm for the elements in $\mathcal{P}$ for the device m after game round l
$\pi_s^m(l)$	Probability for RL algorithm for the element s in $\mathcal{P}$ for the device m after game round l
π_{QL}	Action selection policy for QL
$\pi_{QL}(i)$	The Best action for any state i
$\mathbb{1}_c$	Indicator function with condition c

4.3.1 Device and Network Coordination

To establish device and network coordination, a DL broadcast frame is sent on the LB at the end of each UL frame [138, 140]. In contrast to conventional approaches, not only information on the occupancy of UL time slots but also information on device and network coordination like instructions and data on switching the band, initial power control and critical areas are also sent to the devices through the same frame. In addition, a co-located AP is used to establish co-ordination among wireless cellular NR, NR-U and WiFi networks. For accessing the UB also, the devices are coordinated through another DL broadcast information frame sent through the LB. Instructions on managing the transmission of the AP are sent to it by the BS as indicated by the double-headed dashed arrows in Fig. 4.2 according to the basic network coordination principles [158, 159]. To utilize radio resources in the UB, a duty cycle based periodic access mechanism is suggested for the UL of the NR-U system. Communication through the AP is disabled for WiFi devices when the duty cycle is on for the mobile cellular devices that are seeking network access through NR-U UL transmissions.

In certain scenarios, the devices are allowed to access both bands simultaneously, however, not by the same device. To avoid undue collisions, transmission of an UL frame by any of the devices on any of the bands is allowed only through an empty slot found after listening to a DL broadcast frame. Critical or priority areas are determined by the BS using historical data on both networks. Information related to these areas is shared with the devices enabling them to be used by both devices in those areas and the BS, appropriately.

By using a DL broadcast frame, one of the main challenges in data exchange is mitigated. With the availability of location-based data through this frame, challenges of situation and location awareness, and fast adaptation to the situation and the environment are successfully addressed.

4.3.2 Q-learning with Network Coordination

In this study, a coordinated QL scheme is suggested as a solution for the RACH access problem in 3D SCs while efficiently utilizing the opportunistic radio resources. This solution is further improved by jointly considering the device prioritization schemes and location-specific information. Compared to conventional algorithms [140], time slots are granted based on $w^m_{(x,y,z)} C^V_m$ with the assistance of initial transmit power control.

This QL algorithm, a model-free RL scheme, is developed based on the agent-environment relationship with the action-reward function given by a Q-table [57, 140] where this environment can be described by a Markov Decision Process (MDP). At each time-step in this MDP, an agent in state i takes an action $k \in \mathcal{K}_A$ trying to maximize own reward at time t given by r_t and reaching the next state i', $\{i, i'\} \in \mathcal{I}_S$, under a certain transition probability where $\mathcal{I}_S$ and $\mathcal{K}_A$ are the sets of states and actions, accordingly. Considering a certain action selection policy π_{QL} and state-action pair $\{i, k\}$, Q-function and the optimum Q-function are given as $Q^{\pi_{QL}}(i, k)$ and $Q^*(i, k) = \max_{\pi_{QL}} Q(i, k)$, respectively. The action is selected based on the highest Q-value as $\pi_{QL}(i) = \arg \max_k Q(i, k)$. Then, the Q-value at iteration or time $t + 1$ could be updated as

$$Q_{t+1}(i, k) \leftarrow (1 - \lambda)Q_t(i, k) + \lambda\left\{r_t + \gamma \max_{k'} (Q_t(i', k'))\right\}, \tag{4.4}$$

where λ, $\{i', k'\}$ and γ are the learning rate, next state-action pair and the discount factor, accordingly.

In this QL solution, device m is allowed to select time slot k and Q-value is updated at the end of each frame as

$$Q_{t+1}(m, k) = Q_t(m, k) + \lambda(R(m, k) - Q_t(m, k)), \tag{4.5}$$

where reward function is defined as

$$
R_{(x,y,z)}(m,k) = \begin{cases} \dfrac{w^m_{(x,y,z)} C^V_m}{C^V_{\text{CAvg}}} & \text{success,} \\[2mm] -R_{\text{C}}(k) & \text{otherwise.} \end{cases}
\tag{4.6}
$$

C^V_{CAvg} and $R_{\text{C}}(k)$ are the average volume capacity for the cell and penalty for a collision due to simultaneous packet access, respectively. When there are K time slots, the congestion report is defined as $\mathbf{R}_{\text{C}} = \frac{1}{M}\left[R_{(x,y,z)}(m,1), R_{(x,y,z)}(m,2), \dots, R_{(x,y,z)}(m,k), \dots, R_{(x,y,z)}(m,K)\right]$ and sent with the DL broadcast frame. As it is explained in Fig. 4.4, for the time slot or sub-frame k, $R_{\text{C}}(k)$ is set to 1 when the slot is not assigned to a device. With this design, challenges of minimization of collision in devices accessing the channel simultaneously, avoidance of accessing already occupied slots and undue congestions caused by continuously attempting machine type devices are addressed.

Multi-factor Prioritization Scheme for Access Granting

Even though the devices and services are prioritized, solutions cannot be implemented if the link quality is neglected. In this case, to allocate time slots for the devices, a multi-factor, weighting assisted, situation aware, location dependent prioritization policy is used while considering QoS aspects. For this strategy, to determine the weighting factors given as $w^m_{(x,y,z)}$, necessary information is sent to the BS by the devices with bids for time slots. In the absence of current data, these weights are calculated based on the historical data provided by the devices operated at the same location previously. A device in the vicinity of a critical area has the option to use the most favorable set of data from historical or current data sets. In order to a device to be get qualified for this process, condition that the distance from that device to the center of the nearest critical area d^m_{C} should be less than or equal to the maximum allowed distance $d^{\text{C}}_{\text{max}}$ is to be fulfilled as indicated by $d^m_{\text{C}} \le d^{\text{C}}_{\text{max}}$.

As it is indicated in Fig. 4.4, there may be situations where a given time slot is accessed by a single device, more than one device or no device with sufficient receive signal power enabling

UL Frame

DL Coordination Fame

C C C C C C I C I C C R_C I I C I I R_C C C C C I C C C C

☐ Free   ☐ Occupied $\boxed{I}$ Initial value $\boxed{R_C}$ Penalty $\boxed{C}$ Capacity

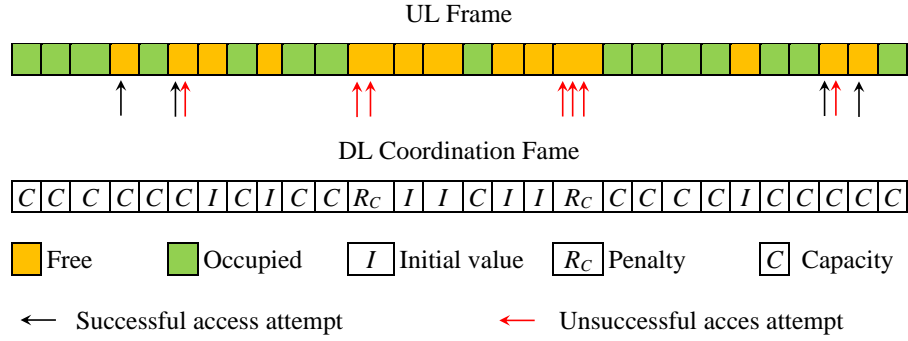← Successful access attempt   ← Unsuccessful acces attempt

Figure 4.4: RACH attempts in UL frame no l and corresponding DL broadcast coordination frame used for the QL scheme.

the devices to be detected at the BS. In a case of multiple devices bidding for a time slot, there may be a situation where more than one or more devices are detected for that particular vacant slot. In that kind of situation, the prioritization scheme is used to grant the slot to the device with the highest weighted volume capacity $w_{(x,y,z)}^m C_m^V$. If there are two or more devices with the same $w_{(x,y,z)}^m C_m^V$ value, access is given based on z_m. However, if those devices are in the same height, access is granted to a randomly selected device. If no device is identified, no action is needed. If one device is detected, access would be granted to that device. Subsequently, the congestion report is generated accordingly. If an alternative band is not available for a device, high priority is given for that device through weighting trying to secure a band and a time slot for that device.

With this scheme technical challenges of getting priority for certain devices and avoidance of long waiting times to get channel access are successfully addressed. In other words, attractive solutions are provided for the challenges of access delay minimization and access probability maximization for prioritized devices.

Scheme for Transmission Device Power Adjustment

To determine the initial transmission power, both current 3D location-based and historic prioritization information are considered. As it is explained in Algorithm 7, if a device is in the close vicinity of a critical area, it is allowed to select the highest transmit power value out of s_m and

s_C at the first attempt itself. Here, s_m and s_C are the power control step selected according to self estimated device priority level and power control step recommended by the BS, respectively. The step s_C is based on the historical data on the location and that information is passed to the devices through the DL broadcast frame as a part of device and network coordination. All the other occasions, power control step index s is incremented by one ($s \leftarrow s + 1$) while increasing p_s^m. This process is continued until channel access is granted. Transmit power values set $\mathcal{P}$ is given as $\mathcal{P} = \{p_1, p_2, p_3, \ldots, p_s^m, \ldots, p_S\}$ with $\mathcal{S} = \{1, 2, 3, \ldots, s, \ldots, S\}$, $S = |\mathcal{P}|$, and with the highest transmit power p_S. This approach is with a clear difference compared to many of the open-loop or closed-loop gradual power control mechanisms used at the devices, particularly in determining initial transmission power values [160, 161]. Moreover, this solution enables the devices to reach the most suitable initial transmit power values quickly and efficiently. In addition, with the congestion report, instructions are sent on transmit power adjustments based on the interference limits given in (4.2). In LB, after receiving access, devices are allowed to adjust the power levels based on the same principle until the maximum safe limits are reached. Flowcharts for the operations of the devices and the BSs are given in Fig. 4.5. Functions related to the transmission process at a device and the BS are explained in Fig. 4.5(a) and Fig. 4.5(b), respectively.

4.3.3 Communication in UB

In this solution, use of UB is considered as a form of utilization of opportunistically available radio resources for communication when and only when the LB time slots are fully occupied. Furthermore, simultaneous access attempts or connections to the UB enabled BS through both bands by the same device are also not allowed. Due to frequency dependent nature of the path loss characteristics, a separate set of location-specific values is expected for the path loss parameters in the UB [15]. In addition, this band cannot be fully occupied by the devices operated through NR-U channels and should be shared with the other wireless networks like WiFi [151] in a fair manner.

Algorithm 7: Algorithm for Device Initial Transmit Power

1: **Initialization**
2: Obtain s_C from the last DL broadcast frames
3: Calculate distances to the nearest congestion point d_C^m
4: **if** $d_C^m \leq d_{max}^C$ **then**
5:      **if** $s < \max\{s_C, s_m\}$ **then**
6:         Update $(s \leftarrow \max\{s_C, s_m\})$, p_s^m
7:      **else**
8:         Update $(s \leftarrow s + 1)$ under (4.3d) and (4.3e), p_s^m
9:      **end**
10: **else**
11:      **if** $s < s_m$ **then**
12:         Update $(s \leftarrow s_m)$, p_s^m
13:      **else**
14:         Update $(s \leftarrow s + 1)$ under (4.3d) and (4.3e), p_s^m
15:      **end**
16: **end**

(a) Operations at the devices.   (b) Operations at the BSs.
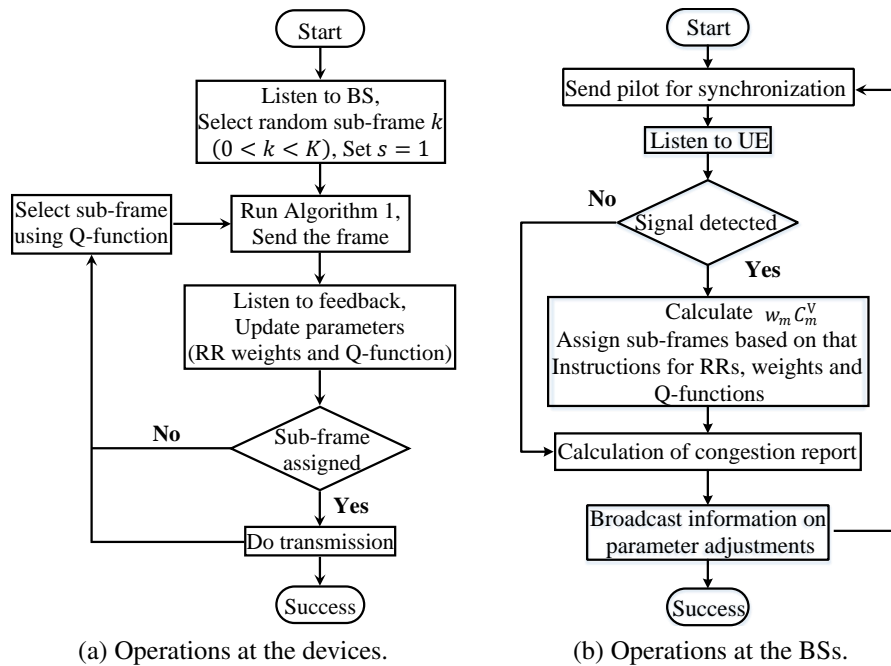
Figure 4.5: Flowcharts for operations at devices and BSs: (a) Functions at devices on transmission and parameter adjustments. (b) Operations at a BS on data reception and parameter calculations.

In this scenario also, devices are allowed to make the decision on accessing the channel using the QL algorithm and to select the most suitable transmit power values using Algorithm

7. In conventional approaches, UB channel access is entirely managed by UB enabled BSs where there were no proactive devices [132]. This band is accessed and used according to the time division duplex (TDD) frame of the same length as of LB using a NR-U interface and a duty cycle where the structure is presented in Fig. 4.6. Percentages of duty cycles are allocated based on the amount of WiFi traffic available at that occasion through the co-located WiFi AP where higher the WiFi traffic lower the duty cycle percentage for communication through the NR-U interface. Furthermore, NR-U operation is coordinated by the AP by switching on and off the WiFi transmissions appropriately. For the simplicity, access beacons or the guard frames are not discussed. Each TDD frame is capable of serving a number of devices as indicated by different colors. At the start, all the devices are allocated with equal time durations. In this study, a heavily congested environment is considered where there are more than or equal number of devices than the number of slots in a frame.

Once access is granted, to get the optimum utilization of opportunistic radio resources, time durations allocated for the devices are dynamically adjusted using device and network coordination. That would lead to unevenly allocated time durations for the devices at the point of convergence based on their performance. In contrast to conventional LB operations, in this method devices get the opportunity to adjust both transmit time and power to reach a sub-optimum solution for the optimization problem presented in (4.3a) using RBL principles [58].

To implement this solution, the RBL game $\mathcal{G} = \left\{ \mathcal{M}_U, \{\mathcal{A}_m\}_{\{m \in \mathcal{M}_U\}}, \left\{ w^m_{(x,y,z)} C^V_m \right\}_{\{m \in \mathcal{M}_U\}} \right\}$ is developed considering (4.3a).

- **Players:** Device set $\mathcal{M}_U$ in the SC is defined as the players. A game round or an iteration l is played by each player m, $m \in \mathcal{M}_U$.

- **Actions:** The action set $\mathcal{A}_m$ is defined for player m as $\mathcal{A}_m = \left\{ p^m_s, t^m_q \right\}_{\{s \in \mathcal{S}, q \in Q\}}$ where the action can be changed over iterations. For the round l, player m is allowed to select transmission power p^m_s, $p^m_s \in \mathcal{P}$ and t^m_q, $q \in Q$. If current weighted capacity is greater than the that of previous the previous iteration, time allocation is increased by one division as $(q \leftarrow q + 1)$ and vice versa while guaranteeing a minimum amount for each
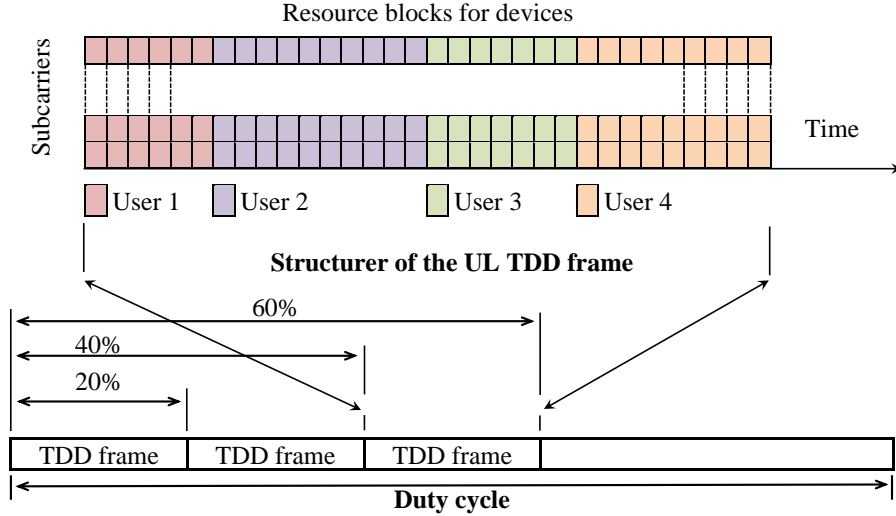
Figure 4.6: Duty cycle for the UL of the devices operated in the unlicensed band.

user. Similarly, all the players in the cell are facilitated to select their own transmission power values under equal opportunity conditions. In a occasion where $C_{\text{Sum}}^{\text{W},V} < C_{\text{tar}}^{V}$ or $w_{(x,y,z)}^{m} C_{m}^{V} < \{C_{\text{min}}^{V}\}$, s is increased by one leading to an increment in p_{s}^{m} to maintain the QoS requirements. C_{tar}^{V} is the target capacity. Further, adjustments for p_{s}^{m} is subjected to a set of constraints and the probability function as well.

- **Utility function:** Weighted volume capacity of the device m at a given location $w_{(x,y,z)}^{m} C_{m}^{V}$ is used as the utility function.

Probability value set for the elements in $\mathcal{P}$ after game round l of total rounds L is given by $\pi_{m}(l)$. $\pi_{s}^{m}(l) \in \pi_{m}(l)$, $\pi_{m}(l) = \{\pi_{1}^{m}(l), \pi_{2}^{m}(l), \dots, \pi_{S}^{m}(l)\}$, is the probability of achieving volume capacity target C_{tar}^{V} for p_{s}^{m}. Since sum weighted volume capacity of a cell is optimized, cell level values are used to update the probability function. When $s = s'$, $s' \in \mathcal{S}$ and with $\pi_{s}^{m}(l)$, $\pi_{s'}^{m}(l + 1)$ is given [58] as

$$\pi_{s'}^{m}(l + 1) = \pi_{s'}^{m}(l) + \tau(l)g_{m}(l)(\mathbb{1}_{\{s'=s\}} - \pi_{s'}^{m}(l))\mathbb{1}_{\{C_{\text{Sum}}^{\text{W},V} < C_{\text{tar}}^{V}\}}, \ \forall s' \in \mathcal{S}, \tag{4.7}$$

where C_{max}^{V} is the maximum volume capacity that the SC can achieve after iteration l with $\tau(l) = \frac{1}{l+1}$ and $g_{m}(l) = \frac{C_{\text{max}}^{V} + C_{\text{Sum}}^{\text{W},V} - C_{\text{tar}}^{V}}{2C_{\text{tar}}^{V}}$. $\mathbb{1}_{c}$ is the indicator function with condition c. $p_{s}^{m}(l + 1) = p_{s}^{m}$

is chosen with $s = \arg\max\limits_{s' \in \mathcal{S}} \left(\pi_{s'}^m(l) \right)$ followed by an increment in time with $(q \leftarrow q + 1)$ for the next iteration $t_q^m(l + 1) = t_q^m$. The process of optimization and strategy of the game $\mathcal{G}$ are explained in Algorithm 8 and the complete operations on the UB is managed by Algorithm 9.

Algorithm 8: Algorithm for Sum Weighted Volume Capacity Optimization

---

1: **Initialization**
2: Determine UL slots in UB for devices, set $C_{\max}^V$ and C_{tar}^V.
3: **Initialization; $\mathcal{G}$:**
4: Set $\pi_s^m(0) = \frac{1}{S}$, $\forall s \in \mathcal{S}$, $\forall m \in \mathcal{M}_U$.
5: **for** $l = 1, 2, 3, ..., L$ **do**
6:     **for** $m = 1, 2, 3, ..., M_U$ **do**
7:         Execute the action $\mathcal{A}_m$, Calculate $C_{\text{Sum}}^{W,V}$.
8:         **if** (4.2) **then**
9:             **if** $C_{\text{Sum}}^{W,V} > C_{\text{tar}}^V$ and (4.3e) **then**
10:                 Update (4.7), Select $p_s^m(l + 1) = p_s^m$, $s = \arg\max\limits_{s' \in \mathcal{S}} \left(\pi_{s'}^m(l) \right)$.
11:             **if** (4.3b) **then**
12:                 Update $(q \leftarrow q + 1)$, t_q^m.
13:             **end**
14:             **else**
15:                 **if** (4.3d) **then**
16:                     Update $(s \leftarrow s + 1)$, p_s^m.
17:                     **if** (4.3f) **then**
18:                         Update $(q \leftarrow q - 1)$, t_q^m.
19:                   **end**
20:               **end**
21:             **end**
22:         **else**
23:             **if** (4.3c) **then**
24:                 Update $(s \leftarrow s - 1)$, p_s^m.
25:             **end**
26:         **end**
27:     **end**
28: **end**

Over iterations, convergence of the game $\mathcal{G}$ is expected to be achieved reaching the convergence equilibrium for all $m \in \mathcal{M}_U$ and $\{s \in \mathcal{S}, q \in \mathcal{Q}\}$ with $\pi_s^m(l) > 0$ [58]. This is under the assumption, that the game has at least one equilibrium under pure strategies. In contrast to equilibrium achieved in game theory [58], the equilibrium achieved in the RBL can be unstable over time under considerably dynamic environmental conditions. In this kind of situation,

---

Algorithm 9: Algorithm for Communication in UB

1: **Initialization**
2: Set initial values for the Q-tables, transmitters.
3: **repeat**
4:    Coordinate with WiFi network, determine duty-cycle.
5:    Switch off the WiFi AP as of the duty-cycle.
6:    **repeat**
7:       **repeat**
8:          Execute the process in Fig. 4.5 in UB for NR-U.
9:       **until** *Convergence*;
10:       Run Algorithm 8.
11:    **until** *WiFi traffic flow is stable*;
12: **until** *LB is full*;

---

again the agents can achieve new convergence equilibrium under new conditions. In this case, with RBL, always convergence equilibrium is expected giving sub-optimal solution for the optimization problem.

4.3.4 Device and Network Coordination for Simultaneous Operation of LB and UB

In order to further reduce channel access delays while improving utilization efficiency of opportunistically available radio resources, a device and network coordination based approached is introduced for simultaneous use of LB and UB. In this solution, the challenge of coordination of wireless cellular and WiFi networks is mitigated by using a co-located BS and a WiFi AP. The challenge of making the devices more proactive is mitigated by allowing them to select an appropriate time slots by themselves using the same QL algorithm. This decision is further supported with information provided by the BS on availability of time slots on either bands. However, the same device is not permitted to access both bands at the same time. As it is explained in Fig. 4.7, an integrated DL coordination frame is used to provide data for the Q-tables of the devices. This frame is designed combining information from both bands and transmitted it through the LB.

Step by step operations related to device and network coordination in allocation of time

slots in LB and UB is explained by Algorithm 10. In this algorithm, the number of devices detected, the set of detected devices and the set of time slots in a frame are given by M_D, $\mathcal{M}_\text{D}$ and $\mathcal{K}$, respectively. $L_m^\text{P,L}$ and $L_m^\text{P,U}$ are used to represent the path loss values for the device m in LB and UB, accordingly. In this scheme also, the vacant slots are assigned to the device based on the prioritization scheme. For a given instance, when both LB and UB are available, the algorithm is capable of coordinating the devices and the two networks to assign the band with the minimum path loss to the device with the highest weighted volume capacity and the remaining band to the device with the second highest weighted volume capacity irrespective of the bands that the devices attempted to access the channel.

4.4   Simulation Results

A spherical SC of approximate radius of 20 m is considered where the BS is at the center of it. This is the layer 2 SC in Fig. 4.1 containing 10 critical or priority areas where each of them is 4 m in radius. The maximum allowed distance from a device to the center of the nearest critical area d_max^C is also set to 4 m. The devices are with the maximum and the minimum transmit power values of 2.6 dBm and 26 dBm, respectively where there are discrete power control steps in between them. The threshold power value for the cell coverage P_E is set to -90 dBm.

For the path loss model, parameter values for the LB operated in the 28 GHz band are set as $61 \leq \alpha_{(x,y,z)} \leq 72$, $2 \leq \beta_{(x,y,z)} \leq 2.8$ and $\xi_{(x,y,z)}^m \sim \mathcal{N}\left(0, \sigma_\text{PL}^2\right)$ where σ_PL, $\sigma_\text{PL} = 8.7$, is an estimated random value based on the location [15]. Values for the same set of parameters used in the UB operated in 6 GHz band are specified as $31.4 \leq \alpha_{(x,y,z)} \leq 34.7$, $3.49 \leq \beta_{(x,y,z)} \leq 3.85$ and $\xi_{(x,y,z)}^m \sim \mathcal{N}\left(0, \sigma_\text{PL}^2\right)$ with $\sigma_\text{PL} = 4$, accordingly [15]. All the parameters are made sensitive to vertical angle in the range of 0° - 90° (i.e., $z \geq 0$) by randomly selecting the parameters including the LOS scenarios [15, 25]. However, for the vertical angle in the range of -90° - 0° (i.e., $z < 0$) LOS is not allowed. TDD data frames of 10 ms are used for the 5G NR and NR-U transmissions with 100 time slots or sub-frames. The algorithms are implemented at the BS

Algorithm 10: Algorithm for Device and Network Coordination in Allocation of Time Slots in LB and UB

1: **Initialization**
2: Devices: Set $s = 1$, Set initial values for Q-tables, $Q(k', m) = \frac{1}{K}$, $\forall m \in \mathcal{M}$, $\forall k \in \mathcal{K}$
3: BS: Opens LB and UB, set duty cycle percentage, send DL coordination frame
4: **repeat**
5: $\quad$ Devices: Run Algorithm 7, set p_s^m
6: $\quad$ Devices: Select the band with min $\left\{L_m^{\text{P,L}}, L_m^{\text{P,U}}\right\}$ and k, $k = \arg\max_{k' \in \mathcal{K}} (Q(k', m))$, $\forall m \in \mathcal{M}$, access the channel
7: $\quad$ **for** $k = 1, 2, 3, ..., K$ **do**
8: $\quad\quad$ BS: Listen to devices, check for LB or UB parallel slots, detect symbols in slots
9: $\quad\quad$ **if** *Already allocated* **then**
10: $\quad\quad\quad$ BS: Include $\frac{w_{(x,y,z)}^m C_m^V}{C_{\text{CAvg}}^V}$ with (4.6) to the relevant slot/s in the DL coordination frame
11: $\quad\quad$ **else if** *Empty* **then**
12: $\quad\quad\quad$ BS: Set value 0 to the relevant slot/s in the DL coordination frame
13: $\quad\quad$ **end**
14: $\quad\quad$ **if** *Collision detected in LB and UB* **then**
15: $\quad\quad\quad$ BS: Include $-R_{\text{C}}(k)$ with (4.6) to the relevant slots in the DL coordination frame for LB and UB
16: $\quad\quad$ **else if** $M_D > 0$ **then**
17: $\quad\quad\quad$ **if** *Collision detected in LB or UB* **then**
18: $\quad\quad\quad\quad$ BS: Include $-R_{\text{C}}(k)$ with (4.6) to the relevant slot in the DL coordination frame for LB or UB
19: $\quad\quad\quad\quad$ BS: Estimate $L_m^{\text{P,L}}$ or $L_m^{\text{P,U}}$ for available band, calculate $w_{(x,y,z)}^m C_m^V$, $\forall m \in \mathcal{M}_D$
20: $\quad\quad\quad\quad$ BS: Assign the slot in available band to m, $m = \arg\max_{m' \in \mathcal{M}_D} \left(w_{(x,y,z)}^{m'} C_{m'}^V\right)$
21: $\quad\quad\quad\quad$ BS: As in (4.6), include $\frac{w_{(x,y,z)}^m C_m^V}{C_{\text{CAvg}}^V}$ to the corresponding slot in the DL coordination frame for LB or UB
22: $\quad\quad\quad$ **else**
23: $\quad\quad\quad\quad$ BS: Estimate $L_m^{\text{P,L}}$ and $L_m^{\text{P,U}}$, calculate $w_{(x,y,z)}^m C_m^V$, $\forall m \in \mathcal{M}_D$
24: $\quad\quad\quad\quad$ **if** $M_D \geq 2$ **then**
25: $\quad\quad\quad\quad\quad$ BS: Assign LB and UB slots (Sequence: low to high $L_m^{\text{P,L}}$ and $L_m^{\text{P,U}} \leftarrow$ device highest to lowest $w_{(x,y,z)}^m C_m^V$)
26: $\quad\quad\quad\quad\quad$ BS: Include $\frac{w_{(x,y,z)}^m C_m^V}{C_{\text{CAvg}}^V}$ with (4.6) to the relevant slots in the DL coordination frame for LB and UB
27: $\quad\quad\quad\quad$ **else**
28: $\quad\quad\quad\quad\quad$ BS: Assign the slot from the band with min $\left\{L_m^{\text{P,L}}, L_m^{\text{P,U}}\right\}$
29: $\quad\quad\quad\quad\quad$ BS: Include $\frac{w_{(x,y,z)}^m C_m^V}{C_{\text{CAvg}}^V}$ with (4.6) to the relevant slot in the DL coordination frame for LB or UB
30: $\quad\quad\quad\quad$ **end**
31: $\quad\quad\quad$ **end**
32: $\quad\quad$ **end**
33: $\quad$ **end**
34: $\quad$ BS: Send DL coordination frame
35: $\quad$ Devices: Listen to BS, update Q-tables
36: **until** *Convergence*;
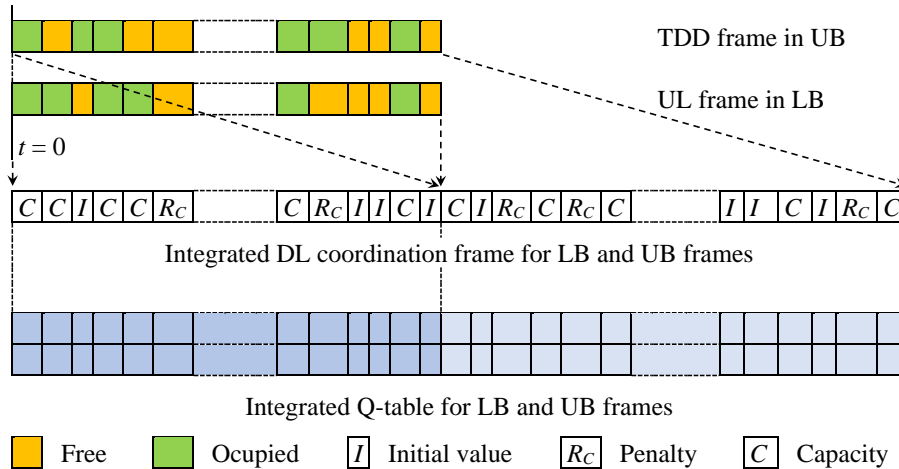37: Run Algorithm 8

Figure 4.7: Integrated DL coordination frame and integrated Q-table used in devices for the LB and UB frames started at the same time instance when the devices are allowed to access both bands simultaneously.

and the collaborative devices based on the assumption that all the devices, BS and servers are properly synchronized with no additional core network or processing delays. Default learning rate for the QL algorithm is set to $\lambda = 0.1$ unless otherwise it is mentioned.

In calculating weighted capacities, three prioritization weighting factors $w_{(x,y,z)}^{1,m}$, $w_{(x,y,z)}^{2,m}$ and $w_{(x,y,z)}^{3,m}$ are considered representing operating height of the devices, user data criticality and availability of alternative band for communication. The minimum and the maximum limits for each weighting factor are set as of 0 and 1 with five intermediate levels. For the first weighting factor, weights are assigned proportionately to the altitudes of the devices. In the second weighting factor, the data carrying control or emergency information is given the highest priority by allocating the highest weights. For the third weighting factor, weight of 1 is assigned when there is no alternative band available for communication and 0 when there is an available band. As an example, if the channel access attempt is on UB and if the LB is fully occupied, weight 1 is assigned. If still there are some vacant slots in the LB, no weight is added in favor of that device.

4.4.1 Evaluation of Coordination Efficiency

Three simple performance metrics namely coordination efficiency $E_{C,t}$, sum volume capacity enhancement $C_{E,t}^V$ and overall coordination efficiency $E_{OC,t}$ are used to further evaluate the performance enhancement due to device network coordination. In all these metrics, performance is evaluated with respect to the same iteration of a reference solutions and they are defined as $E_{C,t} = \frac{O_t - O_t^R}{O_t^R} \times 100\%$, $C_{E,t}^V = \frac{C_{Sum,t}^V - C_{Sum,t}^{R,V}}{C_{Sum,t}^{R,V}} \times 100\%$ and $E_{OC,t} = \frac{E_{C,t} + C_{E,t}^V}{2} \times 100\%$. Here, O_t, O_t^R, $C_{Sum,t}^V$ and $C_{Sum,t}^{R,V}$ are frame occupancy at iteration t with the proposed solution, frame occupancy at iteration t under reference method, sum volume capacity at iteration t with the proposed solution and sum volume capacity at iteration t under a reference method, respectively.

4.4.2 Communication in LB

In accessing UL radio channel and radio resource allocation, performance of the coordinated QL-assisted S-ALOHA algorithm for numerous device distribution densities is given in Fig. 4.8. Convergence of the algorithm for weighted sum volume capacity values is shown in Fig. 4.8(a) where corresponding volume capacity values are given in Fig. 4.8(b). Here weighted sum values are used as a performance measure for decision making in assigning time slots or allocation of resources where values without weights are used as a performance measure for the system. In addition, the difference between with and without prioritization scheme [140] is a performance measure for the efficiency of the improved device and network coordination assisted solutions suggested in this study. The results for device densities of 20, 60 and 100 (or more) are investigated. Generally, sum volume capacity values are increased with the increase of number of devices until the maximum number is reached. Channel access interference and packet collisions are reduced due to two reasons. First reason is that the devices have to listen to the broadcast message containing congestion report and other information before sending access request messages. Second reason is that the channel access time slots are selected based on the learning algorithm. Dee to these reasons, comparatively better or faster convergence

is shown by the algorithm with device prioritization mechanism compared to the reference method [140].

Performance of QL schemes with and without prioritization scheme for the cell is shown in Fig. 4.9. Occupancy of the sub-frames or slots with $\lambda = 0.1$ is shown in Fig. 4.9(a). Fast occupancy is indicated with the prioritization scheme at the early iterations. In the case of 100 or more (maximum number of devices), for the iterations 1-4, better frame occupancy rates are shown for the algorithm with prioritized slot allocation mechanism compared to the reference scheme [140] as 68.42%, 43.33%, 29.73% and 16.67%, respectively. Further, with the prioritization scheme full channel occupancy is achieved with 50% less time or 200% faster than regular scheme (i.e., 5 iterations with and 10 iterations without prioritization scheme). Similar kind of behaviors are shown for the other device densities as well. This is a very important characteristic when serving the devices with urgent or emergency data. Convergence of those two coordinated QL schemes under different learning rates are shown in Fig. 4.9(b). Faster convergence could be observed with the increase of learning rate giving evidence for proper functionality and the implementation accuracy of the algorithms.

4.4.3   Communication in UB

Occupancy of the sub-frames or slots when number of devices are greater than the number of available slots is shown in Fig. 4.10 under three duty cycle percentages 20%, 40% and 60%. For all these duty cycle percentages, curves with prioritization scheme coincide with each other. Similarly, curves without prioritization scheme also coincide each other. However, for all the duty cycle percentages there is a considerable time reduction in achieving 100% frame occupancy for the schemes with prioritization schemes over the conventional method [140]. In UB also, with the prioritization scheme full channel occupancy is achieved with 50% less time or 200% faster than regular scheme (i.e., 5 iterations with and 10 iterations without prioritization scheme). In addition, better frame occupancy rates are shown for the algorithm with prioritized slot allocation mechanism compared to the regular algorithm [140] for the
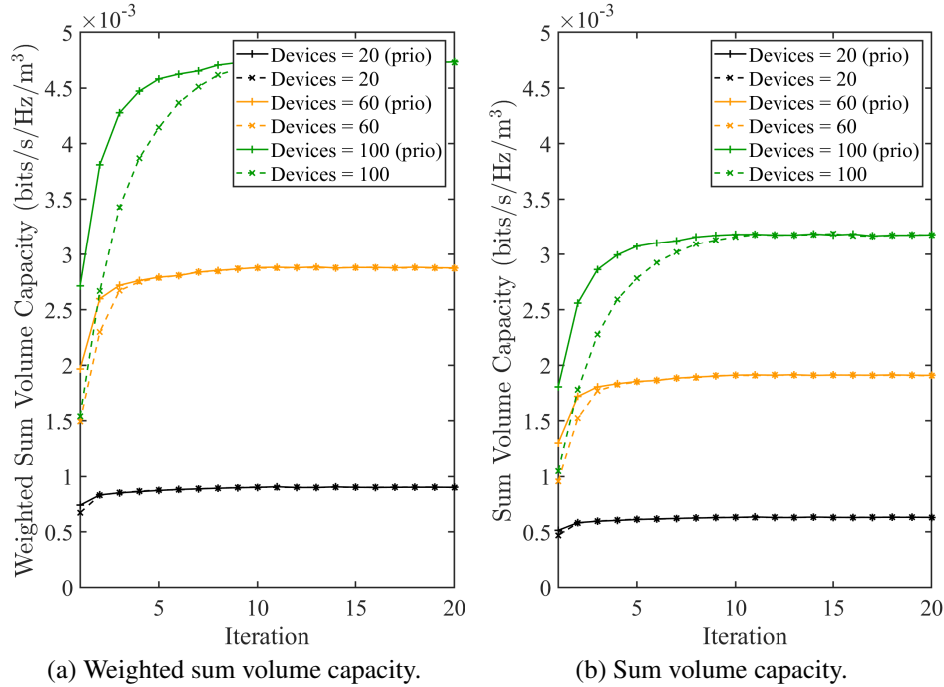
(a) Weighted sum volume capacity.

(b) Sum volume capacity.

Figure 4.8: Convergence of throughput capacity with QL ($\lambda = 0.1$) under different device distributions with and without prioritized slot allocation mechanism: (a) Weighted sum-capacity vs. iterations with three weighting factors. (b) Sum-capacity vs. iterations without weighting.

iterations 1-4 as 73%, 44%, 27% and 17%, respectively. These results are clear indicators of the success of the device and network coordination assisted mechanisms used for this work.

Results for QL algorithm in UB under different duty cycle percentages are shown in Fig. 4.11. Here, it is considered that the number of devices are greater than available time slots. Convergence of the plots for the weighted sum volume capacity values are shown in Fig. 4.11(a). It is indicated that when the device prioritization scheme is used, convergence is achieved faster than regular occasions [140] while supporting QoS and other requirements of the devices and the SC. Corresponding sum volume capacity plots are shown in Fig. 4.11(b) which are the true performance indicators of the system.

Upon getting access to the BS, communication performance is further improved with radio resource management done through RBL principles assisted algorithm. This algorithm is expected to better utilize opportunistically acquired radio resource in the UB. At the start, in a given duty cycle about 10% of the resources are allocated for a single device instead of one

(a) Frame occupancy.

(b) QL algorithm.

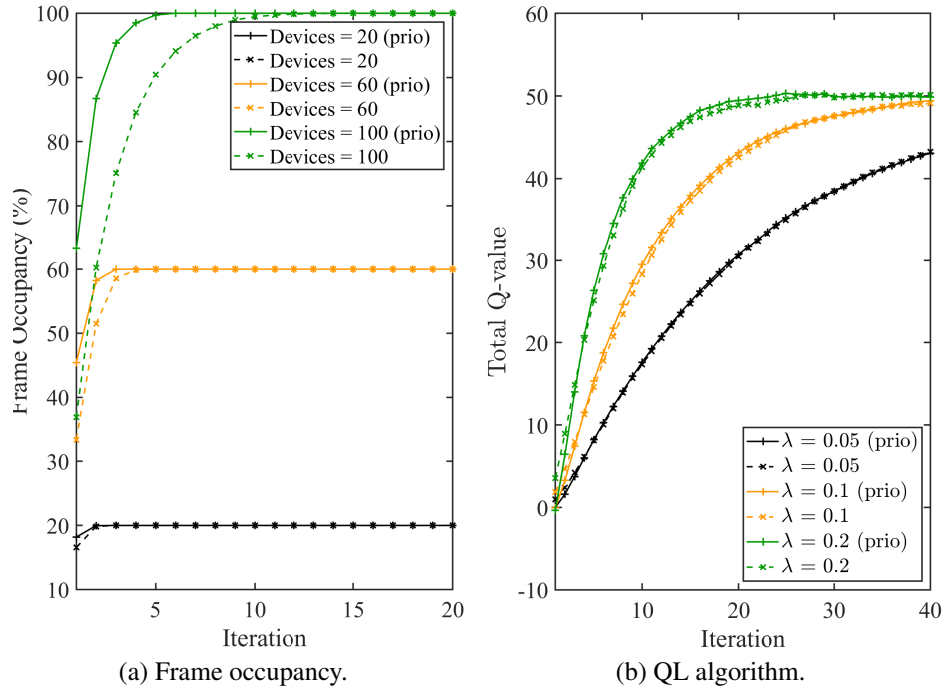Figure 4.9: Performance of the algorithm and convergence of QL scheme with and without prioritized slot allocation mechanism: (a) Convergence of algorithms for different device distributions. (b) Convergence of QL algorithms for different λ values ($M_b = 100$).
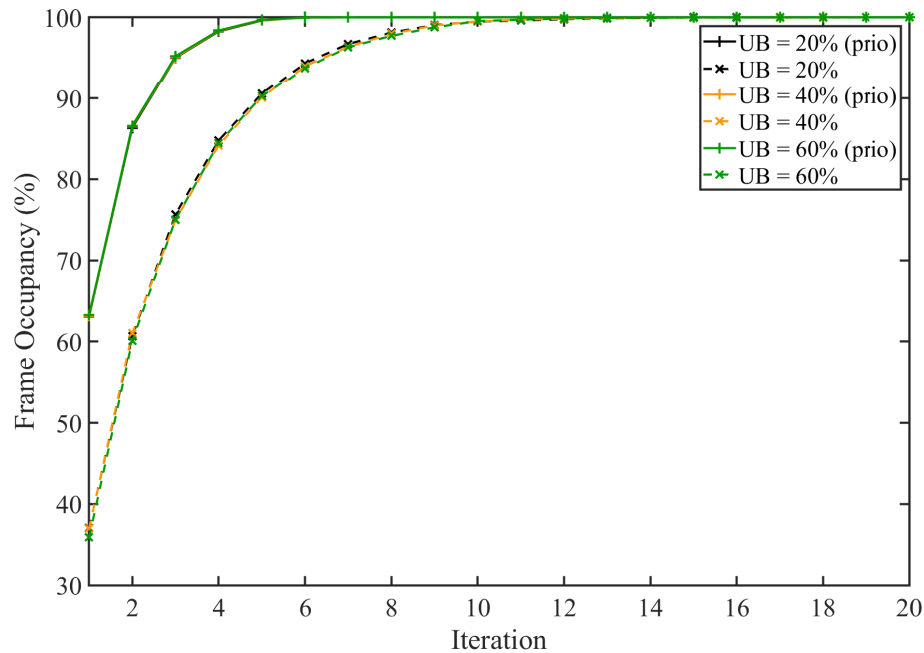

Figure 4.10: Frame occupancy in the UB with for different duty cycle duration with and without consideration of prioritization scheme.

(a) Weighted sum volume capacity.
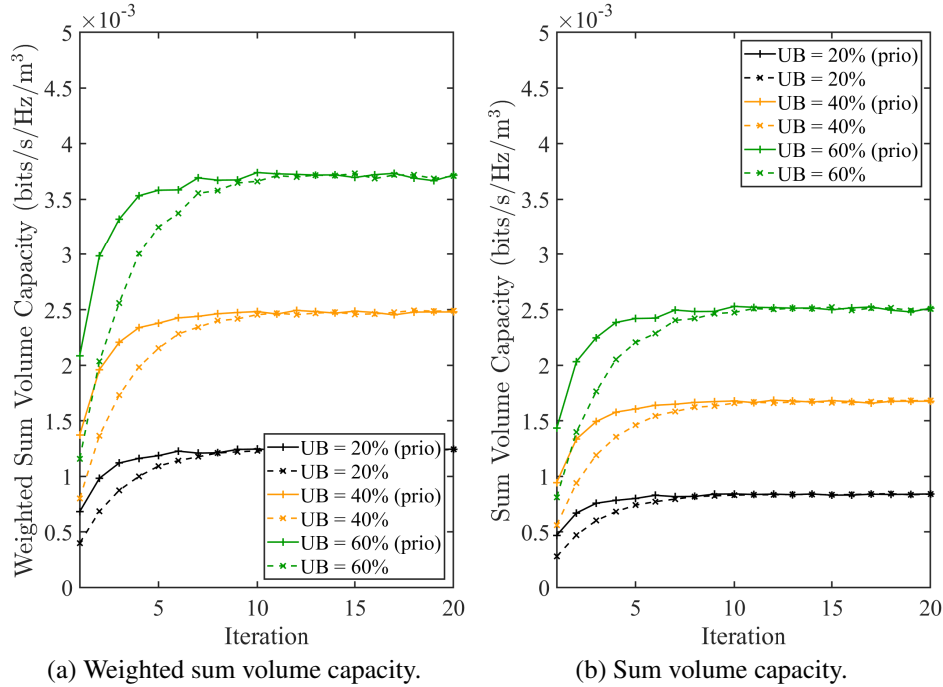
(b) Sum volume capacity.

Figure 4.11: Convergence of throughput capacity in UB with QL algorithm is used to get access for the communication channel under different duty cycle percentages with and without prioritized slot allocation mechanism: (a) Weighted sum volume capacity vs. iterations with two weighting factors. (b) Sum volume capacity vs. iterations without weighting.

slot. Subsequently, allocated time for each device and power are adjusted (remaining in the same duty cycle) to get the sub-optimum sum volume capacity performance while utilizing available radio resources in an efficient manner. Overall performance of this scheme for the SC is shown in Fig. 4.12 under different duty cycle percentages. Convergence of the plots for the weighted sum volume capacity values under different duty cycle percentages are shown in Fig. 4.12(a) and corresponding sum volume capacity plots are shown in Fig. 4.12(b). In this case also, true performance of the system is reflected with the sum volume capacity plots.

Both QL and RBL principles based schemes are capable of converging almost below 15 iterations while showing acceptable sum volume capacity values at the convergence. This is a clear indication that the schemes are capable of being used for real-time operations in the wireless communication systems very successfully.

(a) Weighted sum volume capacity.
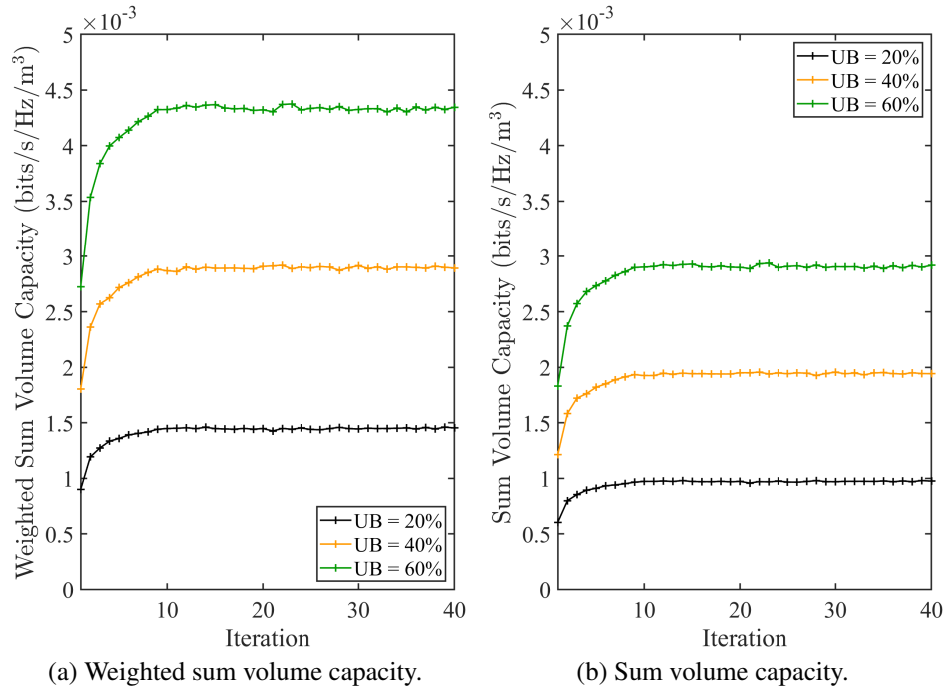
(b) Sum volume capacity.

Figure 4.12: Convergence of throughput capacity in UB with RL under different band occupancy levels: (a) Weighted sum volume capacity vs. iterations with two weighting factors. (b) Sum volume capacity vs. iterations without weighting.

4.4.4 Coordination Efficiency of LB and UB Operations

Relative performance improvement of the device prioritization assisted QL algorithm compared against reference QL algorithm is shown in Fig. 4.13. The device and network coordination assisted mechanism and the device prioritization scheme are the two main reasons behind these impressive results. In this case, device and network coordination efficiency for LB and the UB are given in Fig. 4.13(a) and Fig. 4.13(b), accordingly. Considering scenario of 100 devices or more in the LB and all the scenarios in the UB, nearly 70% and over 75% coordination efficiency values are shown with the solution suggested with this study at the initial iterations, respectively. With both O_t and O_t^{R} reaching to 100% over iterations, the difference $\left(O_t - O_t^{\mathrm{R}}\right)$ becomes zero leading to have zero coordination efficiency over iterations. Corresponding, sum volume capacity enhancement values for LB and the UB are given in Fig. 4.13(c) and Fig. 4.13(d), accordingly. In these cases also, nearly 70% and over 75% sum volume capacity en-

(a) Coordination efficiency for the LB.

(b) Coordination efficiency for the UB.

(c) Enhanced volume capacity in LB.

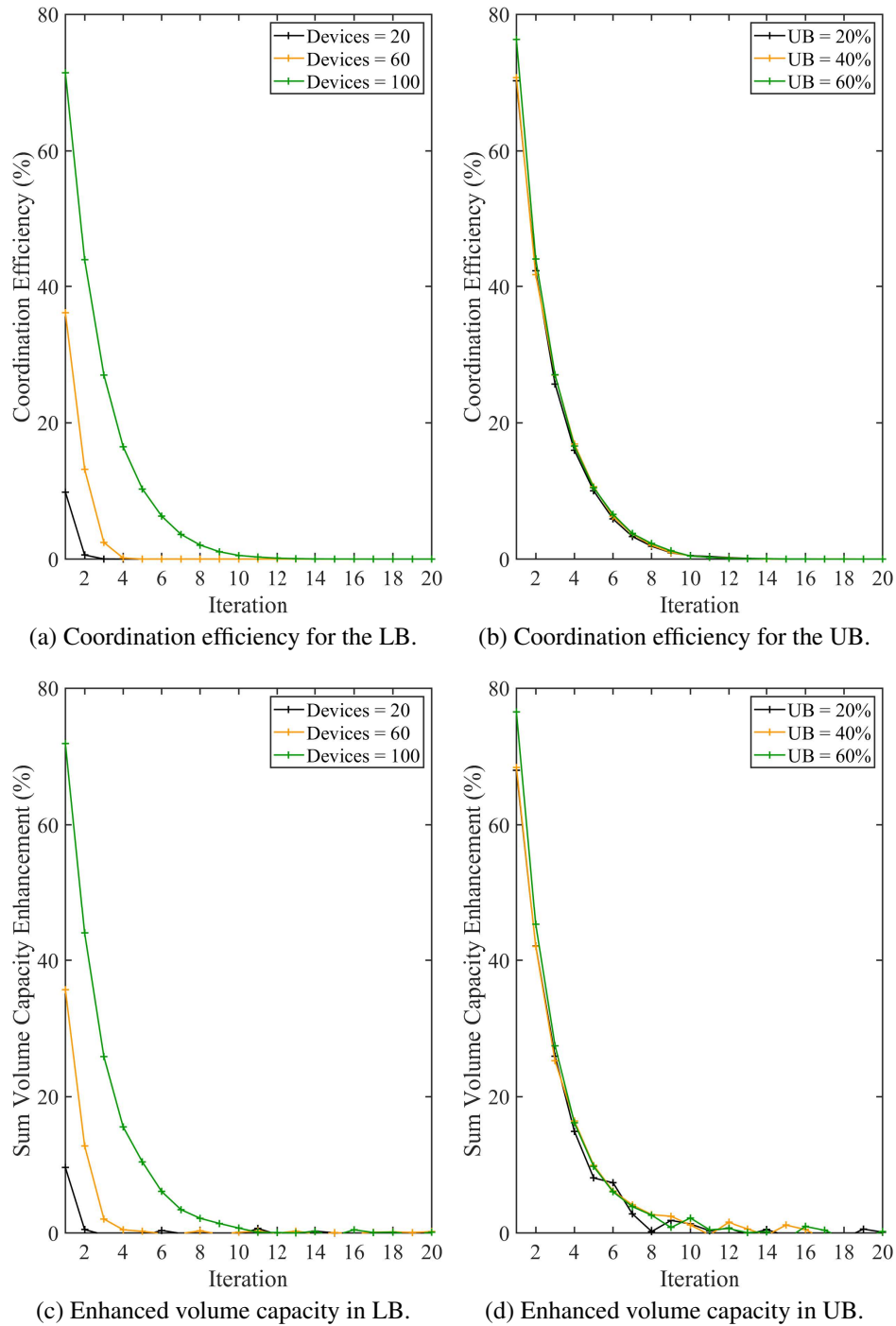(d) Enhanced volume capacity in UB.

Figure 4.13: Relative performance improvement in device access process at early iterations due to coordination assisted mechanism, QL and device prioritization mechanism: (a) Device and network coordination efficiency for LB (b) Device and network coordination efficiency for UB (c) Sum volume capacity enhancement in LB (d) Sum volume capacity enhancement in UB.

hancement values are shown with the solution suggested with this study at the initial iterations for the scenario with 100 devices or more in the LB and all the scenarios in the UB, respectively. When it comes to sum volume capacity enhancement also, for the case of 100 devices or more in the LB and for all the scenarios in the UB, approximately 70% and 75% performance results are shown for the early iterations, accordingly. With both $C_{\text{Sum},t}^{V}$ and $C_{\text{Sum},t}^{R,V}$ reaching to their sub-optimum values over iterations, the difference $\left(C_{\text{Sum},t}^{V} - C_{\text{Sum},t}^{R,V}\right)$ is drastically reduced leading to have very low sum volume capacity enhancement values over iterations.

Overall coordination efficiency with the proposed algorithm over reference method is shown in Fig. 4.14 where values for the LB under different device densities is shown in Fig. 4.14(a) and values for different duty cycle percentages are presented in Fig. 4.14(b). Approximately, 70% performance is shown for the cases of 100 devices (or more) in the LB and for all the duty cycle scenarios of the UB. With drastic reduction of both $E_{\text{C},t}$ and $C_{\text{E},t}^{V}$ over iterations, the summation $\left(E_{\text{C},t} + C_{\text{E},t}^{V}\right)$ is also reduced leading to have very low or near zero overall coordination efficiency values over iterations.

4.4.5 Device and Network Coordination for Simultaneous Operation in LB and UB

In order to get much better understanding on efficient utilization of opportunistically available radio resources, performance of device and network coordination for simultaneous operation of LB and UB is studied against that of the sequential operation. Overall sum volume capacity of the BS in accessing and utilizing opportunistically available radio resources on LB and UB sequentially and in parallel with and without device access prioritization scheme are shown in Fig. 4.15. Always UB is accessed under the scenario of with 100 devices or more where three duty cycle percentages 20%, 40% and 60% are considered for that. In Fig. 4.15(a), UB is accessed once the LB is fully occupied. The device prioritization algorithm is capable of allocating all the opportunistic radio resources in the LB during first 7 iterations for scenario of device density of 100 or more. Then, the remaining devices are facilitated to access the

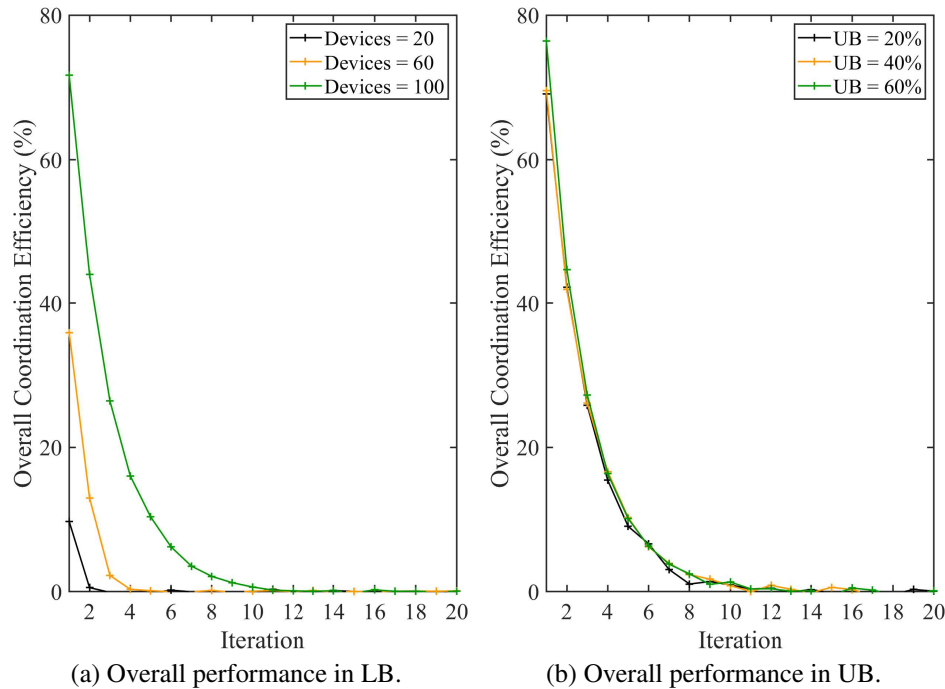(a) Overall performance in LB.　　　　(b) Overall performance in UB.

Figure 4.14: Overall coordination efficiency with of the proposed method over reference algorithm: (a) Overall coordination efficiency vs. iterations in LB with different device densities. (b) Overall coordination efficiency vs. iterations under different duty cycle percentages in UB.

opportunistically available radio resources in the UB where they are captured and allocated by the same algorithm from iteration 8 to 13, until the convergence. Starting from iteration 14, for all the duty cycle percentages RBL algorithm is used to optimize the radio resource utilization efficiency. In summary, with and without prioritization mechanism, about 20 and 35 iterations are spent to reach the final sub-optimum solutions, accordingly. As it is indicated in Fig. 4.15(b), in the case of device density is more than 100, for all the duty cycle percentages both UB and LB are accessed in parallel. With the device prioritization algorithm, radio resources in both bands are allocated within first 7 iterations. Starting from iteration 8, RBL algorithm is used to optimize the radio resource utilization efficiency. About 11 and 20 iterations are used to reach the sub-optimum solutions with and without device prioritization scheme, respectively.

Relative performance enhancement on device and network coordination related to parallel access of LB and UB for the prioritized QL scheme against the regular reference method measured for the SC is given in Fig. 4.16. Device and network coordination efficiency is given in
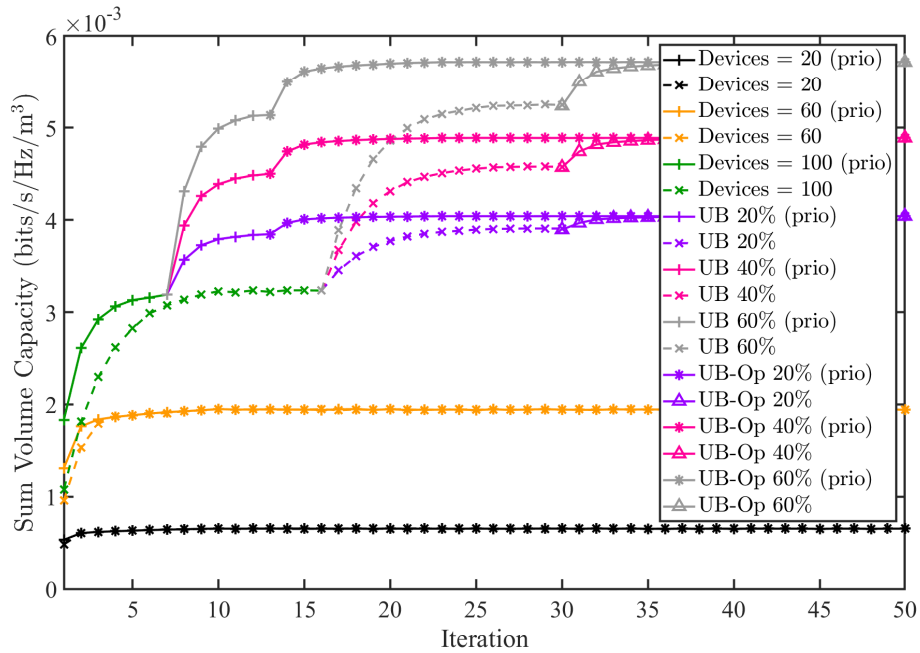
(a) LB and UB access is in sequntial manner.
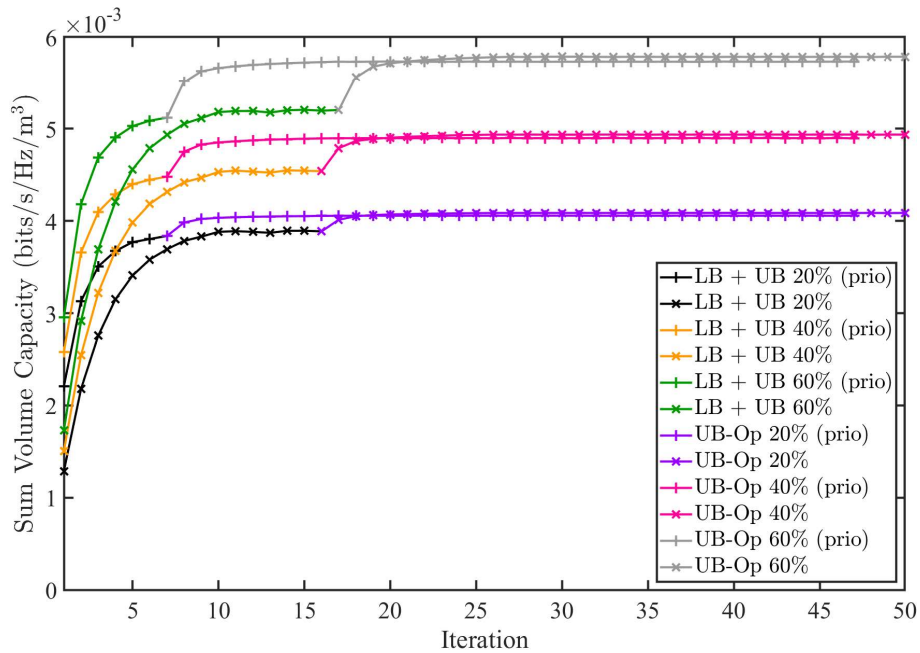
(b) LB and UB access is in parallel manner.

Figure 4.15: Overall sum volume capacity performance measured at the BS with and without device prioritization scheme: (a) UB is accessed when LB is fully occupied. (b) Both UB and LB are simultaneously accessed.

Fig. 4.16(a) and sum volume capacity enhancement is given in Fig. 4.16(b). In both subplots, performance values are over 70% at the start of the iterations and they begin to decline over

(a) Coordination efficiency.
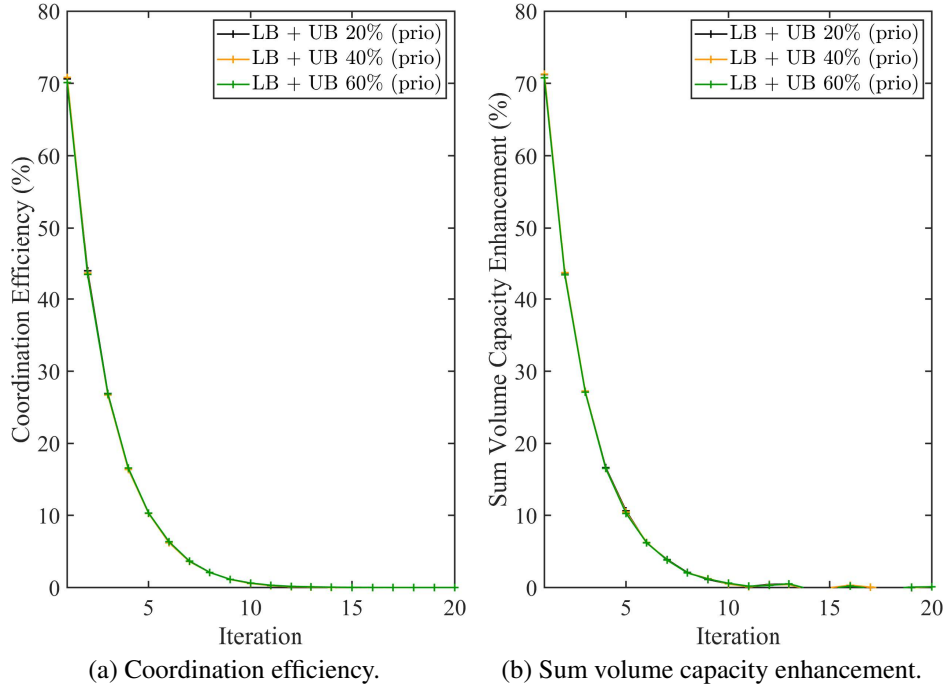
(b) Sum volume capacity enhancement.

Figure 4.16: Performance measured for the SC when LB and UB are accessed in parallel: (a) Device and network coordination efficiency for both bands (b) Sum volume capacity enhancement for both bands.

iterations based on the same reasons given for the sequential band access scenarios.

Overall coordination efficiency for the 3D SC is given in Fig. 4.17. Overall coordination efficiency measured for the device prioritization scheme against conventional approach when LB and UB are accessed in parallel is given in Fig. 4.17(a). Here also, performance values are over 70% at the beginning and start to fall due to the reasons explained under the sequential band access scenarios. Then, overall coordination efficiency measured for LB and UB when they are accessed in parallel with device prioritization against when they are accessed in sequential manner using conventional method is presented in Fig. 4.17(b). For this, $E_{C,t}$ and $C_{E,t}^V$ are defined considering sequential and parallel band utilization modes as $E_{C,t} = \frac{O_t^{\text{Para}} - O_t^{\text{Seq}}}{O_t^{\text{Seq}}} \times 100\%$ and $C_{E,t}^V = \frac{C_{\text{Sum},t}^{\text{Par},V} - C_{\text{Sum},t}^{\text{Seq},V}}{C_{\text{Sum},t}^{\text{Seq},V}} \times 100\%$, accordingly. Here, O_t^{Para} and O_t^{Seq} are the occupancy values measured in parallel and sequential band access modes with device prioritization, accordingly. Then, $C_{\text{Sum},t}^{\text{Par},V}$ and $C_{\text{Sum},t}^{\text{Seq},V}$ are the sum volume capacity values for the sequential and parallel band utilization modes with device prioritization scheme, respectively.
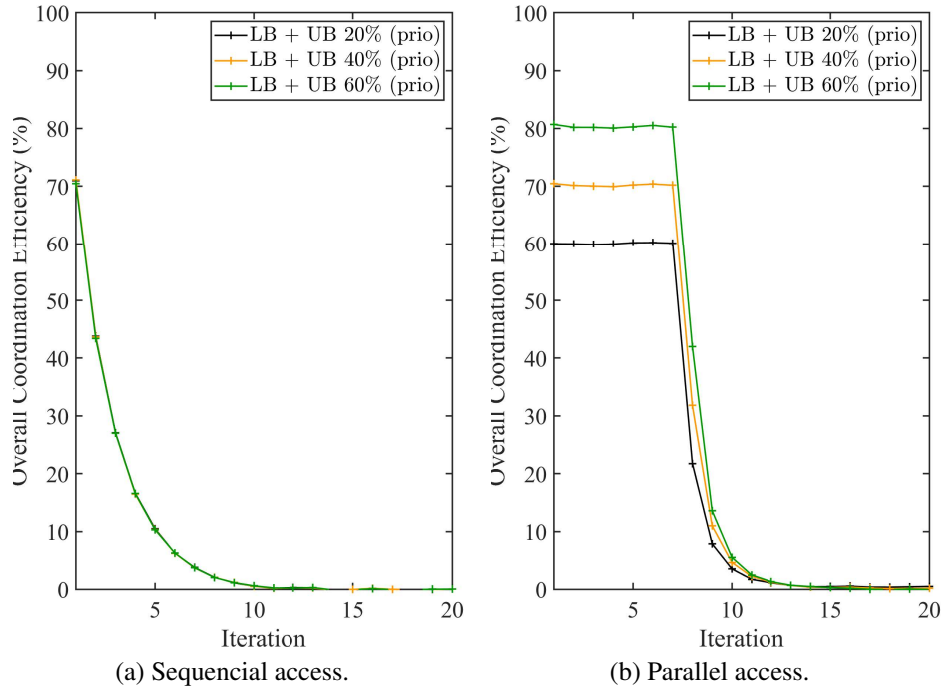
Figure 4.17: Overall coordination efficiency for the SC: (a) Measured for the device prioritization scheme against conventional approach when LB and UB are accessed in sequential manner (b) Measured for LB and UB when they are accessed in parallel with device prioritization compared to band sequential access.

In the case of sequential band access, radio resources in the UB remains unoccupied until all resources in the LB are allocated. Due to this reason O_t^{Para} increases in parallel to O_t^{Seq} with a significant gap until the LB resources are fully allocated where the behavior of $C_{\text{Sum},t}^{\text{Par},V}$ and $C_{\text{Sum},t}^{\text{Seq},V}$ pair is also the same. This has led to have constant and very high overall communication efficiency values approximately within first 7 iterations in Fig. 4.17(b). However, those efficiency values start to fall sharply with the start of allocation of radio resources in the UB in the reference or the sequential band access method after about iteration 7.

4.5 Chapter Summary

Device and Network coordination assisted mechanisms for opportunistic utilization of radio resource in 3D SC HetNets were studied in this work. For that, approaches for fast resource allocation and efficient resource utilization for the devices in dense wireless communication net-

works are presented while meeting different requirements of the applications and the devices. In this case, the problem of performance reduction due to negligence of different location-based information, priority requirements of their data types, availability of LB for communication, delays in radio resource allocation in a 3D network is addressed while satisfying the QoS requirements of the devices. For this problem, QL and S-ALOHA principles based solution is developed with the help of device and network coordination which is even capable of ameliorating the RACH congestion problem. Subsequently, a RBL algorithm is presented to utilize UB radio resources in a very efficient manner. In all these solutions, location-specific and 3D spatially distributed radio resources in LB and UB are utilized while recognizing their limited and opportunistic availability for the devices in heavily congested device distributions. The effectiveness and success of the study are shown with a set of an attractive results presented in terms of several performance metrics including sum volume capacity and overall coordination efficiency.

Chapter 5

Neighboring Station Coverage Identification and Dynamic Resource Utilization for 3D Cells in NR-U Networks

With the ongoing proliferation of wireless networks and the dramatic growth of data traffic, offloading cellular network traffic to UB enabled NR BSs becomes one of the critical alternatives to address the radio resource constraint. Due to ongoing network densification and reduced SC coverage, this solution can be further improved through efficient and dynamic utilization of 3D spatially distributed common UB radio resources while deviating from current inefficient 2D concepts. For that, accurate 3D coverage information of nearby NR-U BSs is vital information. The overall objective of this study is to better estimate the location-specific signal or interference power values in a 3D SC due to operations of neighbor UB BSs enabling that information to be used for efficient and dynamic radio resource utilization in the overlapped 3D coverage space. In the first part of this study, the problem of determining the receive signal power at a given location due to a transmission done by a neighboring NR-U BS operated in the 6 GHz band is addressed. As a solution, a deep regression neural network (DRNN) based algorithm is introduced to predict the receive signal or interference power of a neighbor BS at

121

a given location of a 3D SC, gaining the benefit of bypassing the complex path loss parameter estimation process. In the second part of the study, the problem of efficient radio resource management is considered while dynamically utilizing the UB spectrum for NR-U transmissions. For that, a collaborative double Q-learning (DQL) algorithm is introduced while exchanging mutual cell radio information within the learning process and using the outcomes of the first part of this study. In this case, under ideal, estimated and theoretical categories of predictions, approximately 11%, 23% and 20% better performance results are shown by the DQL based approach over conventional QL based solutions, respectively. However, for the same categories, approximately 59%, 212% and 67% faster algorithm convergence results are indicated by the DQL based method over QL based solutions, accordingly. With the estimated path loss parameters, over 200% faster algorithm convergence is achieved by the DQL based method over conventional solutions.

5.1 Introduction

Over the last few decades, there is a continuous and exponential increase in the density of heterogeneous devices [124] operated under diverse operational and terrain conditions while catering to numerous requirements of various applications. Consequently, it has become a primary design goal to facilitate flexible, intelligent, and self-healing communication systems that are capable of providing joint communication, environment sensing and computing services under extremely scarce radio resource conditions. Deployment of this type of communication system may lead to a strategic and holistic paradigm shift toward more sophisticated future wireless networks. In meeting the technical targets of upcoming 6G and beyond communication systems, data rates are to be significantly increased up to 4.3 Tb/s with latency reduction up to submillisecond in serving prospective applications including high-fidelity holograms with immersive reality, tactile/haptic based communications, and mission-critical applications [28]. This revolutionary shift may lead to excessive network densification while exerting tremendous

pressure to utilize all available scarce radio resources, including UB, to meet the diverse QoS requirements of the radio links in a much more efficient manner [162] than ever before.

Network densification together with migration to high frequency bands may dramatically reduce the size of the wireless cells towards SCs [96] where those SCs can be served by NR-U enabled BSs while facilitating ever-growing data traffic [163]. However, in a dense environment, it is highly possible that the radio resources in UB could also be very inefficiently utilized with chaotic and abrupt transmissions resulting in very heavy interference. With the reduced cell sizes, the third spatial dimension is also being considered for wireless coverage planning leading to 3D SCs. At the same time, it is a necessity to consider spatially distributed radio resources on a real-time basis for efficient radio resource utilization while minimizing different types of interferences where coverage and radio resource management are two sides of the same coin [102]. This situation has drawn the attention of the communication systems designers who are working on upcoming versions of WiFi and NR systems to come up with efficient solutions to manage UB radio resources through UB enabled BSs or NR-U BSs [164, 165].

Due to the site-specific deployment patterns, propagation characteristics and coverage scenarios, it is extremely challenging to manually set different optimum or sub-optimum parameter values for all the BSs to maintain the best coverage for the devices while minimizing mutual interference and utilizing radio resources efficiently. As a solution, autonomous and adaptive systems are being developed to fulfill those requirements [101]. Through this improvement, some of the adverse effects caused to the communication systems due to several changes in the environment like rapid urbanization with high-rise buildings, increased use of flying devices and continuous industrialization are successfully minimized.

Due to their versatility, ease of implementation and high performance, ML techniques have attracted the interest of designers in almost all sectors of engineering, including wireless communication [166]. For the NR-U deployment scenarios in this study, solutions are heavily supported by ML principles where the algorithms are expected to learn and extract knowledge by interacting with the environment under complex environmental conditions. Even though there

are many studies to estimate propagation parameters, interference and receive signal power, only on very few occasions those objectives are achieved in an autonomous and intelligent manner in 3D environments [70, 74]. On most occasions, satellite images are processed with DCNNs to determine the characteristics of the terrains [70, 74]. However, these approaches are far away from reality, as the phenomenon of radio wave propagation is heavily dependent on the medium of propagation and the propagation characteristics can only be effectively identified through observation of the waves traveling through a particular medium.

This work is mainly motivated by a number of technical problems and limitations in NR-U deployment scenarios with 3D SCs. One of the main reasons for this is that many of the current networks operated in UB have no proper coverage deployment plans, even in 2D space, which has led to a situation with very high interference and inefficient radio resource utilization. Increasing demand to utilize the third spatial dimension for proper coverage planning, particularly for NR-U deployment scenarios to meet the requirements of future wireless networks is another key reason behind this study. Due to the scarcity of radio resources, it is vital to consider the spatial distribution of opportunistically available radio resources and interference in managing radio resources efficiently for dense 3D coverage deployment scenarios. The second reason is the requirement of having radio information on neighboring BSs based on observations that are free from influences caused by certain types of interferences and noise. Receive signals and interference are highly affected by environments with spatially distributed and unknown propagation characteristics. Moreover, most of the data that is important to provide continuous NR-U coverage while efficiently managing the radio resources in a dense environment with reduced interference to neighbouring SCs and good QoS [167] is changed over time. Development of infrastructure facilities for future super-active (i.e., situation aware, ultra-fast and proactive), deterministic, adaptive and intelligent communication systems and networks [168] can be introduced as another main motivation behind this study.

5.1.1 Technical Challenges

There is a number of technical challenges against solving the problem of determining the receive signal power at a given location due to a transmission by a neighboring BS or coverage identification of neighbor stations while managing radio resources in a NR-U deployment scenario efficiently. With the involvement of the third spatial dimension, several limitations are also imposed on the applicability of conventional techniques and methods used in 2D deployments.

When considering some of the important challenges, the first challenge is the lack of knowledge on 3D spatially distributed path loss parameters to estimate receive signal power or interference values in developing solutions for radio resource and interference management. Unevenly distributed device locations in 3D space are identified as the second challenge where readings at desired locations are always preferred in certain conventional path loss estimation and coverage prediction mechanisms. The third challenge is to increase the resolution or the granularity of the readings and thereby increasing the accuracy of the solutions. In addition, there are always some conventional challenges, including getting rid of the signal coming from the serving BS when monitoring the neighbor stations and designing a network architecture to facilitate operations related to data collection, data processing, resource allocation, communication and network control [27].

5.1.2 Proposed Solution

This study is developed with the overall objective of better estimation of location-specific signal or interference power values in a 3D SC coverage space due to the operations of UB enabled neighbor BSs. The main purpose of these estimations is to facilitate efficient and dynamic radio resource utilization in an overlapped 3D coverage space. Discussions on the solutions to the problems are initiated with a design for data gathering from overlapped NR-U coverage spaces. In the collection of data, a set of communication devices connected to the serving BS that is in

the overlapped volume is used. In this study, a DRNN [64,65,169,170] based approach is used to predict the receive signal power or interference values at a given location while solving the first problem. That is followed by a solution developed for the problem of dynamic spectrum utilization and radio resource allocation using the principle of DQL with cooperative learning. Even though access to a NR-U enabled network can be managed by channel access schemes like LAA [17] or LBT [147], still there is no mechanism to identify the distribution of radio information including the coverage and provide a situation and environment aware proactive solution. In this case, it is very important to establish mechanisms to utilize radio resources very efficiently, even after acquiring them through a channel access mechanism in UB in a chaotic and abrupt transmission environment.

There are several advantages in using ML techniques to solve a problem. First, they are capable of outperforming conventional signal processing techniques even under complex conditions and constraints. Secondly, deep learning and reinforcement learning techniques are with fast prediction and convergence properties, accordingly while giving sub-optimum solutions with acceptable accuracy. The third advantage is, in general, ANN and other supervised learning methods are outperformed by deep learning techniques [63] provided that sufficient amounts of data, training time and processing power are available. However, DQL has the advantage of being operated on a real-time basis without prior training data [171]. As a whole, these solutions are with the general advantage of having backward and forward compatibility with existing and near future networks, systems, protocols and their performance aspects. Especially they can be well-matched with intelligent and autonomous concepts.

The way that the location-specific parameters are used for the coverage predictions is the main difference between the recent coverage prediction techniques presented for 3D SCs in LB [15] and the solutions discussed in this work. In the previous approaches [15], location-specific path loss parameters are used for the coverage predictions where the same outcomes are achieved without estimation of path loss parameters in the ML based solutions discussed in this study. In addition, the availability of device clusters together with different data collection and

processing mechanisms is a requirement for some of the solutions in the previous study [15].

In this study, a set of the most appropriate solutions is discussed for some of the problems and challenges identified in designing the UB operations of NR-U enabled 3D SCs [15]. The solutions become most appropriate as: 1. DNN based solutions are highly compatible with the future radio transceiver architectures or the upcoming integrated neural processing units for communication [66], 2. they facilitate proactive, intelligent, situation aware, environment aware and adaptive systems and networks, 3. they are convenient to deploy with no model selection, no model customization or no generalization to the coverage volumes (i.e., self-configurable solutions suitable for coverage volumes with multiple cells).

5.1.3 Technical Contributions

Within this study, much attention is paid to coverage identification of neighbor 3D NR-U BSs and post-channel access radio resource management related problems in UB. The contributions of this study are summarized as:

- To address the problem of estimation of location-specific receive signal or interference power values of a 3D NR-U enabled neighbor BSs operated in UB, a DRNN based solution is presented. Some of the challenges faced by conventional solutions like having knowledge of a suitable propagation model, estimation of path loss parameters for that, taking readings at desired locations for the path loss parameters and performing these operations on a real-time basis are mitigated with this approach. With this solution, at a point of 12 m towards transmit BS from the monitoring BS, 17% better performance for receive power estimation is shown compared to conventional theoretical calculations.

- To solve the problem of inefficient utilization of UB radio resources in the overlapped areas of 3D SCs, a DQL principle assisted collaborative learning algorithm is introduced. Subsequently, a performance metric is also established to quantify the strength of the collaborations. Several challenges like neighbor cell interference management and uti-

lization of mutual information for collaborative learning in real-time operations under complex environmental conditions are addressed with this solution. With the estimated interference values, about 23% better sum volume capacity values and over 200% faster algorithm convergence are achieved over the QL based scheme at the end of 200 iterations.

- To overcome the challenges related to the management of radio information from 3D SCs for training the neural networks, subsequent real-time operation and elimination of inaccuracies associated with readings taken through opportunistic observations, a supporting algorithm is discussed for the training and utilization of DRNNs. Furthermore, a simple data preprocessing stage is also included in the same algorithm to reduce both impulse noise (IN) and AWGN noise.

- To facilitate 3D NR-U coverage deployment scenarios, smooth flow of data and information, data processing, resource management, real-time operations, network control and convenient implementation of solutions, a network architecture of a 3D cellular network containing NR-U BSs and devices is also discussed.

5.2   Network Architecture and Problem Formulation

A layout of a primary 3D NR-U SC that is heavily overlapped with a similar neighbor cell is considered in Fig. 5.1. This can be considered as the network architecture of the 3D network as well. Both primary and the neighbor SCs are approximately equal in size and they are with randomly dropped devices served through UB radio links. However, only the devices in the overlapped coverage region are considered in this study and they are capable of receiving signals from both BSs. In the common coverage space, belongs to each SC, there are randomly dropped M devices indexed with m, $m \in \mathcal{M}$, $\mathcal{M} = \{1, 2, 3, \ldots, m, \ldots, M\}$ where M can be a specific number for each cell. UB interference power values due to the transmission done by the neighbor BS and the own location information are opportunistically reported to the serving
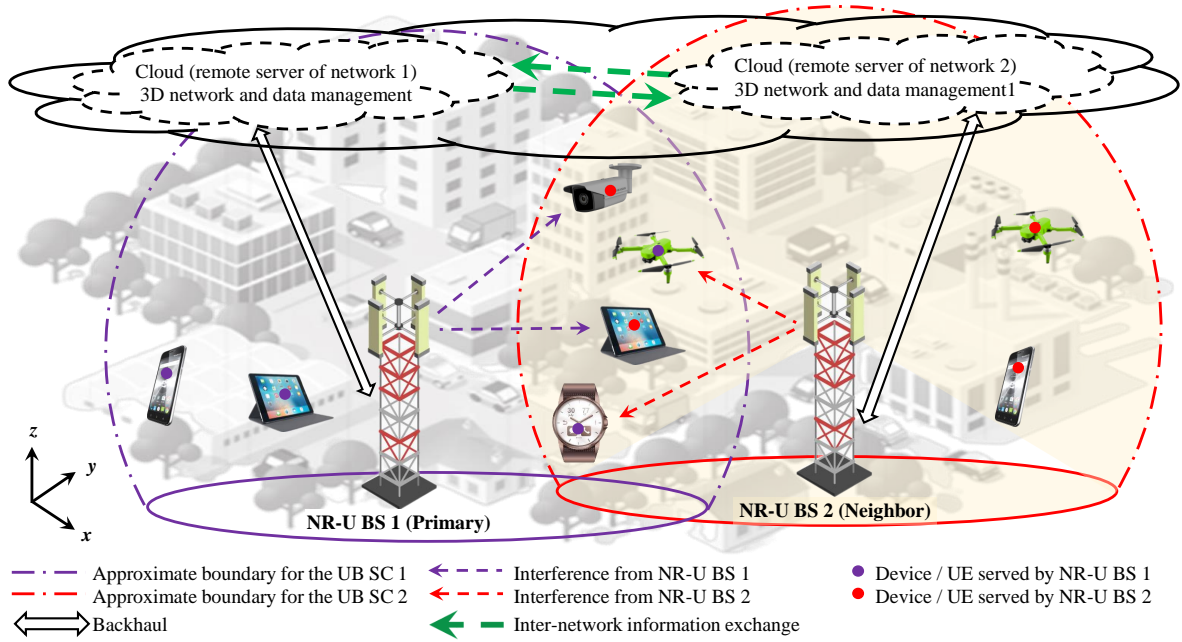
Figure 5.1: Network architecture of 3D network containing NR-U capable primary and neighbor BS with their device distributions.

BS by the devices. Moreover, UB interference is continuously monitored by the serving BS as well. Locations of the transmit antennas of the BSs are considered as the origins of the Cartesian coordinate systems of the 3D SCs.

5.2.1   Overview on Network Architecture

The network architecture of the 3D network is designed to facilitate three main functions in supporting this study namely, data gathering, data processing and information utilization. Here, a 3D network refers to a cellular network containing 3D SCs with NR-U enabled BSs. In certain occasions, 3D service coverage of a BS in UB is introduced as a 3D coverage volume that is equal in size and shape to a 3D SC [15]. Functions related to the cellular network operated on the LB are not discussed in this architecture. In this study, work related to data gathering, storage and processing is introduced as data management and the operations related to processed radio data or information are named as radio information management.

When briefing the operations supported by the network architecture of a 3D network shown

in Fig. 5.1, radio data like RSP, SINR, interference and location information are collected at the devices through opportunistic observations and passed to the BS. For observation of a neighbor BS coverage, DL signal or the interference from that station is used. Intermediate data preprocessing and radio resource management operations can be done at the BSs. BSs are expected to manage the 3D coordinate systems for their own service areas as well. To construct own 3D coverage maps, data gathered by own devices is normally processed at the BSs instead of being passed to the cloud. From the BSs, necessary data and information are passed to the cloud through the backhaul link. Similarly, information needed for DL transmission, resource management and other network operations is passed to the BS through the same link.

As shown in Fig. 5.1, the cloud is used for network management, information management, data processing and data storage functionalities. If the BSs are from different networks, separate clouds are used as indicated by the dashed black lines. If they are from the same network, a common cloud can be used as shown by the solid black line. Either at the cloud or BSs, data is processed using different intelligent algorithms and techniques to achieve the objectives. If there are two networks, certain data and information related to the collaborative learning process, neighbor BSs and interference management are exchanged between the two networks and subsequently among the BSs. Each BS is capable of gathering radio data by observing the UB transmit signals of the neighbor BSs. That information is also exchanged among relevant BSs. Information like RSP (or interference) from DLs of neighbor NR-U BSs is stored and utilized at the observing BSs and the cloud for learning algorithms and other objectives like radio resource management. However, from the perspective of latency, the cloud is the best location to store common data needed for real-time radio resource management functionalities.

There are two additional advantages to this network architecture due to the mitigation of two drawbacks associated with conventional techniques. The first drawback is the difficulties and costs (in terms of capital and labor) associated with the deployment of measurement devices all over the cell to take readings amid access restrictions in certain locations. The second shortcoming is the network overhead and costs of using a dedicated channel or frames

for the data collection process. These drawbacks are mitigated with opportunistic reading and reporting of data using available devices and network resources in an autonomous manner. In this way, even location access restrictions can be avoided. Since data is collected using more than one device in the coverage volume with more than one reading from each device, device-specific inaccuracies can also be avoided.

5.2.2 Problem Formulation

There are two main parts to the research problem namely, neighbor BS coverage identification and efficient radio resource allocation for dynamic spectrum utilization. Furthermore, discovered radio information from the first part of the problem is to be used to find the solutions for the subsequent part of the study.

Neighbor Base Station Coverage Identification

In the first part of this study, the problem of estimation of location-specific and dynamically changing receive power values due to a transmission from a BS in a neighbor 3D SC is addressed. In other words, the problem of estimation of coverage of a neighbor 3D SC on a real-time basis under dynamic conditions is investigated. Consideration of NR-U deployments in UB is of significant importance as communication could be disturbed by chaotic and abrupt transmissions as all the transmitters don't follow disciplined access principles like LBT [147] or don't listen to the nearby transmissions. The purpose of solving this problem is to use that information for radio resource management and coverage prediction including dynamic utilization of spectrum among both cells through individual cell radio resource allocation. This work also leads to efficient interference management operations where location-specific, spatially distributed RSP values can be used for that on a real-time basis.

The transmit signal of a neighbor NR-U station can be sensed by the devices in the overlapped coverage volume and the primary NR-U station. Other than the known interference, practical wireless communication channels are contaminated by location related IN or un-

known interference [172, 173] as well. The strength and the occurrence or contamination possibility of IN are very high in the UB. Then, the observed receive or interference signal from the neighbor NR-U station with observations done by a receiver at (x, y, z) at time t from transmit frame n, $y^n_{(x,y,z)}[t]$, with AWGN $\eta[t]$, $\eta[t] \sim \mathcal{N}_c\left(0, \sigma^2\right)$ and IN $i_{(x,y,z)}$, $i_{(x,y,z)} \sim \mathcal{N}_c\left(0, \sigma^2_i\right)$ is given as $y^n_{(x,y,z)}[t] = \sqrt{p'}h'_n x'[t] + \sqrt{p}h_n x[t] + i_{(x,y,z,n)} + \eta_n$. $x[t]$, $x'[t]$, p and p' are the transmit symbol from the neighbor NR-U station, transmit symbol from the serving NR-U station, transmit power of the neighbor NR-U station and transmit power of the serving NR-U station, accordingly. h_n and h'_n are the channel coefficients for the radio links from neighbor and serving stations in a UMi open squire (OS) NLOS environment [18, 20], accordingly. Since $\mathbb{E}\left[x[t]^2\right] = \mathbb{E}\left[x'[t]^2\right] = 1$, the receive signal power of a symbol from frame n, observed by a receiver at (x, y, z) is given as

$$p^n_{R(x,y,z)} = \left|y^n_{(x,y,z)}[t]\right|^2 = p'\left|h'_n\right|^2 + p\left|h_n\right|^2 + i^2_{(x,y,z,n)} + \eta^2_n. \tag{5.1}$$

To identify neighbor NR-U station coverage, $I^n_{R(x,y,z)}$ at a given location is to be discovered or predicted.

When facing the conventional challenge of avoiding the signals transmitted by the serving BS, two mechanisms could be used viz. taking opportunistic readings by opportunistically available devices when the serving BS is not transmitting and applying an interference cancellation scheme [174] for the primary signal. However, by considering the convenience of implementation and energy efficiency, it is decided to take opportunistic readings to collect training data at the expense of time. Then the receive signals without signals from own BS $I^n_{R(x,y,z)}$ is given as,

$$I^n_{R(x,y,z)} = \left|y^n_{(x,y,z)}[t]\right|^2 = p\left|h_n\right|^2 + i^2_{(x,y,z,n)} + \eta^2_n. \tag{5.2}$$

To beat the long-established challenge of removal of some of the other interruptions like IN

or unknown ad-hoc interference and noise from the desired neighbor station signals, a signal preprocessing stage is employed.

Since IN and AWGN are uncorrelated, considering a sufficiently large number of frames N, $\frac{1}{N} \sum_{n=1}^{N} i_{(x,y,z,n)}^2 + \eta_n^2 = p_{\sigma_i} \sigma_i^2 + \sigma^2 = \sigma_{\text{Sum}}^2$ where p_{σ_i} is the occurrence probability of IN in a given time instance [173]. When σ_{Sum}^2 is known, it can be deducted from the averaged observe signal to get the signal with reduced influences from noise as, $I_{\text{R}(x,y,z)} = \frac{1}{N} \sum_{n=1}^{N} I_{\text{R}(x,y,z)}^n - \sigma_{\text{Sum}}^2$. This preprocessing stage is very important, particularly when a overlapped coverage volume is served by several NR-U transmissions in parallel disregarding LBT type access schemes [147]. Duty cycle based DL channel access mechanisms [132] are typical examples for them.

Efficient 3D Radio Resource Allocation and Dynamic Spectrum Utilization

In the second stage of the study, the problem of efficient radio resource allocation for dynamic spectrum utilization is addressed. The main reasons to address this problem are to eliminate the latency due to information exchange (i.e., receive power, interference or signal-to-noise ratio (SNR) values) among neighbor stations while maintaining device cooperation for other purposes like cooperative learning. In this case, an optimization problem is formulated to maximize the sum volume capacity $C_{\text{Sum}}^{\text{v}}$ of the small cell for efficient utilization of radio resources under a set of constraints as:

$$\underset{p_{s_{m,b}}, f_{m,b}}{\text{maximize}} \quad C_{\text{Sum}}^{\text{v}} = \sum_{b=1}^{2} \sum_{m=1}^{M} C_{(m,b)}^{\text{v}} \tag{5.3a}$$

$$\text{subject to} \quad I_{m,b}, I_b \leq I_{\text{Th}}, \quad \forall m \in \mathcal{M}, \forall b \in \{1,2\} \tag{5.3b}$$

$$p_{s_{m,b}} \geq p_{\min}, \quad \forall m \in \mathcal{M}, \forall b \in \{1,2\} \tag{5.3c}$$

$$p_{s_{m,b}} \leq p_{\max}, \quad \forall m \in \mathcal{M}, \forall b \in \{1,2\} \tag{5.3d}$$

$$C_{(m,b)}^{\text{v}} \geq C_{\min}^{\text{v}}, \quad \forall m \in \mathcal{M}, \forall b \in \{1,2\} \tag{5.3e}$$

$$f_{m,b} \geq f_{\min}, \quad \forall m \in \mathcal{M}, \forall b \in \{1,2\} \tag{5.3f}$$

$$f_{m,b} \leq f_{\max}, \quad \forall m \in \mathcal{M}, \forall b \in \{1,2\} \tag{5.3g}$$

where, $I_{m,b}$, I_b and I_{Th} are the total interference felt by device m served by NR-U BS b, total interference sensed by NR-U BS b and the interference threshold, respectively. The relationship between them is sown by (5.3b). $s_{m,b}$, $s_{m,b} \in \mathcal{S}$, $\mathcal{S} = \{s_1, s_2, s_3, \ldots, s_{|\mathcal{P}|}\}$, is the power control step for device m served by NR-U BS b leading to have transmit power $p_{s_{m,b}}$, $p_{s_{m,b}} \in \mathcal{P}$ and with transmit power value set $\mathcal{P}$, $\mathcal{P} = \{p_1, p_2, p_3, \ldots, p_{\text{max}}\}$. p_{min} and p_{max} are the minimum and maximum transmit power values where they are related to $p_{s_{m,b}}$ as in (5.3c) and (5.3d), accordingly. $f_{m,b}$ is the number of subcarriers allocated for device m served by BS b. f_{min} and f_{max} are the minimum and maximum limits for $f_{b,m}$, accordingly. Their relationships to $f_{b,m}$ are established by (5.3f) and (5.3g), respectively. $C_{(m,b)}^{\text{v}}$ is the volume capacity for the device m in NR-U BS b and $C_{\text{min}}^{\text{v}}$ is the minimum volume capacity needed to maintain the QoS requirements as indicated by (5.3e). Here, volume capacity is defined as the throughput capacity that can be achieved for a unit volume of a cell and calculated as $C_{(m,b)}^{\text{v}} = \frac{C_{(m,b)}}{\pi R_b^3} = \frac{\sum_{f=1}^{f_{m,b}} w_f}{\pi R_b^3} \log_2\left(1 + \text{SINR}_f\right)$ where $C_{(m,b)}$, w_f and R_b are the throughput capacity of device m served by BS b, subcarrier bandwidth and the radius of the cell, respectively. SINR value on subcarrier f, SINR_f, is given as $\text{SINR}_f = \frac{P_{\text{R}(x,y,z)}^n}{I_{\text{R}(x,y,z)}^n}$.

5.3 Intelligent 3D Neighbor SC Coverage Identification and Efficient Radio Resource Allocation

Solutions to the problems are derived from two main branches. One is aimed at the problem of neighbor NR-U BS coverage identification and the other is on efficient radio resource allocation and dynamic spectrum utilization. The outcomes of the first part are effectively used for the second part as well.

5.3.1 Neighbor BS Coverage Identification with Deep-Learning

For the first problem definition, a learning based solution is presented using the principles of DRNN [64, 65, 169] to achieve the objective of finding and prediction of coverage (i.e, receive

signal and interference powers) at a given location at a neighbor 3D NR-U coverage volume in real-time with receive signal observations. In this approach, no propagation characteristics are needed to predict a receive signal or interference power value where the third challenge is also easily mitigated. In addition, with this solution, the second challenge is also successfully addressed as there is no requirement to have readings taken at a particular location in a given volume similar to conventional measurements-based approaches.

Utilization of discovered radio information for efficient radio resource management is the main purpose of finding it. The primary reason to select a DNN based approach over other ML techniques is that, in the long run, DNN can outperform most of the conventional ML techniques, provided that a sufficient amount of data is available [63]. In addition, the DRNN method is well compatible with the linearity properties of the transmit and receive power values while supporting regression type input-output relationships. Widely used DCNN based solutions are much more suitable for solving problems with image processing [70,74] and they are not going to be the best solutions for this study.

This solution is with several advantages as well. Since DNNs can be centrally implemented, most probably at a BS, subsequently estimated receive power or interference values related to different locations could be obtained with low or no communication latency, provided that they are used by different algorithms at the same BS. Further, as receive power or interference could be directly obtained, all the work related to the estimation of path loss parameters can be eliminated saving computational resources and energy. The solution becomes more effective than conventional methods used to determine receive power or interference values as no predefined path loss models, including propagation parameters are required to be assumed or known to estimate the receive signal values. Since training data can be collected over a long period of time, inaccuracies caused by the dynamism of the environment and the device deployment scenarios are also successfully beaten.
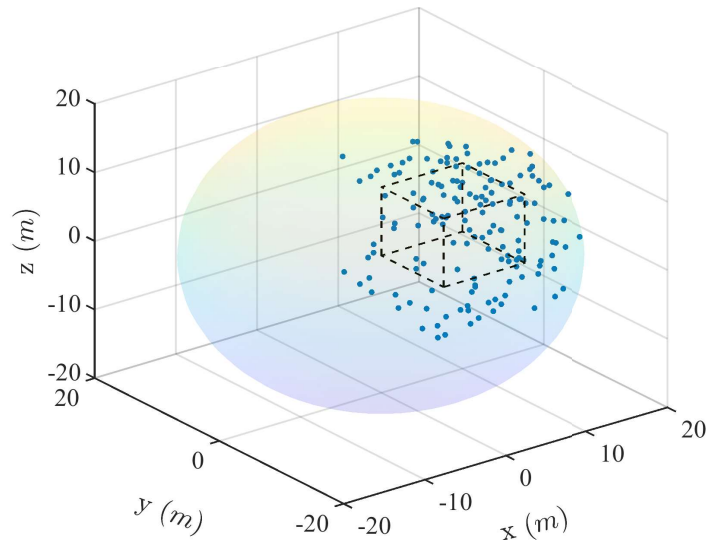
Figure 5.2: Layout of a 3D coverage volume with neighbor BS monitoring devices and one of the cubic volume containing a DNN.

Layout Preparation

A DNN may become overly generalized if data from all over the cell is used to train it. This is due to the influence of the data collected from different locations in the coverage volume containing different properties. Even within the volume considered, there is a possibility of having a considerably large diversity in data due to different types of reflection and scattering surfaces [175]. This technical problem and the first challenge are overcome by dividing 3D coverage into cubic volumes as indicated in Fig. 5.2 for DNN network training and utilization purposes while facilitating the use of a single DNN for each cube. This may lead to more accurate location-specific predictions.

DRNN Model

The model developed for prediction of the interference or receive power from a neighbor NR-U capable BS using the principles of DRNN [64, 65, 169] is shown in Fig. 5.3. In this supervised learning model, labeled data is used after pre-processing and normalization stages. The data includes the location coordinates of the observation device with respect to the transmitter, distance to the transmitter, transmit power and observed interference power from the neighbor
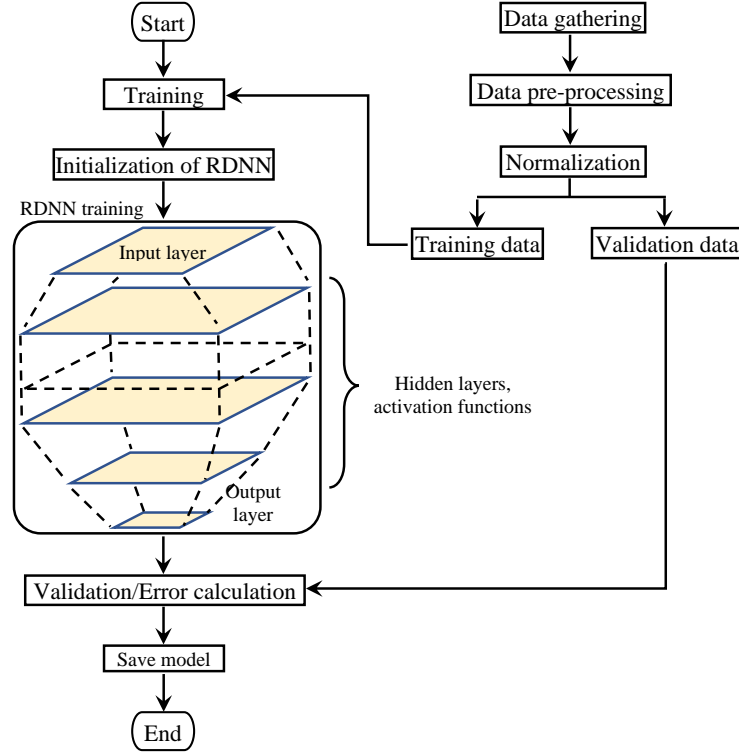
Figure 5.3: Block diagram for the DRNN network for the network training process.

NR-U BS. A segment of randomly selected data is used for validation as well. Hyperparameters of the DNN are determined based on the random parameter optimization method [176] and Rectified Linear Unit (ReLU) function [177] is used as the activation function. In the case of location prediction, a procedure developed based on the principles of multi-output regression [178] is used. One complete DRNN for each cube is implemented and the dynamism of the devices and the environment could be captured by periodically training the networks. The whole process of data gathering, DNN training and value prediction, including the data update cycle is given in Algorithm 11. For that, cubic volumes V_c operated over total time of T_w is used. However, if the mean square error for validation MSE_v is grater than the threshold MSE_{Th}, the model belongs to cubic volume v_c trained at time window t_w, c, $DRNN_{t_w,c}$, is replaced with previously trained model $DRNN_{t_w-1,c}$.

Algorithm 11: Algorithm for Training and Utilization of DRNNs

---

1: **Initialization**
2: Initial data gathering
3: **for** $t_w = 1, 2, 3, \dots T_w$ **do**
4:      **for** $c = 1, 2, 3, ..., V_c$ **do**
5:          Data gathering through opportunistic observations
6:          Data pre-preprocessing and normalization
7:          Addition of new data to the data base
8:          Data separation for training and validation
9:          Initialization of $DRNN_{t_w,c}$
10:        Training $DRNN_{t_w,c}$.
11:        Model validation
12:        **if** $MSE_v \leq MSE_{Th}$ **then**
13:          Save the $DRNN_{t_w,c}$
14:        **else**
15:          Replace $DRNN_{t_w,c} \leftarrow DRNN_{t_w-1,c}$
16:        **end**
17:        Removal of oldest data of volume v_c from the database
18:      **end**
19:      Use $DRNN_{t_w,c} \; \forall v_c \in \{1, 2, 3, ..., V_c\}$ for prediction of interference $\hat{I}_{R(x,y,z)}$.
20: **end**

5.3.2 DQL Based 3D Radio Resource Allocation and Dynamic Spectrum Utilization

Utilization of the radio spectrum in a dynamic manner through an efficient 3D radio resource allocation mechanism is the main objective of the second part of the problem. However, the processes of channel access in UB are not considered in this study. It is assumed that all the participating NR-U capable BSs (i.e., primary and neighbor) have already acquired necessary UB spectrum for DL transmissions through duty cycle based [132] or any other spectrum access mechanisms [179] used in UB. Then, a solution is developed to reduce the inference for the devices served by the neighbor NR-U BSs while increasing the efficient utilization of the spectrum. Interference management is achieved through a systematic management of 3D radio resources, namely transmit power values, time and number of subcarriers at the serving NR-U BSs accounting for estimated mutual interference at the locations of the devices as well as the BSs. In this case, the principle of DQL [171] are used to develop an algorithm to collaboratively

learn the most suitable radio resource allocation for both serving NR-U BSs. Furthermore, ϵ greedy policy is employed [59, 171] for the algorithm. The reason and purpose of the selection of the greedy policy are to ensure that all the state/action pairs are explored as the number of iterations goes to infinity. Mutual interference is estimated much more accurately using the DRNN based approach presented in the first part of this study for the overlapped cell coverage area. Subsequently, those values are used to calculate the volume capacity values as well.

Some of the advantages associated with the DQL schemes [171] over conventional QL based algorithms [57] is the main reason to develop a DQL based solution for this problem. Generally, fast convergence with less training are shown by DQL based schemes than QL based algorithms. In addition, particularly in this study, a collaborative learning process with a nearby device can be established while reducing intense competition among devices for the radio resources through situation awareness. Intense competition in QL based solutions can degrade overall system performance due to two reasons. The first one is excessive acquisition of radio resources by one device leaving less resources for the other devices. The second reason is undue interference generated by some devices.

In this solution, device cooperation for the learning process is achieved by mutually exchanging and updating the Q-function values between two nearby devices served by each NR-U BS. In this case, devices are paired only for algorithm training purposes. Here onward, index m is changed from random to two mutually nearby devices. Considering two NR-U BSs, the device pair is indexed as (m, b), $m \in \mathcal{M}$, $b \in \{1, 2\}$. That means, two devices indexed as $(m, 1)$ and $(m, 2)$ are considered to be in the close vicinity of the overlapped coverage volume and paired for algorithm learning while being served by BS 1 and 2, respectively. Furthermore, there is a possibility that the locations of both devices may have the same 3D path loss values for information signals and interference from the BSs where an information signal from one device is the interference for the other device and vice versa. However, to avoid excessive complexity, one device is paired with only one other device. This method is highly capable of overcoming the technical challenges of the limited time available for training, dynamic environments and

collection of data for training during real-time operations. In addition, this approach is highly effective not only due to the aforementioned properties but also due to its inherent capacity to enhance the learning experience through the exchange of training information between device pairs while converging fast to sub-optimal solutions.

This model-free DQL algorithm is designed considering the agent-environment relationship with the action-reward function given by a Q-table [57] described by a MDP. In this MDP, at each time-step, an action $k \in \mathcal{K}_A$ is taken by an agent in state i trying to maximize own reward at time t given by r_t and reaching the next state i', $\{i, i'\} \in \mathcal{I}_S$, under a certain transition probability. $\mathcal{I}_S$ and $\mathcal{K}_A$ are the sets of states and actions, accordingly. Considering the Q-function $Q^\pi(i, k)$ in QL [57], the optimum Q-function is given as $Q^*(i, k) = \max_\pi Q(i, k)$ for a certain policy π and state-action pair $\{i, k\}$. The action is selected based on the highest Q-value given as $\pi(i) = \arg\max_k Q(i, k)$. When DQL [171] is considered, two value functions are updated using separate experiences as $Q_{t+1}^{(m,b)}(i, k)$, $b \in \{1, 2\}$, for the iteration or time $t + 1$ as

$$Q_{t+1}^{(m,1)}(i,k) \leftarrow (1 - \lambda(i,k))Q_t^{(m,1)}(i,k) + \lambda(i,k)\left\{r_t + \gamma Q_t^{(m,2)}\left(i', \arg\max_{k'} Q_{t+1}^{(m,1)}(i,k')\right)\right\} \quad (5.4)$$

$$Q_{t+1}^{(m,2)}(i,k) \leftarrow (1 - \lambda(i,k))Q_t^{(m,2)}(i,k) + \lambda(i,k)\left\{r_t + \gamma Q_t^{(m,1)}\left(i', \arg\max_{k'} Q_{t+1}^{(m,2)}(i,k')\right)\right\} \quad (5.5)$$

where λ, $\{i', k'\}$ and γ are the learning rate, next state-action pair and the discount factor, respectively.

Definitions for Actions, States and Cost

The state action pair for the Q-functions of device (m, b) at time t is introduced as $\left\{j_t^{(m,b)}, s_{m,b}\right\}$. Then, the definitions for the action set, states and cost for the learning algorithm are given as

- **Action:** Action set is $\mathcal{S} = \{s_1, s_2, s_3, \ldots, s_{|\mathcal{P}|}\}$.

- **State:**

$$
\mathcal{J} = \begin{cases}
1, & C^{n,v}_{(m,b)} < 0.1 \\
2, & 0.1 \leq C^{n,v}_{(m,b)} < 0.2 \\
3, & 0.2 \leq C^{n,v}_{(m,b)} < 0.3 \\
4, & 0.3 \leq C^{n,v}_{(m,b)} < 0.4 \\
5, & 0.4 \leq C^{n,v}_{(m,b)} < 0.5 \\
6, & 0.5 \leq C^{n,v}_{(m,b)} < 0.6 \\
7, & 0.6 \leq C^{n,v}_{(m,b)} < 0.7 \\
8, & 0.7 \leq C^{n,v}_{(m,b)} < 0.8 \\
9, & 0.8 \leq C^{n,v}_{(m,b)} < 0.9 \\
10, & 0.9 \leq C^{n,v}_{(m,b)}
\end{cases}
\tag{5.6}
$$

- **Cost:** $C^{n,v}_{(m,b)} = \dfrac{C^{v}_{(m,b)}}{C^{v,\max}_{(m,b)}}$

Where $C^{n,v}_{(m,b)}$ and $C^{n,\max}_{(m,b)}$ are the normalized volume capacity for device m served by BS in the SC b and the maximum average volume capacity for the same cell.

In applying DQL, each device in pair (m, b), $m \in \mathcal{M}$, $b \in \{1, 2\}$, is allowed to select transmit power value $p_{m,b}$, $m \in \mathcal{M}$, $b \in \{1, 2\}$ independently. At the end of transmit times allocated for the devices in that pair, the Q-values of them are updated using (5.7) and (5.8).

$$
\begin{aligned}
Q^{(m,1)}_{t+1}\left(j^{(m,1)}_t, s_{m,1}\right) &\leftarrow (1 - \lambda)Q^{(m,1)}_t\left(j^{(m,1)}_t, s_{m,1}\right) \\
&. \; + \lambda\left\{C^{n,v}_{(m,1)} + \gamma Q^{(m,2)}_t\left(j^{(m',1)}_{t+1}, \arg\max_{s'} Q^{(m,1)}_{t+1}\left(j^{(m',1)}_{t+1}, s'\right)\right)\right\}
\end{aligned}
\tag{5.7}
$$

$$
\begin{aligned}
Q^{(m,2)}_{t+1}\left(j^{(m,2)}_t, s_{m,2}\right) &\leftarrow (1 - \lambda)Q^{(m,2)}_t\left(j^{(m,2)}_t, s_{m,2,}\right) \\
&. \; + \lambda\left\{C^{n,v}_{(m,2)} + \gamma Q^{(m,1)}_t\left(j^{(m',2)}_{t+1}, \arg\max_{s'} Q^{(m,2)}_{t+1}\left(j^{(m',2)}_{t+1}, s'\right)\right)\right\}
\end{aligned}
\tag{5.8}
$$

Policies for Interference Management and Subcarrier Allocation

In a case of $\{I_{m,b}, I_b\} \geq I_{\text{Th}}$ and $\left\{C^{\text{v}}_{(m,b)}, C^{\text{v,Pr}}_{(m,b)}\right\} \geq C^{\text{v}}_{\text{min}}$ transmit power step of the neighbor device is reduced as $(s_{m,b} \leftarrow s_{m,b} - 1)$ leading to have a power reduction as $p_{s_{m,b}} \leftarrow p_{(s_{m,b}-1)}$. $C^{\text{v,Pr}}_{(m,b)}$ is the precalculated capacity of the device after subcarrier adjustment. $C^{\text{v,Pr}}_{(m,b)}$ is calculated with an already trained DNN designed to give 3D location-specific receive power values.

At the start, all the devices are allocated with at least the minimum number of subcarriers as $f_{b,m} \geq f_{\text{min}}$. If $\left\{I^{\text{Pr}}_{m,b}, I^{\text{Pr}}_b\right\} < I_{\text{Th}}$ and $f_{b,m} < f_{\text{max}}$ number of subcarriers for a device is increased by one as $(f_{m,b} \leftarrow f_{m,b} + 1)$ where $I^{\text{Pr}}_{m,b}$ and I^{Pr}_b are the precalculated values for the interference at device (m, b) and the interference at the observing BS, respectively. $I^{\text{Pr}}_{m,b}$ and I^{Pr}_b are determined using an already trained DNN designed to give 3D location-specific receive power values. However, if $\{I_{m,b}, I_b\} \geq I_{\text{Th}}$ and $f_{b,m} > f_{\text{min}}$, the number of subcarriers for that device is decreased by one as $(f_{m,b} \leftarrow f_{m,b} - 1)$. Dynamic vs fixed utilization of spectrum in terms of subcarrier allocation for DL of a mobile radio channel is shown by Fig. 5.4.

After Q-function is updated with the cost $C^{\text{n}}_{(m,b)}$ received for the current state action pair, $\left\{j^{(m,b)}_t, s_{m,b}\right\}$, $j^{(m,b)}_t \in \mathcal{J}$ and $s_{m,b} \in \mathcal{S}$, a new action is to be selected for the next state. For that greedy policy [59, 171] is used while considering exploration purposes. In this case, if a generated random number r, $r \sim \mathcal{U}(0, 1)$ is with the property $r < \epsilon$, an random action is selected as $s_{m,b} \in \mathcal{U}(1, |p_{\text{max}}|)$. Otherwise action is selected as $p_{s_{m,b}}$, $s_{m,b} = \arg\max_{s'} Q^{(m,b)}_{t+1}\left(j^{(m,b)}_t, s'\right)$. This DQL based algorithm is summarized in Algorithm 12.

Contribution from Collaboration

In order to analyze and quantify the impact of the collaborative learning process against the conventional processes, a separate performance metric is defined using the values available in the Q-tables. Performance metrics used to evaluate the system output are not used for that due to two main reasons. The first reason is that system performance can be influenced by other factors other than device collaborations. The second reason is that collaborations take place by exchanging the values in the Q-tables.
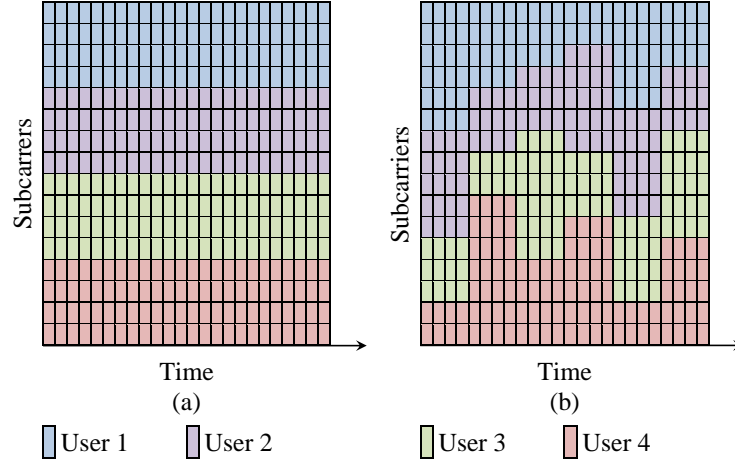
Figure 5.4: Utilization of the spectrum for different devices considering a DL serving to four devices: (a) Fixed utilization (b) Dynamic utilization

---

Algorithm 12: Algorithm for Dynamic Spectrum Utilization and Radio Resource Allocation

---

1: **Initialization**
2: Set, $s_{m,b} \in \mathcal{U}(1, |p_{\max}|)$, $f_{m,b} = f_{\min}$ and I_{Th} $C_{(m,b)}^{\text{v,max}}$, $\forall m \in \mathcal{M}$, $\forall b \in \{1, 2\}$.
3: **for** $t = 1, 2, 3, \ldots, T$ **do**
4:     **for** $m = 1, 2, 3, ..., M$ **do**
5:         **for** $b = 1, 2$ **do**
6:             Execute $p_{s_{m,b}}$, update (5.7) or (5.8).
7:             **if** (5.3b) *and* $\left\{C_{(m,b)}^v, C_{(m,b)}^{v,Pr}\right\} \geq C_{min}^v$ **then**
8:                 Update, $(s_{m,b} \leftarrow s_{m,b} - 1)$, $p_{s_{m,b}}$
9:                 **if** (5.3f) **then**
10:                     Update, $(f_{m,b} \leftarrow f_{m,b} - 1)$
11:                 **end**
12:             **else**
13:                 Generate a random number r, $r \sim \mathcal{U}(0, 1)$
14:                 **if** $(r < \epsilon)$ **then**
15:                     Set, $s_{m,b} \in \mathcal{U}(1, |p_{\max}|)$, $p_{s_{m,b}}$
16:                 **else**
17:                     Set, $s_{m,b} = \arg \max_{s'} Q_{t+1}^{(m,b)}\left(j_t^{(m,b)}, s'\right)$, $p_{s_{m,b}}$
18:                 **end**
19:                 **if** (5.3g) *and* $\left\{I_{m,b}^{Pr}, I_b^{Pr}\right\} \geq I_{Th}$ **then**
20:                   Update, $(f_{m,b} \leftarrow f_{m,b} + 1)$
21:                 **end**
22:             **end**
23:         **end**
24:     **end**
25: **end**

Considering the Q-tables, let $Q_t^{(m,m')}\left(j_t^{(m,m')}, s_{m,m'}\right)$ and $Q_t^{(m,m')'}\left(j_t^{(m,m')}, s_{m,m'}\right)$ be the Q-values for the device m' of collaborating device pair m with and without collaboration or exchanging the Q-values, accordingly. In this case, collaboration contribution $C_{(t,m)}^{(C,m')}$ of a device m' at iteration t is measured as,

$$C_{(t,m)}^{(C,m')} = \left| Q_t^{(m,m')}\left(j_t^{(m,m')}, s_{m,m'}\right) - Q_t^{(m,m')'}\left(j_t^{(m,m')}, s_{m,m'}\right) \right|. \tag{5.9}$$

Here, $Q_t^{(m,m')'}\left(j_t^{(m,m')}, s_{m,m'}\right)$ is selected from an already trained reference Q-tables of a conventional QL or DQL algorithms. Then the overall collaboration contribution $C_{(t,m)}^{C}$ for the device pairs at iteration t is given as

$$C_{(t,m)}^{C} = \frac{1}{2M} \sum_{m=1}^{M} \sum_{m'=1}^{2} C_{(t,m)}^{(C,m')}. \tag{5.10}$$

5.4   Simulation Results

Two overlapped 3D NR-U SCs are considered and each cell is approximately similar in size with a 20 m in radius. NR-U BSs are in the centers of them. In addition, the centers of the SCs are 20 m away from each other and approximately on the same horizontal plane. In the overlapped space, there is a set of randomly dropped devices (a random number between 40 and 160) served by each NR-U BS in the DL operated in the 6 GHz frequency band. For the device deployments, path loss parameters are randomly selected within a set of ranges. These ranges and the rest of the simulation parameters for the deployment operated in a UMi OS NLOS environment [18, 20] are given in Table 5.1 where simulated data is used to model the device deployment scenarios.

In real life, the path loss is identified as a location-specific property rather than conventional site-specific models [15]. In addition, based on a particular environment, parameter values of a path loss model can vary dynamically over time subject to a certain range. In this case, to be more realistic, dynamic parameters are used for the path loss model for a given location.

Table 5.1: Simulation parameters for the 3D NR-U deployment in a UMi OS NLOS environment.

Parameter	Value
Propagation parameter, α	2.4
Propagation parameter, $\beta_{(x,y,z)}$	$3.96 \leq \beta_{(x,y,z)} \leq 4.84$
Propagation parameter, $\xi_{(x,y,z)}$	$\xi_{(x,y,z)} \sim \mathcal{N}(0, \sigma_{PL}^2)$
Parameter, γ_f	1.9
Parameter, σ_{PL}	7.8
Maximum transmit power	28 dBm
Minimum transmit powers	2.8 dBm
Power control steps	10
The threshold power for P_E	-80 dBm
Interference threshold, I_{Th}	-100 dBm/Hz
Variance for channel coefficient, σ_h^2	0.5
Variance for AWGN, σ^2	-120 dBm/Hz
Variance for IN, σ_i^2	$10\,\sigma^2$
Occurrence probability of IN, p_{σ_i}	0.001

Furthermore, the relationship between those parameter values at a given location and those of nearby devices are also taken into account. Most of the time, there shouldn't be a significant change in those path loss parameters at a given location compared to the parameter values at the locations of the nearby devices. The path loss model used in this study, the process of modeling the location-specific path loss parameters, their behavior based on a given location and their evolution over time are explained in APPENDIX A.

Each frame is confined to 10 ms where scheduling and resource allocations are supported through network coordination. In the case of receive signal prediction using DRNNs, each SC is divided into 64 cubes having equal dimensions of 4 m and one DRNN for each cube. For the purpose of training, a labeled data set of 10,000 entries is created where each entry from any location is generated with 1,000 opportunistic readings ($N = 1,000$) for the removal of IN and AWGN. The same set of simulated data is used for the empirical models as well. In this DRNN, MSE is used as the loss function and the root mean square propagation (RMSprop) algorithm is used as the training optimization algorithm. The eest of the simulation parameters related to DRNN models are given in Table 5.2.

In developing these solutions, a set of assumptions is also made. First, it is considered that

Table 5.2: Simulation parameters for the to DRNN models.

| Parameter	Location Prediction	Power Prediction
Layers	4	
Number of neurons for each layer	5, 300, 75, 3	4, 300, 75, 1
Inputs	$x_m, y_m, z_m, p_{s_{m,b}}, I_{R_{\{x,y,z\}}}$	$x_m, y_m, z_m, p_{s_{m,b}}$
Outputs	$\hat{x}, \hat{y}, \hat{z}$	$\hat{I}_{R_{\{x,y,z\}}}$
Loss function	MSE	
Activation function	ReLU, $f(x) = x^+ = max(0, x)$	
Learning rate	0.001	
Optimization tool	Keras RMSprop	
Size of labeled data set	10,000 entries	
Training to testing ratios of data	80% : 20%	
Model validation ratio of data	20% out of testing data	

all devices, BSs and servers are properly synchronized in both the time and frequency domains. Furthermore, they are well coordinated and without delays due to any of the network related operations.

5.4.1 DRNN-Assisted Neighbor BS Coverage Identification

Trained DRNN and performance curves are used to predict the interference values at desired locations in a 3D SC where they are explained in Fig. 5.5. The value of this prediction is very high in industrial applications they can be used for important decisions like device positioning and avoiding high interference locations. Observations from NR-U BSs are made with high accuracy as the location information and receiver-specific parameters are precisely known. However, the data reported by the devices may contain slight errors related to location information and receiver-specific noise. Since observation data can be collected through a NR-U BS and the devices served by it, the MSE for the received power or interference prediction algorithm under different combinations of observation data sets is given in Fig, 5.5 (a). The MSE is given as MSE $= \frac{1}{3n_T} \sum_{n_i=1}^{n_T} \left((\hat{x}_{n_i} - x_{n_i})^2 + (\hat{y}_{n_i} - y_{n_i})^2 + (\hat{z}_{n_i} - z_{n_i})^2 \right)$ for n_T samples. The prediction of location distribution of receive power or interference values for P_E -80 dBm to -60 dBm using the device-BS observation data combination of 75%-25% is given in Fig. 5.5 (b). Using simulations, the optimum epochs for device percentages of 25%, 50%, 75% and
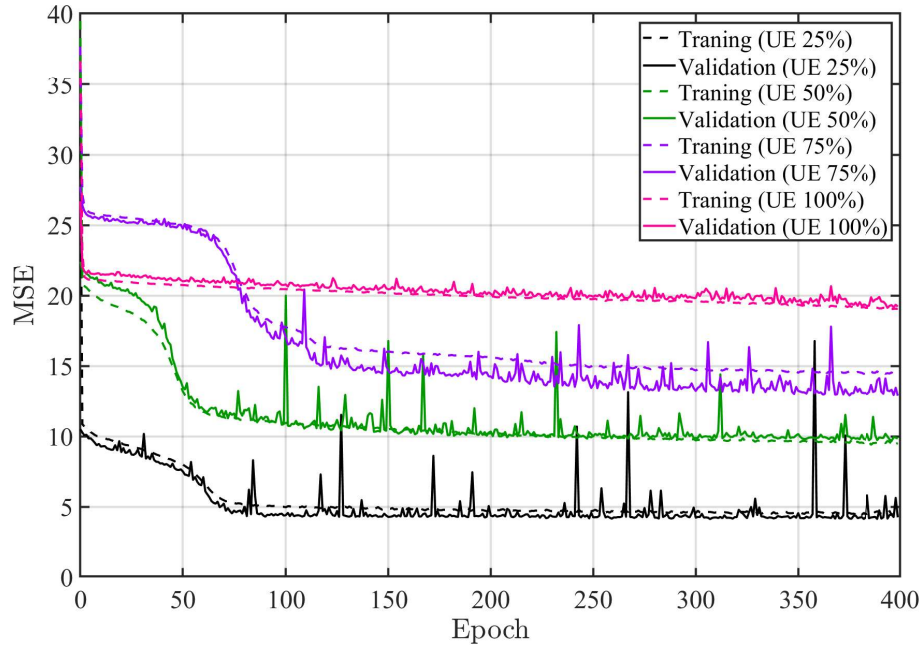
(a) MSE for algorithm.
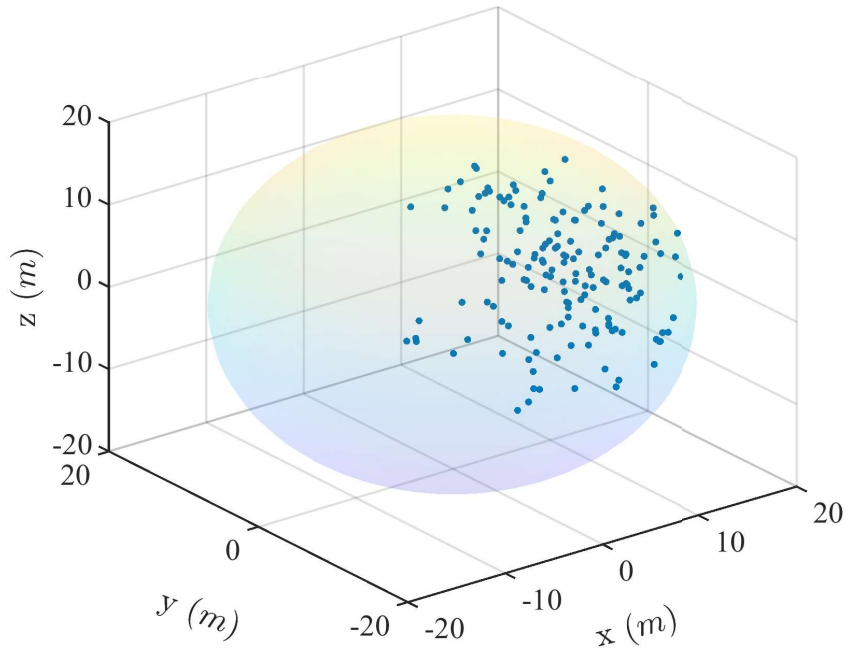
(b) Prediction of locations.

Figure 5.5: Performance of DRNN algorithm in 3D space: (a) MSE for algorithm under different percentages of observation data collected from the devices. (b) Location distribution of receive power or interference value P_E -80 dBm to -60 dBm.

100% to have the minimum difference for training and validation errors are identified as 74, 62, 122, and 4, accordingly. Simulation parameters related to DRNN model are given in Table

5.2. Once network is trained, receive power at a given location could be obtained.
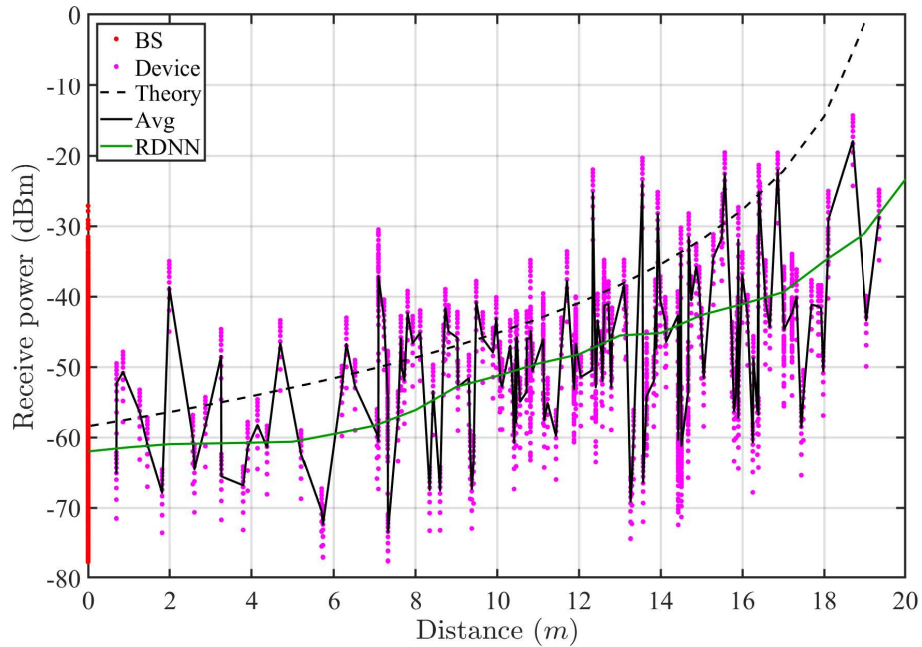
The performance results in a narrow strip in 3D space between the two centers of the coverage volumes (i.e., on the vertical plane connecting the centers of the two cells) is shown in Fig. 5.6. The importance of this scenario is that it can be used to compare the performance of the DRNN algorithm against conventional methods used for receive power, interference power or path loss predictions. In this scenario also, data can be gathered through readings taken from both the NR-U BS and the devices served by it. Then, the MSE for the receive power or interference prediction algorithm under different combinations of observation data is given in Fig, 5.6 (a). The MSE is given as $\text{MSE} = \frac{1}{n_\text{T}} \sum_{n_i=1}^{n_\text{T}} \left(\hat{I}_{n_\text{i},R_{\{x,y,z\}}} - I_{n_\text{i},R_{\{x,y,z\}}} \right)^2$. The receive or interference power observations done by BS and the devices together with curves for prediction done with theory, average values of the observations and prediction done with DRNN are given in Fig. 5.6 (b). For the DRNN, device-BS observation data combinations of 25%-75% is used. In the case of theoretical prediction, cell-specific path loss parameters $\alpha = 2.4$ and $\beta = 4.4$ with path loss estimation equation L_P, $L_m^\text{P} = \alpha + 10\beta \log_{10}(d_m) + 10\gamma_f \log_{10} \frac{f_\text{UB}}{1\text{GHz}}$ are used to calculate the path loss for a device m at distance d_m [24]. Using simulations, 68, 60, 50 and 12 are identified as a set of optimum epochs for device percentages of 25%, 50%, 75% and 100% to have the minimum difference for training and validation errors, respectively. Once network is trained, location of a desired power could be obtained. Simulation parameters related to DRNN model are given in Table 5.2.

5.4.2 DQL Based 3D Radio Resource Allocation and Dynamic Spectrum Utilization

In the second part of the study, the predicted receive power or interference of neighbor NR-U stations is used for 3D radio resource allocation to facilitate dynamic spectrum utilization while maximizing the volume capacities of the primary coverage volumes. To maintain the flexibility of radio resource allocation, the number of devices considered in the overlapped coverage volume is limited to 40. The convergence of the volume capacity values for DQL and QL
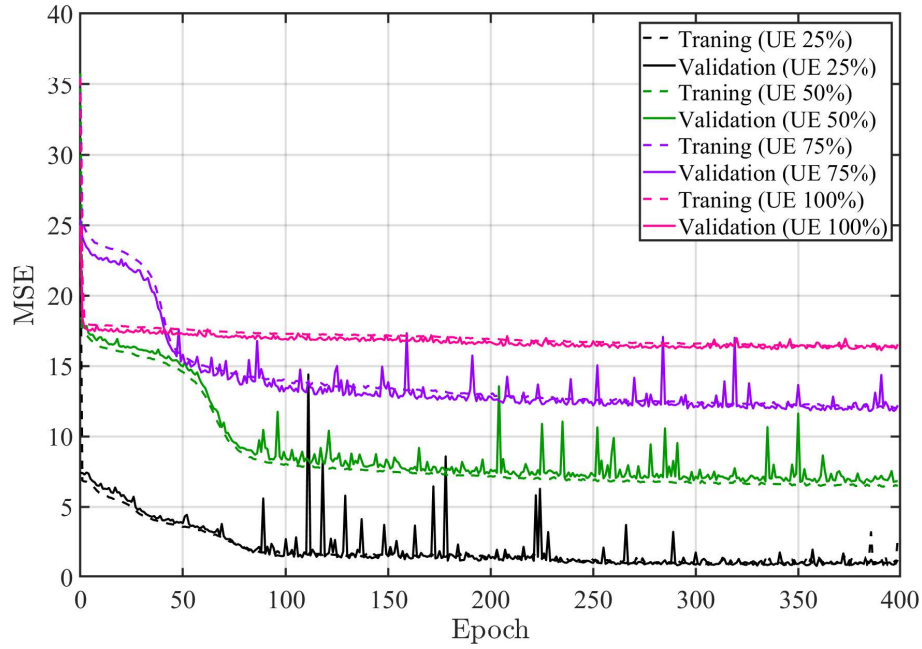
(a) MSE for the algorithm.

(b) Receive or interference power monitoring and prediction.

Figure 5.6: Performance of DRNN algorithm in a narrow strip in 3D space between two NR-U stations (i.e., on the vertical plane connecting centers of the two approximately spherical coverage volumes): (a) MSE for algorithm under different percentages of observation data collected from the devices. (b) Receive or interference power observations done by the BS and the devices together with curves for prediction done with theory, average values of the observations and prediction done with DRNN.

algorithms are shown in Fig. 5.7. In Figs. 5.7 (a), 5.7 (b) and 5.7 (c) ideally calculated interference, interference estimated with the first part of this study and interference estimated with the path loss estimation equation are used, accordingly. Under these three categories, approximately 11%, 23% and 20% better volume capacity values are achieved by the DQL based approach over conventional QL at the end of 200 iterations, respectively. Furthermore, for the same categories, approximately 59%, 212% and 67% faster algorithm convergence values are indicated by the DQL based method over the QL based approach, accordingly.

A volume capacity comparison for the coverage space of the primary NR-U deployment for the two algorithms DQL and QL under the three categories of interference estimations, namely ideally assumed, estimated with DRNN and estimated with the path loss estimation equation are shown in Fig. 5.8. The convergence values of the DQL and QL algorithms are given in Fig. 5.8 (a) and Fig. 5.8 (b), respectively. In both cases, better performance is shown for the scenario when interference is estimated with DRNN over the case when interference is estimated with the theoretical method.

The collaboration contribution of the DQL algorithm is shown in Fig. 5.9. To obtain these results, the system is operated under ideal, estimated, and theoretically derived interference power values. Performance with Q-table values of the regular QL algorithm is used as the reference scheme as in Fig. 5.9 (a). Similarly, the results considering the Q-table values of the DQL algorithm without collaborations are shown in Fig. 5.9 (b). In both scenarios, the highest values are shown for the theoretically determined interference values. This is due to the highest level of interference generated by that scenario. That means the degree of contribution from the algorithm to increase the system performance remains highest when the level of interference is also very high. Based on the same reason, coordination contributions for the scenarios with estimated and ideally calculated interference values receive the second and third positions, accordingly. In all the scenarios, overall collaboration contributions decrease with the convergence of the algorithm over iterations. In this case, overall collaboration contribution values considered against QL at iteration 200 for the scenarios with theoretically calculated and
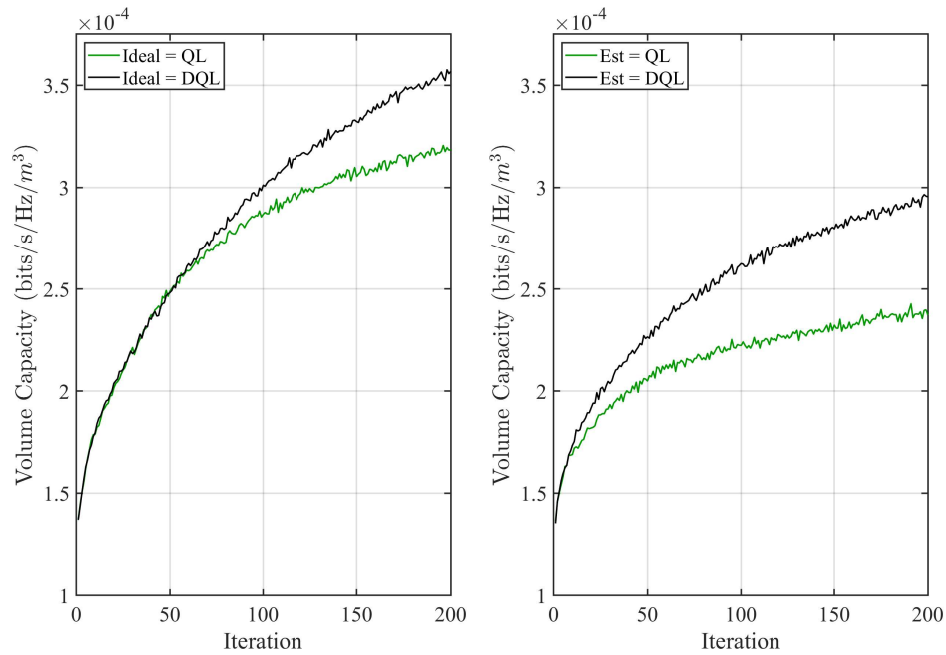
(a) Ideally calculated receive interference values.

(b) Estimated receive interference values.
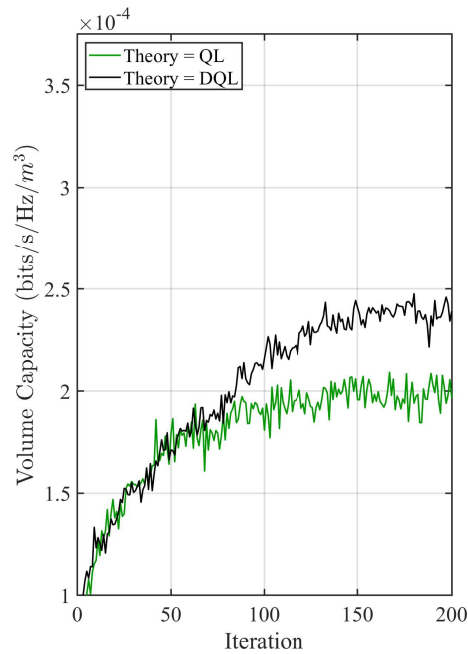
(c) Interference values derived from theory.

Figure 5.7: Volume capacity comparison of algorithms DQL and QL when interference powers are evaluated as: (a). Ideally calculated or known (b). Estimated with DRNN (c). Taken from theory.

(a) Performance of QL algorithm.   (b) Performance of DQL algorithm.
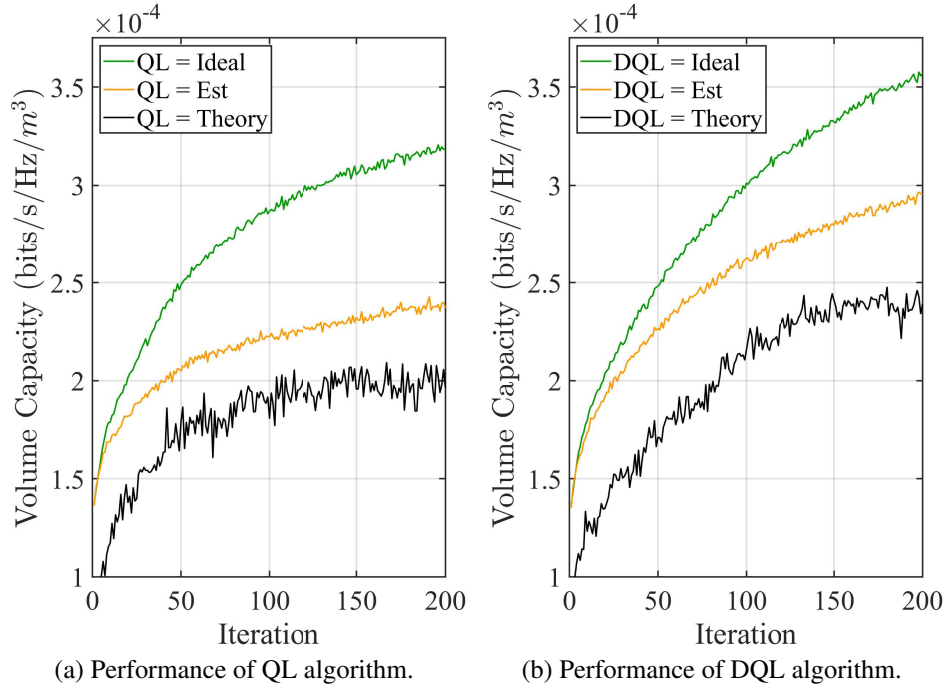
Figure 5.8: Performance comparison of two algorithms for ideal, estimated and theoretically derived interference power values: (a) Volume capacity of QL algorithm. (b) Volume capacity of DQL algorithm.

estimated interference values are 25.33% and 8.6% greater than the overall collaboration contribution value estimated with ideally calculated interference, respectively. Similarly, overall coordination contribution values considered against DQL without collaboration at iteration 200 for the same cases are 12.03% and 5.74% greater than the overall collaboration contribution value estimated with ideally calculated interference, accordingly.

5.5   Chapter Summary

By understanding the importance of accurate knowledge on the coverage of nearby NR-U BS deployment in the allocation and utilization of scarce radio resources to meet the QoS requirements of different applications of devices connected in upcoming dense 3D coverage spaces in UB, the problem of neighbor NR-U station coverage identification was addressed in the first part of this study. As a solution, an algorithm based on DRNN is discussed to predict
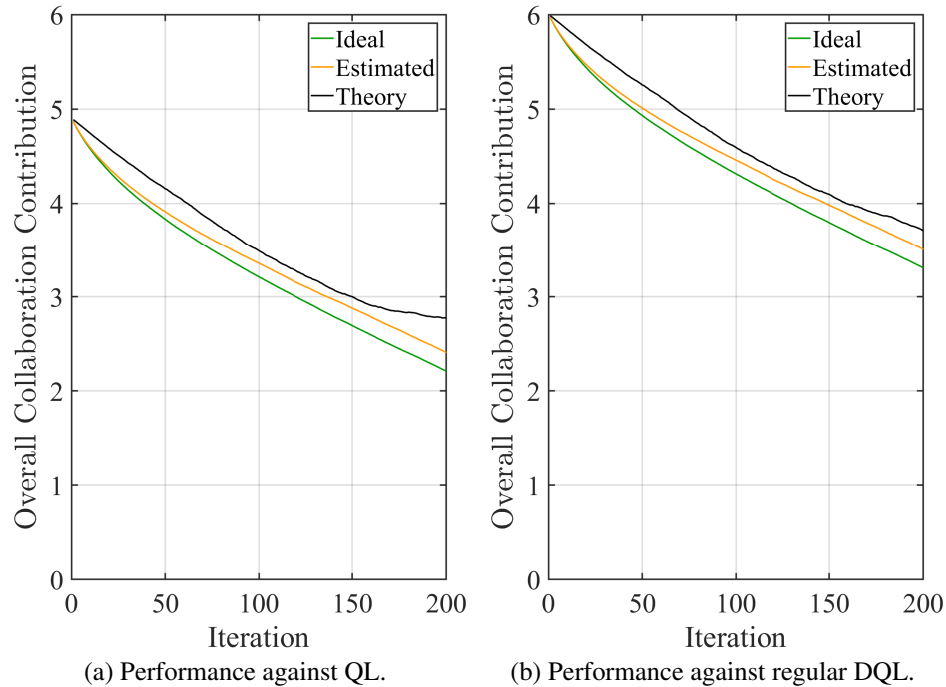
Figure 5.9: Overall collaboration contribution of DQL based solution under ideal, estimated and theoretically derived interference power values: (a) Considering QL algorithm as the reference. (b) Considering regular DQL algorithm without collaboration as a reference.

the receive interference power from a neighbor station at a given location in a 3D coverage space. Then, the problem of efficient radio resource allocation for dynamic spectrum utilization is addressed by presenting a solution based on the DQL technique with device collaboration while facilitating dynamic spectrum utilization. For that, the outcomes of the first part are used and volume capacity values are compared against those of conventional independent QL. When considering all the contributions, this study can be identified as a fruitful attempt to make devices more proactive while reducing real-time performance dependencies and constraints like radio information arriving through the network and associated delays while efficiently using the spectrum and other radio resources in the 3D NR-U deployment.

Chapter 6

Conclusion and Future Work

6.1 Conclusion

With the identification of evolving trends in the numerous sectors of wireless mobile communication, demand for sophisticated wireless communication systems and increasing demand for scarce radio resources, this study was carried out to expand the dimensions of the cellular networks beyond their conventional horizon while stepping towards the concept of 3D networks. In this case, at the start of this work, fundamental limitations and upcoming challenges against the progress or future usage of the long-lasting concept of "2D cellular networks" are identified. Most importantly, "2D cellular networks" is the predominant technology used for areal coverage in cellular networks since its inception, almost throughout all the generations of mobile wireless communications up to 5G over several decades.

In order to overcome the limitations and foreseen challenges of 2D networks, a number of solutions are presented with this work while paving a clear path to replace 2D networks with 3D networks, including maintenance of backward compatibility. In this case, this study is inaugurated with the identification of fundamental limitations with existing cellular networks and key challenges faced in developing technologies for 3D SC networks. However, comparatively high attention is paid to lifting the numerous natural constraints imposed on the usage

of the spectrum like the scarcity of it through efficient management of radio resources while considering their distribution in the 3D space.

Preliminary information is presented in Chapter 2 for the study conducted to investigate efficient information management schemes for ultra-dense 3D HetNets. Emerging and pioneering technologies related to 6G and beyond communication systems are discussed as the basis for introducing the 3D HetNets and enabling technologies. At the beginning, some of the upcoming and very recently developed technologies related to coverage planning, spectrum management and ML technologies used in 3D space and 3D HetNets are discussed under the subtopic of recent developments on 3D HetNets. That is followed by a brief discussion on recently launched or suggested ML and signal processing based receive signal estimation methods for 3D environments. Advantages, different types and use cases of RL and ANN technologies are discussed with the subtopic on ML technologies used in 3D space. Some of the reasons and benefits of efficient information management in wireless networks are also briefly discussed.

In Chapter 3, a detailed study is carried out for path loss estimation and dynamic coverage management in 3D wireless networks with dense SCs. In this work, crowdsensing-assisted algorithm is used to collect data in a dynamic environment without employing dedicated devices. The objective of this study was to increase the efficiency of radio resource utilization of dense and dynamic 3D SCs. In this case, at the first part of the study, three mechanisms, namely LA, OLS and GD are used to discover spatially distributed location-specific path loss parameters while comparing their performance. That is followed by development of two schemes, namely IDW and NMS to extend the 3D communication distance at cluster's farthest borders. For that, propagation characteristics are extrapolated with a reasonable degree of accuracy. On all the occasions RIMs or radio resource managements (RRMs) over 3D space are constructed facilitating radio resources to be used more efficiently in meeting anticipated QoS values for the applications. It is always emphasized the importance of maintaining connectivity at the cluster boundary with an acceptable level of QoS even for an efficient handover process. A number of

challenges are mitigated in providing the solutions. Difficulties with the deployment of measurement equipment at desired locations to take readings, facing the dynamism of both devices and the environment, elimination of device dependent errors on readings, reduction of communication overhead for data exchange and provision of required processing power could be highlighted as some of them. When all the contributions and challenges addressed related to this study are considered, it could be recognized as another progressive step taken to build up infrastructure facilities for 3D SC networks in a very efficient and effective manner through efficient utilization of spatially distributed location-specific radio resources. Furthermore, these solutions are compatible with the existing 2D network deployment scenarios as well.

In Chapter 4, enabling technologies are studied for device and network coordination in the utilization of opportunistically available radio resources in 3D networks. Here it is assumed that information on spatially distributed location-specific radio resources is available when it is needed. In this work, primarily attention is paid to improve the device-network coordination in granting access to the devices upon their requests for communication while considering different requirements like data priority, QoS and connectivity. In addition, the variation of those requirements based on device elevation is also taken into account, as that is going to be a non-negligible factor in future wireless networks. While considering these factors, the problem is converted to a RACH congestion problem, leading to a fast resource allocation solution while reducing network access delays. Since maximum and efficient radio resource utilization techniques are considered, limited and opportunistically available radio resources in both LB and UB are considered. The solutions are developed based on QL and S-ALOHA principles with the assistance of device-network coordination established through common DL broadcast frames. In addition, occupancy of UB is decided using a duty cycle based approach while guaranteeing a fair share of spectrum for the other devices. Upon acquisition of radio resources in UB, UL radio resources utilization efficiency is further increased with the RBL. Several challenges like minimization of collisions in accessing the UL channel, avoidance of accessing already occupied slots, getting the priority for certain devices and reduction of

long waiting times to get channel access are also addressed. In general, with this study, radio resource utilization efficiency of 3D SC is considerably increased with the minimization of access delay, time allocation for devices and control of transmit power.

Neighbor station coverage identification, dynamic spectrum utilization and resource allocation for 3D SC NR-U networks are the main objectives considered in Chapter 5. In developing solutions for these problems a set of challenges is also addressed including overcoming the costs associated with measuring device deployments, device, avoiding interference coming from the monitoring BS and mitigation of device-specific errors associated with the readings taken from the devices. When addressing these problems and challenges, learning based solutions are selected due to several reasons like their capacity to outperform conventional methods and their ability to be operated in an autonomous manner. In this case, a DRNN based algorithm is suggested to predict receive interference power from a neighbor BS at a given location of a 3D SC. When addressing the problem of efficient radio resource allocation for dynamic spectrum utilization, an algorithm based on DQL and device collaboration is presented. With this solution, a number of advantages could also be enjoyed over other techniques and algorithms. As the DNN is centrally implemented, most probably at a BS, estimated receive power or interference values related to different locations could be obtained with low communication latency values for subsequent use of them for other calculations and algorithms implemented at the same BS. In addition, computational resources and energy can be saved as trained DRNN facilitates to directly calculate the receive power or interference without any additional processing like path loss parameter estimations. Furthermore, these learning algorithms based solutions are highly compatible with the emerging integrated neural processing units for communication as well. Based on these reasons, it is very clear that the employment of these solutions in upcoming 3D SC networks could lead to both technical and non-technical benefits at a very low cost.

6.2 Future Work

Several technical problems and challenges related to the design and deployment of 3D SC networks have been addressed in this research study. However, in order to bring this concept to the forefront further improvements are to be done while addressing several other research problems and challenges.

6.2.1 Improvements and Extensions for This Study

As a general practice of the design process, it is prudent to make several improvements and fine-tune the solutions of this study before they are deployed and integrated into a real-life wireless communication network.

- Opportunistic reporting with crowdsensing: Due to the opportunistic nature of reporting, there may be occasions where the devices may not be at the locations and at the time where the readings are needed. In this case, it is identified as a challenge how to take a report from a given location at a given time instance. To address this issue, two solutions are recommended. First one is to use interpolation algorithms covering both time and location parameters. The second solution is to compensate for the readings with readings taken at the same location at different time instances. For the second solution, there should be an algorithm to monitor and identify the repetitive patterns of the environment. However, attention is to be paid to the default challenges with crowdsensing like privacy and security related issues. Since those areas of research are far away from this study and they are not exclusively discussed.

- Accurate positions for the devices: In this study, it is assumed that the devices are capable of reporting the location information accurately. However, attention is to be paid to get accurate location information from the devices. To overcome this challenge, reference points based position determination or position accuracy increasing algorithms can be

used at the data preprocessing stage.

- Device calibration: In this study, it is assumed that the device dependent parameters are known at the receivers. However, it is necessary to have an operator independent centralized database to know the device-specific parameters. That information together with the already identified typical interference level at the location (if there is any) can be used to calibrate the devices and to get better readings on location-specific radio information. This is an important technical problem as unexpected fading and interference are identified as critical challenges in the process of path loss estimation or determination of path loss parameters.

- Deep learning techniques: In this study, a number of solutions are presented based on simple ML techniques based on some reasons like real-time operations, convenience of implementation at the devices, and to achieve fast training without prior data. However, over the time, by monitoring device availability patterns, their data patterns, available radio resources and the device type, many of them can be converted to better performance oriented deep learning techniques. Moreover, some of the coordinated learning techniques can be replaced with federated learning techniques [180].

- Cooperative and coordinated solutions: Device and network coordination is discussed in this study. However, positioning and placement of UAV BSs are discussed in the literature under different application scenarios [48, 83], which are very highly sensitive in terms of accuracy and radio resource utilization. Because, inaccuracy can lead to severe interference to the neighbor cells. Moreover, this increases the dynamism of the environment as well. In this case, device and network coordination aspects are to be further extended to manage UAV BS placements through real-time, cooperative and coordinated solutions.

- Other networks for data collection: Based on the location, availability and compatibility, other wireless networks like sensor networks can be used to collect the data on radio

resources on cellular bands. However, these networks may not communicate using the cellular bands and data is to be collected through their servers. Moreover, their data is to be separately processed and integrated as there may be a separate set of device dependent errors than the regular devices used in the cellular networks.

- Cost of Implementation: Considerable attention has been paid during the design process for the implementation of these solutions in a cost effective manner. Most of the solutions presented in this study are based on software modules. In this case, it is recommended to maintain the same trend for the rest of the developments related to this work like hardware integration while leading the whole set of solutions to an economical viable and technically feasible system.

- Commissioning Time: Some of the solutions presented in this work are based on ML techniques that depend on prior data. In this case, a separate study is to be carried out to determine the most effective and efficient amount of data needed for proper training of those NNs. Since this data is to be collected in real-time at the real locations, this time could be added to the commissioning time of the system or the SC as well. However, this should be a reasonable duration based on the scenario.

6.2.2   Enhancements on Supportive Technologies

In order to use the concept of 3D networks in a very effective and efficient manner, the support technologies must also be developed in parallel. Some of the supportive techniques in demand related to sophisticated mobility management schemes for 3D SC HetNets can be briefed as

- Proactive and dynamic handover mechanisms: Proactive and dynamic handover mechanisms are to be further developed to cope with different mobility patterns and radio resource conditions in 3D space. Selection of a handover can be to an another cell, another network (e.g., WiFi) or to a cell of another operator. Because, there could be a significant variation in radio resource conditions (including interference) with the change of

frequency band where the frequency band can be significantly changed with a handover. It is always very important to have better handover techniques for the applications with V2X data traffic [181].

- 3D beam steering techniques: Apparently, beam steering (or beamforming) with narrow beams and accurate positioning can improve the performance of 3D HetNets by reducing interference. For these technologies also, it is very important to provide accurate radio information. The situation is the same with extra-large scale MIMO arrays or SM-MIMO systems [182] and HBF [43]. Better performance can be achieved with accurate and precise reflection directions and transmit power values. However, in all of these approaches, to achieve the best performance location-specific and spatially distributed radio resource information and path loss parameter values should be updated on a real-time basis.

- Best navigation paths: With the availability of RIM for almost all the cells, several associated studies can be developed. Finding the navigation paths with the best radio information would be one application. These paths would be on land, water, sky or combinations of them. By considering dynamic radio information conditions, these paths could also be dynamically updated to maintain the QoS requirements. Having navigation paths with good radio link conditions is important for certain autonomous delivery vehicles like drones under adverse weather conditions like snow, rain and dust. Because they are currently being used for many essential and critical services like medical supplies, disaster recovery programs and military operations.

- Motion tracking and location tracing techniques: For the occasions where there is no satellite available to support tracking and tracing functions, attention is to be paid to further develop conventional radio information assisted motion tracking and location tracing techniques. Particularly they are very important in indoor environments. For these techniques, more accurate algorithms can be developed to support these operations in 3D space. This work can be further extended or used to predict the communication

coverage for the extended locations or for the locations where there are no devices to report radio information. This work can be done jointly with the techniques used for motion and trajectory prediction [183, 184].

- 3D location information for identification and authentication: Access management is an area where the devices try to establish radio links with the serving BSs. It is very important to have a high degree of signal detection at this stage. However, this process includes not only physical layer signal detection but also higher layer access requests, device identification and authentication. In order to maintain a high degree of accuracy for this process other than signal detection, 3D location-specific radio information including precise 3D location information can be used for a multi factor verification process. Because, most of the time almost all the transceivers are in their unique locations and they are with location-specific radio information as well.

Bibliography

[1] P. Kryszkiewicz, A. Kliks, and H. Bogucka, "Small-Scale Spectrum Aggregation and Sharing," *IEEE J. Sel. Areas Commun.*, vol. 34, no. 10, pp. 2630–2641, Oct. 2016.

[2] T. Huang, W. Yang, J. Wu *et al.*, "A Survey on Green 6G Network: Architecture and Technologies," *IEEE Access*, vol. 7, pp. 175 758–175 768, 2019.

[3] E. Martini and S. Maci, "Theory, Analysis, and Design of Metasurfaces for Smart Radio Environments," *Proceedings of the IEEE*, vol. 110, no. 9, pp. 1227–1243, Sep. 2022.

[4] Y. Han, Y. Chen, R. Wang, J. Wu, and M. Gorlatova, "Intelli-AR Preloading: A Learning Approach to Proactive Hologram Transmissions in Mobile AR," *IEEE Internet Things J.*, vol. 9, no. 18, pp. 17 714–17 727, Sep. 2022.

[5] W. Saad, M. Bennis, and M. Chen, "A Vision of 6G Wireless Systems: Applications, Trends, Technologies, and Open Research Problems," *IEEE Netw.*, vol. 34, no. 3, pp. 134–142, May 2020.

[6] Z. Zhang, Y. Xiao, Z. Ma *et al.*, "6G Wireless Networks: Vision, Requirements, Architecture, and Key Technologies," *IEEE Veh. Technol. Mag.*, vol. 14, no. 3, pp. 28–41, Sep. 2019.

[7] H. Gacanin, "AI-Enabled Future Wireless Networks: Challenges, Opportunities, and Open IssuesAutonomous Wireless Systems With Artificial Intelligence: A Knowledge Management Perspective," *IEEE Veh. Technol. Mag.*, vol. 14, no. 3, pp. 51–59, Sep. 2019.

[8] H. A. Ammar, R. Adve, S. Shahbazpanahi, G. Boudreau, and K. V. Srinivas, "User-Centric Cell-Free Massive MIMO Networks: A Survey of Opportunities, Challenges and Solutions," *IEEE Commun. Surveys Tuts.*, vol. 24, no. 1, pp. 611–652, Firstquarter 2022.

[9] S. Gopi, S. Kalyani, and L. Hanzo, "Cooperative 3D Beamforming for Small-Cell and Cell-Free 6G Systems," *IEEE Trans. Veh. Technol.*, vol. 71, no. 5, pp. 5023–5036, May 2022.

[10] M. Mozaffari, A. T. Z. Kasgari, W. Saad, M. Bennis, and M. Debbah, "Beyond 5G with UAVs: Foundations of a 3D Wireless Cellular Network," *IEEE Trans. Wireless Commun.*, vol. 18, no. 1, pp. 357–372, Jan. 2019.

[11] Z. Yang, C. Pan, M. Shikh-Bahaei *et al.*, "Joint Altitude, Beamwidth, Location and Bandwidth Optimization for UAV-Enabled Communications," *IEEE Commun. Lett.*, vol. 22, no. 8, pp. 1716–1719, Aug. 2018.

[12] H. Jiang, Z. Zhang, L. Wu, and J. Dang, "Three-Dimensional Geometry-Based UAV-MIMO Channel Modeling for A2G Communication Environments," *IEEE Commun. Lett.*, vol. 22, no. 7, pp. 1438–1441, Jul. 2018.

[13] M. D. H. Tataria, M. Shafi and S. Sun, "Six Critical Challenges for 6G Wireless Systems: A Summary and Some Solutions," *IEEE Veh. Technol. Mag.*, vol. 17, no. 1, pp. 16–26, Mar. 2022.

[14] Y. L. Lee, D. Qin, L. C. Wang, and G. H. Sim, "6G Massive Radio Access Networks: Key Applications, Requirements and Challenges," *IEEE Open Journal of Vehicular Technology*, vol. 2, no. 3, pp. 54–66, Jun. 2021.

[15] M. G. S. Sriyananda, X. Wang, and R. K. Rao, "Crowdsensing-Assisted Path Loss Estimation and Management of Dynamic Coverage in 3D Wireless Networks With Dense Small Cells," *IEEE Access*, vol. 9, pp. 112 670–112 685, 2021.

[16] G. Caso, L. D. Nardis, and M. G. D. Benedetto, "Toward Context-Aware Dynamic Spectrum Management for 5G," *IEEE Wireless Commun.*, vol. 24, no. 5, pp. 38–43, Oct. 2017.

[17] M. Zhang, X. Zhang, Y. Chang, and D. Yangn, "Dynamic Uplink Radio Access Selection of LTE Licensed-Assisted Access to Unlicensed Spectrum: An Optimization Game," *IEEE Commun. Lett.*, vol. 20, no. 12, pp. 2510–2513, Dec. 2016.

[18] S. Sun, T. Rappaport, T. Thomas *et al.*, "Investigation of Prediction Accuracy, Sensitivity, and Parameter Stability of Large-Scale Propagation Path Loss Models for 5G Wireless Communications," *IEEE Trans. Veh. Technol.*, vol. 65, no. 5, pp. 2843–2860, May 2016.

[19] S. Y. Seidel and T. S. Rappaport, "Site-specific propagation prediction for wireless in-building personal communication system design," *IEEE Trans. Veh. Technol.*, vol. 43, no. 4, pp. 879–891, Nov. 1994.

[20] S. Sun, T. Rappaport, S. Rangan *et al.*, "Propagation Path Loss Models for 5G Urban Micro- and Macro-Cellular Scenarios," in *Proc. IEEE 83rd Veh. Tech. Conf. (VTC Spring)*, Nanjing, China, 2016.

[21] S. Ju, Y. Xing, O. Kanhere, and T. S. Rappaport, "Millimeter Wave and Sub-Terahertz Spatial Statistical Channel Model for an Indoor Office Building," *IEEE J. Sel. Areas Commun.*, vol. 39, no. 6, pp. 1561–1575, Jun. 2021.

[22] J. Hu and K. Ma, "Analysis and Design of a Broadband Receiver Front End for 0.1-to-40-GHz Application," *IEEE Trans. Circuits Syst.*, vol. 68, no. 6, pp. 2393–2403, Jun. 2021.

[23] J. Seo, I. Yoon, J. Jung *et al.*, "Miniaturized Dual-Band Broadside/Endfire Antenna-in-Package for 5G Smartphone," *IEEE Trans. Antennas Propag.*, vol. 69, no. 12, pp. 8100–8114, Dec. 2021.

[24] H. Braham, S. B. Jemaa, G. Fort, E. Moulines, and B. Sayrac, "Fixed Rank Kriging for Cellular Coverage Analysis," *IEEE Trans. Veh. Technol.*, vol. 66, no. 5, pp. 4212–4222, May 2017.

[25] M. R. Akdeniz, Y. Liu, M. K. Samimi *et al.*, "Millimeter Wave Channel Modeling and Cellular Capacity Evaluation," *IEEE J. Sel. Areas Commun.*, vol. 32, no. 6, pp. 1164–1179, Jun. 2014.

[26] L.-C. Wang, G. L. Stuber, and C.-T. Lea, "Architecture design, frequency planning, and performance analysis for a microcell/macrocell overlaying system," *IEEE Trans. Veh. Technol.*, vol. 46, no. 4, pp. 836–848, Nov. 1997.

[27] H. Chen, R. Abbas, P. Cheng *et al.*, "Ultra-Reliable Low Latency Cellular Networks: Use Cases, Challenges and Approaches," *IEEE Wireless Commun.*, vol. 56, no. 12, pp. 119–125, Dec. 2018.

[28] H. Tataria, M. Shafi, A. F. Molisch *et al.*, "6G Wireless Systems: Vision, Requirements, Challenges, Insights, and Opportunities," *Proceedings of the IEEE*, vol. 109, no. 7, pp. 1166–1199, Jul. 2021.

[29] H. Boostanimehr and V. K. Bhargava, "Unified and Distributed QoS-Driven Cell Association Algorithms in Heterogeneous Networks," *IEEE Trans. Wireless Commun.*, vol. 14, no. 3, pp. 1650–1662, Mar. 2015.

[30] U. Challita, W. Saad, and C. Bettstetter, "Cellular-connected UAVs over 5G: Deep reinforcement learning for interference management," *available online: arxiv.org/abs/*, vol. 1801.05500, 2018.

[31] G. Lin, S. Chang, and H. Wei, "Estimation and Adaptation for Bursty LTE Random Access," *IEEE Trans. Veh. Technol.*, vol. 65, no. 4, pp. 2560–2577, Apr. 2016.

[32] G. Zhang, A. Huang, H. Shan *et al.*, "Design and Analysis of Distributed Hopping-Based Channel Access in Multi-Channel Cognitive Radio Systems with Delay Constraints," *IEEE J. Sel. Areas Commun.*, vol. 32, no. 11, pp. 2026–2038, Nov. 2014.

[33] M. Ishigami and T. Sugiyama, "A Novel Drone's Height Control Algorithm for Throughput Optimization in Disaster Resilient Network," *IEEE Trans. Veh. Technol.*, vol. 69, no. 12, pp. 16 188–16 190, Dec. 2020.

[34] T. S. Rappaport, Y. Xing, O. Kanhere *et al.*, "Wireless Communications and Applications Above 100 GHz: Opportunities and Challenges for 6G and Beyond," *IEEE Access*, vol. 7, pp. 78 729–78 757, 2019.

[35] H. Huang and A. V. Savkin, "An Algorithm of Efficient Proactive Placement of Autonomous Drones for Maximum Coverage in Cellular Networks," *IEEE Wireless Commun. Lett.*, vol. 7, no. 6, pp. 994–997, Dec. 2018.

[36] I. Bor-Yaliniz and H. Yanikomeroglu, "The New Frontier in RAN Heterogeneity: Multi-Tier Drone-Cells," *IEEE Commun. Mag.*, vol. 54, no. 11, pp. 48–55, Nov. 2016.

[37] S. Sekander, H. Tabassum, and E. Hossain, "Multi-Tier Drone Architecture for 5G/B5G Cellular Networks: Challenges, Trends, and Prospects," *IEEE Commun. Mag.*, vol. 56, no. 3, pp. 96–103, Mar. 2018.

[38] I. Bor-Yaliniz, S. S. Szyszkowicz, and H. Yanikomeroglu, "Environment-Aware Drone-Base-Station Placements in Modern Metropolitans," *IEEE Wireless Commun. Lett.*, vol. 7, no. 3, pp. 372–375, Jun. 2018.

[39] M. Giordani, M. Polese, M. Mezzavilla, S. Rangan, and M. Zorzi, "Toward 6G Networks: Use Cases and Technologies," *IEEE Commun. Mag.*, vol. 58, no. 3, pp. 55–61, Mar. 2020.

[40] M. K. Shehzad, L. Rose, M. M. Butt *et al.*, "Artificial Intelligence for 6G Networks: Technology Advancement and Standardization," *IEEE Veh. Technol. Mag.*, vol. 17, no. 3, pp. 16–25, Sep. 2022.

[41] B. Zong, C. Fan, X. Wang *et al.*, "6G Technologies: Key Drivers, Core Requirements, System Architectures, and Enabling Technologies," *IEEE Veh. Technol. Mag.*, vol. 14, no. 3, pp. 18–27, Sep. 2019.

[42] S. Hu, F. Rusek, and O. Edfors, "Beyond Massive MIMO: The Potential of Data Transmission With Large Intelligent Surfaces," *IEEE Trans. Signal Process.*, vol. 66, no. 10, pp. 2746–2758, May 2018.

[43] R. Deng, B. Di, H. Zhang, Y. Tan, and L. Song, "Reconfigurable Holographic Surface: Holographic Beamforming for Metasurface-Aided Wireless Communications," *IEEE Trans. Veh. Technol.*, vol. 70, no. 6, pp. 6255–6259, Jun. 2021.

[44] J. Carle, J. Myoupo, and D. Seme, "A basis for 3-D cellular networks," in *Proc. 15th International Conference on Information Networking*, Beppu City, Oita, Japan, 2001.

[45] S. M. Nazrul Alam and Z. J. Haas, "Coverage and connectivity in three-dimensional networks with random node deployment," *Ad Hoc Networks*, vol. 34, no. 6, pp. 157–169, Jun. 2015.

[46] M. Alzenad, A. El-Keyi, and H. Yanikomeroglu, "3-D Placement of an Unmanned Aerial Vehicle Base Station for Maximum Coverage of Users With Different QoS Requirements," *IEEE Wireless Commun. Lett.*, vol. 7, no. 1, pp. 38–41, Feb. 2018.

[47] X. Wang and M. C. Gursoy, "Coverage Analysis for Energy-Harvesting UAV-Assisted mmWave Cellular Networks," *IEEE J. Sel. Areas Commun.*, vol. 37, no. 12, pp. 2832–2850, Dec. 2019.

[48] M. A. Kishk, A. Bader, and M. S. Alouini, "On the 3-D Placement of Airborne Base Stations Using Tethered UAVs," *IEEE Trans. Commun.*, vol. 68, no. 8, pp. 5202–5215, Aug. 2020.

[49] M. Alzenad and H. Yanikomeroglu, "Coverage and Rate Analysis for Vertical Heterogeneous Networks (VHetNets)," *IEEE Trans. Wireless Commun.*, vol. 18, no. 12, pp. 5643–5657, Mar. 2019.

[50] P. K. Sharma and D. I. Kim, "Random 3D Mobile UAV Networks: Mobility Modeling and Coverage Probability," *IEEE Trans. Wireless Commun.*, vol. 18, no. 5, pp. 2527–2538, May 2019.

[51] C. Zhang and W. Zhang, "Spectrum Sharing for Drone Networks," *IEEE J. Sel. Areas Commun.*, vol. 35, no. 1, pp. 136–144, Jan. 2017.

[52] A. Ellatifi, "Tiling and 3D frequency planning," in *Proc. 5th IEEE International Symposium on Personal, Indoor and Mobile Radio CommunicationsWireless Communications and Networking Conference (PMIRC)*, The Hague, Netherlands, 1994.

[53] C. Chen, J. Zhang, X. Chu, and J. Zhang, "On the Deployment of Small Cells in 3D HetNets with Multi-Antenna Base Stations," *IEEE Trans. Wireless Commun.*, vol. 21, no. 11, pp. 9761–9774, Nov. 2022.

[54] T. M. Mitchell, *Machine Learning*. New York: McGraw-Hill, 1997.

[55] M. Zhang, S. Fu, and Q. Fan, "Joint 3D Deployment and Power Allocation for UAV-BS: A Deep Reinforcement Learning Approach," *IEEE Commun. Lett.*, vol. 10, no. 10, pp. 2309–2312, Oct. 2021.

[56] R. S. Sutton and A. G. Barto, *Reinforcement Learning: An Introduction*, 2nd ed. Cambridge, MA, USA: The MIT Press, 2018.

[57] J. Nie and S. Haykin, "A Q-learning-based dynamic channel assignment technique for mobile communication systems," *IEEE Trans. Veh. Technol.*, vol. 48, no. 5, pp. 1676–1687, Sep. 1999.

[58] M. Simsek, M. Bennis, and İ. Güvenç, "Learning Based Frequency- and Time-Domain Inter-Cell Interference Coordination in HetNets," *IEEE Trans. Veh. Technol.*, vol. 64, no. 10, pp. 4589–4602, Oct. 2015.

[59] J. Langford and T. Zhang, "The Epoch-Greedy Algorithm for Contextual Multi-armed Bandits," in *Annual Conf. on Neural Information Processing Systems*, Vancouver, B.C., Canada, Dec. 2007.

[60] H. Zou, M. Jin, H. Jiang, L. Xie, and C. J. Spanos, "WinIPS: WiFi-based Non-intrusive Indoor Positioning System with Online Radio Map Construction and Adaptation," *IEEE Trans. Wireless Commun.*, vol. 16, no. 12, pp. 8118–8130, Dec. 2017.

[61] X. Tang, J. Chen, T. Liu, Y. Qin, and D. Cao, "Distributed Deep Reinforcement Learning-Based Energy and Emission Management Strategy for Hybrid Electric Vehicles," *IEEE Trans. Veh. Technol.*, vol. 70, no. 10, pp. 9922–9934, Oct. 2021.

[62] E. Ostlin, H. Zepernick, and H. Suzuki, "Macrocell Path-Loss Prediction Using Artificial Neural Networks," *IEEE Trans. Veh. Technol.*, vol. 59, no. 6, pp. 2735–2747, Jul. 2010.

[63] A. Tang, R. Tam, A. Cadrin-Chênevert *et al.*, "Canadian Association of Radiologists White Paper on Artificial Intelligence in Radiology," *Canadian Association of Radiologists Journal*, vol. 69, Apr. 2018.

[64] Y. Guo, K. Zhao, X. Hao, and M. Yu, "Deep Regression Neural Network for End-to-End Person Re-Identification," *IEEE Access*, vol. 7, pp. 92 825–92 837, 2019.

[65] J. Thrane, D. Zibar, and H. L. Christiansen, "Fast and Precise Positioning in PCBs Using Deep Neural Network Regression," *IEEE Trans. Instrum. Meas.*, vol. 69, no. 7, pp. 4692–4701, Jul. 2020.

[66] K. Teng, T. Wu, X. Liu, Z. Yang, and C. Heng, "A 400 MHz Wireless Neural Signal Processing IC With 625 × On-Chip Data Reduction and Reconfigurable BFSK/QPSK Transmitter Based on Sequential Injection Locking," *IEEE Trans. Biomed. Circuits Syst.*, vol. 11, no. 3, pp. 547–557, Jun. 2017.

[67] J. Du, C. Jiang, J. Wang, Y. Ren, and M. Debbah, "Machine Learning for 6G Wireless Networks: Carrying Forward Enhanced Bandwidth, Massive Access, and Ultrareliable/Low-Latency Service," *IEEE Veh. Technol. Mag.*, vol. 15, no. 4, pp. 122–134, Dec. 2020.

[68] H. Yang, A. Alphones, Z. Xiong *et al.*, "Artificial-Intelligence-Enabled Intelligent 6G Networks," *IEEE Netw.*, vol. 34, no. 6, pp. 272–280, Nov. 2020.

[69] Y. Xiao, G. Shi, Y. Li, W. Saad, and H. V. Poor, "Toward Self-Learning Edge Intelligence in 6G," *IEEE Commun. Mag.*, vol. 58, no. 12, pp. 34–40, Dec. 2020.

[70] J. Thrane, D. Zibar, and H. L. Christiansen, "Model-Aided Deep Learning Method for Path Loss Prediction in Mobile Communication Systems at 2.6 GHz," *IEEE Access*, vol. 8, pp. 7925–7936, 2020.

[71] L. Dai and H. Zhang, "Propagation-Model-Free Base Station Deployment for Mobile Networks: Integrating Machine Learning and Heuristic Methods," *IEEE Access*, vol. 8, pp. 83 375–83 386, 2020.

[72] O. Ahmadien, H. F. Ates, T. Baykas, and B. K. Gunturk, "Predicting Path Loss Distribution of an Area From Satellite Images Using Deep Learning," *IEEE Access*, vol. 8, pp. 64 982–64 991, 2020.

[73] L. Wu, D. He, B. Ai *et al.*, "Artificial Neural Network Based Path Loss Prediction for Wireless Communication Network," *IEEE Access*, vol. 8, pp. 199 523–199 538, 2020.

[74] H. F. Ates, S. M. Hashir, T. Baykas, and B. K. Gunturk, "Path Loss Exponent and Shadowing Factor Prediction From Satellite Images Using Deep Learning," *IEEE Access*, vol. 7, pp. 101 366–101 375, 2019.

[75] A. Gupta, J. Du, D. Chizhik, R. A. Valenzuela, and M. Sellathurai, "Machine Learning-based Urban Canyon Path Loss Prediction using 28 GHz Manhattan Measurements," *IEEE Trans. Antennas Propag.*, vol. 70, no. 6, pp. 4096–4111, Jun. 2022.

[76] K. Qiu, S. Bakirtzis, H. Song, J. Zhang, and I. Wassell, "Pseudo Ray-Tracing: Deep Leaning Assisted Outdoor mm-Wave Path Loss Prediction," *IEEE Wireless Commun. Lett.*, vol. 11, no. 8, pp. 1699–1702, Aug. 2022.

[77] Y. Egi and C. E. Otero, "Machine-Learning and 3D Point-Cloud Based Signal Power Path Loss Model for the Deployment of Wireless Communication Systems," *IEEE Access*, vol. 7, pp. 42 507–42 517, 2019.

[78] C. X. Wang, J. Huang, H. Wang *et al.*, "6G Wireless Channel Measurements and Models: Trends and Challenges," *IEEE Veh. Technol. Mag.*, vol. 15, no. 4, pp. 22–32, Dec. 2020.

[79] M. K. Samimi and T. S. Rappaport, "3-D Millimeter-Wave Statistical Channel Model for 5G Wireless System Design," *IEEE Trans. Microw. Theory Techn.*, vol. 64, no. 7, pp. 2207–2225, Jul. 2016.

[80] J. H. Tarng, W. R. Chang, and B. J. Hsu, "Three-dimensional modeling of 900-MHz and 2.44-GHz radio propagation in corridors," *IEEE Trans. Veh. Technol.*, vol. 46, no. 2, pp. 519–527, Jul. 1997.

[81] A. G. Kanatas, I. D. Kountouris, G. B. Kostaras, and P. Constantinou, "A UTD propagation model in urban microcellular environments," *IEEE Trans. Veh. Technol.*, vol. 46, no. 1, pp. 185–193, Feb. 1997.

[82] Q. Zhu, K. Mao, M. Song *et al.*, "Map-based Channel Modeling and Generation for U2V mmWave Communication," *IEEE Trans. Veh. Technol.*, vol. 71, no. 8, pp. 8004–8015, Aug. 2022.

[83] D. Alkama, M. A. Ouamri, M. S. Alzaidi *et al.*, "Downlink Performance Analysis in MIMO UAV-Cellular Communication With LOS/NLOS Propagation Under 3D Beamforming," *IEEE Access*, vol. 10, pp. 6650–6659, 2022.

[84] X. Zhang, J. Wang, and H. V. Poor, "Joint Optimization of IRS and UAV-Trajectory: For Supporting Statistical Delay and Error-Rate Bounded QoS Over mURLLC-Driven 6G Mobile Wireless Networks Using FBC," *IEEE Veh. Technol. Mag.*, vol. 17, no. 2, pp. 55–63, Jun. 2022.

[85] G. Sun, R. He, B. Ai *et al.*, "A 3D Wideband Channel Model for RIS-Assisted MIMO Communications," *IEEE Trans. Veh. Technol.*, vol. 71, no. 8, pp. 8016–8029, Aug. 2022.

[86] K. Kalliola, H. Laitinen, P. Vainikainen *et al.*, "3-D double-directional radio channel characterization for urban macrocellular applications," *IEEE Trans. Antennas Propag.*, vol. 51, no. 11, pp. 3122–3133, Jul. 2003.

[87] S. Gong, C. Xing, N. Yang, Y. C. Wu, and Z. Fei, "Energy Efficient Transmission in Multi-User MIMO Relay Channels With Perfect and Imperfect Channel State Information," *IEEE Trans. Wireless Commun.*, vol. 16, no. 6, pp. 3885–3898, Jun. 2017.

[88] E. G. Larsson, O. Edfors, F. Tufvesson, and T. L. Marzetta, "Massive Massive MIMO for Next Generation Wireless Systems," *IEEE Commun. Mag.*, vol. 52, no. 2, pp. 186–195, Feb. 2014.

[89] S. Chen, S. Sun, Q. Gao, and X. Su, "Adaptive Beamforming in TDD-Based Mobile Communication Systems: State of the Art and 5G Research Directions," *IEEE Trans. Wireless Commun.*, vol. 23, no. 6, pp. 81–87, Dec. 2016.

[90] M. N. Tehrani, M. Uysal, and H. Yanikomeroglu, "Device-to-device communication in 5G cellular networks: challenges, solutions, and future directions," *IEEE Commun. Mag.*, vol. 52, no. 5, pp. 86–92, May 2014.

[91] E. Hossain, M. Rasti, H. Tabassum, and A. Abdelnasser, "Evolution toward 5G multi-tier cellular wireless networks: An interference management perspective," *IEEE Wireless Commun. Lett.*, vol. 21, no. 3, pp. 118–127, Jun. 2014.

[92] N. Zhang, N. Cheng, A. T. Gamage *et al.*, "Cloud assisted HetNets toward 5G wireless networks," *IEEE Commun. Mag.*, vol. 53, no. 6, pp. 59–65, Jun. 2015.

[93] C. D. M. M. Rahman and S. Affes, "Design Optimization of Wireless Access Virtualization Based on Cost & QoS Trade-Off Utility Maximization," *IEEE Trans. Wireless Commun.*, vol. 15, no. 9, pp. 6146–6162, Sep. 2016.

[94] P. Schulz, M. Matthe, H. Klessig *et al.*, "Latency Critical IoT Applications in 5G: Perspective on the Design of Radio Interface and Network Architecture," *IEEE Commun. Mag.*, vol. 55, no. 2, pp. 70–78, Feb. 2017.

[95] H. Ji, S. Park, J. Yeo *et al.*, "Ultra-Reliable and Low-Latency Communications in 5G Downlink: Physical Layer Aspects," *IEEE Wireless Commun.*, vol. 25, no. 3, pp. 124–130, Jun. 2018.

[96] V. M. Nguyen and M. Kountouris, "Performance Limits of Network Densification," *IEEE J. Sel. Areas Commun.*, vol. 35, no. 6, pp. 1294–1308, Jun. 2017.

[97] Q. Wu, G. Y. Li, W. Chen, D. W. K. Ng, and R. Schober, "An Overview of Sustainable Green 5G Networks," *IEEE Trans. Wireless Commun.*, vol. 24, no. 4, pp. 72–80, Aug. 2017.

[98] F. Khan, "Multi-comm-core architecture for terabit-per-second wireless," *IEEE Commun. Mag.*, vol. 54, no. 4, pp. 124–129, Apr. 2016.

[99] M. Samir, S. Sharafeddine, C. M. Assi, T. M. Nguyen, and A. Ghrayeb, "UAV Trajectory Planning for Data Collection from Time-Constrained IoT Devices," *IEEE Trans. Wireless Commun.*, vol. 19, no. 1, pp. 34–46, Jan. 2020.

[100] I. Bor-Yaliniz, A. El-Keyi, and H. Yanikomeroglu, "Spatial Configuration of Agile Wireless Networks with Drone-BSs and User-in-the-loop," *IEEE Trans. Commun.*, vol. 18, no. 2, pp. 753–768, Feb. 2019.

[101] G. Cao, Z. Lu, X. Wen, T. Lei, and Z. Hu, "AIF: An Artificial Intelligence Framework for Smart Wireless Network Management," *IEEE Commun. Lett.*, vol. 22, no. 2, pp. 400–403, Feb. 2018.

[102] M. Mozaffari, A. T. Z. Kasgari, W. Saad, M. Bennis, and M. Debbah, "Beyond 5G with UAVs: Foundations of a 3D Wireless Cellular Network," *IEEE Trans. Wireless Commun.*, vol. 18, no. 1, pp. 357–372, Jan. 2019.

[103] V. J. Kotagi, R. Thakur, S. Mishra, and C. S. R. Murthy, "Breathe to Save Energy: Assigning Downlink Transmit Power and Resource Blocks to LTE Enabled IoT Networks," *IEEE Commun. Lett.*, vol. 20, no. 8, pp. 1607–1610, Aug. 2016.

[104] A. Ö. Kaya and D. Calin, "On the Wireless Channel Characteristics of Outdoor-to-Indoor LTE Small Cells," *IEEE Trans. Wireless Commun.*, vol. 15, no. 8, pp. 5453–5466, Aug. 2016.

[105] H. Q. Ngo, A. Ashikhmin, H. Yang, E. G. Larsson, and T. L. Marzetta, "Cell-Free Massive MIMO Versus Small Cells," *IEEE Trans. Wireless Commun.*, vol. 16, no. 3, pp. 1834–1850, Mar. 2017.

[106] Y. J. C. Feng and S. Jin, "Interference and Outage Probability Analysis for Massive MIMO Downlink with MF Precoding," *IEEE Signal Process. Lett.*, vol. 23, no. 3, pp. 366–370, Mar. 2016.

[107] J. J. Egli, "Radio Propagation above 40 MC over Irregular Terrain," *Proceedings of the IRE*, vol. 45, no. 10, pp. 1383–1391, Oct. 1957.

[108] E. G. Richards, "The estimation of transmission loss in the trans-horizon region," *Proceedings of the IEE - Part B: Radio and Electronic Engineering*, vol. 105, no. 8, pp. 177–183, 1958.

[109] *Evolved Universal Terrestrial Radio Access (E-UTRA); User Equipment (UE) radio transmission and reception*, document TS 36.101, V. 17.1.0, 3GPP, Apr. 2021.

[110] *Study on 3D channel model for LTE*, document TR 36.873, V. 12.7.0, 3GPP, Jan. 2018.

[111] *Study on channel model for frequencies from 0.5 to 100 GHz*, document TR 38.900, V. 16.1.0, 3GPP, Jan. 2020.

[112] K. Sato and T. Fujii, "Kriging-Based Interference Power Constraint: Integrated Design of the Radio Environment Map and Transmission Power," *IEEE Trans. on Cogn. Commun. Netw.*, vol. 3, no. 1, pp. 13–25, Mar. 2017.

[113] E. Sakhaee and A. Jamalipour, "Stable Clustering and Communications in Pseudolinear Highly Mobile Ad Hoc Networks," *IEEE Trans. Veh. Technol.*, vol. 57, no. 6, pp. 3769–3777, Nov. 2008.

[114] Z. Niu, S. Zhou, Y. Hua, Q. Zhang, and D. Cao, "Energy-Aware Network Planning for Wireless Cellular System with Inter-Cell Cooperation," *IEEE Trans. Wireless Commun.*, vol. 11, no. 4, pp. 1412–1423, Apr. 2012.

[115] H. B. A. Sidi and Z. Altman, "Small Cells' Deployment Strategy and Self-Optimization for EMF Exposure Reduction in HetNets," *IEEE Trans. Veh. Technol.*, vol. 65, no. 9, pp. 7184–7194, Sep. 2016.

[116] Y. Al-Eryani and E. Hossain, "The D-OMA Method for Massive Multiple Access in 6G: Performance, Security, and Challenges," *IEEE Veh. Technol. Mag.*, vol. 14, no. 3, pp. 92–99, Sep. 2019.

[117] X. Zhang, Z. Yang, Y. Liu, J. Li, and Z. Ming, "Toward Efficient Mechanisms for Mobile Crowdsensing," *IEEE Trans. Veh. Technol.*, vol. 66, no. 2, pp. 1760–1771, Feb. 2017.

[118] L. Xiao, T. Chen, C. Xie, H. Dai, and H. V. Poor, "Mobile Crowdsensing Games in Vehicular Networks," *IEEE Trans. Veh. Technol.*, vol. 67, no. 2, pp. 1535–1545, Feb. 2018.

[119] J. Talvitie, M. Renfors, and E. S. Lohan, "Distance-Based Interpolation and Extrapolation Methods for RSS-Based Localization With Indoor Wireless Signals," *IEEE Trans. Veh. Technol.*, vol. 64, no. 4, pp. 1340–1353, Apr. 2015.

[120] D. Shepard, "A Two-dimensional Interpolation Function for Irregularly-spaced Data," in *23rd ACM National Conference*, Las Vegas, NV, USA, Aug. 1968, pp. 517–524.

[121] J. A. Nelder and R. Mead, "A simplex method for function minimization," *Computer Journal*, vol. 7, pp. 308–313, 1965.

[122] M. Lee and D. Han, "Voronoi Tessellation Based Interpolation Method for Wi-Fi Radio Map Construction," *IEEE Commun. Lett.*, vol. 16, no. 3, pp. 404–407, Mar. 2012.

[123] M. Elsayed and M. Erol-Kantarci, "AI-Enabled Future Wireless Networks: Challenges, Opportunities, and Open Issues," *IEEE Veh. Technol. Mag.*, vol. 14, no. 3, pp. 70–77, Sep. 2019.

[124] M. Condoluci, M. Dohler, G. Araniti, A. Molinaro, and K. Zheng, "Toward 5G Densenets: Architectural Advances for Effective Machine-Type Communications Over Femtocells," *IEEE Commun. Mag.*, vol. 53, no. 1, pp. 134–141, Jan. 2015.

[125] K. Huang and H. Wang, "Identifying the Fake Base Station: A Location Based Approach," *IEEE Commun. Lett.*, vol. 22, no. 8, pp. 1604–1607, Aug. 2018.

[126] S. Srirangarajan, A. H. Tewfik, and Z. Luo, "Distributed sensor network localization using SOCP relaxation," *IEEE Trans. Wireless Commun.*, vol. 7, no. 12, pp. 4886–4895, Dec. 2008.

[127] J. D. Kelleher, B. M. Namee, and A. D'Arcy, *Fundamentals of Machine Learning for Predictive Data Analytics: Algorithms, Worked Examples, and Case Studies*. Reading, Massachusetts: The MIT Press, 2015.

[128] *New frequency range for NR (24.25-29.5 GHz)*, document TR 38.815, V. 15.0.0, 3GPP, Jul. 2018.

[129] W. Ji, T. Ebrahimi, Z. Li *et al.*, "Guest Editorial: Emerging Visual IoT Technologies for Future Communications and Networks," *IEEE Trans. Wireless Commun.*, vol. 28, no. 4, pp. 10–11, Aug. 2021.

[130] X. Shao, X. Chen, and R. Jia, "A Dimension Reduction-Based Joint Activity Detection and Channel Estimation Algorithm for Massive Access," *IEEE Trans. Signal Process.*, vol. 68, pp. 420–435, 2020.

[131] M. Aazam and E. Huh, "Fog Computing: The Cloud-IoT/IoE Middleware Paradigm," *IEEE Potentials*, vol. 55, no. 3, pp. 40–44, May 2016.

[132] N. Rupasinghe and İ. Güvenç, "Reinforcement Learning for Licensed-Assisted Access of LTE in the Unlicensed Spectrum," in *Proc. IEEE Wireless Commun. Networking Conf. (WCNC)*, New Orleans, LA, USA, Mar. 2015.

[133] M. Chen, W. Saad, and C. Yin, "Echo State Networks for Self-Organizing Resource Allocation in LTE-U With Uplink–Downlink Decoupling," *IEEE Trans. Wireless Commun.*, vol. 16, no. 1, pp. 3–16, Jan. 2017.

[134] J. Mark, "Distributed Scheduling Conflict-Free Multiple Access for Local Area Communication Networks," *IEEE Trans. Commun.*, vol. 28, no. 12, pp. 1968–1976, Jan. 1980.

[135] H. O. Burton and D. D. Sullivan, "Errors and error control," *Proceedings of the IEEE*, vol. 60, no. 11, pp. 1293–1301, Jan. 1972.

[136] A. J. Viterbi, A. M. Viterbi, and E. Zehavi, "Performance of power-controlled wideband terrestrial digital communication," *IEEE Trans. Commun.*, vol. 41, no. 4, pp. 559–569, Aug. 1993.

[137] F. H. C. Neto, D. C. Araújo, M. P. Mota, T. F. Maciel, and A. L. F. de Almeida, "Uplink Power Control Framework Based on Reinforcement Learning for 5G Networks," *IEEE Trans. Veh. Technol.*, vol. 70, no. 6, pp. 5734–5748, Jun. 2021.

[138] Y. Chu, P. D. Mitchell, and D. Grace, "Reinforcement learning based ALOHA for multi-hop Wireless Sensor Networks with Informed Receiving," in *Proc. IET Conference on Wireless Sensor Systems (WSS 2012)*, London, 2012.

[139] J. Moon and Y. Lim, "Access control of MTC devices using reinforcement learning approach," in *Proc. International Conference on Information Networking (ICOIN 2017)*, Da Nang, Vietnam, 2017.

[140] S. K. Sharma and X. Wang, "Collaborative Distributed Q-Learning for RACH Congestion Minimization in Cellular IoT Networks," *IEEE Commun. Lett.*, vol. 23, no. 4, pp. 600–603, Apr. 2019.

[141] Z. Yang, C. Pan, M. Shikh-Bahaei *et al.*, "Joint Altitude, Beamwidth, Location, and Bandwidth Optimization for UAV-Enabled Communications," *IEEE Commun. Lett.*, vol. 22, no. 8, pp. 1716–1719, Aug. 2018.

[142] H. Bao, Y. Huo, X. Dong, and C. Huang, "Joint Time and Power Allocation for 5G NR Unlicensed Systems," *IEEE Trans. Wireless Commun.*, vol. 20, no. 9, pp. 6195–6209, Sep. 2021.

[143] S. Lien, J. Lee, and Y. Liang, "Random Access or Scheduling: Optimum LTE Licensed-Assisted Access to Unlicensed Spectrum," *IEEE Commun. Lett.*, vol. 20, no. 3, pp. 590–593, Mar. 2016.

[144] J. Yuan, A. Huang, H. Shan, T. Q. S. Quek, and G. Yu, "Design and Analysis of Random Access for Standalone LTE-U Systems," *IEEE Trans. Veh. Technol.*, vol. 67, no. 10, pp. 9347–9361, Oct. 2018.

[145] J. So and R. Srikant, "Improving Channel Utilization via Cooperative Spectrum Sensing With Opportunistic Feedback in Cognitive Radio Networks," *IEEE Commun. Lett.*, vol. 19, no. 6, pp. 1065–1068, Jun. 2015.

[146] Y. Zeng, Y. Liang, and R. Zhang, "Blindly Combined Energy Detection for Spectrum Sensing in Cognitive Radio," *IEEE Signal Process. Lett.*, vol. 15, pp. 649–652, Feb. 2008.

[147] S. Lagen, L. Giupponi, S. Goyal *et al.*, "New Radio Beam-Based Access to Unlicensed Spectrum: Design Challenges and Solutions," *IEEE Commun. Surveys Tuts.*, vol. 22, no. 1, pp. 8–37, 2020.

[148] Y. Wang, Y. Zeng, S. Sun, and Y. Nan, "High Accuracy Uplink Timing Synchronization for 5G NR in Unlicensed Spectrum," *IEEE Wireless Commun. Lett.*, vol. 10, no. 3, pp. 604–608, Mar. 2021.

[149] F. K. Jondral, "Cognitive Radio: A Communications Engineering View," *IEEE Wireless Commun.*, vol. 14, no. 4, pp. 28–33, Aug. 2007.

[150] D. Niedzwiecki, M. J. Sherman, C. S. Myers, and P. D. Fiore, "Recent advances in cognitive communications," *IEEE Commun. Mag.*, vol. 45, no. 10, pp. 54–61, Oct. 2007.

[151] R. Yin, G. Yu, A. Maaref, and G. Y. Li, "LBT-Based Adaptive Channel Access for LTE-U Systems," *IEEE Trans. Wireless Commun.*, vol. 15, no. 10, pp. 6585–6597, Oct. 2016.

[152] C. She, C. Yang, and T. Q. S. Quek, "Cross-Layer Optimization for Ultra-Reliable and Low-Latency Radio Access Networks," *IEEE Trans. Wireless Commun.*, vol. 17, no. 1, pp. 127–141, Jan. 2018.

[153] C. Sun, C. She, C. Yang *et al.*, "Optimizing Resource Allocation in the Short Block-length Regime for Ultra-Reliable and Low-Latency Communications," *IEEE Trans. Wireless Commun.*, vol. 18, no. 1, pp. 402–415, Jan. 2019.

[154] J. Lu, S. Wan, X. Chen *et al.*, "Beyond Empirical Models: Pattern Formation Driven Placement of UAV Base Stations," *IEEE Trans. Wireless Commun.*, vol. 17, no. 6, pp. 3641–3655, Jun. 2018.

[155] W. S. Jeon and D. G. Jeong, "Combined Channel Access and Sensing in Cognitive Radio Slotted-ALOHA Networks," *IEEE Trans. Veh. Technol.*, vol. 64, no. 5, pp. 2128–2133, May 2015.

[156] S. Sesia, I. Toufik, and M. Baker, *LTE - The UMTS Long Term Evolution: From Theory to Practice*, 2nd ed.   West Sussex, United Kingdom: John Wiley & Sons, 2011.

[157] X. Li, C. Li, S. Jin, and X. Gao, "Interference Coordination for 3-D Beamforming-Based HetNet Exploiting Statistical Channel-State Information," *IEEE Trans. Wireless Commun.*, vol. 17, no. 10, pp. 6887–6900, Oct. 2018.

[158] C. Pan, C. Yin, N. C. Beaulieu, and J. Yu, "Distributed Resource Allocation in SDCN-Based Heterogeneous Networks Utilizing Licensed and Unlicensed Bands," *IEEE Trans. Wireless Commun.*, vol. 17, no. 2, pp. 711–721, Feb. 2018.

[159] Q. Chen, G. Yu, and Z. Ding, "Optimizing Unlicensed Spectrum Sharing for LTE-U and WiFi Network Coexistence," *IEEE J. Sel. Areas Commun.*, vol. 34, no. 10, pp. 2562–2574, Oct. 2018.

[160] C. Ye, M. C. Gursoy, and S. Velipasalar, "Power Control for Wireless VBR Video Streaming: From Optimization to Reinforcement Learning," *IEEE Trans. Commun.*, vol. 67, no. 8, pp. 5629–5644, Aug. 2019.

[161] X. Liu, Y. Liu, Y. Chen, and L. Hanzo, "Trajectory Design and Power Control for Multi-UAV Assisted Wireless Networks: A Machine Learning Approach," *IEEE Trans. Veh. Technol.*, vol. 68, no. 8, pp. 7957–7969, Aug. 2019.

[162] I. Bor-Yaliniz, A. El-Keyi, and H. Yanikomeroglu, "Spatial Configuration of Agile Wireless Networks with Drone-BSs and User-in-the-loop," *IEEE Trans. Wireless Commun.*, vol. 18, no. 2, pp. 753–768, Feb. 2019.

[163] R. Bruschi, F. Davoli, P. Lago, and J. F. Pajo, "A Multi-Clustering Approach to Scale Distributed Tenant Networks for Mobile Edge Computing," *IEEE J. Sel. Areas Commun.*, vol. 37, no. 3, pp. 499–514, Mar. 2019.

[164] B. K. M. Hirzallah, M. Krunz and B. Hamzeh, "5G New Radio Unlicensed: Challenges and Evaluation," *IEEE Trans. on Cogn. Commun. Netw.*, vol. 7, no. 3, pp. 689–701, Sep. 2021.

[165] F. Liu, E. Bala, E. Erkip, M. C. Beluri, and R. Yang, "Small-Cell Traffic Balancing Over Licensed and Unlicensed Bands," *IEEE Trans. Veh. Technol.*, vol. 64, no. 12, pp. 5850–5865, Dec. 2015.

[166] M. G. Kibria, K. Nguyen, G. P. Villardi *et al.*, "Big Data Analytics, Machine Learning, and Artificial Intelligence in Next-Generation Wireless Networks," *IEEE Access*, vol. 6, pp. 32 328–32 338, 2018.

[167] C. X. Wang, F. Haider, X. Gao *et al.*, "Cellular Architecture and Key Technologies for 5G Wireless Communication Networks," *IEEE Commun. Mag.*, vol. 52, no. 2, pp. 122–130, Feb. 2014.

[168] R. Li, Z. Zhao, X. Zhou *et al.*, "Intelligent 5G: When Cellular Networks Meet Artificial Intelligence," *IEEE Trans. Wireless Commun.*, vol. 24, no. 5, pp. 175–183, Oct. 2017.

[169] "Basic regression: Predict fuel efficiency," *https://www.tensorflow.org/tutorials/keras/regression*.

[170] "Deep Neural Networks for Regression Problems," *https://towardsdatascience.com/deep-neural-networks-for-regression-problems-81321897ca33*.

[171] H. van Hasselt, A. Guez, and D. Silver, "Deep Reinforcement Learning with Double Q-learning," in *Thirtieth AAAI Conf. on Artificial Intelligence (AAAI-16)*, Arizona, USA, Feb. 2016.

[172] U. Epple, D. Shutin, and M. Schnell, "Mitigation of Impulsive Frequency-Selective Interference in OFDM Based Systems," *IEEE Wireless Commun. Lett.*, vol. 1, no. 5, pp. 484–487, Oct. 2012.

[173] S. Sharma, A. Gupta, and V. Bhatia, "Impulse Noise Mitigation in IR-UWB Communication Using Signal Cluster Sparsity," *IEEE Wireless Commun. Lett.*, vol. 22, no. 3, pp. 558–561, Mar. 2018.

[174] M. Wildemeersch, T. Q. S. Quek, M. Kountouris, A. Rabbachin, and C. H. Slump, "Successive Interference Cancellation in Heterogeneous Networks," *IEEE Trans. Commun.*, vol. 62, no. 12, pp. 4440–4453, Dec. 2014.

[175] C. Kloch, G. Liang, J. B. Andersen, G. F. Pedersen, and H. L. Bertoni, "Comparison of measured and predicted time dispersion and direction of arrival for multipath in a small cell environment," *IEEE Trans. Antennas Propag.*, vol. 49, no. 9, pp. 1254–1263, Sep. 2001.

[176] J. Bergstra and Y. Bengio, "Random Search for Hyper-Parameter Optimization," *Journal of Machine Learning Research*, vol. 13, no. 10, pp. 281–305, 2012.

[177] I. Goodfellow, Y. Bengio, and A. Courville, *Deep Learning*. Cambridge, MA, USA: The MIT Press, 2016.

[178] "Deep Learning Models for Multi-Output Regression," *https://machinelearningmastery.com/deep-learning-models-for-multi-output-regression/*.

[179] M. G. S. Sriyananda and M. Bennis, "Learning-Based Small Cell Traffic Balancing Over Licensed and Unlicensed Bands," *IEEE Wireless Commun. Lett.*, vol. 6, no. 5, pp. 694–697, Oct. 2017.

[180] S. R. Pandey, N. H. Tran, M. Bennis *et al.*, "A Crowdsourcing Framework for On-Device Federated Learning," *IEEE Trans. Wireless Commun.*, vol. 19, no. 5, pp. 3241–3256, May 2020.

[181] P. Sun, N. AlJeri, and A. Boukerche, "An Energy-Efficient Proactive Handover Scheme for Vehicular Networks Based on Passive RSU Detection," *IEEE Sustain. Comput.*, vol. 5, no. 1, pp. 37–47, Mar. 2020.

[182] V. Croisfelt, A. Amiri, T. Abrao, E. de Carvalho, and P. Popovski, "Accelerated Randomized Methods for Receiver Design in Extra-Large Scale MIMO Arrays," *IEEE Trans. Veh. Technol.*, vol. 70, no. 7, pp. 6788–6799, Jul. 2021.

[183] Y. Jeong and K. Yi, "Target Vehicle Motion Prediction-Based Motion Planning Framework for Autonomous Driving in Uncontrolled Intersections," *IEEE Trans. Intell. Transp. Syst.*, vol. 22, no. 1, pp. 168–177, Jan. 2021.

[184] S. X. Wei, A. Dixit, S. Tomar, and J. W. Burdick, "Moving Obstacle Avoidance: a Data-Driven Risk-Aware Approach," *IEEE Control Syst. Lett*, vol. 24, no. 4, pp. 72–80, Aug. 2022.

Appendices

Appendix A

Path Loss Model with Dynamic Parameters

Consider a receive signal sample from the frame n of the device m at location (x_m, y_m, z_m), $y^n_{(x,y,z)}[t]$, $y^n_{(x,y,z)}[t] = \sqrt{p'} h'_n x'[t] + \sqrt{p} h_n x[t] + i_{(x,y,z,n)} + \eta_n$. The channel coefficient h_n in the receive signal is modeled as $|h_n|^2 = |h^f_n|^2 \, 10^{-\frac{L^P_m}{10}}$, $h^f_n \sim \mathcal{N}_c\left(0, \sigma^2_h\right)$ where h^f_n and L^P_m are the location based fading coefficient path loss (in dB), accordingly. For this study, path loss L^P_m based on UMi OS NLOS environment [18, 20] is expressed as

$$L^P_m = \alpha + 10\beta_{(x,y,z)} \log_{10}(d_m) + 10\gamma_f \log_{10} \frac{f_{\text{UB}}}{1\text{GHz}} + \xi_{(x,y,z)}, \text{ dB} \tag{A.1}$$

where γ_f is the coefficient for the dependence of path loss on frequency and d_m is the distance to the receiver from the BS. α, $\beta_{(x,y,z)}$ and $\xi_{(x,y,z)}$, $\xi_{(x,y,z)} \sim \mathcal{N}\left(0, \sigma^2_{\text{PL}}\right)$, are least square fit of floating intercept, slope over the measured distances and log-normal shadowing, respectively. α is an optimized offset value for the UMi OS NLOS environment [18, 20], $\beta_{(x,y,z)}$ is non-optimized parameter for a given distance and shadowing $\xi_{(x,y,z)}$ is a specific parameter for a given location. Both $\beta_{(x,y,z)}$ and $\xi_{(x,y,z)}$ are made sensitive to the location [15, 24] and indexed with Cartesian coordinates representing path loss as a location-specific parameter. Even though these two parameters are indexed with 3D Cartesian coordinates, for the simplicity L^P_m is not

indexed with them. Variance for $\xi_{(x,y,z)}$, σ^2_{PL}, is also an estimated value for the UMi OS NLOS environment [18, 20]. The channel coefficient h' is also modeled similar to h considering the path of the signal from the serving NR-U enabled BS.

In a case of a device at (x_m, y_m, z_m) which is surrounded by several other M' nearby devices, path loss parameters $\beta'_{(x,y,z)}$ and $\xi'_{(x,y,z)}$ are given with reference to those of the locations of the nearby devices as

$$\beta'_{(x,y,z)} = \frac{1}{M'} \sum_{m'}^{M'} \beta^{m'}_{(x,y,z)} (1 \pm \epsilon_{m'}) \tag{A.2}$$

$$\xi'_{(x,y,z)} = \frac{1}{M'} \sum_{m'}^{M'} \xi^{m'}_{(x,y,z)} \left[1 \pm 8 d^2_{m'} \sin(\theta_{m'}) \right] \tag{A.3}$$

where $\theta = 2\pi \left(4 \left(d_{m'} + n_{\text{no}} + r_{m'} \right) \bmod 4 \right)$, $0 < d_{m'} \leq 1$, $n_{\text{no}} = \frac{(n \bmod 10^3)}{10^3}$, $r_{m'} \sim \mathcal{U}(0, 1)$ and $\epsilon_{m'} \sim \mathcal{U}(0, 0.05)$. $d_{m'}$ is the distance to the locations of the nearby devices from the device m. It is assumed that there is a slight variation for the parameter $\beta^{m'}_{(x,y,z)}$ which can be modeled as a random parameter $\epsilon_{m'}$ and it is changed over frames. Furthermore, it is assumed that variation of the parameter $\xi^{m'}_{(x,y,z)}$ can be represented with $8 d^2_{m'} \sin(\theta_{m'})$ with a reasonable accuracy. $8 d^2_{m'} \sin(\theta_{m'})$ evolves over time as n_{no} and $r_{m'}$ are changed from frame to frame. With the parameter $r_{m'}$, a certain degree of randomness is also maintained for this evolution.

Curriculum Vitae

Name: M. G. S. Sriyananda

Post-Secondary   2016 - present, Ph.D. candidate
Education and   The University of Western Ontario
Degrees: London, Ontario, Canada.

                     2010 - 2014, Ph.D.
                     University of Jyväskylä
                     Jyväskylä, Finland

                     2003 - 2005, M.Sc.
                     University of Moratuwa
                     Moratuwa, Sri Lanka

                     1998 - 2003, B.Sc.Eng.
                     University of Moratuwa
                     Moratuwa, Sri Lanka

Honours and   2017, Outstanding Young Professional - IEEE London
Awards: Section

Related Work   Research Assistant
Experience: University of Western Ontario
                     2016 - present.

                     Teaching Assistant
                     University of Western Ontario
                     2016 - present.

Publications:

Published

[1] M. G. S. Sriyananda, X. Wang, and S. Primak, "Device and Network Coordination for Opportunistic Utilization of Radio Resources in 3D Networks," *IEEE Open Journal of Vehicular Technology*, vol. 3, pp. 408-425, 2022.

[2] M. G. S. Sriyananda, X. Wang, and R. K. Rao, "Crowdsensing-Assisted Path Loss Estimation and Management of Dynamic Coverage in 3D Wireless Networks With Dense Small Cells," *IEEE Access*, vol. 9, pp. 112 670–112 685, 2021.

[3] M. G. S. Sriyananda, X. Wang, and S. Primak, "Learning-Assisted Access Management for Dense 3D Small Cell Networks," in *Proceedings of IEEE Canadian Conference on Electrical and Computer Engineering (CCECE)*, Canada, Sep. 2021.

[4] G. Zafari, M. Koca, X. Wang and M. G. S. Sriyananda, "Antenna Grouping in Dual-Polarized Generalized Spatial Modulation," in *IEEE 86th Vehicular Technology Conference (VTC-Fall)*, Toronto, ON, Canada, Sep. 2017.

Under Review

[1] M. G. S. Sriyananda and X. Wang, "Learning Based Neighboring Station Coverage Identification and Dynamic Resource Utilization for 3D Cells in NR-U Networks," *IEEE Systems Journal*.